Near Real-time Seasonal Drought Forecasting and Retrospective Drought Analysis Using Simulated Multi-layer Soil Moisture from Hydrological Models at Sub-watershed Scales

Vinit Sehgal

Thesis submitted to the faculty of the
Virginia Polytechnic Institute and State University
in partial fulfillment of the requirements for the degree of

Master of Science
in
Biological Systems Engineering

Venkataramana Sridhar (Chair)
Jactone A. Ogejo
Luke Juran

15th June 2017
Blacksburg, Virginia

Keywords: Drought, Soil moisture, Water balance,
Southeastern US, Hydroclimatology, SWAT, CFSv2

Near Real-time Seasonal Drought Forecasting and Retrospective Drought Analysis Using Simulated Multi-layer Soil Moisture from Hydrological Models at Sub-watershed Scales

Vinit Sehgal

ABSTRACT

This study proposes a stratified approach of drought severity assessment using multi-layer simulated soil moisture. SWAT (Soil & Water Assessment Tool) models are calibrated for 50 watersheds in the South-Atlantic Gulf region of the Southeastern US and a high-resolution daily soil moisture dataset is obtained at Hydrologic Unit Code (HUC-12) resolution for a period of January 1982 through December 2013. A near real-time hydrologic simulation framework by coupling the calibrated SWAT models with the National Centers for Environmental Prediction (NCEP) coupled forecast system model version 2 (CFSv2) weather data is developed to forecast various water balance components including soil moisture (SM), actual evapotranspiration (ET), potential evapotranspiration ET (PET), and runoff (SURQ) for near-real time drought severity assessment, and drought forecasting for a lead of 9-months. A combination of the surface and total rooting depth soil moisture percentiles proves to be an effective increment over conventional drought assessment approaches in capturing both, transient and long-term drought impacts. The proposed real-time drought monitoring approach shows high accuracy in capturing drought onset and propagation and shows a high degree of similarity with the U.S. Drought Monitor (USDM), the long-term (PDSI, PHDI, SPI-9 and SPI-12), and the short-term (Palmer Z index, SPI-1 and SPI-6) drought indices.

Near Real-time Seasonal Drought Forecasting and Retrospective Drought Analysis Using Simulated Multi-layer Soil Moisture from Hydrological Models at Sub-watershed Scales

Vinit Sehgal

GENERAL AUDIENCE ABSTRACT

Drought, a recurring and worldwide phenomenon, with spatial and temporal characteristics varying significantly from across globe, lead to long-term and cumulative environmental changes. Often referred to as creeping phenomena, droughts are difficult to predict and constant monitoring is required to capture the signs of the onset of drought. Spatial variability in drought severity requires an understanding of the hydrology of the region and a knowledge of the relationship between drought inducing climatic extremes and other regional or local characteristics which help build, sustain and propagate droughts. In the absence of long-term observed hydrologic variables like soil moisture, evapotranspiration, simulated hydrologic variables serve an important purpose in understanding the impact of drought on various components of the water budget. However, several continental scale, physics-based models, and large scale remote sensing products find themselves restricted in explaining the watershed scale and sub-watershed scale variability in relation to drought. This study provides a high-resolution simulation of hydrological variables for 50 watersheds in the South-Atlantic Gulf region of the Southeastern US. The high resolution hydrologic simulations provide bedrock for retrospective drought simulations and understanding the response of various hydrologic variables of these watersheds to drought. It also aids in understanding the spatial variability in the relationship, and understanding the impact of seasonality and hydroclimatology on drought. The understanding of the interplay of various water budget components at watershed scale is used in developing a reliable seasonal drought forecasting framework based on the forecasted hydrologic variables from SWAT-CFSv2 coupled models for application in real time with a lead time of 9 months.

Table of Contents

List of Figures

List of Tables

Chapter 1 :
Introduction

Droughts are a worldwide phenomenon, with spatial and temporal characteristics varying significantly from region to region (Tallaksen and Van Lanen, 2004). The impact of drought manifests in all components of the hydrologic budget, namely, in water supply (precipitation), storage (soil moisture, snowpack, groundwater, and surface water), and exchange or flux (evapotranspiration, snowmelt, drainage/recharge, runoff, and streamflow) (Anderson et al., 2013). McEvoy (2015) reported that the severity of the recent droughts in the United States has been accentuated by high temperatures and evaporative demand. With increasing human population and associated demand for freshwater resources and food production, global food security has come under severe risk (Mu et al., 2013). The Southeastern U.S. has experienced widespread droughts three times within a span of 15 years since early 2000 and nearly 40% of the region is under moderate to exceptional drought conditions as of early 2017. Several studies have expressed concerns over increasing drought vulnerability of the region owning to continued growth and subsequent industrial, agricultural and metropolitan demand throughout the southeast (Manuel, 2008; Pederson et al., 2012; Seager et al., 2009) and suggest that the threat of water-related conflict in the region has potential to grow more intense in the coming decades.

Dynamical seasonal forecasting systems, based on coupled atmosphere-ocean-land general circulation models (CGCMs), have been widely used for drought forecasting in recent years (Dutra et al., 2013; Ma et al., 2015). Seasonal climate forecasts are useful in improving farm production, particularly in rain-fed systems (Wetterhall et al., 2015). Skillful prediction of the field moisture availability is important to decide crop type, resource use, and crop insurance and contract

renewals (Shafiee-Jood et al., 2014). Several studies have highlighted the applicability of climate forecast system reforecast and reanalysis (Saha et al., 2010) products in drought monitoring and prediction, seasonal soil moisture estimation, and understanding the land-surface interaction (Dirmeyer, 2013; Mace et al., 2015; McEvoy et al., 2016b; Mo et al., 2011; Mo et al., 2012b; Roundy et al., 2014). Physically-based hydrological models are popularly used to simulate complex water resource systems to simulate the impacts of land use and climate change and other anthropogenic activities on the hydrological cycle (Cao et al., 2006; Muttiah and Wurbs, 2002). These model provide a physical representation of spatially variable hydrological processes (Xu et al., 2009) and key hydrological components along with the temporal variability and interrelationship with hydroclimatological influences. While some hydrological variables like precipitation, streamflow are more frequently recorded and reported, similar long-term soil moisture observations are scarce. Estimation of another important water budget component, namely evapotranspiration, is carried out using several remotely sensed platforms. However, inter-comparisons of multiple spatial datasets reveal significant uncertainties, with relative errors of 15%–30% between the products, thus accentuating the need of using physics based models for simulating the hydrologic variables for effective drought monitoring and prediction.

Chapter 2 develops an adjusted, high-resolution soil moisture dataset for drought reconstruction for the Contiguous United State (CONUS) using a multi-resolution regression of Noah and Mosaic Land Surface Models against *in-situ* soil moisture dataset obtained from the U.S. Climate Reference Network (USCRN) stations. A layer-wise correlation analysis is carried out to highlight the response of soil moisture to various drought indices (DIs) representing short-term (Palmer Z index, SPI-1 and SPI-6) and long-term (PDSI, PHDI, SPI-9, SPI-12 and SPI-24) predictability of drought. The study also highlights the difference in the spatial and inter-layer

patterns in the persistence of the soil moisture, pertaining to different soil layers, thus establishing a need for multi-layer perspective in drought analysis. These novel insights are used for a layer-wise (stratified) drought reconstruction approach which is applied to recent drought occurrences, for capturing drought in the Southern U.S. (from April' 2011- December 2011) as a case study.

Droughts are recurrent features of the natural system and are primarily driven by climate and weather patterns. However, these extremities are significantly moderated at a watershed-scale, where the confluence of several factors related to watershed-scale water balance and, in some cases, anthropogenic activities, may exacerbate or alleviate drought conditions (Garner et al., 2015). Several catchment-scale processes associated with droughts like extension of meteorological droughts into a long-term hydrological drought (pooling); attenuation of meteorological droughts in groundwater storage; a lag between the meteorological, soil moisture, and hydrological drought; lengthening of droughts-where drought characteristics change from meteorological to soil moisture to hydrological drought; are controlled by both catchment characteristics and climate (Van Loon and Van Lanen, 2012). The characteristics of meteorological anomalies leading to droughts vary spatially (between climatic regions) and temporally (between seasons) and interact with the physical characteristics of the catchment (e.g. area, soils, geology and land use) that govern basin water storage and transfer processes to determine river flow response (Garner et al., 2015; Van Loon and Van Lanen, 2012). Above discussion highlights the importance of a catchment/watershed scale understanding of drought dynamics in the context of drought predictability and inclusive drought impact assessment.

Chapter 3 identifies the inadequacy in current literature in linking the global scale weather models like CFSv2 to regional hydrologic models for simulating high-resolution hydrologic variables and using watershed-scale process understanding in near-real time seasonal forecasting.

This part of the study focusses on implementing SWAT models to simulate various hydrologic variables at the sub-watershed scale for the South Atlantic-Gulf (SAG) region of the Southeastern U.S. (SEUS) at HUC-12 (12-digit Hydrologic Unit Code) resolution. The study uses multi-layer observed soil moisture dataset from USCRN to test the accuracy of the models in simulating sub-watershed scale surface soil layer and root zone soil moisture. A near real-time forecasting framework at sub-watershed scale for soil moisture and evapotranspiration is developed in this study using calibrated SWAT models initialized with climate drivers from the National Centers for Environmental Prediction (NCEP) coupled forecast system model version 2 (CFSv2) models with a lead time of up to 9 months at a daily time step.

Once the high-resolution hydrologic data obtained by implementing SWAT models for the 50 watersheds is obtained from the study in *Chapter 3*, a stratified drought analysis as proposed in *Chapter 2* is implemented for SEUS for drought severity estimation using the top soil layer for analyzing transient and low intensity droughts, and total column soil moisture for long term, severe droughts using sub-watershed scale (at HUC-12 resolution) soil moisture. This study is provided in *Chapter 4*. A retrospective drought analysis for the SAG region with a focus on three recent drought occurrences in the year 2000- 02, 2006- 09 and 2011-13 using the proposed layer-wise approach. Furthermore, a real-time drought forecasting framework using high-resolution, SWAT-based simulated soil moisture initialized using climate drivers from CFSv2 with a lead time of up to 9 months at a weekly time step is also developed for effective early drought forecasting in the region.

Hydrologic variability in the SEUS in terms of precipitation and streamflow can be partly explained by the phase of various hydroclimatological teleconnections (Engström and Waylen, 2017a; Kahya and Dracup, 1993; Labosier and Quiring, 2013). These hydroclimatic anomalies and

internal variation in the coupled ocean-atmospheric-land systems are strongly related to climatic extremes across the world thus serving as natural drivers of droughts. The hydroclimatological variability ranges from interannual to decadal timescale and can significant impact the climate across the globe (Sheffield and Wood, 2012). Previously, Labosier and Quiring (2013) reviewed the hydroclimatology of the Southeastern USA and concluded that the region is strongly impacted by Southeast is primarily controlled by El Niño/Southern Oscillation (ENSO), the Pacific North American (PNA) pattern, the Bermuda High, and tropical cyclones. El Niño-Southern Oscillation, The North Atlantic Oscillation and Pacific North American Pattern, all found to significantly change seasonal precipitation and runoff in southeastern U.S (Engström and Waylen, 2017a).

Chapter 5 evaluates the response of four water budget components namely soil water storage (SW), precipitation (PCP), surface runoff (SURQ) and potential evapotranspiration (PET) to various hydroclimatological indices for 50 watersheds in the SEUS. The study assesses the strength of interrelationship between hydroclimatology and long and short-term drought predictability in the region using various water budget components at watershed scale. The highlights the spatial variability in the association between watershed scale hydrology and climatic indices for the SEUS and compliments the drought forecasting efforts made in previous chapters.

Chapter 2 :
Stratified drought analysis using a stochastic ensemble of simulated and in- situ soil moisture observations

Key Points:

a) Soil moisture ensembles from Noah and Mosaic simulations, and *in-situ* dataset using multi-wavelet, multi- resolution models with Bayesian Model Averaging

b) Highlight significant variation in behavior of soil moisture from three layers to drought, pertaining to difference in persistence and statistical properties

c) A layer-wise soil moisture percentile approach is proposed and used for drought reconstruction for Texas drought (Jan- Dec' 2011)

1. Abstract

This study proposes a multi- wavelet Bayesian ensemble of two Land Surface Models (LSMs) using in- situ observations for accurate estimation of soil moisture for Contiguous United States (CONUS). In the absence of a continuous, accurate *in-situ* soil moisture dataset at high spatial resolution, an ensemble of Noah and Mosaic LSMs is derived by performing a Bayesian Model Averaging (BMA) of several wavelet-based multi- resolution regression models (WR) of the simulated soil moisture from the LSMs and *in-situ* volumetric soil moisture dataset obtained from the U.S. Climate Reference Network (USCRN) field stations. This provides a proxy to the *in- situ* soil moisture dataset at $1/8^{th}$ degree spatial resolution called Hybrid Soil Moisture (HSM) for three soil layers (1-10 cm, 10- 40 cm and 40- 100 cm) for the CONUS. The derived HSM is used further to study the layer- wise response of soil moisture to drought, highlighting the necessity of the ensemble approach and soil profile perspective for drought analysis. A correlation analysis between HSM, the long-term (PDSI, PHDI, SPI-9, SPI-12 and SPI-24) and the short-term (Palmer Z index, SPI-1 and SPI-6) drought indices is carried out for the nine climate regions of the U.S. indicating a higher sensitivity of soil moisture to drought conditions for the Southern U.S. Furthermore, a layer-wise soil moisture percentile approach is proposed and applied for drought reconstruction in CONUS with a focus on the Southern U.S. for the year 2011.

Keywords: Soil Moisture, Land Surface Models, Drought, Wavelet analysis, Bayesian model averaging, Ensemble, NLDAS- v2

2. Introduction

Drought and its impacts are not only incremental and a factor in long-term and cumulative environmental changes, but also comes into existence as a slow-onset or creeping event (Pulwarty and Sivakumar, 2014). Because it is difficult to establish a generally acceptable definition of drought for use in various water sectors, four types of droughts are defined as meteorological, agricultural, hydrological, and socioeconomic drought (Mozny et al., 2012; Wilhite and Glantz, 1985). Due to the slow onset and recovery, determining the beginning and end of a particular drought period is often difficult (Iglesias et al., 2009). In the wake of climate change, the likelihood of occurrence of extreme drought events with greater severity in the future in many regions of the globe is expected to rise significantly (Dai, 2011; Kundzewicz et al., 2010; Peterson et al., 2012; Trenberth and Fasullo, 2012). The areal extent of droughts increased more than 50% during the last century over the globe, while changes in the areal extent of wet regions were relatively small (Trenberth et al., 2004). Hence, great emphasis has been laid out worldwide on the drought strategies, with a specific focus on comprehensive drought monitoring (Hayes et al., 2011).

Many studies have established the usefulness of soil moisture anomalies for characterizing drought onset and demise (Hunt et al., 2009). Soil moisture modulates the atmospheric surface energy balance and hence has a significant impact on the vertical distribution of turbulent heat fluxes, as well as the boundary layer structure (Alapaty et al., 1997). Soil moisture is a pivotal element in the hydrological process of converting precipitation into runoff and groundwater storage. Mozny et al. (2012) used *in-situ* soil moisture dataset for drought monitoring in the Czech Republic using a Soil Moisture Index (SMI) and found soil moisture based drought index to be useful in rapid-onset drought monitoring. Ford et al. (2015) used *in-situ* soil moisture observations for developing a flash drought early warning framework for Oklahoma. Sims and Raman (2002)

established strong inter-relationship of two drought indices: Palmer Drought Severity Index (PDSI) values and Standardized Precipitation Index (SPI) with soil moisture for North Carolina. Lakshmi et al. (2004) showed that the deep layer soil moisture anomaly is a good drought indicator and has a higher memory than Palmer Drought Severity Index (PDSI).

To understand the interrelationship between soil moisture and drought at a large spatial scale, long-term data of soil moisture is required. However, in most regions of the world, the lack of spatially extensive soil moisture monitoring networks precludes the inclusion of soil moisture in drought monitoring systems (Ford et al., 2015) . While some hydrological variables like precipitation, streamflow are more frequently recorded and reported, similar long-term soil moisture observations are scarce. There has been an extensive application of near-surface soil moisture information obtained through remote sensing in agriculture and meteorology. However, in most applications the magnitudes of modeled, in situ, and remotely sensed soil moisture often do not correlate well without any posterior bias correction (Narayan and Lakshmi, 2008; Sridhar et al., 2013). Also, near surface soil moisture in not sufficient to comprehensively assess drought severity. Hence, the use of simulated soil moisture from land surface models (LSMs) has become popular and has been applied to several studies to understand the dynamics and impact of drought. With the advancements in computational power, it is now feasible to generate operational land surface hydrological data products over large scales using telemetry, remote sensing based dataset and modeled meteorological data from atmospheric forecast models (Mitchell et al., 2004b). Though, the lack of high-resolution data to perform any physically based distributed hydrological modeling remains a limitation to researchers (Sridhar and Hubbard, 2009).

Previously, Sridhar et al. (2008) used simulated soil moisture using a hydrologic model developed by Robinson and Hubbard (1990) across different land-use conditions in Nebraska, US,

to develop a Soil Moisture Index (SMI) for quantifying agricultural drought. The results were compared with the SMI derived from *in-situ* soil moisture. It was concluded that developing SMI using a simulation model-based approach should be considered pragmatic considering the difficulty in establishing a soil moisture observation-based drought index over large areas on a continuous long term. Sheffield et al. (2004a) used the Variable Infiltration Capacity (VIC) model to derive a model-based drought index and evaluated its agreement with the PDSI. Zhang et al. (2016a) applied Australian Community Atmosphere Biosphere Land Exchange model (CABLE) LSMs to predict near-real-time drought in China. Yuan et al. (2013) used the VIC model for obtaining simulated soil moisture for probabilistic seasonal forecasting of droughts in Africa. Xia et al. (2014a) used the North American Land Data Assimilation System (NLDAS) (Mitchell et al., 2004a) dataset to derive *Objective Blended NLDAS Drought Index* (OBNDI) for Conterminous United States (CONUS). Wang et al. (2009) developed a multimodal ensemble of several LSMs for reconstruction of drought over the U.S. AghaKouchak (2014) used precipitation and soil moisture dataset from NASA Modern-Era Retrospective analysis for Research and Applications (MERRA) for probabilistic drought forecasting using a standardized soil moisture index. Sheffield et al. (2014) used the VIC model to derive soil moisture for developing a drought monitoring and forecasting framework in Sub- Sahara region of Africa. Tang and Piechota (2009) used soil moisture obtained from the VIC model for spatial- temporal evaluation of drought variability in the Upper Colorado River Basin. Mo (2008) used Noah and VIC models from NLDAS in order to estimate soil moisture percentiles and runoff indices for drought analysis over U.S. AghaKouchak (2015) proposed a multivariate approach integrating soil moisture percentiles and precipitation for a persistence based drought prediction for East Africa. Soil moisture anomalies from NLDAS were used in assessing the evolution of soil moisture and vegetation conditions in extreme flash drought

in Otkin et al. (2016). Wang et al. (2011) used an ensemble of four physically- based hydrology models to obtain soil moisture percentiles which were used to estimate the severity of agricultural drought. Sohrabi et al. (2015) developed a Soil Moisture Drought Index (SODI) to characterize droughts.

It is therefore evident the scientific community is interested in exploring the application of soil moisture in drought analysis. This study points the importance of differential response of soil profile soil moisture to drought. This insight augments the current understanding of soil moisture to drought correlation. This adds to the existing literature by proposing a layer- wise soil moisture percentile based drought reconstruction approach by using shallow soil layers for short- term, low-intensity drought reconstruction and deeper soil layers for capturing long-term and severe droughts, respectively. The study of the inter-relationship between droughts and soil moisture at a large spatial scale is restricted to the use of several hydrological models which are themselves known to possess a high degree of uncertainties and biases (Mo et al., 2012a). Although LSM-derived soil moisture shows encouraging consistency in the depiction of large-scale drought events, the development of a drought index based on soil moisture at a smaller scale appears to differ considerably across models(Xia et al., 2014a). This is partly due to discrepancies in simulated soil moisture as well as sub-grid scale variability. Some recent studies have attempted to provide a stochastic approach to estimate *in-situ* soil moisture using hydrological models (Kim et al., 2015) but do not address the non- stationarity and multi-scale nature of the underlying process. This study utilizes an ensemble of Noah and Mosaic Land Surface Models (LSMs), obtained using a wavelet- based regression coupled with a Bayesian Model Averaging (BMA) approach (termed as WBR in this study) to simulate and evaluate soil moisture and its correlation with drought indices. The proposed wavelet-based multi-resolution modeling addresses to the non-

stationarity and multiscale variability of soil moisture dataset by modeling the inputs in their sub-time series domain at multiple time- frequency resolutions. BMA is used to counter the subjectivity in the choice of mother wavelet function for time series decomposition into its sub- time series and uncertainty related to the ability of the selected wavelet to satisfactorily represent the process dynamics at the chosen level of time- frequency resolution.

The objectives of this study are as follows:

a) To develop an adjusted, high-resolution soil moisture dataset for carrying out drought sensitivity and reconstruction analysis for Contiguous United State (CONUS) using the proposed multi- resolution regression of Noah and Mosaic LSMs against *in-situ* soil moisture dataset obtained from U.S. Climate reference network (USCRN) stations.
b) To perform a layer- wise correlation analysis to understand the response of soil moisture to drought indices (DIs) representing short term (Palmer Z index, SPI-1 and SPI-6) and long term (PDSI, PHDI, SPI-9, SPI-12 and SPI-24) predictability of drought.
c) To highlight the difference in the spatial and inter- layer patterns in the persistence of the soil moisture pertaining to different soil layers, thus establishing a need for multi-layer perspective in drought analysis and reconstruction using soil moisture.
d) To propose a new layer- wise drought reconstruction approach and apply to recent drought occurrences, for capturing drought in the Southern US (from April 2011- December 2011) as a case study.

Section 2 of the paper provides a short description of the dataset used in this study. An overview of the Wavelet analysis and Bayesian Model Averaging is provided in Section 3. Development of the WBR models is explained in Section 4. Results are provided in Section 5 whereas Section 6 provides a detailed discussion on the observed results. The paper is concluded in Section 7.

3. Data Description

3.1. In-situ soil moisture dataset:

In-situ soil moisture observations for this study is obtained from the US Climate reference network (USCRN) (Bell et al., 2013) database. USCRN is a network of climate monitoring stations operated by the National Oceanic and Atmospheric Administration (NOAA). The soil moisture observations are available for five standard soil depths i.e. 5 cm, 10 cm, 20 cm, 50 cm and 100 cm at daily and hourly time step (also sub-hourly time step for 5 cm layer). Currently, there are 114 stations operating in the continental United States out of which 87 stations contain soil moisture observations for all five layers. Furthermore, to facilitate the inter-comparison of dataset available from all layers, only the stations with equal length of dataset available for all layers are chosen.

Missing values in the dataset were filled using a *penalized least square regression based on discrete cosine transform* (DCT-PLS) algorithm proposed by Garcia (2010) and Wang et al. (2012). The PLS regression is a thin-plate spline smoother for generally one-dimensional data array, which trades off fidelity to the data versus roughness of the mean function and thus expresses the data in terms of a sum of cosine functions oscillating at different frequencies (Wang et al., 2012). This algorithm is successfully employed by several other recent studies in order to address the issue of missing temporal data points in soil moisture (Dorigo et al., 2013; Su et al., 2016) , coastal ocean surface currents (Fredj et al., 2016), remotely sensed solar radiation estimated (Chen et al., 2014) etc. However, as a high number of missing values may lead to higher degree of uncertainty in the analysis, the stations with missing values greater than 15% of the total available dataset from the stations for any layer, are deemed to be unfit for this study.

A total of 48 stations meet all the aforementioned criteria of data availability for all layers and maximum missing values (Figure 2-1 (a)) and are termed as control stations in this study. *In-situ* soil moisture observations only from these control stations are used for building and validating the models which will be described later in this paper. Figure. 2-2 provides a plot for the observed soil moisture time series with gaps filled using the DCT- PLS algorithm for the stations with maximum number of missing values (below 15% threshold) for each sensor depth in order to establish the effectiveness of the gap-filling algorithm for this study.

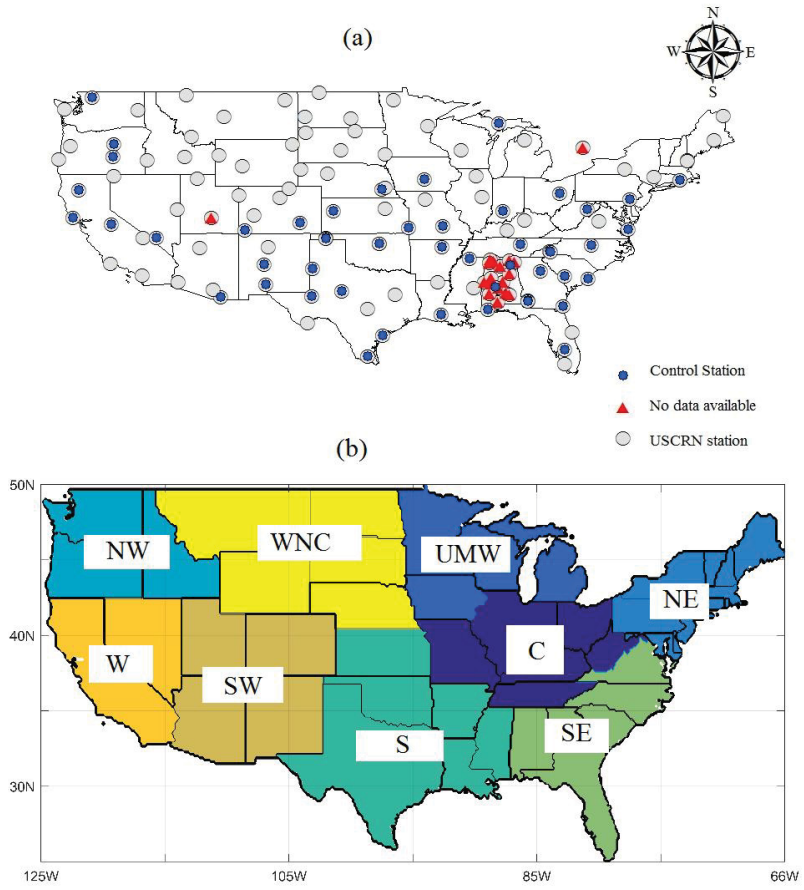

Figure 2-1 : (a) Location of the U.S. Climate reference network (USCRN) stations across US. The red triangle indicates no data is currently available for those stations. Blue circle indicates stations with data available for all five layers. Grey circle indicates control stations. (b) Nine climate

regions of the U.S. (C= Central, UMW=Upper Midwest, NE= North East, NW= North West, S= South, SE= South East, SW= South West, W= West, WNC= West North Central).

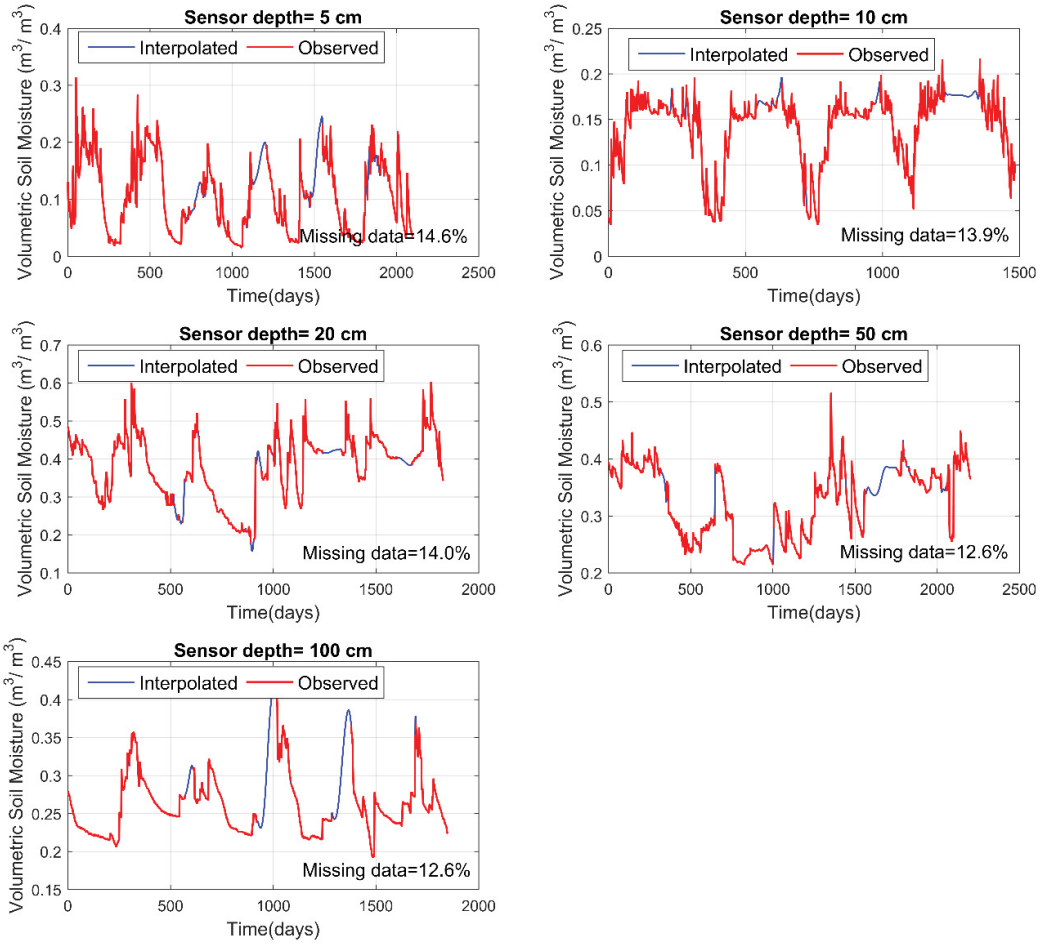

Figure. 2-2: Observed *in- situ* soil moisture data (in red) with interpolated gaps (in blue) at daily time step for five sensor depths. Each plot represents the station with maximum number of missing values (less than the permissible limit of 15%) for a given sensor depth.

3.2. Simulated volumetric soil moisture dataset from Noah and Mosaic LSMs:

Simulated soil moisture dataset for this study is obtained from the North America Land Data Assimilation System Phase 2 (NLDAS-2) products. Simulated volumetric soil moisture variables

from two land surface models namely Noah and Mosaic used in this study are available at a resolution of 1/8th of a degree for an extent of 25°N to 53°N latitude and 125° W to 67° W Longitude.

The Mosaic Land Surface Model (LSM) developed by Koster and Suarez (1994) and implemented by Koster and Suarez (1996) as a tile approach to account the sub-grid vegetation variability. Each vegetation tile carries its own energy, water balance, soil moisture, and temperature. Each tile has three soil layers, first two of which are in the root zone. Noah model (Xia et al., 2012) was developed as the land component of the NOAA- National Centers for Environmental Prediction (NCEP) mesoscale Eta model (Betts et al. (1997); Chen et al. (1997); Ek et al. (2003)) and serves as the land component in the evolving Weather Research and Forecasting (WRF) regional atmospheric model, the Climate Forecast System (CFS), and the Global Forecast System (GFS). The model simulates the soil freeze-thaw process and its impact on soil heating/cooling and transpiration, following (Koren et al., 1999). Unlike Mosaic model, Noah has four soil layers, first three of which form the root zone in non-forested regions, and the fourth layer is included in forested regions (Mitchell et al., 2004a).

3.3. Drought Indices (DIs)

Eight drought indices namely Palmer Drought Severity Index (PDSI), Palmer Hydrological Drought Index (PHDI), Palmer Z Index (ZNDX), Standardized Precipitation Index (SPI) for 1, 6, 9, 12 and 24 months are chosen for analysis in this study. The indices have been selected to facilitate a representation of a diverse set of drought scenarios. While indices like PHDI, PDSI, SPI-12, and SPI-24 relate to long-term droughts, ZNDX, SPI-1 and SPI-6 indicate relatively short-term drought predictability. While PDSI accounts for drought-inducing circulation patterns, PHDI is used to quantify hydrological effects of drought. PDSI, PHDI, and ZNDX are water balance indices

(consider water supply, demand and loss through precipitation, evapotranspiration and runoff respectively), the Standardized Precipitation Index (SPI) is a probability index and relates to precipitation only. Monthly Palmer Drought Indices (PDSI, PHDI, and ZNDX) and SPI are obtained from the NOAA's National Climatic Data Center (NCDC–NOAA) repository for 344 climatic divisions in CONUS. For a given month, each point in a climatic division is assumed to have the same value for a drought index. Detailed information on the difference between these drought indices can be obtained from Mishra and Singh (2010).

Description of the layer thickness for Noah and Mosaic; and sensor location for the *in-situ* observations at USCRN sites is provided in Table 2-1. As the observed USCRN soil moisture is available for only up to first 100 cm of depth, the dataset for this study uses simulated soil moisture for three soil layers i.e. 0-10 cm, 10- 40 cm and 40- 100 cm. Since the soil layers for USCRN data are different from those of Noah and Mosaic, a linear interpolation has been applied to obtain values at a depth of 5cm, 25 and 75 cm for an accurate layer to layer comparison. Soil moisture data from Noah, Mosaic and USCRN is converted to monthly time step for compatibility with the drought indices.

Table 2-1: Description of layer thickness for Noah and Mosaic land surface models; and sensor location for *in-situ* observations at US Climate Reference Network (USCRN) stations

Model/Source	Layer / sensor depth description for Noah, Mosaic and USCRN data					
	Soil column thickness available in model (in cm)					
Noah	0-10	10-40	0-40	40-200	0-100	0-200
Mosaic	0-10	10-40	40-100	0-100	0-200	100-200
	Sensor depth from surface (in cm)					
USCRN	5	10	20	50	100	
	Layer thickness / interpolated sensor depth used in the study					
Noah/ Mosaic	0-10	10-40	40-100			
Interpolated USCRN	5	25	75			

Temporal length of the USCRN data varies from station to station based on installation, time for quality control and testing and operation of the soil moisture sensors. Broadly, the dataset from USCRN stations starts from Jan 2009 and goes up to August 2015. Equivalent lengths of the datasets from Noah, Mosaic have been obtained from their respective grids for model development and validation. For correlation and persistence analysis, and drought reconstruction, the data from Noah and Mosaic models for all three soil layers i.e. 0-10 cm, 10- 40 cm and 40- 100 cm, and, the drought indices, are obtained for a period of Jan 1979 through Aug 2015.

4. Brief overview of the mathematical techniques

4.1.Discrete Wavelet Transform (DWT):

Natural processes are non-stationary and work at different spatial- temporal scales. The wavelet transform is a tool to obtain convolution of a signal or a time series against a particular instance of a wavelet corresponding to various time scales and positions. It breaks up a time series into shifted and scaled versions of wavelets, which are waveforms of effectively limited duration and zero mean, along the full signal in such a way that higher frequency wavelets will be very narrow and lower frequency wavelets will be wide. At each step, a generated wavelet coefficient measures the correlation of the wavelet to the signal in each section. This capability of the wavelet transform to focus on short time intervals for gross features and long intervals for local features makes it well suited for approximating data with sharp changes and discontinuities (Sahay and Sehgal, 2014).

Discrete wavelet transform (DWT) enables to achieve the time-frequency localization and multi-scale resolution of a signal by focusing and zooming around the neighborhood of one's choice (Mallat, 1999) for discrete time series, and a time series is decomposed into Approximation (A) and Detail (D1, D2, D3, etc.) sub-time series or Discrete Wavelet Components (DWCs)

following a number of successive filtering steps . The Approximation components represent the coarse features of a time series which are obtained by correlating stretched version (low-frequency and high-scale) of a wavelet $\psi(n)$ with the original time series. The detail components signify rapidly changing features of time series and are obtained by correlating compressed wavelet (high-frequency and low-scale) with the original time series.

For a discrete time series x_i, DWT is defined as

$$A_{m,n} = 2^{-m/2} \sum_{i=0}^{N-1} x_i \psi(2^{-m} i - n) \quad (1)$$

Where $A_{m,n}$ is the wavelet coefficient for the discrete wavelet of scale $a=2^m$, $b=2^m n$, m and n are positive integer variable and N is the data length which is equal to $2M$. This gives the ranges of m and n as $0 < n < 2^{M-m} - 1$ and $1 < m < M$, respectively.

The original time series may be constructed using the Inverse Discrete Wavelet Transform as

$$x_i = A + \sum_{m=1}^{M} \sum_{n=0}^{2^{M-m}-1} A_{m,n} 2^{-m/2} \psi(2^{-m} i - n) \quad (2)$$

$x_i = \overline{T} + \sum_{m=1}^{M} \sum_{n=0}^{2^{M-m}-1} T_{m,n} 2^{-m/2} \varphi(2^{-m} i - n)$ Or, in simple terms,

$$x_i = \overline{T}(t) + \sum_{m=1}^{M} W_m(t) \quad (3)$$

Where $A(t)$ is called approximation sub-time series at level M and $D_m(t)$ are details sub-time series at levels $m = 1,2, \ldots M$

Non-stationarity in the data such as trends and seasonal variations significantly affect modeling of soil moisture and hence may causes poor predictability in practical applications. Wavelet transforms, by analyzing the time series data in both time and frequency domains, give

considerable information about the physical structure of the data which is useful to analyze time series that contain nonstationary power at many different frequencies (Daubechies, 1990). In the recent past, wavelet analysis has emerged as an attractive technique to deal with non-stationarity and multiscale processes. Wavelets have been applied in areas of hydrological modeling and time-frequency characterization of natural processes (Smith et al. (1998); Chou and Wang (2002); Wang and Ding (2003); Dai et al. (2003)). Extensive literature is available on wavelet-based models for a diverse set of problems in hydrological modeling like monsoonal flood forecasting (Sehgal et al., 2014c), drought forecasting (Kim and Valdés, 2003), streamflow (Adamowski, 2008; Coulibaly and Burn, 2004; Maheswaran and Khosa, 2012b; Nanda et al., 2016), precipitation (Kim, 2004; Lu, 2002; Partal and Kişi, 2007), climatic downscaling (Sehgal et al., 2016), hydrologic regionalization (Agarwal et al., 2016a; Agarwal et al., 2016b), understanding multi-scale nature of climatic extremes (Agarwal et al.; Rathinasamy et al., 2017), and understanding the coherence between different hydro-climatic variables at multiple time-frequency resolutions like soil moisture (Lakshmi et al., 2004; Tang and Piechota, 2009), El Nino and Southern Oscillation (Torrence and Webster, 1998; Torrence and Webster, 1999) etc.

4.2. Bayesian Model Averaging (BMA)

Selection of an appropriate wavelet function poses significant challenges and is governed largely by the problem at hand and some of the distinctive properties of the wavelet function such as its region of support, and the number of vanishing moments (Maheswaran and Khosa, 2012a). Some other recent studies have also highlighted the effect of vanishing moment of the mother wavelet on the accuracy of a wavelet-based time series model (Sehgal et al., 2014a). The region of support relates to the length span of a wavelet thus effecting its feature localization capability, whereas, the vanishing moments, determine the ability of a wavelet to suitably represent the

polynomial behavior of a time series. Thus, it is safe to assume that the performance of a wavelet-based multi- resolution model with a given mother wavelet function is highly dependent on the data, and, is location specific.

The best performing wavelet-based model at a given location may not perform satisfactorily at another location due to the choice of a given mother wavelet. Also, each mother wavelet captures a physical process at different time – frequency resolution. This study deals with a large geographic area (CONUS) with several climate regions having peculiar regional/ local features. Hence, it is incorrect to assume that a single wavelet will be able to capture the physical processes with a satisfactory degree of accuracy for the chosen highest level of decomposition in the study. Mostly, a *single best model* approach is applied in statistical modeling where a single model is chosen from a set of available and viable models based on various performance indices to assess agreement or disagreement of the modeled with the observed dataset. However, there is a possibility that a model which is able to capture some unique features of the processes of interest better than other models is being discarded as the said model may not perform best overall. Additionally, there may be uncertainties associated with estimated parameters for each model. The single best model ignores this aspect and leads to an overconfident estimation of the modeled variable (Fragoso and Neto, 2015; Hoeting et al., 1999).

BMA is a statistical approach for post-processing ensemble estimates from multiple competing models (Leamer, 1978). BMA helps in reducing this overconfidence and uncertainty related to a given model by conditioning on a given set of models. BMA has also been widely used in hydrologic and climatic modeling by providing a multi-model ensemble of for hydrologic predictions and forecasts (Duan et al. (2007), Ajami et al. (2007), Raftery et al. (2005), effective soil moisture estimation (Kim et al., 2015), drought forecasting (Madadgar and Moradkhani,

2013), groundwater modeling (Rojas et al., 2008), addressing model uncertainty (Parrish et al., 2012). Rathinasamy et al. (2013) proposed a multi- model ensemble using different wavelets for multi-scale streamflow forecasting. Vrugt and Robinson (2007) proposed a multi-criteria formulation for post-processing of forecast ensembles and applied on surface temperature and sea level pressure dataset. These studies report that a multi-model combination approach using BMA provides better results than those obtained using the individual models and helps in countering uncertainty associated with parameter estimation of a single model.

This study applies BMA on the top ten best performing wavelet-based regression models (WR) developed in this study in order to generate a combination soil moisture from Noah and Mosaic for each layer. This method assumes that the probability of the observed soil moisture $SM_{obs}(t)$ at time *t* is given by a weighted sum over the probability distributions $g\left(WR^{f}(k,t)\right)$ from the *k* different WR models

$$P\left(SM_{obs}(t)\right) = \sum_{k} w(k)\, g\left(WR^{f}(k,t)\right) \tag{4}$$

The choice of a probability distribution for each individual WR model is assumed to be a normal distribution following similar assumption from some recent studies (Kim et al., 2015; Rathinasamy et al., 2013; Vrugt and Robinson, 2007) with variance $\sigma(k)$

$$g\left(WR^{f}(k,t)|\, SM_{obs}(t), \sigma(k)\right) = \left(1/\sigma(k)\sqrt{2\pi}\right) e^{\left(-\frac{\left(SM_{obs}(t)-WR(k,t)\right)^{2}}{2\sigma(k)^{2}}\right)} \tag{5}$$

For a given set of historic observed and simulated soil moisture using the WR Models, the BMA algorithm is used to obtain the optimal values for $w(k)$ and $\sigma(k)$, such that the likelihood of the overall PDF (Eq. 2) is maximal using an iterative process by consecutively optimizing $w(k)$ and $\sigma(k)$. The iteration is initialized with an estimate for the weights $w(k)$ and $\sigma(k)$ for each

individual model and estimates of matrix $z(k,t)$ using Eq. (3). $z(k,t)$ gives the probability that model *k* is the best estimate for the soil moisture at time *t*

$$z(k,t) = g\big(SM_{obs}(t)|\, WR(k,t), \sigma(k)\big) / \sum_k g\left(SM_{obs}(t)|\, WR_f(k,t), \sigma^2(k)\right) \quad (6)$$

In the second step, an iterative algorithm estimates the weights $w(k)$ and variances $\sigma(k)$ of each of the model's *k* based on the values of $z(k,s,t)$. . The weights are estimated as;

$$w(k) = \frac{1}{n}\sum_t z(k,t) \quad (7)$$

where *n* is the number of observations in the training period *(t)*. The variance $\sigma(k)$ is estimated using

$$\sigma^2(k) = \left(\sum_t z(t)\left(SM_{obs}(t) - WR_f(k,t)\right)^2\right) / \sum_t z(k,t) \quad (8)$$

The last two steps are alternated in this process in order to achieve a desired degree of convergence using Expectation-Maximization (EM) algorithm proposed by (Raftery et al., 2005). For detailed information on the Bayesian Model Algorithm applied in this study, the readers are referred to Fernandez et al. (2001a) and Fernandez et al. (2001b).

5. Development of multi- resolution regression based Bayesian Model Averaging (WBR) models

In order to address the need of an accurate *in-situ* soil moisture dataset at high spatial resolution, and to counter the uncertainty and bias in the soil moisture available from the two LSMs namely, Noah and Mosaic (obtained from NLDAS-v2) for this analysis , a statistical transformation of volumetric soil moisture provided by the two LSMs is carried out to obtain a

Hybrid Soil Moisture (HSM) for the Conterminous United States (CONUS) for three soil layers i.e. 1-10 cm, 10-40 cm and 40-100 cm at a spatial resolution of 1/8th degree.

5.1. Wavelet based multi- resolution regression models (WR models)

The observed soil moisture dataset is obtained from the selected 48 control stations. The *in-situ* and simulated soil moisture dataset obtained from all control stations for USCRN, Noah and Mosaic is appended station-wise in order to obtain a single time series for each source. These time series are used as inputs to the statistical models.

The input time series are first standardized prior to the model development to reduce systematic biases in the mean and variance values of Noah/ Mosaic dataset. A multi-resolution modeling approach is employed in this study where each wavelet sub- time series of the input data is modeled separately using regression-based framework for respective sub- time series of the *in-situ* soil moisture dataset. Each model provides the respective sub-time series of the HSM which is later added to provide the HSM in original time – frequency domain. This modeling approach is called as the Wavelet-based multi- resolution regression (WR) in this study. Selection of suitable level of decomposition is important in a multi-resolution modeling. A schematic of the framework for the WR models in provided in Figure. 2-3.

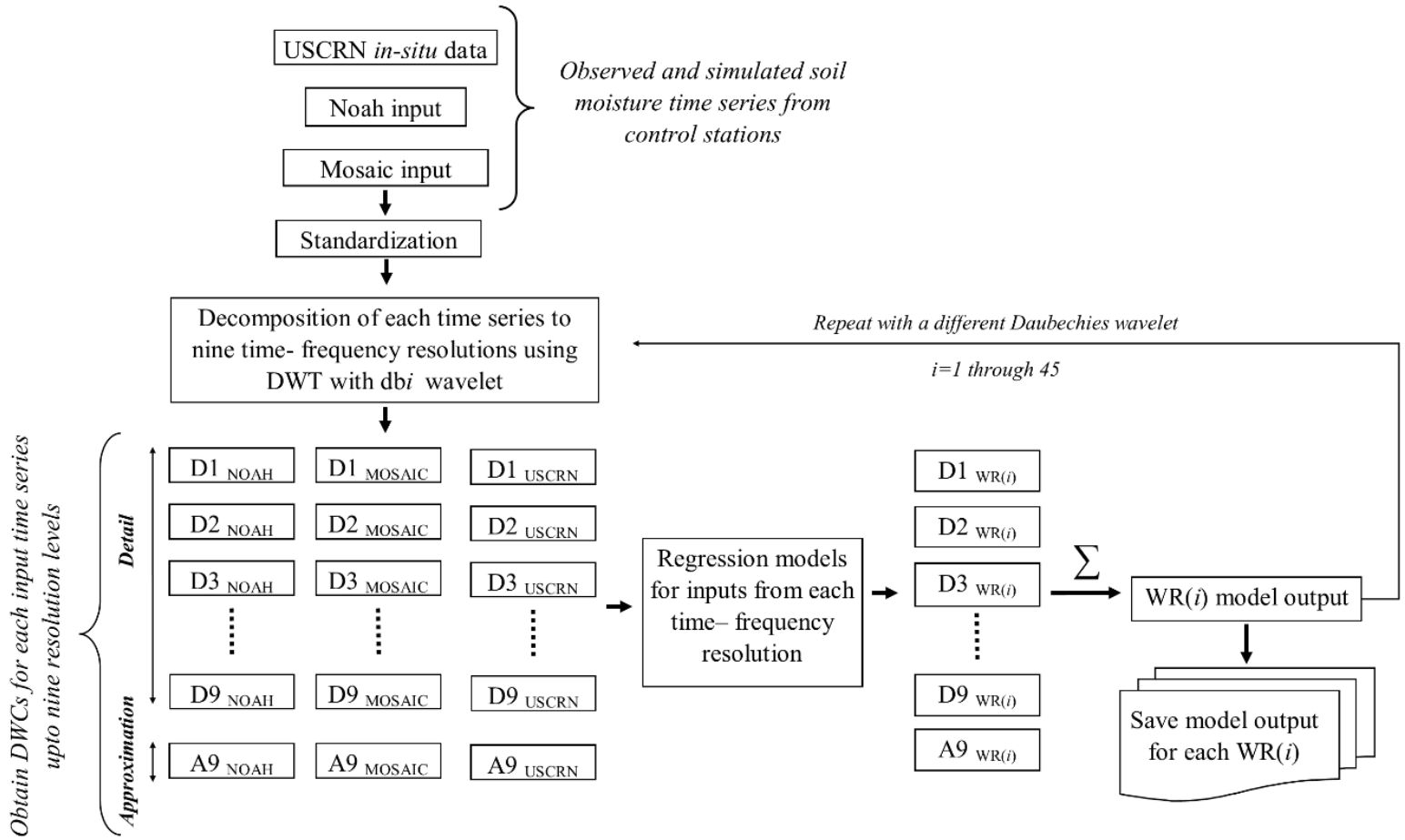

Figure. 2-3: Flowchart for the wavelet-based multi- resolution regression (WR) models. Forty-five WR models are developed corresponding to each *db* wavelet with vanishing moments from 1 to 45 individually for each layer.

5.2. Selection of suitable level of decomposition of input dataset for WR models

Selection of resolution of time series decomposition using DWT is conducted by observing the wavelet spectrum of the observed soil moisture time series. Figure. 2-4 provides the wavelet spectrum of the observed soil moisture using Morlet wavelet. It can be observed that there are significant occurrences around the 9th level of decomposition (256- 512 months) for all three layers. This can be attributed to the effect of El Niño Southern Oscillation (ENSO) and Pacific Decadal Oscillation (PDO) which are two important oceanic-atmospheric indices having a strong influence on the climate variability in large parts of the US (Barnett et al., 1999; Beebee and Manga, 2004). It can be observed from Figure. 2-4 that apart from a consistent annual variability, the soil moisture for all three layers consistently displays a decadal variability pertaining to a 256 to 512-month period. Hence, the dataset from the three sources is decomposed up to nine time-frequency resolutions and modeled separately to obtain the estimated DWC of the HSM at the respective time- frequency resolution.

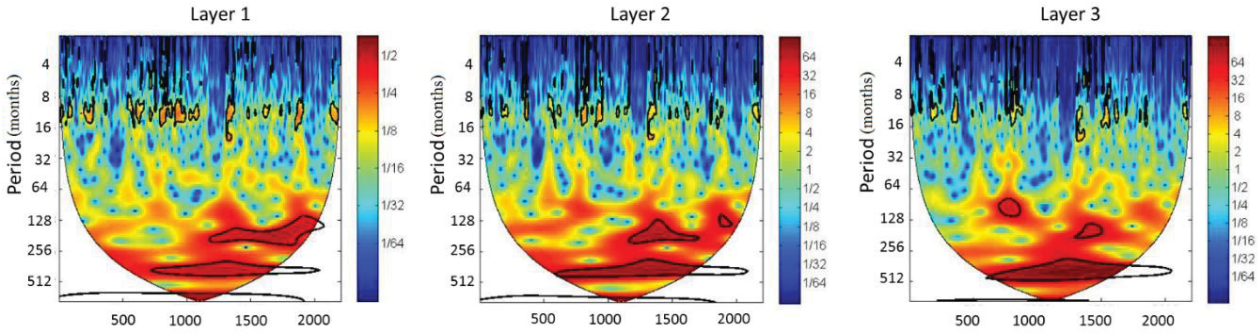

Figure. 2-4: Wavelet spectrums of the observed *in- situ* soil moisture time series from the control stations for training dataset using Morlet wavelet. The thick black contour delineates the 5% significance level against the red noise. Red and blue colours represent stronger and weaker power respectively. It can be observed that the period around 256- 512 is significant for all three layers.

5.3. Selection of wavelets for WR models

Maheswaran and Khosa (2012a) and Sehgal et al. (2014a) showed that wavelets with high support width and higher vanishing moments are better suited to capture the dynamics of a time series at multiple time-frequency resolutions. "*daubechies*" (*db*) wavelets are used in this study which provide a high number of vanishing moments for a given support width (Sehgal et al., 2014b). A WR(*i*) is developed using *db(i)* wavelet for obtaining the DWCs of the input dataset for the models where *i* represent the vanishing moment of the employed mother wavelet for the WR model and ranges from 1 through 45.

5.4. Bayesian Model Averaging of Wavelet based multi- resolution regression Models (WBR models)

BMA is applied to obtain an overall probability distribution function (PDF) of the volumetric soil moisture by taking a weighted average of outputs from top ten individual WR models using standardized Noah and Mosaic soil moisture inputs, each employing a different wavelet as mother functions. Figure. 2-5 provides a schematic of the proposed modeling framework applied in this study. Top ten WR models are selected based on the model's correlation with the observed dataset. These models are then fed into the BMA framework to obtain weights for each WR model which are then used to obtain an ensemble of the top ten WR model by weighted averaging, providing the WBR_{Hybrid} output. The best performing wavelets obtained regression coefficients corresponding to each model run and the respective model weights are recorded in the form of a "*Transformation matrix*" for each layer as this matrix provide all necessary information to obtain the HSM from Noah and Mosaic dataset for each grid cell.

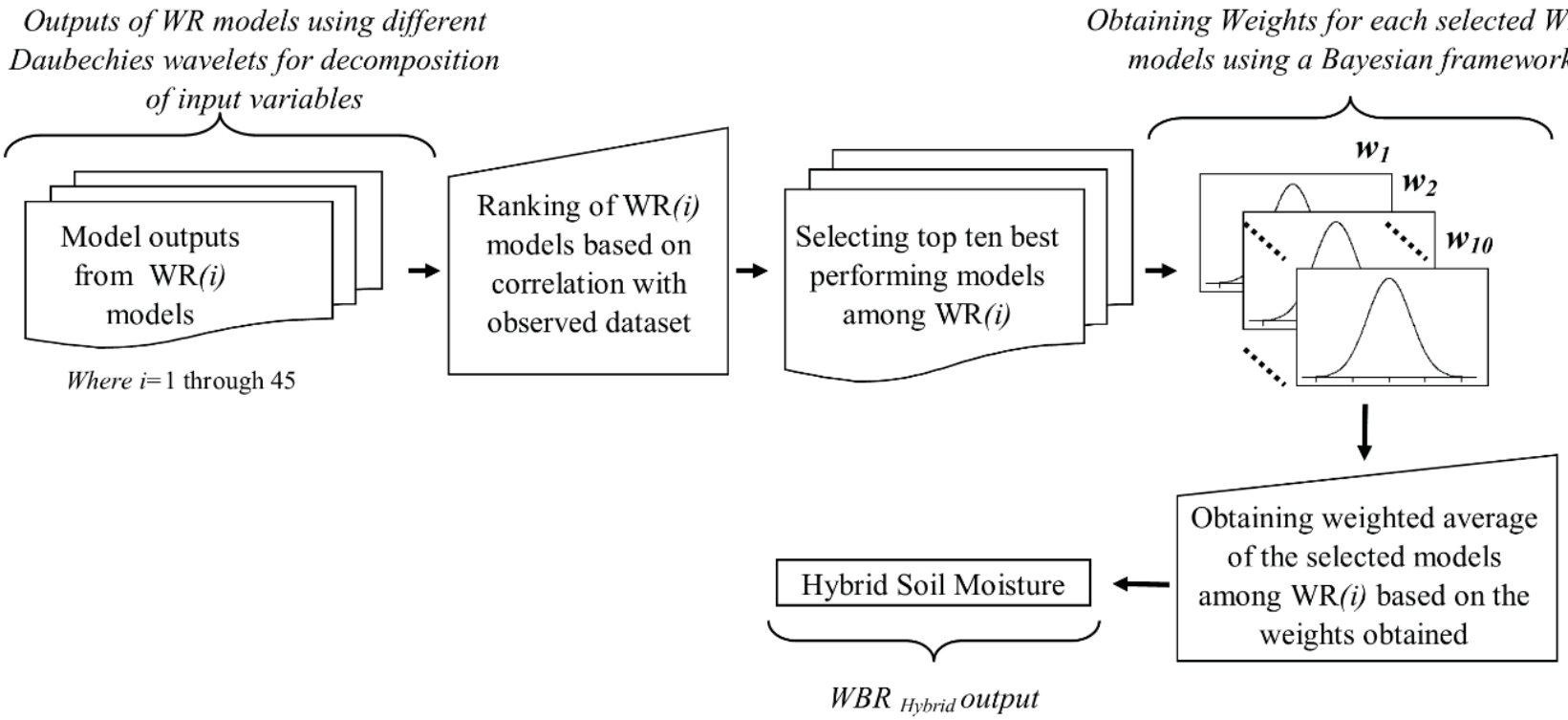

Figure. 2-5: Flowchart for the Bayesian Model Averaging (BMA) of top performing wavelet-based multi- resolution regression (WR) models to obtain Hybrid Soil Moisture. This process is carried out individually for each layer.

6. Results

6.1. Comparison of Noah and Mosaic simulations with observed soil moisture dataset

It is important to analyze the discrepancies in the model simulated soil moisture using Noah and Mosaic compared to the observed *in- situ* soil moisture to establish the necessity of the proposed ensemble approach. An analysis is carried out to understand the problem of over/ underestimation of soil moisture for each control station for the three soil layers. If the estimation of soil moisture using the LSMs is between $\pm 10\%$ of the observed data value, the estimation is termed as satisfactory otherwise the soil moisture is either over/ under predicted. Figure. 2-6 provides the percentage of data points for each control station being over (O)/ satisfactorily (S)/ or under (U) – predicted. It can be observed that for most of the stations, both Noah and Mosaic over-estimated the soil moisture. Overall, the overestimation is observed to increase with layer depth.

A conservative estimate of 10% accuracy band for soil moisture estimation is based on the difference in the maximum and reference volumetric soil moisture for most soil types as shown in Table 2-2. The difference between the maximum and reference volumetric soil moisture is less than 10% for most of the soil types. Only Loamy Sand (32%), Sandy Loam (12%), Silt (44%) and Loam soil (11%) types have higher than 10% difference between the field capacity and maximum soil moisture content (volumetric). Hence, a choice of 10% accuracy bracket represents a significant difference in the estimated and observed soil moisture values for most soil types.

Table 2-2: Maximum soil moisture content (MAX SMC), Reference soil moisture (REF SMC), and Wilting point soil moisture content (WLT SMC) and the difference between maximum and reference volumetric soil moisture (MAX-REF) for different soil types (Chen, 2007).

Soil type	MAX SMC	REF SMC	WLT SMC	MAX-REF
Sand	0.34	0.24	0.01	0.10
Loamy Sand	0.42	0.08	0.03	0.34
Sandy Loam	0.43	0.31	0.05	0.12
Silt	0.48	0.04	0.08	0.44
Loam	0.44	0.33	0.07	0.11
Sandy clay loam	0.40	0.31	0.07	0.09
Silty clay loam	0.46	0.39	0.12	0.08
Clay loam	0.47	0.38	0.10	0.08
Sandy clay	0.41	0.34	0.10	0.07
Silty clay	0.47	0.40	0.13	0.06
Clay	0.47	0.41	0.14	0.06
Organic materials	0.44	0.33	0.07	0.11

6.2. Performance evaluation of developed models

6.2.1. Statistical indices for performance evaluation

To evaluate the performance of developed models, the dataset for each control station is divided into a fraction of 3:1 where first three-quarters are used as a training dataset and the later quarter of the data for each control station is used in the validation process. In total, the training dataset consisted of 2204 data points whereas the validation dataset consisted of 727 values. To assess performance of the developed models, following error metrics are evaluated in this study:

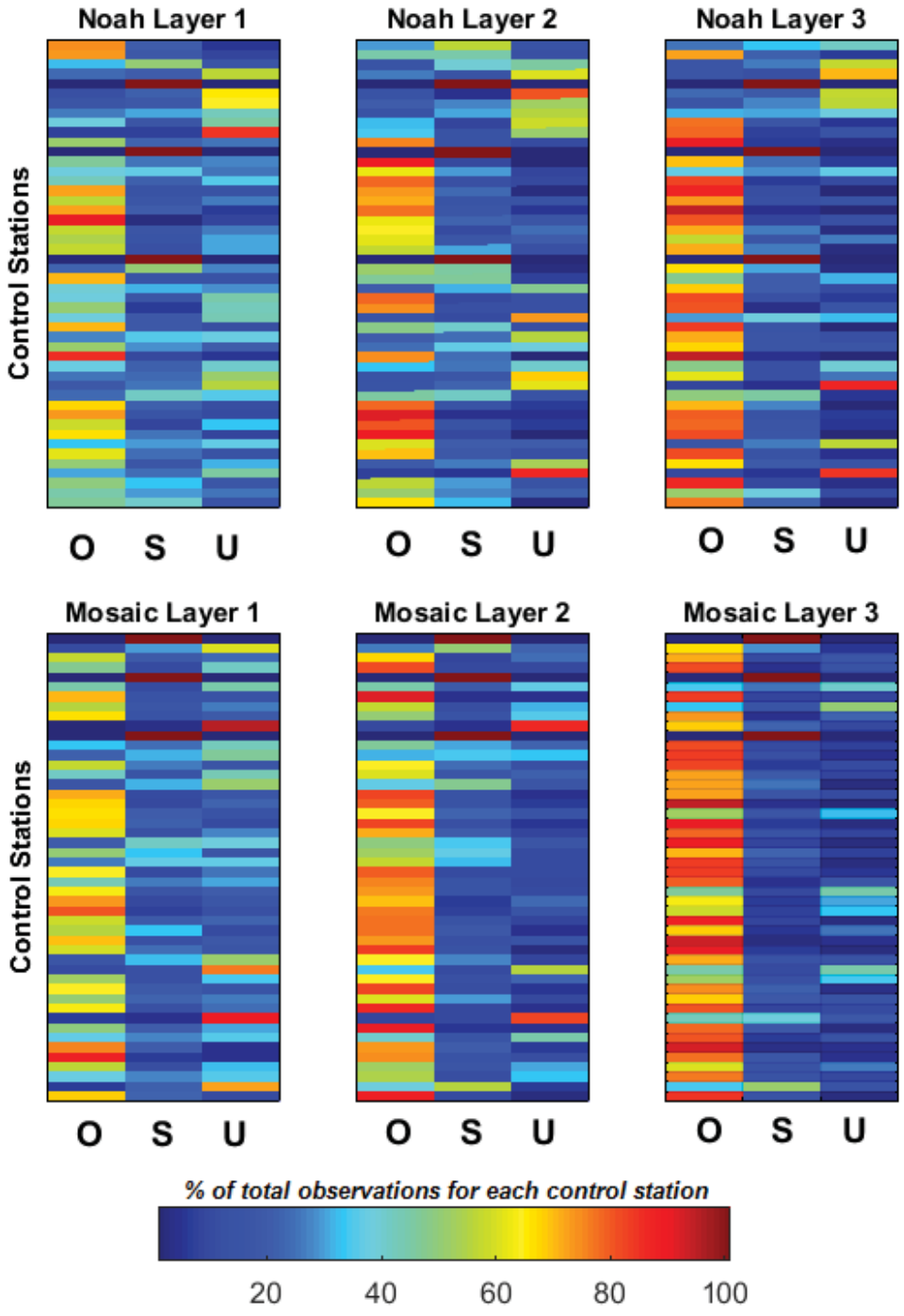

Figure. 2-6: Percentage of *in- situ* observations being over (O)/ satisfactorily(S) / under (U) estimated for each control station by Noah and Mosaic LSMs.

(i) ***Normalized Root Mean Square Error (NRMSE)*** is Root Mean Square Error (RMSE) normalized to a scale [0, 1].

RMSE is expressed as:

$$RMSE = \sqrt{\frac{1}{n}\sum_{i=1}^{n}(O_i - P_i)^2} \quad (9)$$

Where O_i and Pi are the observed and estimated SM time series and n is the number of data points in the series. To facilitate easy comparison of model performances across stations and models, NRMSE is adopted in this study which is expressed as:

NRMSE= RMSE/ Range

Where, Range is the difference between the maximum and the minimum value of the observed dataset.

(ii) ***Nash–Sutcliffe coefficient (E)***. It is expressed as:

$$E = 1 - \frac{\sum_{i=1}^{n}(Oi - Pi)^2}{\sum_{i=1}^{n}(Oi - \overline{Oi})^2} \quad (10)$$

Where $\overline{Oi}$ is the mean of the observed soil moisture.

(iii) ***Correlation coefficient (CC)*** is defined as:

$$CC = \left(\frac{\sum_{i=1}^{n}\left(\mathrm{Oi} - \bar{O}\right)\left(\mathrm{Pi} - \bar{P}\right)}{\sqrt{\sum_{i=1}^{n}\left(\mathrm{Oi} - \bar{O}\right)^2}\sqrt{\sum_{i=1}^{n}\left(\mathrm{Pi} - \bar{P}\right)^2}} \right) \quad (11)$$

Where $\overline{Pi}$ is the mean of the estimated soil moisture.

6.2.2. Performance evaluation

Results of performance analysis for the total dataset (training + validation) is summarized in Table 2-3 (a, b and c) for layer 1, 2 and 3 respectively. In these tables, the performance of the

top 10 WR models is tabulated along with WBR_{Hybrid} models for comparison. These tables also provide the model weights applied to the respective model output. The value in the parenthesis of the WR models provides the vanishing moment of the *db* wavelet selected as mother wavelet for the WR model. For example, *WR(7)* signifies the WR model with *db7* as the mother wavelet function. Figure. 2-7 provides the scatterplots of the observed dataset and HSM for the validation and total dataset. It can be observed from Figure. 2-7 that no systematic over- or under- estimation in the model outputs.

Table 2-4 provides the information about the performance of WBR_{Hybrid} models for each layer for training and validation dataset. For comparison, the performance of the best performing WR models for the respective layer is also included in Table 2-4. For validation data, the HSM (WBR_{Hybrid} output) provides a correlation of 0.78, 0.75 and 0.73 for layer 1, 2 and 3 respectively. The values of E for the three layers for the validation dataset are 0.6, 0.57 and 0.53 whereas NRMSE is found to be 0.15, 0.159, 0.154 for layer 1, 2 and 3 respectively. Respective values for the performance indices for the WR model outputs fall short of the WBR model outputs in performance for both training and validation dataset. The values for correlation, E and NRMSE for layer 1, 2 and 3 for the WR model outputs for validation dataset are 0.78, 0.70 and 0.71; 0.59, 0.48 and 0.50; 0.152, 0.174 and 0.160 respectively.

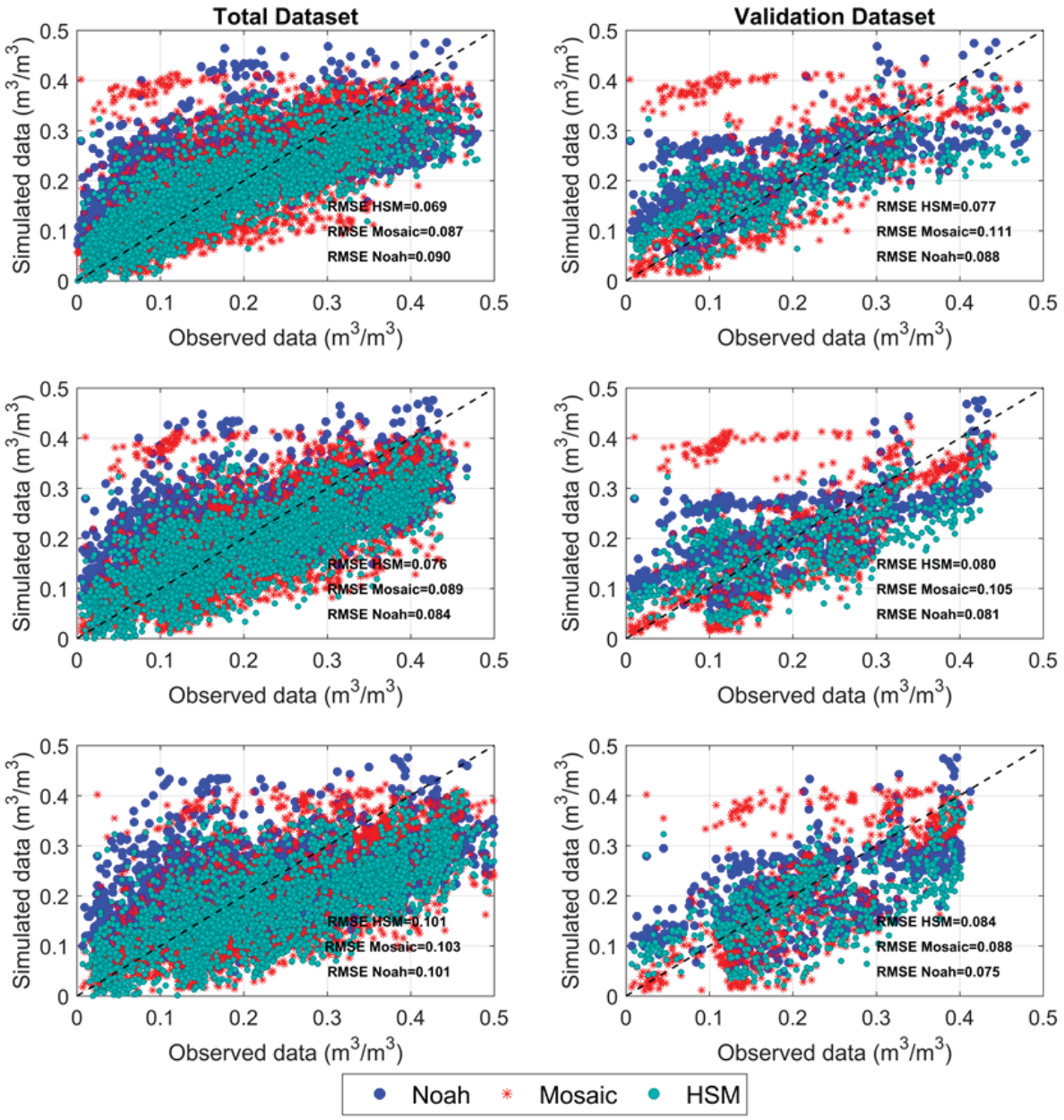

Figure. 2-7: Scatter plots with respective Root Mean Square Error (RMSE) of observed soil moisture v/s Hybrid Soil Moisture, Noah and Mosaic models for all three layers for (a) Validation dataset (b) Total dataset

Table 2-3: Model performance of WBR models with the best performing WR models for the total dataset for (a) Layer 1 (b) Layer 2 (c) Layer 3

(a) Model performance for total data- Layer 1				
Model	**CC**	**E**	**NRMSE**	**Weights**
WR(7)	0.7937	0.6298	0.1423	0.072
WR(3)	0.7930	0.6286	0.1425	0.252
WR(11)	0.7873	0.6192	0.1443	0.024
WR(24)	0.7862	0.6180	0.1446	0.003
WR(33)	0.7854	0.6168	0.1448	0.252
WR(28)	0.7842	0.6148	0.1451	0.048
WR(15)	0.7842	0.6147	0.1452	0.006
WR(20)	0.7840	0.6145	0.1452	0.006
WR(37)	0.7822	0.6118	0.1457	0.087
WR(16)	0.7802	0.6084	0.1464	0.252
WBR_{Hybrid}	0.7924	0.6272	0.1428	

(b) Model performance for total data- Layer 2				
Model	**CC**	**E**	**NRMSE**	**Weights**
WE(3)	0.7596	0.5765	0.1582	0.167
WR(43)	0.7570	0.5728	0.1589	0.167
WR(7)	0.7549	0.5696	0.1594	0.053
WR(33)	0.7548	0.5695	0.1595	0.167
WR(29)	0.7545	0.5692	0.1595	0.060
WR(38)	0.7545	0.5690	0.1596	0.166
WR(42)	0.7538	0.5680	0.1597	0.003
WR(34)	0.7536	0.5677	0.1598	0.004
WR(25)	0.7522	0.5657	0.1602	0.047
WR(37)	0.7521	0.5654	0.1602	0.167
WBR_{Hybrid}	0.7661	0.5855	0.1565	

(c) Model performance for total data-Layer 3				
Model	**CC**	**E**	**NRMSE**	**Weights**
WR(42)	0.7500	0.5616	0.1553	0.415
WR(37)	0.7466	0.5567	0.1562	0.039
WR(33)	0.7455	0.5548	0.1565	0.041
WR(29)	0.7454	0.5551	0.1564	0.011
WR(24)	0.7446	0.5537	0.1567	0.024
WR(41)	0.7445	0.5535	0.1567	0.161
WR(38)	0.7444	0.5531	0.1568	0.022
WR(20)	0.7444	0.5536	0.1567	0.052
WR(28)	0.7436	0.5523	0.1569	0.167
WR(16)	0.7427	0.5507	0.1572	0.070
WBR_{Hybrid}	0.7505	0.5619	0.1552	

Different combinations of inputs and modeling approaches have been explored for their performance in estimating the observed soil moisture for the purpose of comparison with the proposed hybrid model of Noah and Mosaic using Wavelet regression and BMA (WBR_{Hybrid}). These models are WBR_{Noah}, WBR_{Mosaic}, $WBR_{Average}$, and original Noah and Mosaic dataset. A brief description of these models is provided in Table **2-5**.

Table 2-4: Performance evaluation of the proposed models for the training and validation dataset for WBR_{Hybrid} and best performing Wavelet Regression (WR) models for each layer.

	Layer 1		*Layer 2*		*Layer 3*	
	Training					
	WBR_{Hybrid}	**WR**	**WBR_{Hybrid}**	**WR**	**WBR_{Hybrid}**	**WR**
Correlation	0.80	0.79	0.76	0.74	0.75	0.75
E	0.64	0.64	0.59	0.56	0.57	0.57
NRMSE	0.141	0.142	0.159	0.165	0.157	0.157
	Validation					
	WBR_{Hybrid}	**WR**	**WBR_{Hybrid}**	**WR**	**WBR_{Hybrid}**	**WR**
Correlation	0.78	0.78	0.75	0.70	0.73	0.71
E	0.60	0.59	0.57	0.48	0.53	0.50
NRMSE	0.150	0.152	0.159	0.174	0.154	0.160

Table 2-5: A brief description of the models explored in this study

Model name	**Input variables**	**Modelling methodology**	**Wavelet Regression**	**BMA**
WBR_{Hybrid}	Noah + Mosaic	Noah and Mosaic inputs fed to WR modelling scheme followed by BMA	Yes	Yes
WBR_{Noah}	Noah	Noah inputs fed to WR modelling scheme followed by BMA	Yes	Yes
WBR_{Mosaic}	Mosaic	Mosaic inputs fed to WR modelling scheme followed by BMA	Yes	Yes
$WBR_{Average}$	Noah + Mosaic	Noah and Mosaic fed to two separate WR+ BMA schemes and the outputs are averaged	Yes	Yes
Noah	Noah	Original Noah dataset	No	No
Mosaic	Mosaic	Original Mosaic dataset	No	No

Table 2-6 summarizes the performance of the models developed for comparison with WBR_{Hybrid} approach. It is evident that the hybrid approach of modeling performs better than all other models. Also, it can be observed from Table 2-3, Table 2-4 and Table 2-6 that models perform

comparatively better for layer 1 than layer 2 and 3. This can be noticed by observing that the correlation of soil moisture inputs from Noah and Mosaic decreases from layer 1 to layer 3. As the input variables had less correlation with the observed dataset with increasing depth from the surface, the performance of models falls from layer 1 to layer 3. However, it is noted that for each layer, the HSM has a higher correlation with the observed dataset than that of Noah/ Mosaic and observed data. It can be observed from Table 2-6 that WBR $_{Hybrid}$ models outperform the best performing models for all performance indices for layer 2 and 3. For Layer 1, though WBR $_{Hybrid}$ outputs do not provide the best performance, however, the performance is very close to the best WR outputs.

Table 2-6: Performance of models developed for comparison with WBR $_{Hybrid}$ models for total dataset for all three layers

	Model performance for total data				
	Layer 1				
	Noah	**Mosaic**	**WBR $_{Noah}$**	**WBR $_{Mosaic}$**	**WBR $_{Average}$**
Correlation	0.705	0.685	0.740	0.739	0.770
E	0.361	0.402	0.547	0.546	0.588
NRMSE	0.187	0.181	0.157	0.158	0.150
	Layer 2				
	Noah	**Mosaic**	**WBR $_{Noah}$**	**WBR $_{Mosaic}$**	**WBR $_{Average}$**
Correlation	0.665	0.681	0.708	0.726	0.744
E	0.405	0.430	0.502	0.528	0.550
NRMSE	0.181	0.177	0.165	0.161	0.157
	Layer 3				
	Noah	**Mosaic**	**WBR $_{Noah}$**	**WBR $_{Mosaic}$**	**WBR $_{Average}$**
Correlation	0.559	0.665	0.626	0.696	0.699
E	0.272	0.439	0.391	0.485	0.481
NRMSE	0.222	0.195	0.203	0.186	0.187

Figure. 2-8 provides a comparison of the histograms obtained for the correlation of *in- situ* soil moisture from control stations with HSM, Noah, and Mosaic. It can be seen that while the overall correlation of the three datasets with the observed soil moisture falls with an increase in

the layer depth, HSM consistently provides higher number of stations with a higher correlation than Noah and Mosaic for all three layers. To test whether HSM captures the multi- scale variability of the in- situ dataset, a comparison between the wavelet spectrums of the observed in-situ dataset, HSM, Noah and Mosaic dataset is provided in Figure. 2-9. It is evident from the figure that while the observed dataset has significance towards higher periods (due to decadal variability), Noah and Mosaic datasets are not able to reflect significance in this range. However, HSM effectively captures this variability and displays significance around 128 to 512 months similar to the observed dataset.

6.2.3. Performance evaluation using remotely sensed dataset

The developed HSM is validated further with the remotely sensed dataset available from the Soil Moisture Active and Passive (SMAP) mission. The dataset from SMAP is available only for the top soil layer (~5cm). Due to data availability issues, the validation is carried out for two months (June and July 2015). It can be observed from Figure. 2-10 that the HSM is sensitive able to counter the wet bias of the two LSMs and is relatively more sensitive to dry conditions which make it suitable for drought analysis.

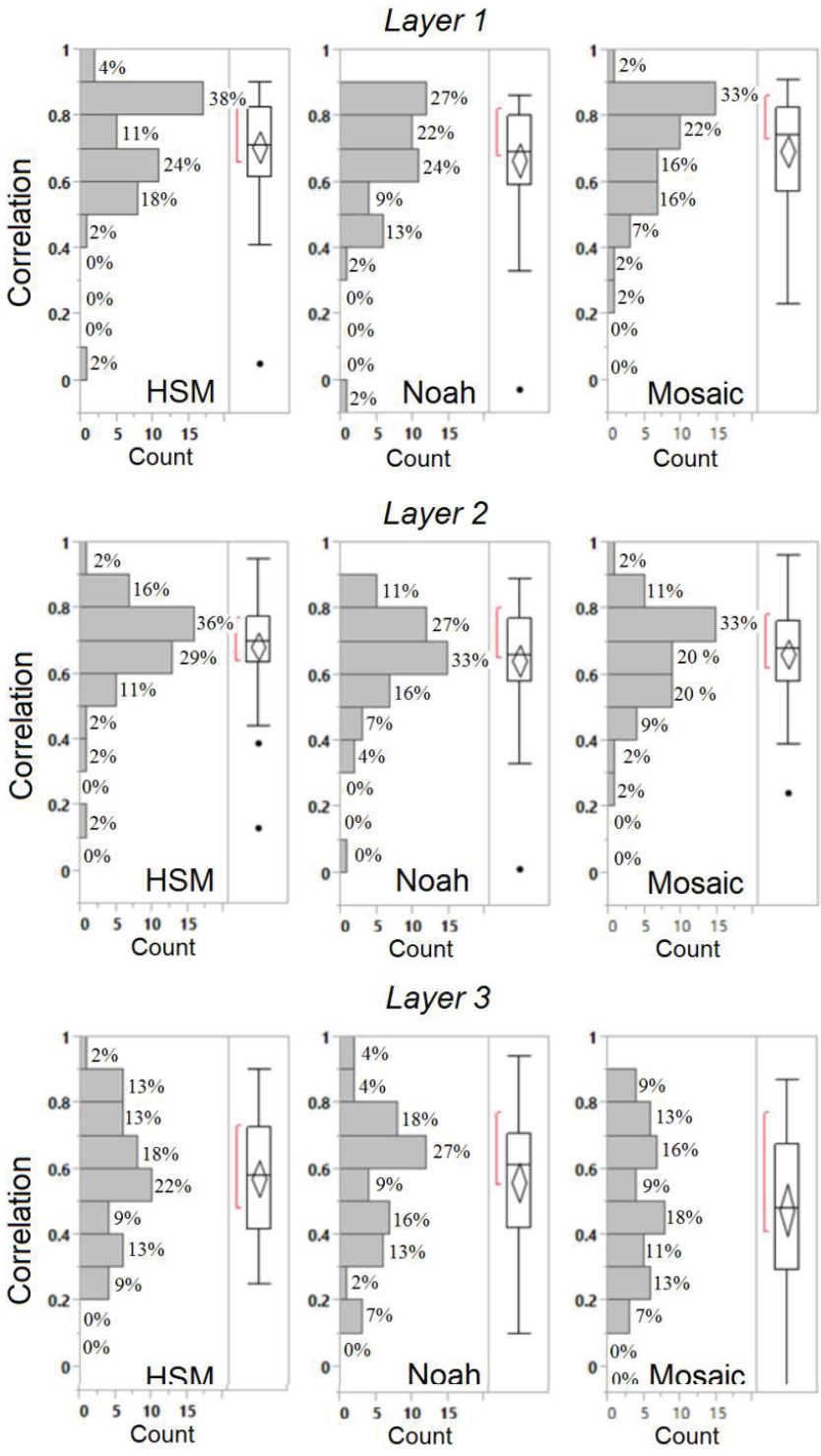

Figure. 2-8: Histograms for correlation of the observed *in- situ* soil moisture from control stations with HSM, Noah and Mosaic for the three layers.

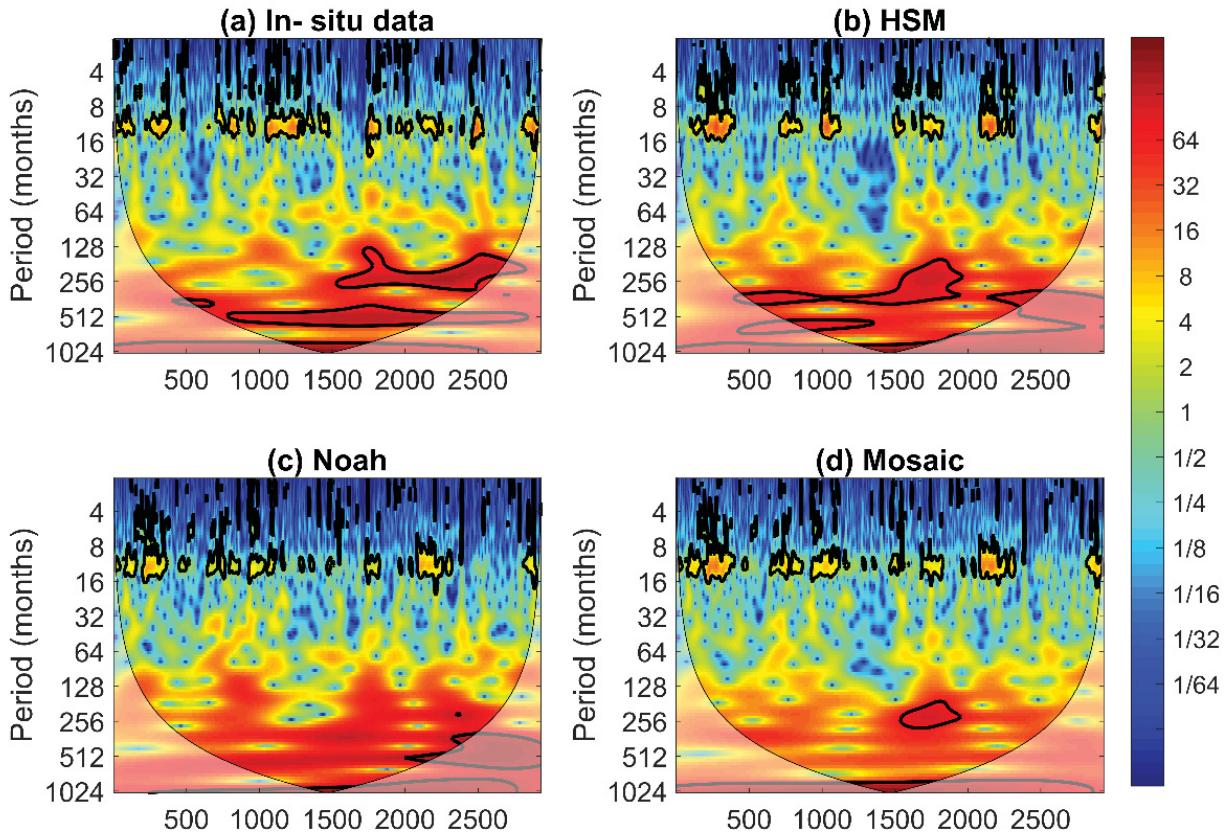

Figure. 2-9: Wavelet spectrums of (a) Observed *in- situ* soil moisture (b) Hybrid Soil Moisture (c) Noah (d) Mosaic time series from the control stations for total dataset for layer 1 using Morlet wavelet. The thick black contour delineates the 5% significance level against the red noise. Red and blue colors represent stronger and weaker power respectively.

7. Drought analysis using HSM

While the knowledge of past climatology is important for obtaining the soil moisture percentiles, the available in-situ dataset for this study is relatively short (<7 years). This may influence the stability of the soil moisture percentiles developed for the purpose of drought reconstruction and/ or the study of persistence of soil moisture for CONUS, and, the correlation between soil moisture and the selected drought indices. Hence, the transformation matrix is applied

to Noah and Mosaic dataset from Jan 1979 to Aug 2015 to obtain a data record of HSM for ~37 years. This dataset is used for further analysis described in this section.

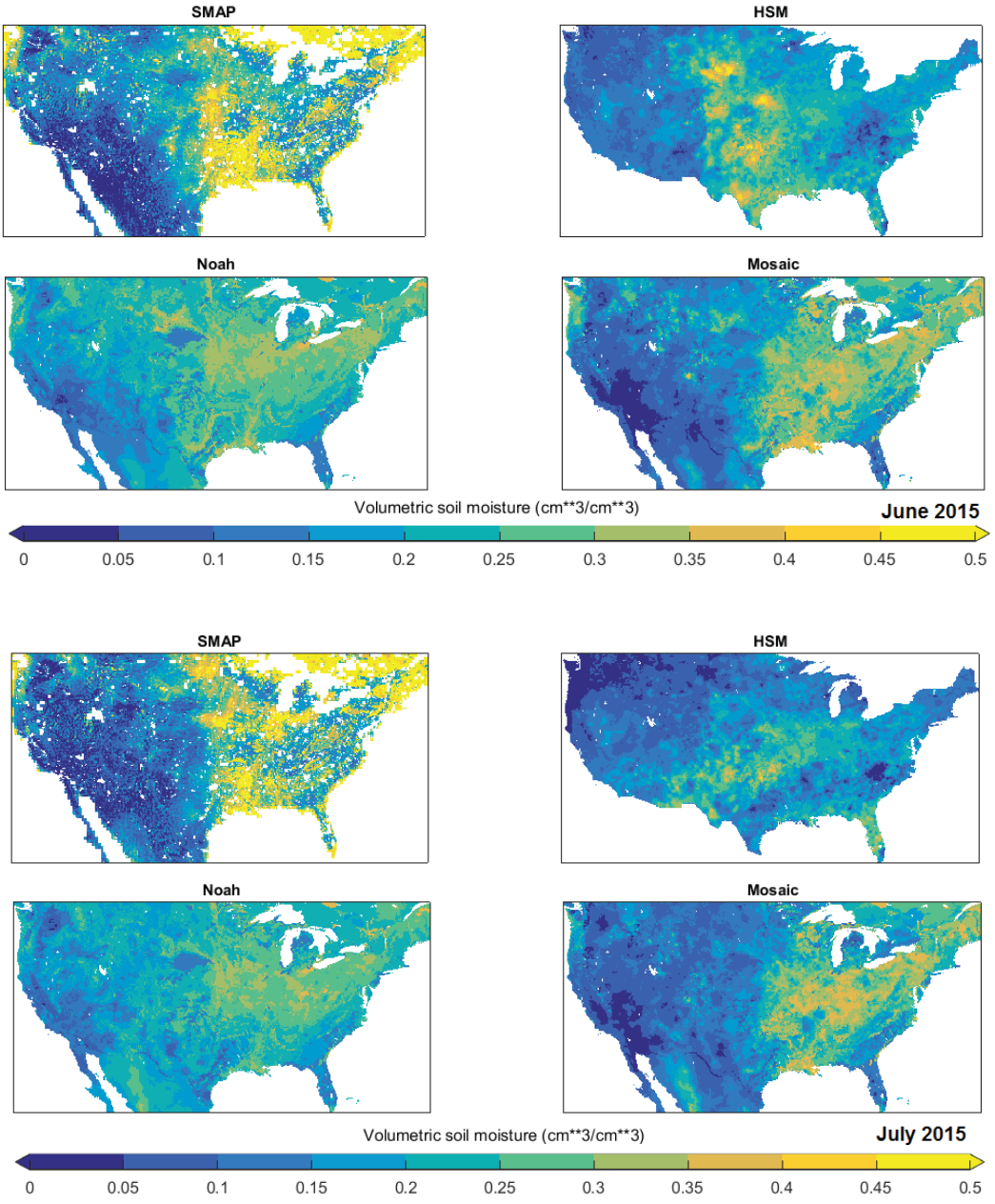

Figure. 2-10: Comparison of op soil layer estimation from SMAP, HSM, Noah and Mosaic for June and July 2015.

7.1.Layer-wise persistence of soil moisture

A layer-wise analysis is conducted to study the persistence of the soil moisture for the CONUS to highlight the variation in the properties of the soil moisture for different soil layers. Persistence is a distinctive characteristic of soil moisture as it exhibits less variability relative to precipitation (Hao and AghaKouchak, 2014). Previously, Mo et al., 2012a illustrated the importance of soil moisture persistence in improving the drought forecasting skills. The persistence of the soil moisture time series is obtained in terms of the response time (T_o) of the HSM for each grid cell. Higher persistence indicates longer memory of the soil moisture, hence delayed response to drought and vice-versa. Response time (T_o) (Delworth and Manabe, 1988; Trenberth, 1984) is defined here as the lag time at which the autocorrelation of the time series of soil moisture has decayed to $1/e$. T_o of a time-series can be calculated from the autocorrelation *R(i)* at lag *i* month for *i*=1 to 30:

$$T_o = 1 + 2\sum_{i=1}^{N}\left(1 - i/N\right)R_i \quad \text{with } N = 30 \tag{12}$$

Figure. 2-11 shows the spatial distribution of T_o obtained from the soil moisture percentiles for the period Jan 2009 to Aug 2015 for CONUS. Further, the response time for each soil layer is averaged for the nine climate regions (as specified by Karl and Koss (1984) and shown in Figure 2-1(b)) of the US and is shown in Figure. 2-12.

It can be observed that the spatial patterns of T_o changes drastically with increasing the layer depth. For Layer 1, the value of T_o over the region that covers Texas, New Mexico, Oklahoma, Kansas, North and South Dakota with some regions of Georgia and South Carolina is observed to be around 7- 9 months compared to Pennsylvania, New York, and Michigan in the East and Washington, Oregon, Idaho and some parts of California which show a higher T_o of about 13- 15

months. For Layer 2, the value for T_o decreases for major parts of Oklahoma, New Mexico, and Texas whereas for the east and northeastern states it increases to 19- 24 months. For Layer 3, the spatial variations in the T_o values show reductions due to overall alleviation in the T_o values across the CONUS with some regions like Oklahoma, and some parts of Texas, North Carolina, and South Carolina showing low T_o values. Overall, it can be observed from Figure. 2-11 and Figure. 2-12 that the T_o for the southern part of the CONUS has lowest response time compared to other regions. This is in accordance with the work of Wang et al. (2009) and Mo (2008) who reported higher persistence of soil moisture across the U.S. Karl (1983) attributed the abnormally wet or dry weather in the Rocky Mountain (around Colorado, Idaho, Montana) and the High Plains states (around Nebraska, Kansas and South Dakota) for higher persistence in soil moisture than the states farther east or west. Wang et al. (2006) highlighted that factors pertaining to soil depth and soil characteristics like porosity, texture, vegetation of a soil are significantly related to the response time of a soil. Hence, it is evident that there is a great degree of variation in the soil moisture behavior across layers with respect to their persistence defined in terms of T_o.

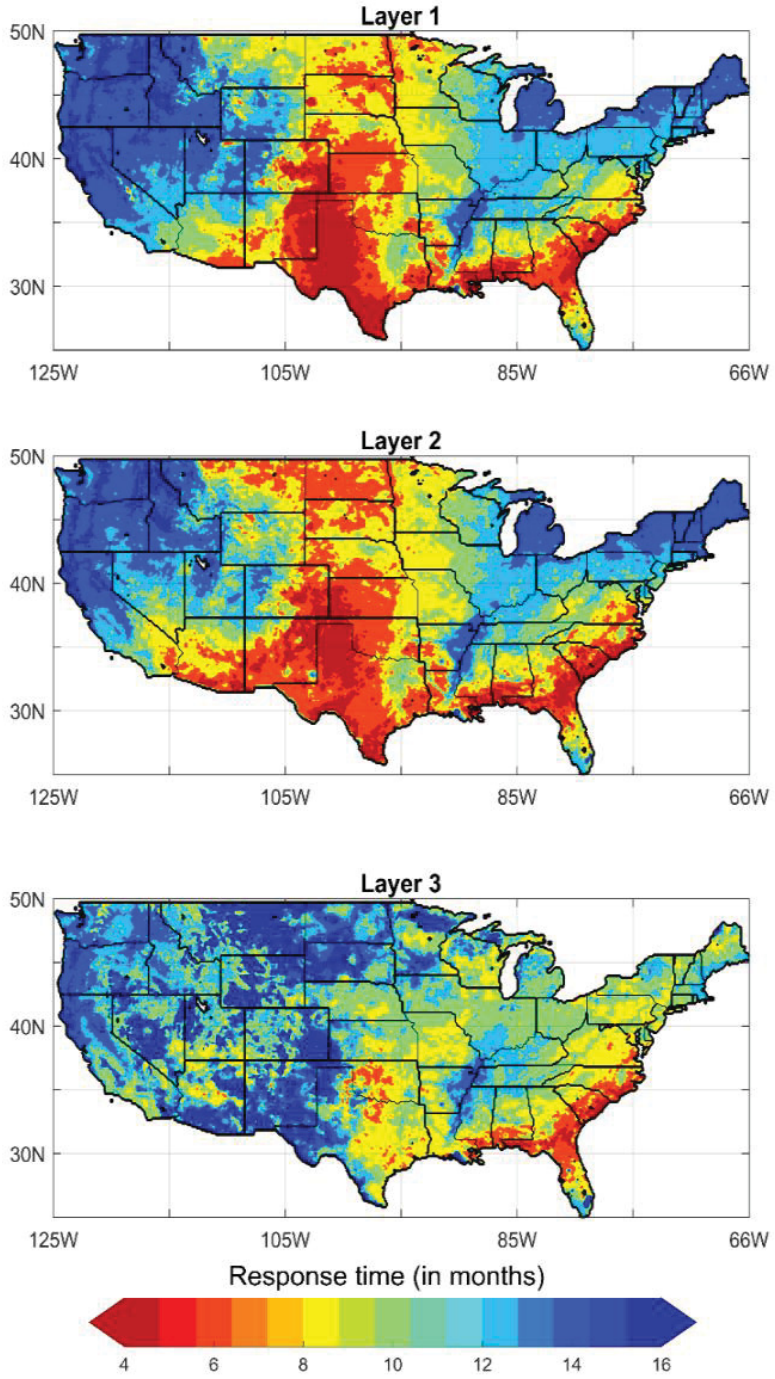

Figure. 2-11: Spatial distribution of Response Time (T_o) of Hybrid Soil Moisture (in months) for the three layers. Red/ Orange represents low persistence whereas Blue/ Cyan represents regions with higher Persistence.

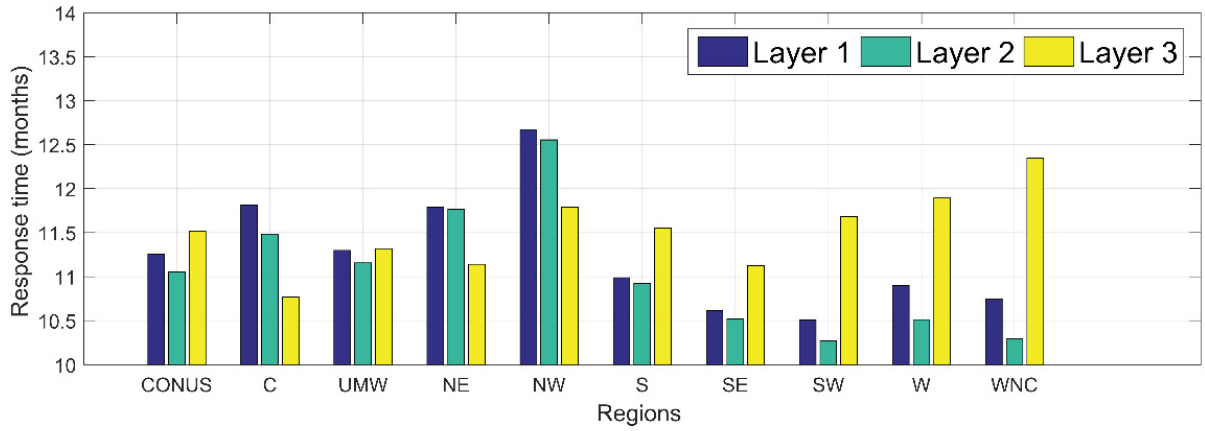

Figure. 2-12: Mean Response time (T_o) for three soil layers for the nine climate regions of the US (C= Central, UMW=Upper Midwest, NE= North East, NW= North West, S= South, SE= South East, SW= South West, W= West, WNC= West North Central).

7.2. Layer-wise sensitivity of soil moisture to drought indices

The *transformation matrix* for each layer contains the information about the top performing wavelets, the regression coefficients for each WR model and the respective model weights. These transformation matrices are applied over all grid cells of NOAH and MOSAIC to obtain HSM at $1/8^{th}$ degree resolution from Jan 1979 to Sep 2015 at monthly scale for all three layers. Once the dataset for all grid cells is obtained, the correlation between the HSM for all three layers with the eight DIs for their respective climate division is obtained for each grid. This exercise provides a spatial map of the inter-relationship between each of the eight DIs under study with the HSM for all three layers. Figure. 2-13 shows the spatial pattern of correlation of soil moisture with the DIs for CONUS. Furthermore, the average correlation of soil moisture with DIs for each climate region is summarized in Figure. 2-14.

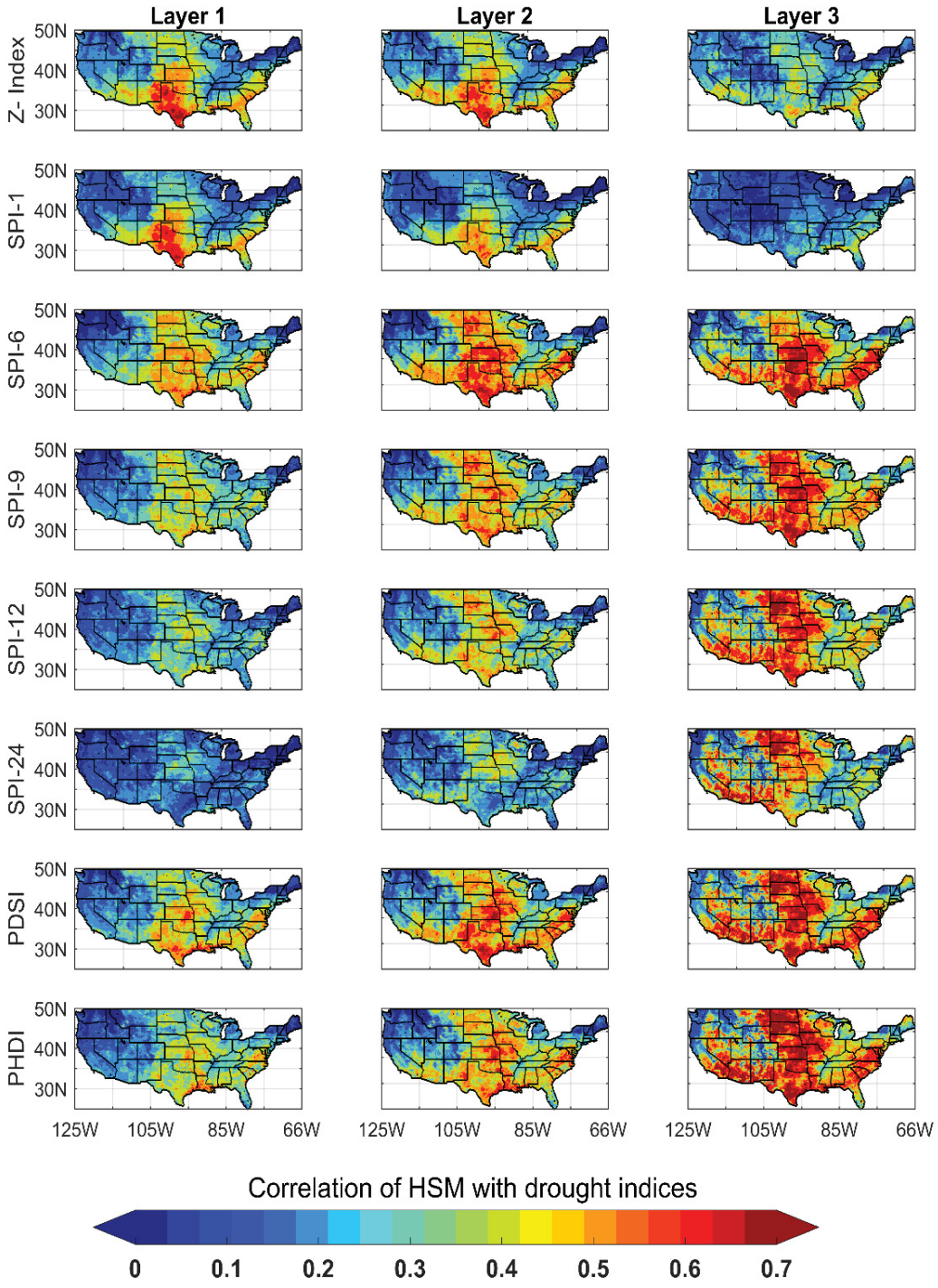

Figure. 2-13: Correlation plots of Hybrid Soil Moisture with the eight drought indices for the three soil layers for CONUS. Red color represents stronger positive correlation whereas Blue color represents near low or negative correlation with the drought indices.

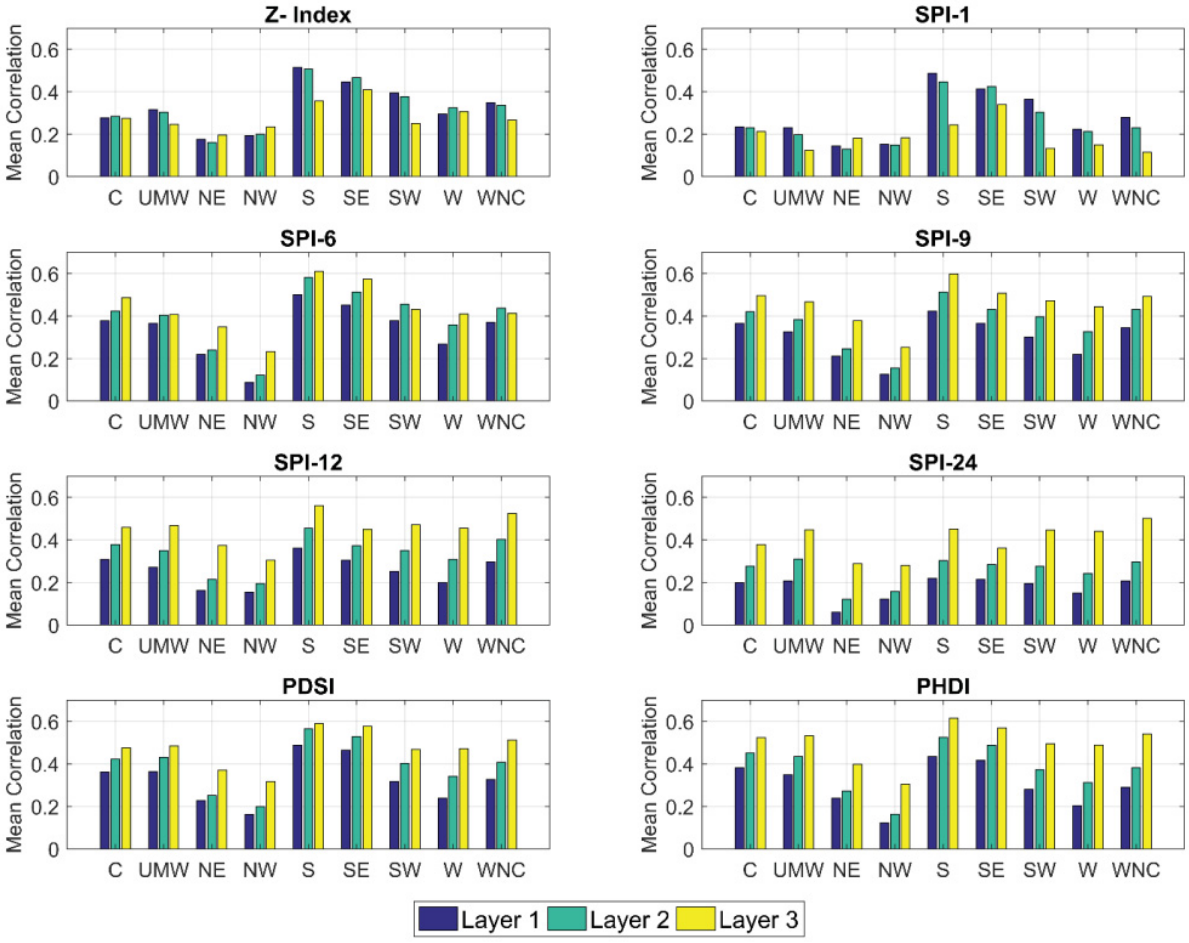

Figure. 2-14: Mean correlation of soil moisture with drought indices (DIs) for the nine climate regions of the U.S. (C= Central, UMW=Upper Midwest, NE= North East, NW= North West, S= South, SE= South East, SW= South West, W= West, WNC= West North Central).

The observable trends can be summarized in the following points: Regions like the west north central part of US around Texas and New Mexico, West south central (Kansas, Nebraska) and regions around Georgia, Alabama and South Carolina typically show a higher correlation with the DIs compared to other regions of respective layers. In contrast, the region around the mid-Atlantic US, New England and the Western US show very low correlation with the drought indices. It is also worth noting that these regions have significant low persistence in comparison with other

regions for the soil moisture of a given layer. Hence, persistence is observed to have a significant impact on the response of soil moisture to drought.

These trends can be attributed to the fact that the role of soil moisture in modulating precipitation generation is extremely high in the 'transition zones' between wet and dry climates, as evaporation becomes sensitive to soil moisture in these areas (Koster et al., 2004). The Great Plains can be characteristically identified with this phenomenon simply due to the fact that evaporation is greater than precipitation during the growing season, thus implying that the region predominantly serves as a source for moisture(Sridhar and Wedin, 2009).

7.3. Effect of autocorrelation in time series on correlation analysis

Significant autocorrelation in the soil moisture and DI time series may impact the correlation analysis (and thus, its inferences). In order to eliminate any significant autocorrelation and seasonal effects, the time series are pre- whitened prior to the correlation analysis. Pre- whitening is carried out using ARIMA (Box and Jenkins, 1976) (2,1,2) models to obtain the residuals for the time series of soil moisture and drought indices for each grid cell. An analysis is carried out to select the most suitable ARIMA model for the purpose of pre- whitening (refer to the Supplementary material). 20 grid points are randomly selected across CONUS and ARIMA (p ,1, q) models are evaluated for the lowest AIC for different combinations of p (autoregressive component) and q (moving average component) where $p \in [0,1,2]$ and $q \in [0,1,2]$. A sample analysis of correlation analysis using the pre- whitened soil moisture and DI time series is shown for Z-index and SPI-1 in Figure. 2-15. On comparing Figure. 2-14 and Figure. 2-15, it is evident that the spatial pattern of correlation between the two DIs and soil moisture for each layer is different when the pre-whitening of the time series is carried out prior to calculating the correlation between the two variables. However, the interpretation about the relative strength of the interrelationship from layer

1 through layer 3 isn't effected. Since the correlation strength is impacted by pre-whitening, while the patterns remain unchanged, it is generally recommended to do pre-whitening. However, care should be given to retain the physical relationship in the variable (in this case soil moisture) and its relationship with DIs. As the ultimate goal is to evaluate if soil moisture can be useful in predicting drought, correlation analysis need not done if the resultant data dilutes the nature of relationship. However, lack of information on soil moisture data for the managed and natural systems, a generalized approach to remove the temporal correlation across the entire domain constrained this study to use the data without pre-whitening. This assumption is consistent with some studies which utilize the autocorrelation in soil moisture as an important property in order to capture the perpetuation of drought conditions. Tang and Piechota (2009) and Lakshmi et al. (2004), based on the autocorrelative structure of soil moisture, conclude that the deep layer soil moisture anomaly possess strong inter-relationship with drought indicators like PDSI. Also, Oglesby et al. (2002) show that deep soil zone anomalies exert a more powerful, long-lasting effect than anomalies in the near-surface soil zone and hence, are more important in explaining interannual to decadal droughts evident in the historic and recent prehistoric records.

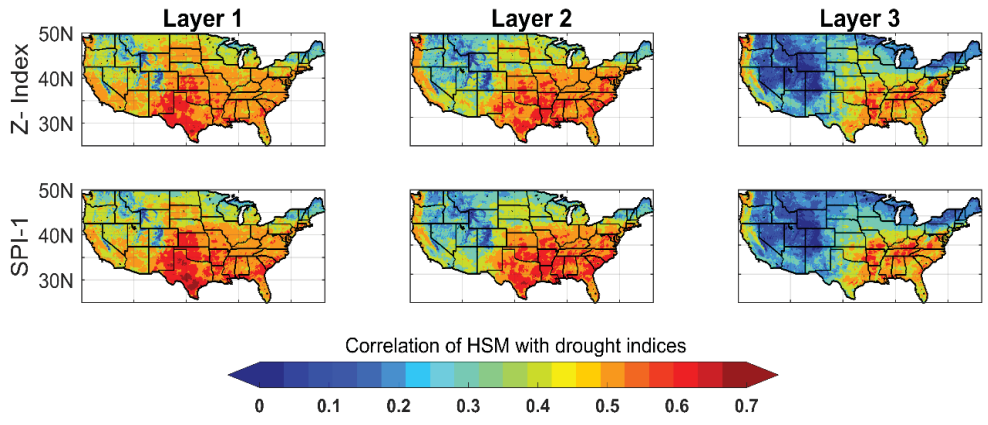

Figure. 2-15: Correlation plots of pre- whitened Hybrid Soil Moisture with pre- whitened Z- index (top row) and SPI-1 (bottom row) for the three soil layers for CONUS. Red color represents

stronger positive correlation whereas Blue color represents near low or negative correlation with the drought indices.

Hence upon comparing the results of correlation between the DIs and soil moisture for all three layers with and without pre- whitening of the input time series, and evaluating related literature, this study utilizes the correlation results of soil moisture and the DIs without pre-whitening.

7.4. Layer-wise drought reconstruction for Southern U.S.

Based on the correlation and sensitivity of drought indices for soil moisture, it is clear that each soil layer responds to drought in a different way. While top soil layer has comparatively low persistence, it is expected to respond quickly to impending drought conditions compared to the deeper layers. At the same time, the deeper soil layer will respond slowly to changing moisture conditions and hence will respond slowly to improving drought conditions.

Currently, soil moisture percentiles used in drought reconstruction provide an estimate of moisture percentiles for total column length of soil moisture (Luo and Wood, 2007; Wood, 2008) and does not account to this inter- layer variations in moisture loss. The U.S. Drought Monitor (USDM) provides a comprehensive drought assessment of current drought conditions for the US and provides a useful reference for socio- economic and agricultural management purposes at a weekly time step (Wang et al., 2009). USDM drought assessment maps are popularly used for validating the drought assessment from various research products with that of an operational product. The USDM classification of drought severity using soil moisture percentile is given in Table 2-7. HSM (Jan 1979 through Aug 2015) is used to in determining the thresholds for each severity level, and all data used in drought severity determinations are considered with reference

to their historical frequency of occurrence for the location and time of year in question in accordance with Svoboda et al. (2002).

Table 2-7: U.S. Drought Monitor (USDM) classification of drought based on soil moisture percentiles

Soil Moisture Percentile	USDM classification	Interpretation
Less than 30	D0	Abnormally dry
Less than 20	D1	Moderate drought
Less than 10	D2	Severe drought
Less than 5	D3	Extreme drought
Less than 2	D4	Exceptional drought

7.5.Layer- wise classification of soil moisture percentile to drought severity

The average squared correlation coefficient (ASCC) (Abatzoglou et al., 2014) is employed to relate the soil moisture percentile with long/ short term drought. ASCC is obtained by averaging the squared correlation coefficient between the drought indices and soil moisture for the three layers obtained for all available data points. The ASCC values obtained from all grids across CONUS are normalized across layers to obtain the normalized average squared correlation coefficient (NASC) to facilitate a comparative assessment of the strength of the relationship between the DI and HSM across different layers as provided in Figure. 2-16 against the values obtained from the *in-situ* observations. The layer-wise sensitivity provides information of the relative sensitivity of a given drought index across layers from the two datasets.

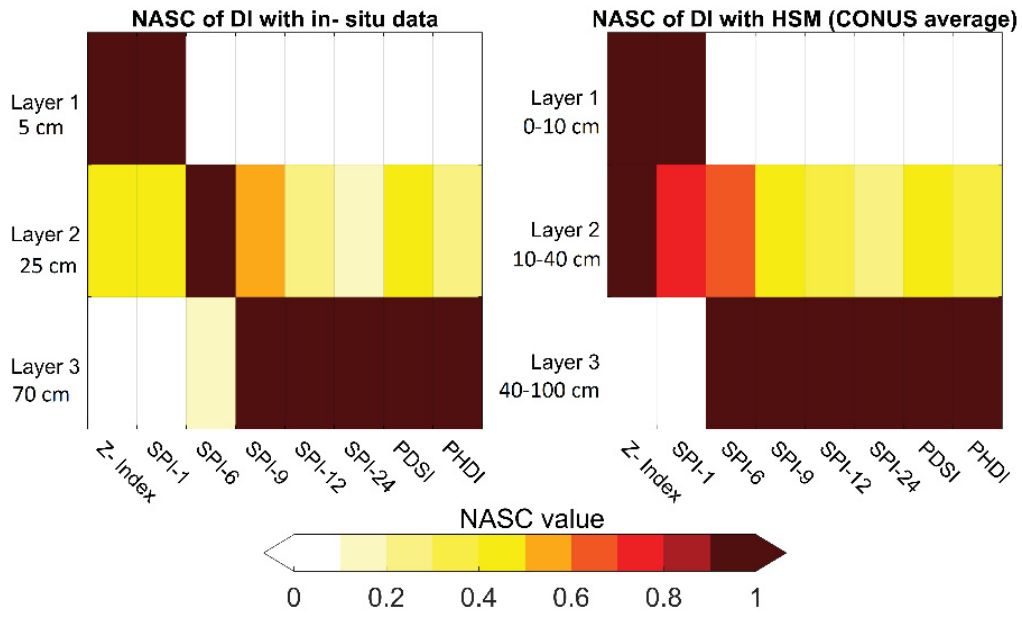

Figure. 2-16: The Averaged Squared Correlation normalized across three soil layers (Read top to bottom) to obtain the Normalized Averaged Squared Correlation (NASC) for both *in- situ* US Climate reference network (USCRN) data and Hybrid Soil Moisture averaged over CONUS. NASC=1 indicates strongest correlation, NASC= 0 indicates weakest, and, 0<NASC<1 indicates intermediate correlation between the soil moisture of the respective layer and a given drought index.

From Figure. 2-16, it can be observed that the top soil layer (Layer 1) is more responsive to the short-term variations in moisture regime due to direct soil evaporation whereas Layer 3 reflects more on the long-term moisture deviations and often display a lagged response to dry conditions. Layer 2 served as a link between the two layers in terms of transition of drought from low to high severity. This understanding is used while proposing a new soil moisture percentile classification to effectively represent drought severity for the Southern U.S. While Layer 1 is used to represent only the transient dry conditions (D0), Layer 3 is used to capture severe and long-term droughts (D2-D4). Layer 2 is used to represent the transition of drought severity from low to high

(D0-D3). The effectiveness of the drought reconstruction approach is carried out against the USDM maps for the concurrent time. The layer-wise soil moisture percentiles and corresponding drought severity proposed in this study are provided in Table 2-8.

Table 2-8: Classification of drought based on layer- wise soil moisture percentiles proposed in this study

Proposed layer- wise classification of drought severity			
Soil Moisture Percentile	Layer 1	Layer 2	Layer 3
Less than 30	D0	D0	D2
Less than 20	D0	D1	D2
Less than 10	D0	D1	D2
Less than 5	D0	D2	D3
Less than 2	D0	D3	D4

**Interpretation of D0,D1,D2,D3,D4 is consistent with USDM*

7.6.Application of proposed multi- layer percentiles for drought reconstruction for CONUS. (April- December 2011)

In the proposed approach, the drought classification is carried out for each layer using the classification provided in Table 2-8. Drought severity maps obtained from each layer are then overlaid with deeper layers getting higher priority than the shallower ones. To illustrate, if we assume the moisture percentile for a grid cell is observed between 5-2 percentile for all layers simultaneously, then the drought will be classified as a D3 drought (Extreme drought).

Drought reconstruction maps using the proposed multi-layer percentile approach for CONUS (with a focus on drought in the southern U.S.) for April- December 2011 is provided in Figure. 2-17. It can be observed that the soil moisture percentiles are able to respond in accordance with the drought conditions as depicted by the USDM maps. Consistent with the USDM approach, the percentiles used for the drought severity classification in this study are standardized for the

time of the year, rather than for all times of the year at once. It is to be noted that though the threshold values for drought severity using the soil moisture percentiles do not correspond exactly to the appropriate soil type-based water holding capacities and their percentiles at all locations across the U.S., they provide a consistent and replicable standard for drought classification utilizing a variable easily understood by the general public. These objective inputs, and subjective adjustments based on local impacts and vulnerability result in a drought indicator based on a convergence of evidence that can be interpreted easily in terms of return periods (Svoboda et al., 2002).

A similar drought reconstruction is carried out using Noah and Mosaic dataset for the purpose of comparison (Figure. 2-18). Discrepancies between the drought maps reconstructed using Noah and Mosaic can be seen in the plots. While two models generally agree on severe droughts in the Southern U.S. for the study period, there remains significant dissimilarities in the models in terms of severity and the region under estimated severity conditions for other regions. A comparison of the area under various drought severity conditions represented by the reconstruction approach using HSM, Noah and Mosaic, and, the USDM for April through Dec-2011 (months of most severe impact) is provided in Figure. 2-19. Figure. 2-20 provides a comparison between the time series of the eight drought indices and monthly soil moisture percentiles using HSM, Noah and Mosaic. It can be seen from Figure. 2-19 and Figure. 2-20 that there remain discrepancies in analysis based on Noah and Mosaic dataset, while HSM provides a reliable ensemble of the two models and is able to estimate in- situ soil moisture with greater accuracy, thus eliminating the subjectivity in choosing one model over another.

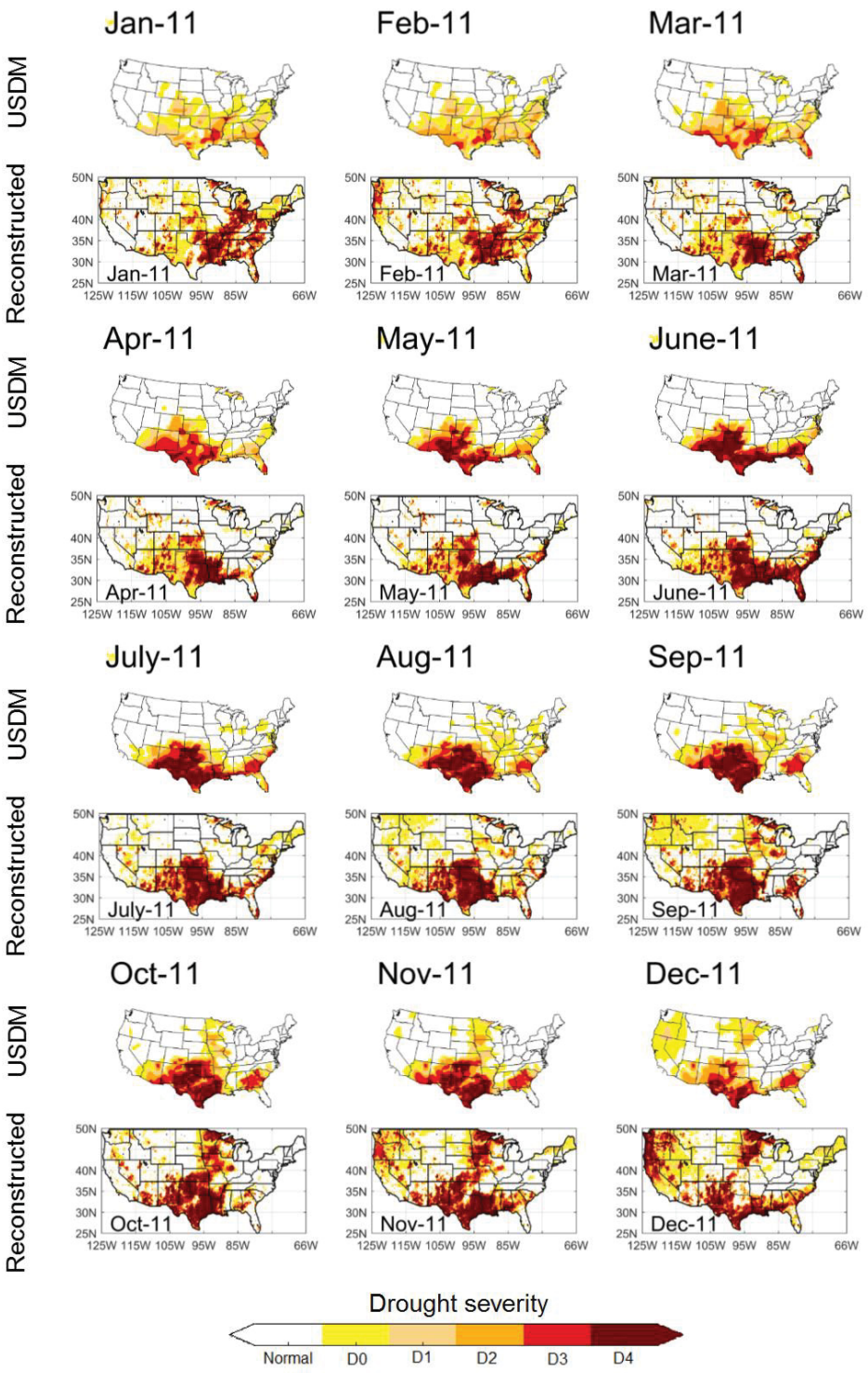

Figure. 2-17: Reconstructed drought maps using the proposed layer-wise soil moisture percentile approach using HSM v/s USDM drought maps for CONUS (Apr'-11 to Dec'- 11)

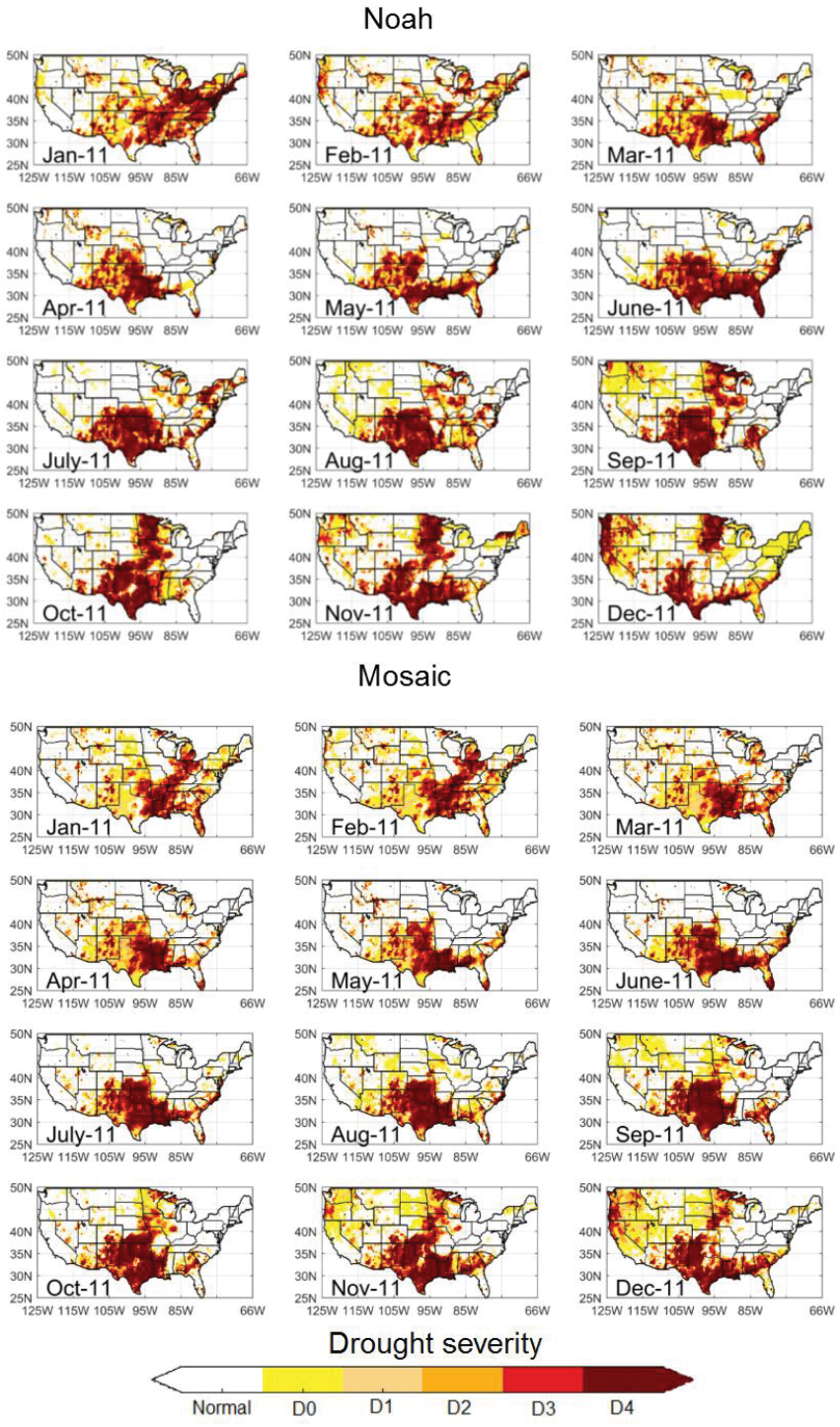

Figure. 2-18: Reconstructed drought maps using the proposed layer-wise soil moisture percentile approach using Noah and Mosaic dataset v/s USDM drought maps for CONUS (Apr'-11 to Dec'-11)

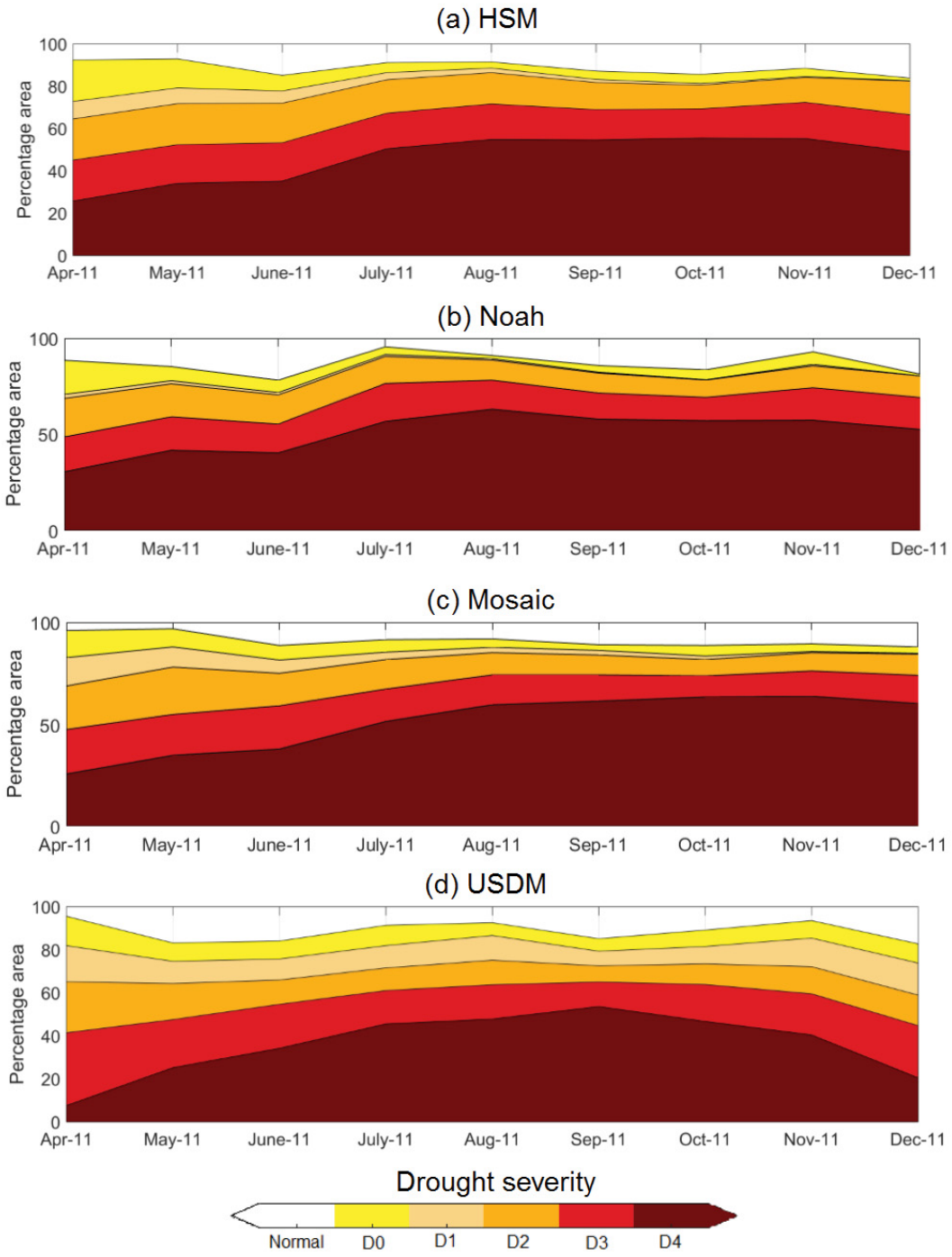

Figure. 2-19: Comparison of the area under various drought severities as obtained from the reconstructed drought maps using (a) HSM (b) Noah (c) Mosaic and (d) USDM maps (Apr'-11 to Dec'- 11) for Southern U.S.

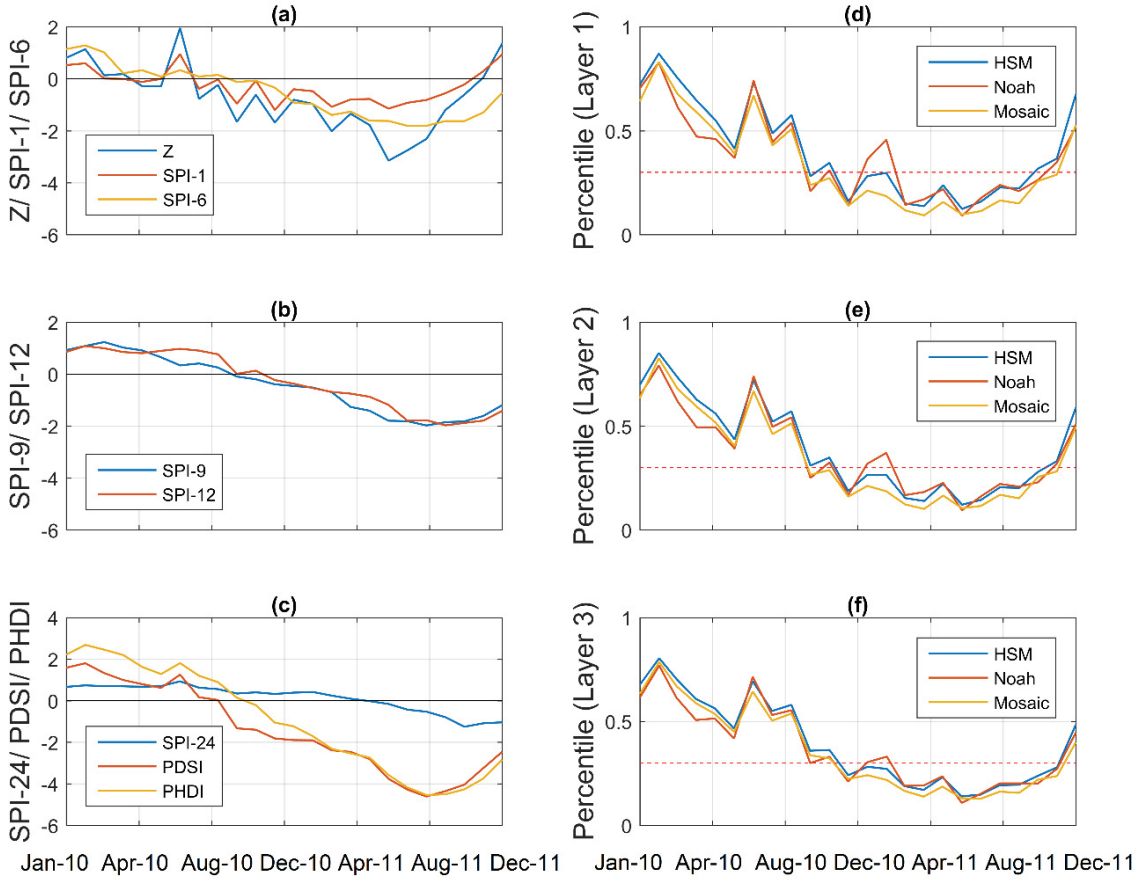

Figure. 2-20: Comparison of average value of the eight drought indices (Left) (a) Z- index, SPI-1 and SPI- 6 months (b) SPI- 9 and SPI- 12 (c) SPI- 24, PDSI and PHDI with monthly soil moisture percentiles obtained using HSM, Noah and Mosaic for (d) Layer 1 (b) Layer2 and (c) Layer 3 for Southern US.

8. Discussion

A layer- wise perspective is imperative to completely represent the water transport dynamics in soil column in the event of drought. While, the drier conditions in the near surface soil layer may indicate short-term meteorological drought it may not be a good measure of agricultural drought if the total root zone water storage is relatively wet. Deficit soil moisture storage in the total soil column may be indicative of hydrological drought but a single storm may

replenish root zone soil moisture enough to relieve agricultural drought, yet hydrological drought could inflict the region over a season (Sheffield et al., 2004b). Deeper layers represent the water availability for plant uptake, aquifer recharge, and, baseflow to streams, whereas, the near- surface soil moisture indirectly indicates the dryness of the deposited plant litter which may indicate susceptibility to other natural hazards like wildfire, essentially, aggravating drought conditions. A detailed study on the dynamics of soil moisture can be found in D'Odorico et al. (2000). It can be observed that the reconstructed maps are quick to respond to transient changes and usually predate the USDM maps in capturing the drought onset. This property can be attributed to the inclusion of moisture percentile information from shallow soil layers in representing flash droughts. Further applicability of the proposed approach for drought early forecasting with satisfactory skill- scores and lead time can be useful to effectively characterize emerging drought conditions over large areas. The proposed representation of drought severity is directly comparable to the USDM maps, which are popular benchmarks for drought analysis, making it easier for the policy makers in taking decisions based on evolving hydrometeorological conditions. While the climatology and dataset for the USDM and this study are not the same, the USDM involves many other factors like county-level information on drought, reservoir levels, snowpack and groundwater which may lead to different interpretation of drought at local scales.

Timely identification of impending drought conditions is important from agricultural and water management perspectives. The two land surface models for this study namely Noah and Mosaic are available at near real- time through the NLDAS- v2 platform. Using the ensemble model proposed in this study, HSM can be generated in near- real time mode and hence carries the potential to be used in an operational drought monitoring setup. Also, soil moisture simulations from multiple physically based models can be derived using the seasonal forecasts from coupled

ocean-atmosphere general circulation models (Wood et al., 2002) and a similar approach can be applied to obtain HSM and thus soil moisture percentiles for forecasting droughts with a lead time of several months.

However, the proposed approach has certain limitations due to the model design and limited availability of observed data. The proposed approach for drought reconstruction is developed in a time independent way, which means, that the drought severity is estimated for the current month and hence compromise on maintaining the continuity during month-to-month transitions and doesn't account for the contribution of the additional soil moisture for hydrologic processes in the next time step.

Currently, this study uses in- situ soil moisture data from 48 observation stations available for a relatively short time duration (Jan 2009 through Aug 2015). This limited sampling could potentially impact the performance of the proposed approach. Although the issue of limited data availability is addressed, to some extent, using a generalized modeling approach consisting of multiple wavelets and BMA to capture the overall variability of the data across CONUS, a higher number of observation stations with longer data record will certainly add to the accuracy and confidence of the model. Recent efforts in soil moisture monitoring like North Atlantic Soil moisture database (Quiring et al., 2015), and advancements in remotely sensed soil moisture missions like SMAP (Brown et al., 2013), will be able to rectify this issue in coming years. It is also to be noted that the current drought reconstruction is performed at a monthly time step. Increasing the temporal resolution will add to the ability of the drought percentiles to capture short term changes.

9. Conclusion

Soil moisture is an important tool in understanding the onset, propagation, and recovery of droughts. However, as an alternative to a long-term, *in- situ* soil moisture data for drought analysis, this study develops an ensemble of Noah and Mosaic Land Surface Model estimated soil moisture and i*n- situ* observations to obtain a combined dataset data called Hybrid Soil Moisture (HSM). The HSM is used to understand the response soil moisture from three layers (0- 10 cm, 10- 40 cm and 40- 100 cm) to eight drought indicators representing long-term and short-term drought predictability. A stratified approach for reconstruction of droughts is proposed in this study and is used for drought reconstruction over Southern U.S. during a recent drought to demonstrate the effectiveness of the proposed approach in capturing the drought dynamics. This study can be summarized as follows:

1. A statistical approach is employed to obtain a hybrid of two Land Surface Models for the CONUS using *in- situ* dataset to reduce bias and error in estimating the true state of soil moisture. A multi- resolution regression coupled with Bayesian Model Averaging is used for transforming the simulated soil moisture from the two LSMs into Hybrid Soil Moisture which is further used as a proxy to *in- situ* soil moisture for CONUS scale statistical analysis and drought reconstruction for Southern U.S.
2. A layer- wise correlation analysis of the soil moisture with eight drought indices namely PDSI, PHDI, Z index, SPI- 1, 6, 9, 12 and 24 shows that shallow soil layers (0-10 cm and 10- 40 cm) respond to short-term drought occurrences with higher correlation whereas deeper layer (40-100 cm) is more responsive to long-term droughts.

3. The three soil layers under study differ significantly with respect to their Response Time, which significantly drives their characteristic response to drought. This strengthens the argument in favor of a layer- wise approach for drought analysis and reconstruction.
4. A new drought classification based on stratified soil moisture percentiles is proposed and applied to the reconstruction of drought over CONUS with a focus on drought in the Southern U.S. for Apr- Dec 2011. The reconstructed drought maps show good correspondence to the USDM drought maps for the concurrent period. The reconstructed maps usually predate the USDM maps in representing low-intensity droughts which can be exploited further in flash drought studies.

Chapter 3 :
High resolution retrospective simulation, and near real-time seasonal forecasting of sub-watershed scale hydrologic variables for Southeastern US using CFSv2 coupled SWAT models

Key points:

a) High resolution, sub-watershed (HUC-12) scale hydrological modeling for 50 watersheds in Southeastern US.

b) Watershed scale model calibration and validation using observed streamflow.

c) Stratified validation of sub-watershed scale soil moisture simulations using *in-situ* soil moisture observations.

d) Framework for near real- time forecasting of hydrologic variables at daily time step with a lead of 9 months by coupling SWAT models with CFSv2 drivers (precipitation and temperature).

1. Abstract

This study provides high resolution modeling of water budget components at HUC-12 (12- digit Hydrologic Unit Code) resolution for 50 watersheds for the South Atlantic– Gulf (SAG) region in the Southeastern US (SEUS). A near real-time hydrologic simulation framework by coupling calibrated SWAT (Soil & Water Assessment Tool) models with the National Centers for Environmental Prediction (NCEP) coupled forecast system model version 2 (CFSv2) weather data is developed to forecast various water balance components including soil moisture (SM), actual evapotranspiration (ET), potential evapotranspiration ET (PET), and runoff (SURQ). CFSv2 models provide global weather data for multiple initializations every month with a lead time of 9 months. The observed streamflow data from 50 USGS gaging stations is used to calibrate (Jan 2003- Dec 2010) and validate (Jan 2011- Dec 2013) the simulated streamflow. Sub-watershed scale, SWAT-simulated soil moisture for two layers: the surface layer and total rooting depth, are compared with the observed *in-situ* data from nine US climate reference stations (USCRN) across SEUS. The water balance analysis show that SWAT models satisfactorily represent the hydrology of the study region and capture the spatial variability in soil moisture, evapotranspiration and streamflow across different regions (Appalachian highlands, plains and coastal wetlands) and across different seasons. SWAT-CFSv2 models based forecast of hydrologic components is provided in this study for the SAG region with a lead time of 9 months (from Mid-March through end of December 2017). The models forecast a relief from dry conditions due to precipitation in May- June' 2017 however, mild to moderate drought conditions may reappear in some parts of the SAG region owning to high PET, low precipitation and soil moisture in the later parts of the year.

Key words: Soil moisture, SWAT, Southeastern US, CFSv2, HUC-12

2. Introduction

Soil moisture and evapotranspiration (ET) are two important components of the hydrologic cycle. Soil moisture impacts the surface and atmospheric boundary layer processes significantly, including the development of mesoscale circulations for various land surface patches with differing soil moisture conditions, the development of deep convection, and the growth and sustainment of large-scale interannual variations such as droughts (Hain et al., 2011). Soil moisture modulates the atmospheric surface energy balance and hence, has a significant impact on the vertical distribution of turbulent heat fluxes, as well as the boundary layer structure, and, is a pivotal element in the hydrological process of converting precipitation into runoff and groundwater storage (Alapaty et al., 1997). ET plays important role in linking water, energy, and carbon cycles and hence is crucial for the climate system and the hydrological cycle (Sun et al., 2017). ET can reach as high as 60% of terrestrial precipitation during precipitation recycling process (Shiklomanov, 1998) whereas in water-limited ecosystems, ET can approach upto 100% of annual rainfall (Budyko, 1971). The latent heat of vaporization (the energy required for evaporating water) serves as the largest single heat source for the atmosphere, plays a crucial role in weather and climate dynamics (Vinukollu et al., 2011) and has important implications for the availability and usage of fresh water resources by humans and terrestrial ecosystems by regulating ET process (Seneviratne et al., 2006; Trenberth et al., 2009).

Both soil moisture and ET exhibit significant spatiotemporal variability across different scales owing to a range of processes such as precipitation, energy and water fluxes., Factors including orography (on all scales), vegetation, and soil texture, etc. (Garnaud et al., 2017) also influence ET diurnally. Hence, accurate soil moisture and ET estimation is essential for delivering (or improving the quality of) reliable meteorological, hydrological and environmental forecasts, such as

precipitation (Ciabatta et al., 2016) , discharge estimates and prediction (Brocca et al., 2010; Laiolo et al., 2016), identifying flash-flood prone areas and flood forecasting (Alvarez-Garreton et al., 2015; Bangira et al., 2015; Nanda et al., 2016), and identification and characterization of droughts (Anderson et al., 2007; Hobbins et al., 2016; Sridhar et al., 2008), understanding soil–vegetation–atmosphere interactions (Mao et al., 2015; Zhang et al., 2016b), and improving water resource management (Sridhar and Anderson, 2017).

Physically based hydrological models are used to simulate complex water resource systems to simulate the impacts of land use and climate change and other anthropogenic activities on the hydrological cycle (Cao et al., 2006; Muttiah and Wurbs, 2002). These model provide a physical representation of the spatially variable hydrological processes (Xu et al., 2009) and key hydrological components like ET and soil moisture. While some hydrological variables like precipitation, streamflow are more frequently recorded and reported, similar long-term soil moisture observations are scarce. ET measurements can be broadly classified in two categories: *(i)* Remote sensing of ET using mechanistic or empirical models with the remotely sensed land surface and atmospheric properties (Jimenez et al., 2009; Jung et al., 2009; Mueller et al., 2011; Zhang et al., 2010) or *(ii)* Physics based hydrological, and Land Surface models (Griensven et al., 2014; Marek et al., 2016; Mueller et al., 2013; Mueller et al., 2011). Inter-comparisons of these large number of remotely sensed ET datasets have indicated significant uncertainties associated with these products, with relative errors of 15%–30% (Mueller et al., 2011; Polhamus et al., 2013; Vinukollu et al., 2011). Hydrological models / Land Surface Model based ET values is effected by the reliability of the atmospheric forcing and land surface properties datasets, parameterizations of the physical and biogeochemical processes, and the spatiotemporal scales and resolutions of the simulations (Best et al., 2015; Liu et al., 2015; Mueller et al., 2013; Sun et al., 2017).

Several studies have employed a combination of the climate forecasts or reanalysis data with hydrological models to simulate hydrometeorological conditions in several parts of the world. Yan et al. (2013) used SWAT model for simulating long-term serial soil moisture and actual evapotranspiration in the Luanhe river basin in North China. Marek et al. (2016) used SWAT models for estimating ET for dryland cropping systems in semiarid Texas High Plains. Wetterhall et al. (2015) evaluated the European Centre for Medium-Range Weather Forecasts (ECMWF) dataset for seasonal predictions of agrometeorological variables in the Limpopo river basin in South Africa. Mace et al. (2015) developed a process-based statistical model to provide an early warning indicator of meteorological conditions for Texas. Sun et al. (2017) developed a multiple-Land Surface Model (LSM) ensemble-averaged ET ensemble of Community Land Model (CLM), Dynamic Land Model (DLM), and Variable Infiltration Capacity model (VIC) to assess spatial–temporal variations over China for the period 1979-2012. Shah and Mishra (2016) coupled forecasts from Global Ensemble Forecast Systems (GEFS) with the VIC model to provide a pan-India drought monitoring with a lead time of 7 days.

Utilizing information from seasonal climate forecast and long-term climate prediction has proven to be of great interest to water planners and decision makers to improve preparedness towards, and mitigation of impacts due to climatic extremes (Hansen, 2005). Dynamical seasonal forecasting systems that are based on coupled atmosphere-ocean-land general circulation models (CGCMs) have been widely used for hydrologic forecasting in recent years (Dutra et al., 2013; Ma et al., 2015). Seasonal climate forecasts are useful in improving farmers' ability for mitigating adversities linked to climate extremes, particularly in rainfed systems (Wetterhall et al., 2015). Skillful prediction of the field scale soil moisture is important to decide crop type, resource use, and crop insurance and contract renewals (Shafiee-Jood et al., 2014). Application of climate

forecast system reforecast and reanalysis (Saha et al., 2010) products in hydrologic monitoring and prediction, seasonal soil moisture estimation and understanding land- atmosphere interactions (Dirmeyer, 2013; Mace et al., 2015; McEvoy et al., 2016b; Mo et al., 2011; Mo et al., 2012b; Roundy et al., 2014) is also extensively explored. Very recently, Zhang et al. (2017) integrated CFSv2 with the VIC model and satellite data to predict drought in Southwestern China.

With increasing population and associated demand for freshwater resources and food production, global food security has come under severe risk (Mu et al., 2013). Several studies have expressed concerns over increasing vulnerability of Southeastern US owning to continued growth and subsequent industrial, agricultural and metropolitan demand throughout the region (Manuel, 2008; Pederson et al., 2012; Seager et al., 2009) and suggested that the threat of water-related conflict in the region has potential to grow more intense in the coming decades. The southeastern US region has experienced widespread droughts three times within a span of 15 years since early 2000 and nearly 40% of the region is under moderate to exceptional drought conditions as of early 2017. As the frequency of future hydrologic extremes is expected to increase, a reliable hydrologic forecast can be useful for efficient planning of available water resources (Madadgar and Moradkhani, 2014). Previously, Lu et al. (2003) developed an empirical model to estimate long-term annual actual evapotranspiration for forested watersheds in the SEUS . Limaye et al. (2001) developed a macroscale hydrologic model for regional climate assessment studies in the SEUS. Seong and Sridhar (2017) evaluated climate, hydrology, and land use change in the Chesapeake Bay (CB) Watershed. Kang and Sridhar (2017) used spatially distributed hydrological models for drought assessment in Virginia. However, most of these studies, in general, focused on retrospective conditions, or long-term future hydrologic conditions. Furthermore, sub-watershed

scale variability at high resolution with a focus on seasonal and sub-seasonal forecasting wasn't captured in the studies.

This study identifies the inadequacy of the current literature in linking global scale weather models like CFSv2 to regional hydrologic models for simulating high resolution hydrologic variables and subsequent near-real time seasonal forecasting. This study captures the local (sub-watershed) scale variations in water balance components and demonstrate an effective approach for hydrologic analysis (retrospective and forecasting) using a bottom- up approach (sub-watershed to region).

The objectives of this study are as follows:

a) To develop SWAT models to simulate various hydrologic variables at the sub-watershed scale for the South Atlantic-Gulf (SAG) region of the Southeastern US (SEUS) at HUC-12 (12-digit Hydrologic Unit Code) resolution.
b) To evaluate the efficiency of high resolution SWAT models in simulating surface soil layer and root zone soil moisture.
c) To develop a near real-time forecasting framework water balance components at sub-watershed scale using calibrated SWAT models initialized with climate drivers from CFSv2 with a lead time of up to 9 months at a daily time step.

3. SWAT model

3.1.Model background

This study uses SWAT model to simulate various components of hydrologic cycle at a sub-watershed scale. SWAT is a comprehensive, semi-distributed, continuous-time, processed-based model (Arnold et al., 2012; Gassman et al., 2007; Neitsch et al., 2011) initially developed to model

the impacts of management practices on the hydrologic cycle, plant growth, and water quality in medium to large basins (Jin and Sridhar, 2012) . SWAT is a continuous time watershed model that operates on a daily time step and its simulation incorporates weather, hydrology, sedimentation, soil temperature, plant growth, nutrients, pesticides and land management (Arnold et al., 1998). The model uses weather (precipitation, radiation and temperature), elevation, soil, land cover/ use data to simulate surface and subsurface hydrology and various chemical, biological and sediment fluxes. Hydrologic cycle simulations by SWAT are based on the water balance concept.

The aquifer system in SWAT can be conceptualized as a two-layer system consisting of a shallow and a deep aquifer. Water in the shallow aquifer can return to soil profile or enter into stream as a groundwater flow, while water in the deep aquifer is supposed to leave the system. The surface, inter and groundwater flow are calculated for each sub-watershed as an area-weighted average of its composing HRUs. The runoff volumes generated from each sub-watershed are then routed to the watershed outlet. Potential evapotranspiration is estimated using *Penman–Monteith* or other temperature dependent equations and the plant growth is modeled with a modified EPIC model for estimating actual plant transpiration (Williams et al., 1984).

The watershed hydrological transport model is implemented by dividing the watershed into sub-watersheds defined by topography and river network. SWAT lumps unique combinations of soil type and land use (and slope if desired) into hydrologic response units (HRUs) during the initialization process for each sub-watershed, thus further dividing the sub-watershed into smaller units and the land phase of the hydrologic cycle is modeled for each HRU. This process ignores the underlying spatial distribution of the input data and reduces the computational complexity, and surface runoff, interflow, plant growth, evapotranspiration and soil water redistribution is simulated for each HRU. These empirical simulations have advantages of keeping data

requirement reasonable while the physical backbone of the model facilitates a transparent simulation of the hydrologic processes (Liu et al., 2008). The model has a physical basis although it contains some empirical simulations, e.g. the Soil Conservation Service Curve Number (SCS-CN) method for estimating surface runoff (Liu et al., 2008).

SWAT is an open source code simulation model and has been extensively used in hydrological modeling community across the globe with applications in studies ranging from catchment to continental scales (Abbaspour et al., 2015). Readers are further referred to SWAT literature database for literature on SWAT for various hydrological modeling applications (SWAT, 2017).

4. Study area, dataset and modeling framework

4.1.Study area

This study is focused on the South Atlantic-Gulf (SAG) region in the Southeastern US. The geographic area of the South Atlantic-Gulf region includes all of Florida and South Carolina, and parts of Alabama, Georgia, Louisiana, Mississippi, North Carolina, Tennessee, and Virginia (USGS, 2017). The South Atlantic-Gulf region spans over 724,326 square kilometers. The northern part of the study region is bounded by Appalachia, and is predominantly forested. Wetlands are common on the southern part of the study region. The elevation decreases from north to south from over 1700 m to sea level elevation at the coasts.

SAG is listed with a 2-digit Hydrologic Unit Code (HUC) of 03 and consists of 18 sub-regions, each listed with the 4-digit HUC codes ranging from 0301 through 0318. Each HUC-4 basin is further divided into smaller watersheds for this study, totaling 50 for the entire SAG region (Figure 3-1), each of which is modeled using SWAT to delineate sub-watersheds matching the HUC12 resolution as provided by the National Hydrology Dataset plus (NHD+). Figure 3-2 (a) provides a

comparison between the total HUC-12 sub-watersheds delineated by SWAT models and those provided by NHD plus, aggregated based on HUC-4 basins. Out of a total of 7453, the SWAT models delineated 7391 sub-watersheds for the entire SAG region. Figure 3-2 (b) shows the histogram of the area of the sub-watersheds delineated by SWAT models at HUC-12 resolution. Table 3-1 provides the complete list of the 18 basins in the SAG region, each referred to by its HUC- 4 identifier with list and name of the sub-watersheds with the outlet U.S. Geological Survey (USGS) stations. Note that the watershed numbers are provided by the authors only for easy referencing and identification of these watersheds in the study and not to be confused with the watersheds at HUC-6 which are larger than these watersheds in most cases.

Table 3-1: List of the 18 basins in the South Atlantic- Gulf region identified with 4- digit Hydrologic Unit Code with name and a 6-digit identification number (not to be confused with HUC-6) for the constituent watersheds, and, respective outlet USGS stations.

Basin	USGS stn.	Watershed	River/ basin
0301	02066000	030101	Roanoke
	02075500	030102	Dan
	02047000	030103	Nottoway
0302	02084000	030201	Tar
	02091814	030202	Neuse
0303	02134500	030301	Lumber
	02106500	030302	Black
	02108000	030303	NE Cape fear
0304	02129000	030401	Pee Dee
	02134500	030402	Lumber
	02132000	030403	Lynches
0305	02147020	030501	Catawba
	02169500	030502	Congaree
	02175000	030503	Edisto
0306	02197000	030601	Savannah
	02198000	030602	Barrier Creek
	02202500	030603	Ogeechee
	02203000	030604	Canoochee
0307	02223500	030701	Oconee
	02215000	030702	Ocmulgee
	02225500	030703	Ohoopee
	02228000	030704	Satilla
0308	02234000	030801	St. Johns (Geneva)
	02244040	030802	St. Johns (Buffalo bluff)
0309	02270500	030901	Arbuckle Cr.
0309	02292900	030902	Caloosahatchee
0310	02296750	031001	Peace
	02301500	031002	Alafia
	02313000	031003	Withlacoochee
0311	02323500	031101	Suwannee
	02317500	031102	Alapaha
0312	02330150	031201	Ochlockonee
0313	02338000	031301	Chattahoochee
	02350512	031302	Flint
	02358700	031303	Apalachicola
0314	02369600	031401	Yellow
	02366500	031402	Choctawhatchee
	02374250	031403	Conecuh
0315	02397000	031501	Coosa (Rome)
	02407000	031502	Coosa (Childersburg)
	02428400	031503	Alabama
0316	02448500	031601	Noxubee
	02466030	031602	Black warrior
	02469761	031603	Tombigbee
0317	02478500	031701	Chickasawhay
	02474500	031702	Tallahala
	02479300	031703	Red Cr.
0318	02482550	031801	Pearl (Carthage)
	02488500	031802	Pearl (Monticello)
	02489500	031803	Pearl (Bogalusa)

Figure 3-1: Map showing the location of the study area. The watersheds in the South Atlantic-Gulf (SAG) region are highlighted in grey shade.

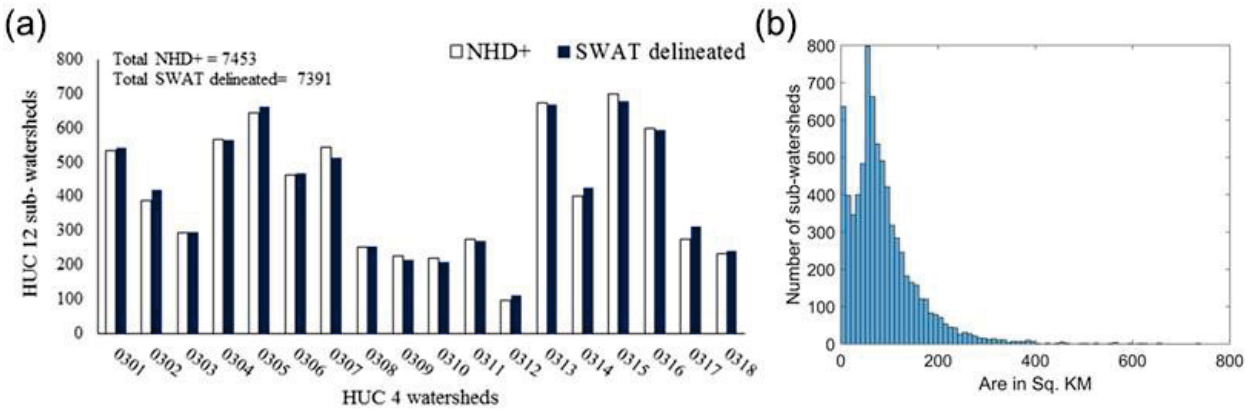

Figure 3-2: (a) Modeled and actual NHD+ HUC-12 watersheds. Against a total of 7453 sub-watersheds at HUC-12 resolution (NHD+), the models delineated a total of 7391 to match with

high spatial resolution. (b) Histogram of the area of the SWAT delineated watersheds at HUC-12 resolution.

4.2. Model dataset

The basic drivers for the SWAT models are the U.S. Geological Survey (USGS)- derived Digital Elevation Model (DEM), STATSGO soil layer and land use/ cover data from National Land Cover Data (NLCD) 20011 (Homer et al., 2015). Weather data (precipitation and temperature) is obtained from the National Centers for Environmental Prediction (NCEP) Climate Forecast System Reanalysis (CFSR) data (Dile and Srinivasan, 2014; Fuka et al., 2013; Saha et al., 2010). CFSR provides a global, high-resolution coupled atmosphere–ocean–land surface–sea ice system to provide the best estimate of the state of these coupled domains for a period of 36 years from 1979 to 2013. One USGS station for each watershed is chosen for calibrating and validating the streamflow generated by the SWAT models (listed in Table 3-1). Figure 3-3 shows the land use and elevation maps and 50 USGS gage stations selected for the SAG region. The western part of SAG is a high elevation region bordered by Appalachia mountains and is predominantly forested region with low development and urbanization. The central and southern part of SEUS is dominated by woody wetlands, open spaces and cultivated crops. The southern tip of Florida is dotted with water bodies and wetlands with some area of cultivated crops and developed spaces.

4.3. Seasonal weather forecast data

CFSR has been extended as an operational, real-time product into the future which provides estimates of the atmospheric variables with a lead time of nine months and are initialized at multiple times a day, and, different days of a month (Table 3-2). Precipitation and temperature time series is obtained from CFSv2 data from 1st April 2011 through 19th Dec 2017 by using the

first output of CFSv2 models from 1st April 2011 through 12th March 2017 and 9-month forecast data is then obtained from the most recent initialization (12th March 2017 in this study). Figure 3-4 provides a schematic of data assimilation for the study. The red ellipse highlights the model run for each initialization which is used for SWAT model implementation with a total number of *K* initializations from 1st April through 12th Match 2017.

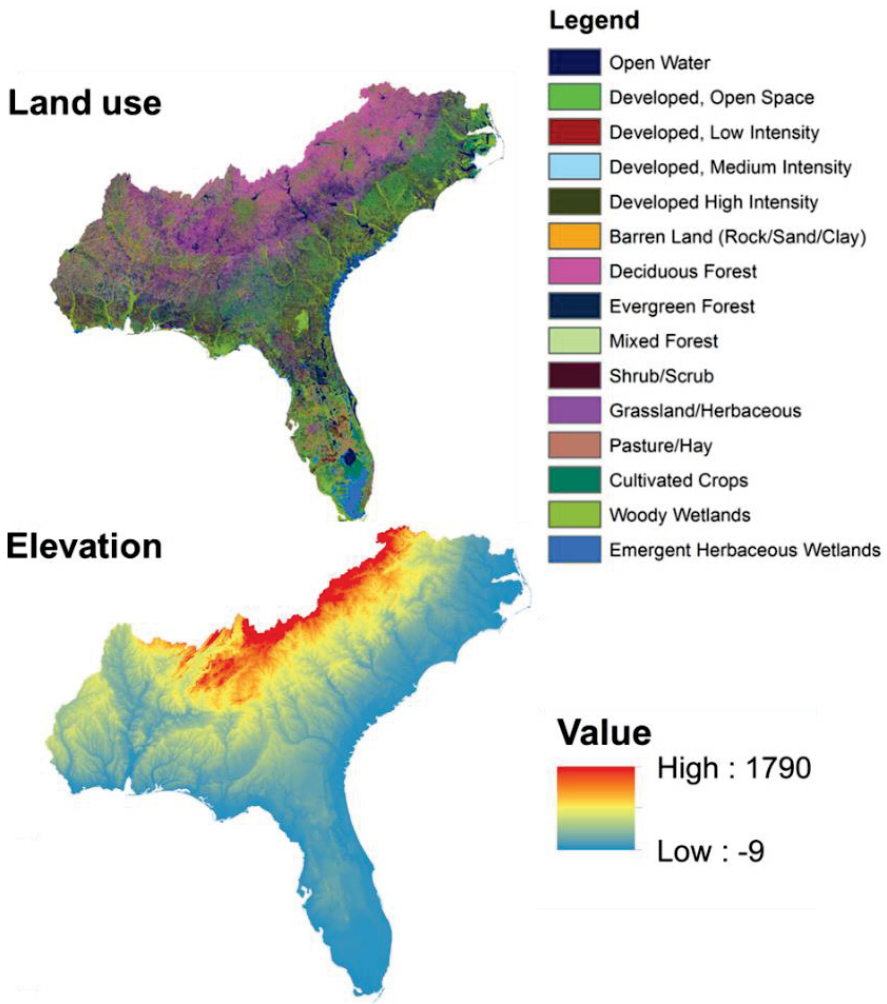

Figure 3-3: (Top) Land use map of the SAG region (NLCD 2011); (Bottom) Digital elevation map of the SAG region.

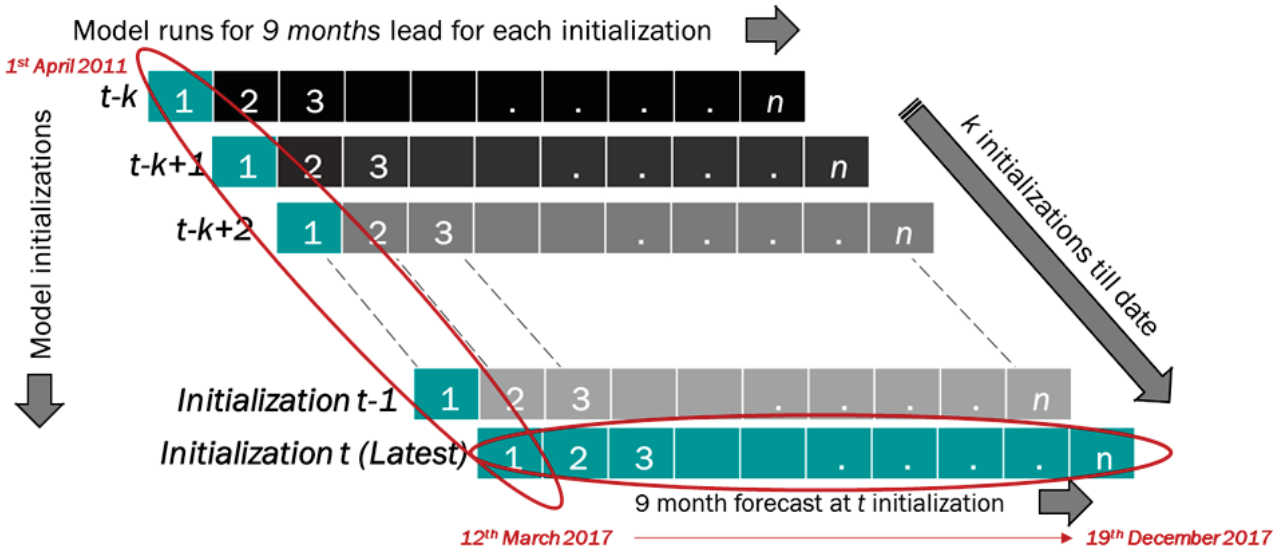

Figure 3-4 : Data assimilation scheme for precipitation and temperature from CFSv2 dataset.

Table 3-2: CFSv2 monthly ensembles with respective initial day of the month for four members initialized at 00Z, 06Z, 12Z, and 18Z. (McEvoy, 2015)

Initialization Month	Total Members	Initialization Days
January	28	1, 6, 11, 16, 21, 26, 31
February	20	5, 10, 15, 20, 25
March	24	2, 7, 12, 17, 22, 27
April	24	1, 6, 11, 16, 21, 26
May	28	1, 6, 11, 16, 21, 26, 31
June	24	5, 10, 15, 20, 25, 30
July	24	5, 10, 15, 20, 25, 30
August	24	4, 9, 14, 19, 24, 29
September	24	3, 8, 13, 18, 23, 28
October	24	3, 8, 13, 18, 23, 28
November	24	2, 7, 12, 17, 22, 27
December	24	2, 7, 12, 17, 22, 27

5. Model development and calibration

5.1. Modeling framework

SWAT models are calibrated for a period of 2003 through 2010 with three years of warm-up period (2000 through 2002) and are validated for a period of 2011 through 2013. The ArcSWAT 2010 interface is used to setup and parameterize the models. Sequential Uncertainty Fitting-2 algorithm (Abbaspour et al., 1997; Abbaspour et al., 2004; Abbaspour et al., 2015) is used to calibrate model parameters for each watershed using SWAT-CUP (calibration/uncertainty or sensitivity program) interface for SWAT. This optimization method calibrates the parameters to achieve best fitness and to the maximum degree to account for the uncertainty between the simulated and the measured data (Jin and Sridhar, 2012). The project was built on a desktop with a 64-bit operating system, 8-core CPU, with 32 GB of RAM and 3.2 GHz processor. The parallel processing routine (Rouholahnejad et al., 2012) available with SUFI-2 is used while simulating 1000 iterations for each watershed. Once the calibrated parameters are obtained from SWAT-CUP, a MATLAB based script is written to update SWAT input- output files and run the SWAT models with calibrated parameters for the validation period and back-run SWAT models for a period of Jan 1982 through Dec 2013 with three years of warm- up period (1979 through 1981) to obtain long term hydrologic variables for this study.

5.2. Calibration of SWAT models using Sequential Uncertainty Fitting (SUFI)-2 algorithm

A set of 24 parameters are chosen for calibration to address various hydrologic components of watershed like surface runoff (Curve number, soil and plant evaporation, surface runoff and Manning's coefficient, and available soil water capacity etc.), baseflow (Groundwater "revap",

aquifer – soil interaction, depth of water in the shallow aquifer, time for water leaving the root zone to reach the shallow aquifer, deep aquifer percolation), storm water (Channel hydraulic conductivity, stormflow lag time etc.), snow (snowmelt rate, snow temperature etc.) etc. The choice and effect of these parameters are very well documented in SWAT literature (Abbaspour et al., 2015; Arnold et al., 2012; Feyereisen et al., 2007; Jin and Sridhar, 2012; Kang et al., 2016; Liu et al., 2008; Sommerlot et al., 2016; Uniyal et al., 2015; Van Liew et al., 2005; Wang et al., 2008) and the selected parameters are consistent with the aforementioned studies. List of the twenty- four parameters selected for this study is provided in Table 3-3. The selected set of 24 parameters is kept consistent for all watersheds modeled in this study to achieve a trade-off between sensitivity analysis for each watershed to a given set of calibration parameters (computationally expensive and time taking process) and obtaining reasonable performance for the entire SAG region. However, with special regard to variable landscape of the study region, the parameters are carefully selected to address to both riparian watershed hydrology (Liu et al., 2008; Martinez-Martinez et al., 2014; Wang et al., 2008) and inland basin characteristics. It is observed that while the values of these parameters varied for each watershed (Figure 3-5), the overall performance of the models for all 50 outlets is found to be satisfactory with the given set of model parameters. Strong influence of land use, topography, soil type and other watershed scale characteristics can be seen on the spatial variability of these parameters. For e.g. predominantly forested areas show higher values for BIOMIX due to increased redistribution of soil constituents due to biota in the soil compared to wetlands or developed watersheds; HRU_SLP and OV_N values are higher for mountainous regions compared to plains and coastal areas; SLSUBBSN is found to be higher for coastal watersheds due to low gradient. Other important parameters like CN2, SOL AWC, ALPHA _BF, EPCO show significant spatial variability. A combination of these

factors determines the response of a watershed to precipitation and the resultant discharge and storage. For example, low ALPHA_BF numbers signify slow response to changing moisture conditions in the baseflow under no recharge to watershed, whereas higher CN2 numbers signify higher discharge for a given precipitation amount. Interaction with groundwater (GW_DELAY, GW_QMN and GW_REVAP) and runoff play major role in partitioning of incoming water in the watershed into runoff, soil and groundwater storage. A slow surface-aquifer interaction, coupled with high curve number, will lead to high values of discharge.

Table 3-3: Selected parameters for calibrating SWAT Models using Sequential Uncertainty Fitting 2 (SUFI2) Algorithm for daily discharge dataset from 1st Jan 2003 through 31st Dec 2010.

Class	Name	Description	Method	Min	Max
HRU	ESCO	Soil evaporation compensation factor (unitless)	Replace (v)	0	1
	CANMX	Maximum canopy index (mm)	Relative (r)	0	100
	EPCO	Plant evaporation compensation factor (unitless)	Relative (r)	0	1
	HRU_SLP	Average slope steepness (mm/ mm)	Relative (r)	0	1
	OV_N	Manning's "*n*" value for overland flow	Replace (v)	0.01	30
	SLSUBBSN	Average slope length (m)	Relative (r)	10	150
MGT	CN2	Initial SCS curve number for moisture condition II (unitless)	Relative (r)	35	98
	BIOMIX	Biological mixing efficiency (unitless)	Relative (r)	0	1
SOL	SOL_AWC	Available water capacity of the soil layer (mm⁄ mm)	Relative (r)	0	1
	SOL_BD	Moist bulk density (Mg/ m^3 org/cm^3)	Replace (v)	0.9	2.5
BSN	SMTMP	Snowmelt base temperature (° C)	Relative (r)	-20	20
	SMFMN	Melt factor for snow on Dec 21 (mm H_2O/ °C-day)	Relative (r)	0	20
	SMFMX	Melt factor for snow on June 21 (mm H_2O/ °C-day)	Relative (r)	0	20
	MSK_CO1	Calibration coefficient used to control the impact of storage time constant (K_m) of normal flow upon when K_m is calculated for the reach	Relative (r)	0	10
	MSK_CO2	Same as above, but for low flows	Relative (r)	0	10
	SURLAG	Surface runoff lag coefficient	Replace (v)	0.05	24
GW	GWQMN	Threshold depth of water in the shallow aquifer required for return flow to occur (mm)	Replace (v)	0	5000
	GW_REVAP	Groundwater revaporation coefficient (unitless)	Replace (v)	0.02	0.2
	GW_DELAY	Groundwater delay (days)	Replace (v)	0	500
	ALPHA_BF	Base flow alpha factor (days)	Replace (v)	0	1
	RCHRG_DP	Groundwater recharge to deep aquifer (fraction)	Relative (r)	0	1
	REVAPMN	Threshold depth of water in the shallow aquifer for revaporation to occur (mm)	Relative (r)	0	500
RTE	CH_N2	Manning coefficient for channel (unitless)	Replace (v)	-0.01	0.3
	CH_K2	Effective channel hydraulic conductivity (mm⁄h)	Replace (v)	-0.01	500

5.3.Hydrologic simulations using CFSv2 coupled calibrated SWAT models

The calibrated SWAT models are coupled with the drivers from CFSv2 from April' 2011 through December' 2017 with a warm-up period of 3 years thus providing simulation outputs from January' 2014 through December' 2017. Combining the retrospective model simulations from CFSR coupled SWAT models and the CFSv2 coupled SWAT models, a seamless daily simulation outputs are obtained from January' 1982 through December' 2017. A schematic of the entire model setup is provided in Figure 3-6. SWAT-CFSv2 model outputs (soil water, evapotranspiration, potential evapotranspiration, surface runoff, watershed precipitation etc.) for the period April through March' 2017 are obtained in near-real time mode since the input meteorological data is taken from the first CFSv2 model runs whereas SWAT-CFSv2 output data from March through December' 2017 are the forecasted model outputs.

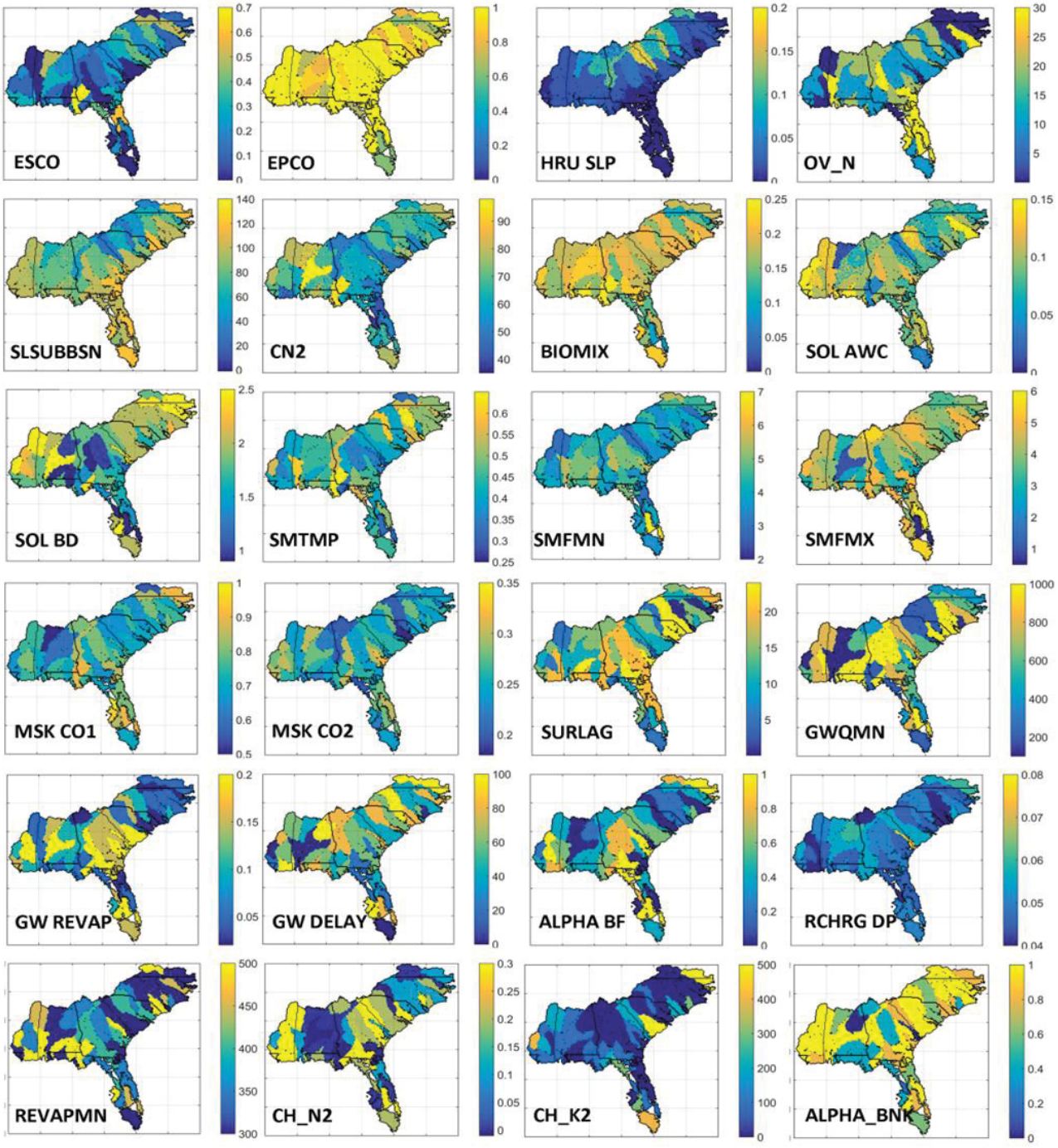

Figure 3-5: Spatial maps of SWAT parameters calibrated using SUFI- 2 algorithm

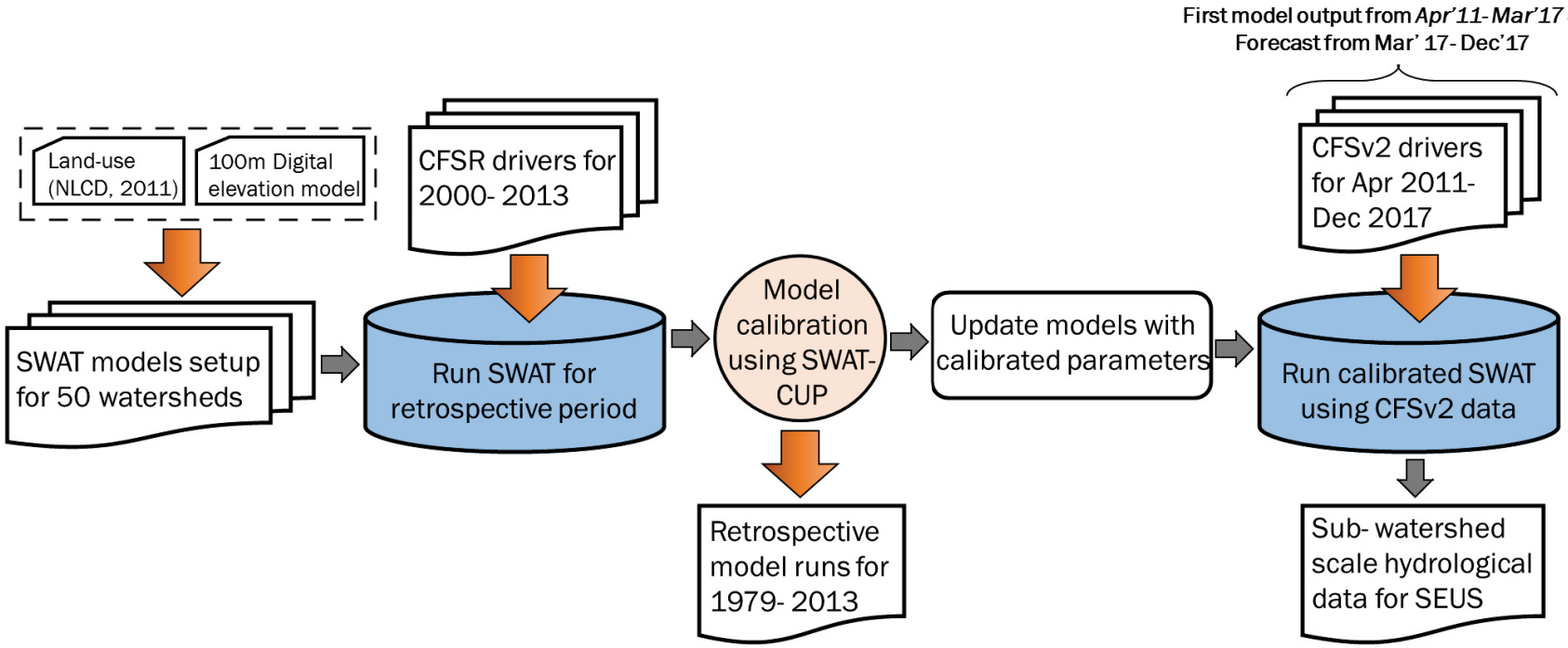

Figure 3-6: Schematic for conceptual framework of forecasting hydrologic variables using CFSv2 dataset in conjunction with SWAT models for the South-Atlantic gulf region.

6. Performance evaluation of model outputs

6.1. Performance evaluation of SWAT models

6.1.1. Streamflow validation

The performance assessment of SWAT models is carried out by comparing the SWAT-simulated discharge at the selected outlet with the observed discharge data from the USGS stations using five statistical performance indices, namely, Coefficient of determination (R^2), Nash Sutcliffe Efficiency (NSE), Normalized mean absolute error (NMAE), Normalized Root mean square error (NRMSE) and Willmott's Index (WI) (Willmott et al., 2012; Willmott et al., 2015). NMAE and NRMSE are normalized values of MAE and RMSE to a range of [0, 1] to facilitate easy comparison of model performance across stations for different watersheds. Figure 3-7 shows the time series of observed and SWAT simulated streamflow for four select watersheds for the calibration (January' 2000-December' 2010) and validation periods (January' 2011- December' 2013). Similar comparison hydrographs for all watersheds are provided in Appendix for the benefit of the readers. It can be observed from Figure 3-7 that the simulated discharge is able to capture the seasonal and annual variations in the daily streamflow dataset. However, the simulated and observed values have some disagreement leading to comparatively lower values some watersheds (Example, Pearl watershed). However, these values of performance indices are considered satisfactorily for two reasons: *(i)* the values of simulated hydrological variables like runoff, soil water, evapotranspiration etc. are aggregated to weekly (or monthly) means for drought analysis, which helps in improving the agreement between the simulated and observed hydrologic variables and *(ii)* Soil moisture tends to have higher persistence (memory) compared to the streamflow values and hence, it is assumed that the accuracy of the watershed scale models in capturing soil moisture variability should be satisfactorily higher.

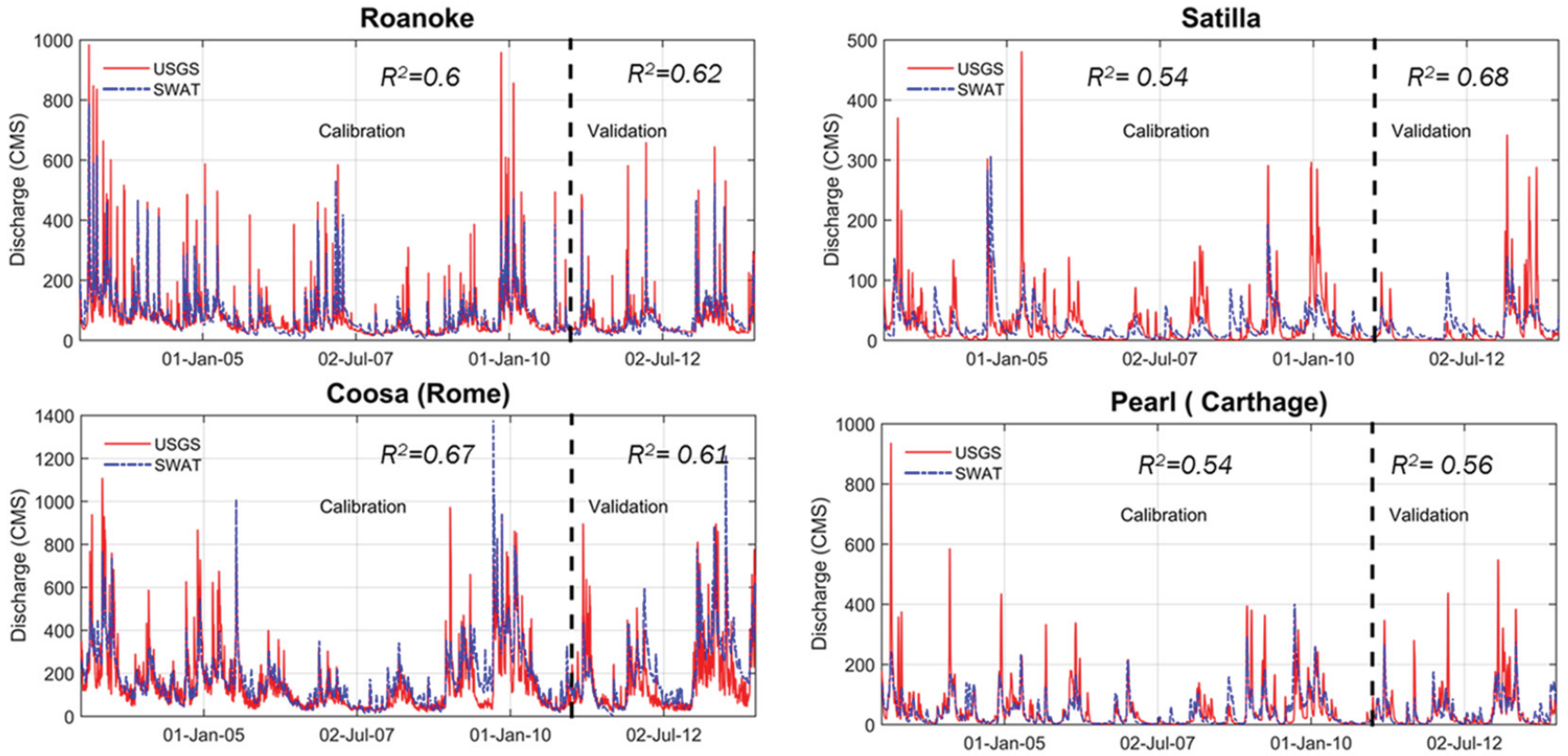

Figure 3-7: Observed v/s daily discharge time series at the outlet for four some selected watersheds. The dotted black line in the plots demarcates calibration period (Jan 2003- Dec 2010) from validation period (Jan 2011- Dec 2013). Similar plots for the rest of the watersheds can be found in the Appendix of this paper.

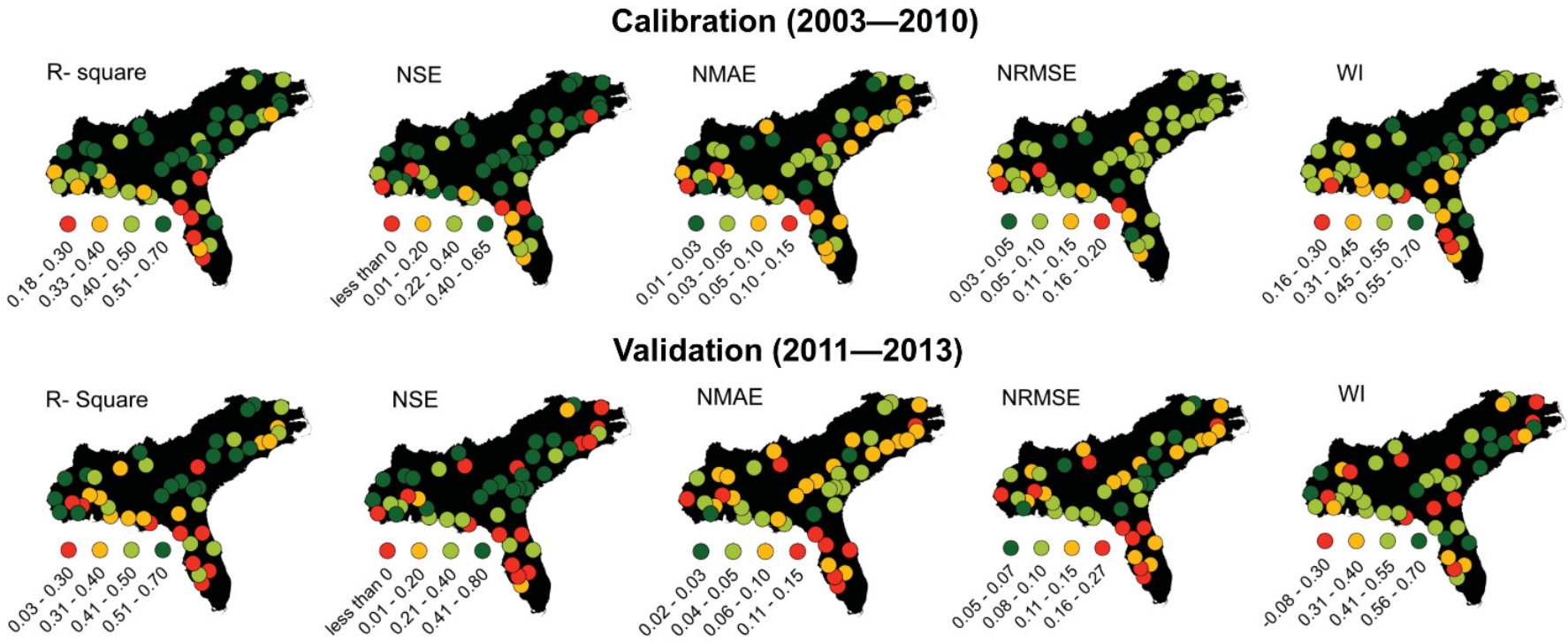

Figure 3-8: Values of the statistical performance indices for the 50 USGS streamflow gaging stations selected for this study for Calibration (2003- 2010) and Validation (2011- 2013) period.

(Statistical indices are defined as: $\boldsymbol{R^2} = \frac{\sum_{i=1}^{n}(\boldsymbol{Oi}-\bar{\boldsymbol{O}})(\boldsymbol{Pi}-\bar{\boldsymbol{P}})}{\sqrt{\sum_{i=1}^{n}(\boldsymbol{Oi}-\bar{\boldsymbol{O}})^2}\sqrt{\sum_{i=1}^{n}(\boldsymbol{Pi}-\bar{\boldsymbol{P}})^2}}, \boldsymbol{NSE} = \boldsymbol{1} - \frac{\sum_{i=1}^{n}(\boldsymbol{Oi}-\boldsymbol{Pi})^2}{\sum_{i=1}^{n}(\boldsymbol{Oi}-\bar{\boldsymbol{Oi}})^2}, \boldsymbol{NMAE} = \frac{\frac{1}{n}\sum_{i=1}^{n}|\boldsymbol{Oi}-\boldsymbol{Pi}|}{(\boldsymbol{Max}\,(\boldsymbol{O})-\boldsymbol{Min}\,(\boldsymbol{O}))}, \boldsymbol{NRMSE} = \frac{\sqrt{\frac{1}{n}\sum_{i-1}^{n}(\boldsymbol{Oi}-\boldsymbol{Pi})^2}}{(\boldsymbol{Max}(\boldsymbol{O})-\boldsymbol{Min}\,(\boldsymbol{O}))}, \boldsymbol{WI} = \boldsymbol{1} - \frac{\sum_{i=1}^{n}[(\boldsymbol{Pi}-\bar{\boldsymbol{O}})-(\boldsymbol{Oi}-\bar{\boldsymbol{O}})]2}{\sum_{i=1}^{n}(|(\boldsymbol{Pi}-\bar{\boldsymbol{O}})|+|(\boldsymbol{Oi}-\bar{\boldsymbol{O}})|)^2}$ (Willmott et al., 2012) where O_i and Pi are the observed and estimated discharge time series and n is the number of data points)

Figure 3-8 provides a spatial visualization of the performance of the SWAT models in simulating stream discharge for the 50 selected outlet points, one for each watershed. It can be observed from Figure 3-8 that while SWAT models perform satisfactorily for inland watersheds, the performance of the models is relatively week in the coastal wetlands especially in the Floridian peninsula. Some of the outlet stations in the coastal lowlands are strongly effected by tides which leads to a significant secondary oscillation of about two weeks' period because of the way the 24.84-hour tidal cycle (a different portion of the dataset) is averaged in successive daily computations of the observed (USGS). Since these oscillations are unrelated to the basin hydrology, the model is not able to capture the hydrologic variability of the effected watersheds. Extensive basin management and regulated streamflow can also impact stream discharge values. A combination of these factors causes deviation of SWAT simulated values from the observed dataset. However, the performance of the models for the rest of the SAG region is assessed to be satisfactory. Figure 3-9 shows the distribution of the performance indices for the 50 watersheds. SWAT models performed satisfactorily for majority watersheds with R^2 and NSE > 0.4, NMAE <0.2, NRMSE <0.1, and WI> 0.4 for daily discharge simulation.

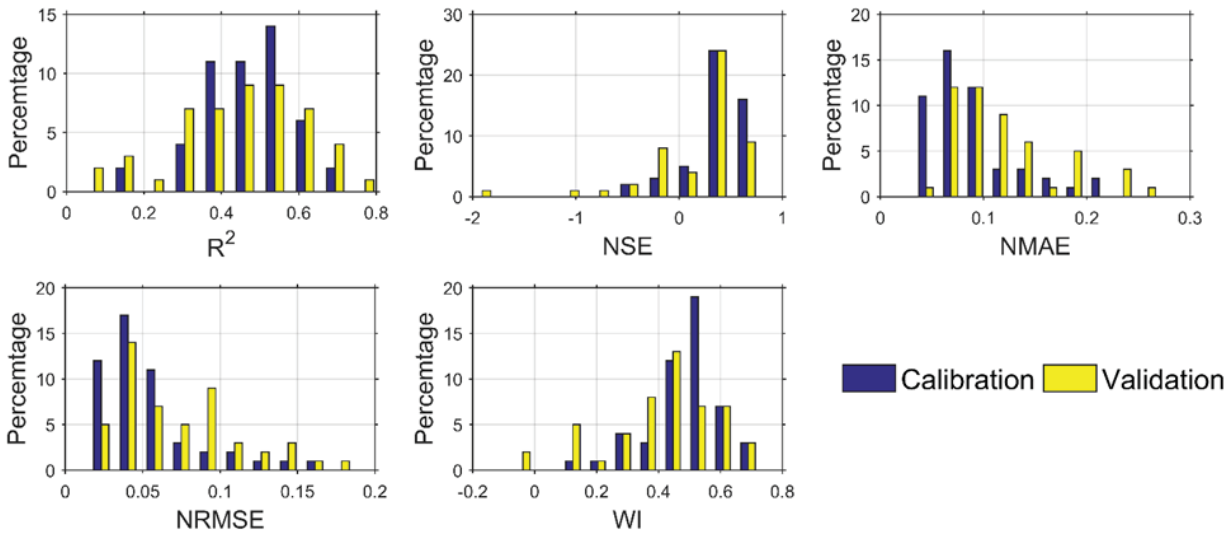

Figure 3-9: Histograms comparing statistical performance indices for all 50 watersheds for calibration and validation period.

6.1.2. Validation of soil moisture data

In-situ soil moisture observations from the US Climate reference network (USCRN) (Bell et al., 2013) database is used to validate the sub-watershed scale (HUC-12) soil moisture simulations from the SWAT models at daily temporal resolution. USCRN is a network of climate monitoring stations operated by the National Oceanic and Atmospheric Administration (NOAA). The volumetric soil moisture observations are available for five standard soil depths i.e. 5 cm, 10 cm, 20 cm, 50 cm and 100 cm at daily and hourly time step (also sub-hourly time step for 5 cm layer). Out of a total of 114 stations operating in the continental United States, 9 stations fall within the study region and are used for obtaining the *in-situ* soil moisture observations. Figure 3-10(a) provides geographic locations of the USCRN stations selected for this study. Figure 3-10(b) provides the SM time series from 5 depths for one of the USCRN stations in the study area.

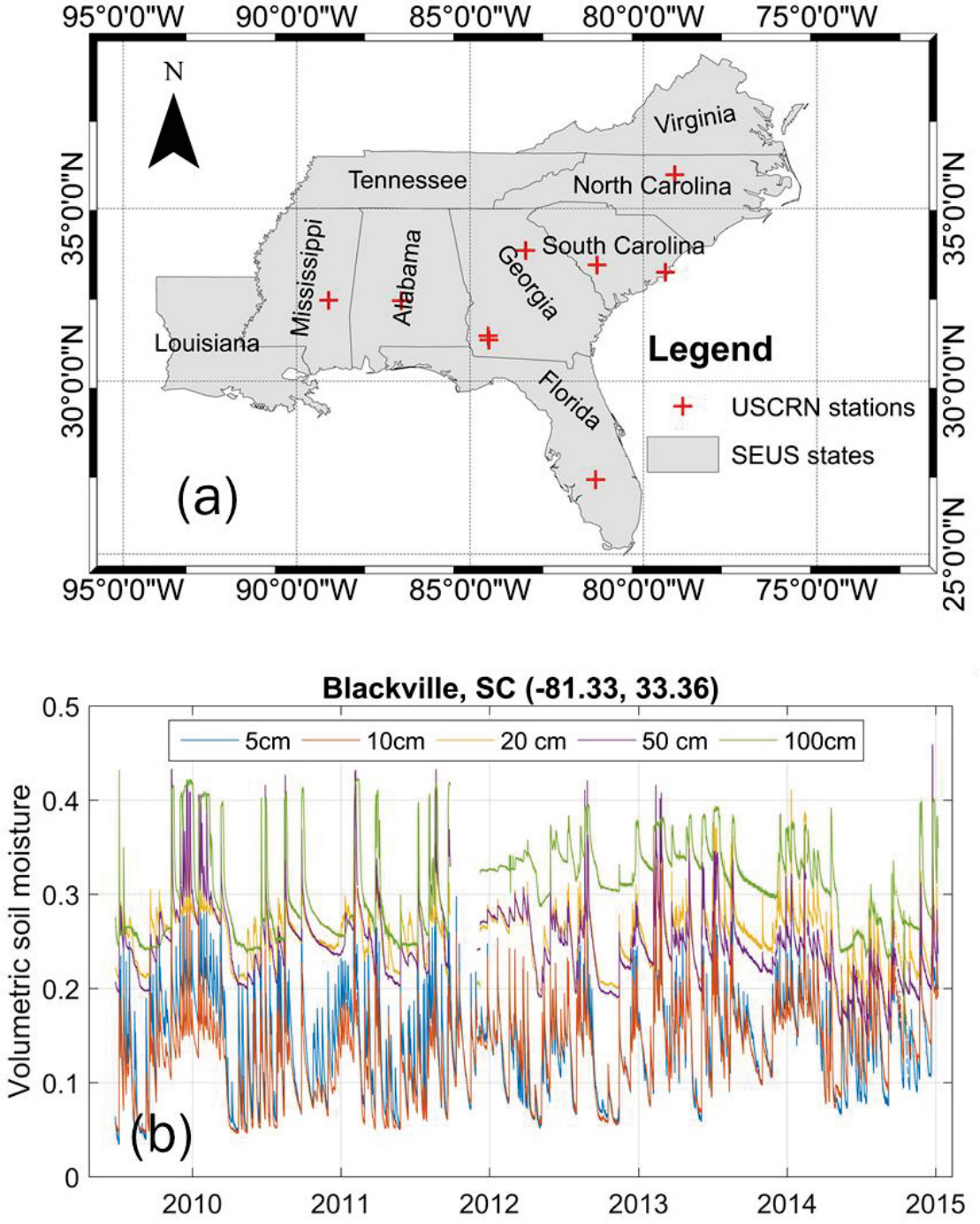

Figure 3-10 : (a) Selected U.S. Climate Reference Network *in-situ* soil moisture observation stations. (b) Time series of soil moisture from 5 sensors at 5 cm, 10 cm, 20 cm, 50 cm and 100 cm depth from the surface from an observation station in Blackville, North Carolina.

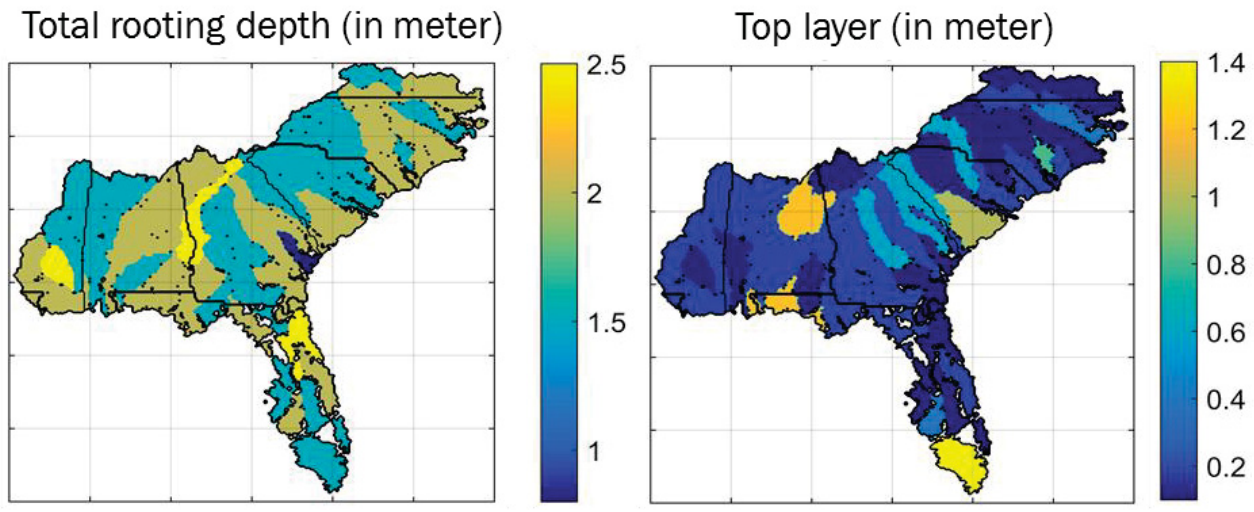

Figure 3-11: Spatially varying depth of the two soil profiles: (Left) Total rooting depth and (Right) Top (surface) layer.

SWAT simulated sub-watershed scale soil water content for two profiles, namely, the Top (surface) layer and, total rooting depth, is compared with the 5 cm and 50 cm sensor data to ascertain the accuracy of soil moisture simulations from SWAT. The soil profiles have spatially varying depth which can be observed in Figure 3-11. The missing values in the *in-situ* data are ignored and only the available values for the corresponding days are compared in the evaluation. Figure 3-12 provides a comparison of the observed (volumetric content, mm/mm) and SWAT simulated soil moisture (soil water content, in mm) values for the two sets of soil profiles and sensor depth. The values are standardized to [0,1] for ease in comparison. Strong seasonality is evident from the plots where soil moisture values can be observed to fall in the summer months and restore in the winter months. However strong local characteristics also influence soil moisture variability esp. at the fine scale of comparison (HUC-12 simulated SM with the observed data) used in the analysis. Hence, while Durham, NC and Newton (SW) stations showed consistency in seasonal and annual variability, McClellanville (SC) and Selma (Al) showed less interannual and

seasonal variability. Correlation between the observed and corresponding sub-watershed scale soil moisture is provided in Figure 3-13. It can be inferred from Figure 3-12 and Figure 3-13 that the correlation values differ within stations as well as within the two soil profiles compared. As discussed previously in this section, the model performance is comparatively low for certain watersheds in the coastal wetlands in Florida which is evident by the low correlation values between observed and simulated soil moisture values for the total rooting depth for the USCRN station in Sebring, Florida. However, the overall performance of the SWAT models to simulate the soil moisture for the two profiles if found to be satisfactory. Overall, the annual and seasonal variability in the soil moisture is well captured by the models. It is to be noted that the comparison is being made between the point location (station) based soil moisture observations with the sub-watershed scale area averaged soil moisture values. This may lead to some discrepancies between the observed versus simulated dataset. However, the primary objective of this inter-comparison is to test the ability of the models in capturing seasonal, sub-seasonal and annual variability of the sub-watershed scale soil moisture, which can be supported based on Figure 3-12.

7. Results and discussion

7.1. Water balance analysis for South-Atlantic Gulf region

This study follows Sridhar and Hubbard (2009) and Singh et al. (2004) in studying the water balance of the study region. The fundamental water balance equation can be expressed as:

$$\frac{\partial S}{\partial t} = P + I - ET - R - D \quad (1)$$

where, S= soil water in the root zone (mm); t=time (day); P = precipitation (mm/day); I=irrigation (mm/day); ET= actual evapotranspiration (mm/day); R= runoff (mm/day); and D= drainage below the root zone (mm/day).

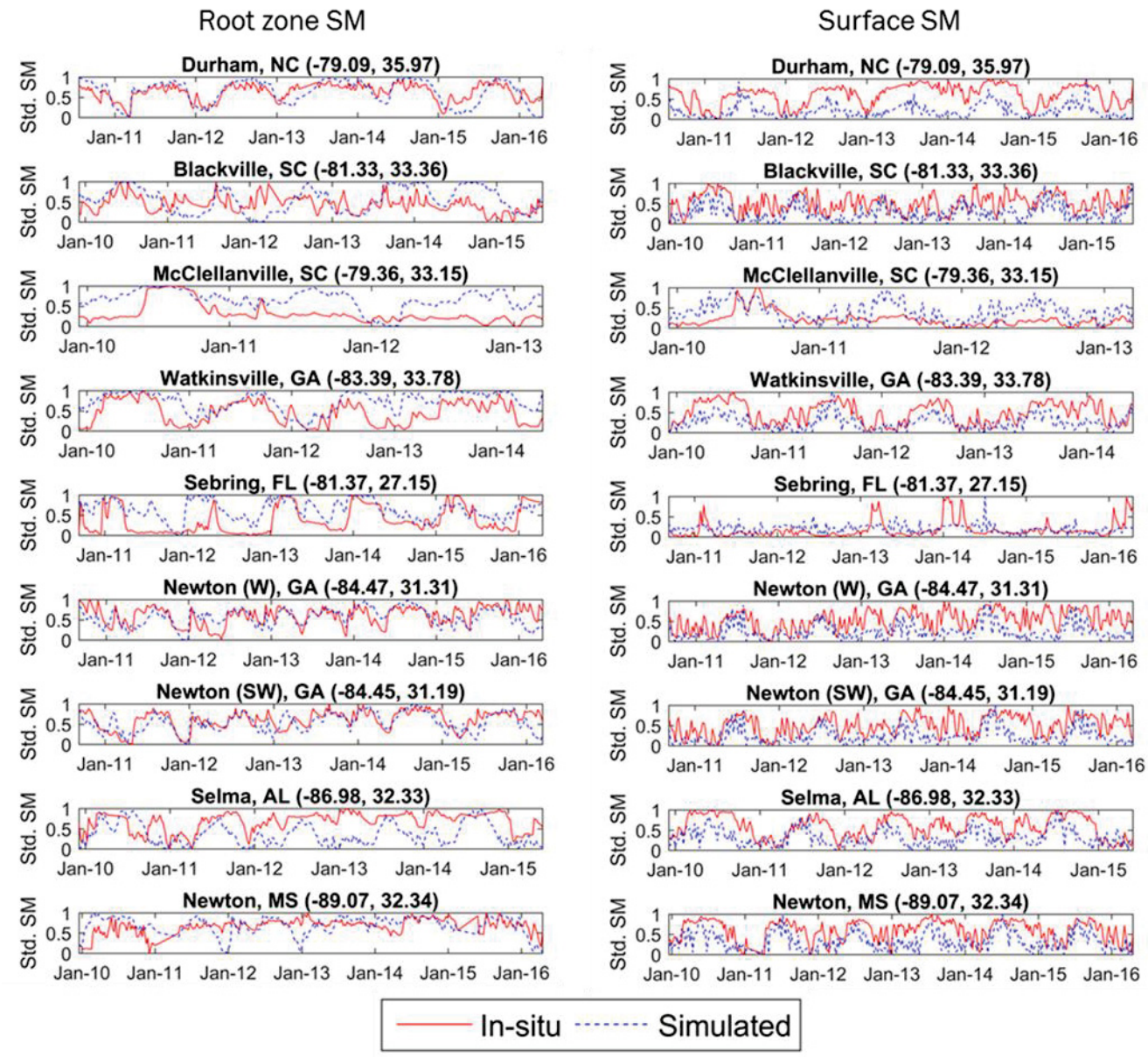

Figure 3-12 : Comparison of observed (*in-situ*) volumetric soil moisture and corresponding sub-watershed (HUC-12) SWAT simulated water content for the two (top and total rooting depth) soil profiles. Please note that the values are standardized for ease in comparison.

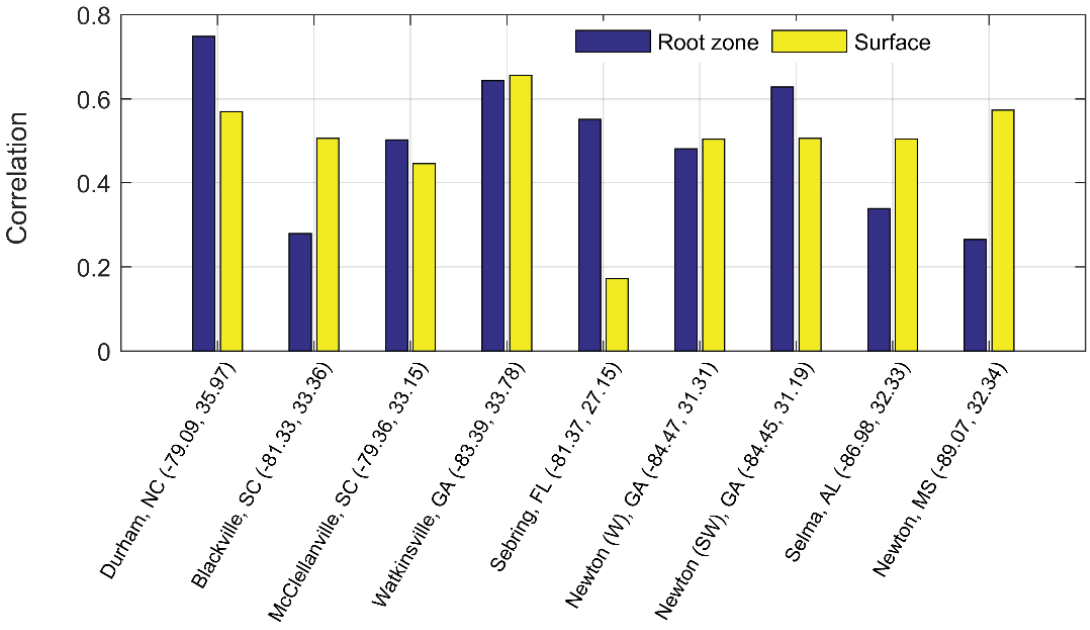

Figure 3-13: Correlation between the observed (*in-situ*) volumetric soil moisture and corresponding sub-watershed (HUC-12) SWAT simulated water content for the two (top and total rooting depth) soil profiles.

The daily estimates of water balance components for each watershed are added to the monthly totals and subsequently used to estimate the routine monthly water balance components for each watershed. Change in soil water storage ΔSW is calculated by subtracting the storage of the previous month from the current month's storage.

$$\Delta SW = SW_i - SW_{i-1} \quad (2)$$

The actual ET (ET) is computed for each month using the change in precipitation and soil water storage.

$$\left.\begin{array}{ll} ET = R - \Delta SW & if\ \Delta SW \leq 0 \\ ET = R + \Delta SW & if\ \Delta SW > 0 \\ ET = PET & if\ \Delta SW > 0 \end{array}\right\} \quad (3)$$

The difference between precipitation (P) and potential ET (PET) i.e. ($P - PET$) is used to calculate water deficit. Surplus water is estimated by subtracting ET from the sum of soil storage and precipitation.

$$\left.\begin{array}{l} Deficit = PET - ET \\ Surplus = P + \Delta SW - ET \end{array}\right\} \quad (4)$$

A positive change in storage indicates availability of additional soil water beyond the soil column storage for ET or drainage. When soil water storage beyond the root zone can be adequate, it is reasonable to assume that plant transpiration can occur at the potential rate (Sridhar and Hubbard, 2009).

Figure 3-14 shows the monthly water budget for the 50 watersheds in the study, summarized in the form of a box plot. Most watersheds in the study region receive precipitation during summer (June- August). With high temperatures and available moisture, precipitation in summer rises to its peak value in summers. Soil water remains relatively consistent in the region with a minor dip during summer months. High temperatures during April through August leads to higher PET compared to ET, thus causing water deficit conditions. Water surplus condition is attained with

incoming precipitation in summer months and subsequent fall in temperature in late spring and fall seasons. Figure 3-15 provides water budget plots for two select watersheds namely Roanoke and Pearl river. Differences in the water budget for the two watersheds is evident from Figure 3-15 and is primarily driven by the climatology of these watersheds. Roanoke watershed receives precipitation of around 100 mm throughout the year. Increasing temperatures in summer leads to fall in soil water storage. However, low temperatures in late fall and winters help bring soil water back to values above 150 mm. Pearl river falls receives highest rainfall in summer months (June-August) and is often affected by the tropical cyclones. Soil water for the watershed consistently remains higher than 150 mm. High summer temperatures and moisture availability fuels high evapotranspiration in the watershed, especially during summers. Since Figure 3-14 and Figure 3-15 are not indicative of the spatial variability in the water budget for the entire SAG region, Figure 3-16 provides a spatial representation of the variation in four water budget components along with the state of excess water and water deficit for the SAG region. Spatial variability in different water budget components is evident from Figure 3-16 and is reflective of the hydroclimatology of the region. It can be observed from Figure 3-16(c) that Georgia, Alabama, the Carolinas face water deficit in the growing season (April- June). This makes the region more sensitive to water management practices and more vulnerable to droughts.

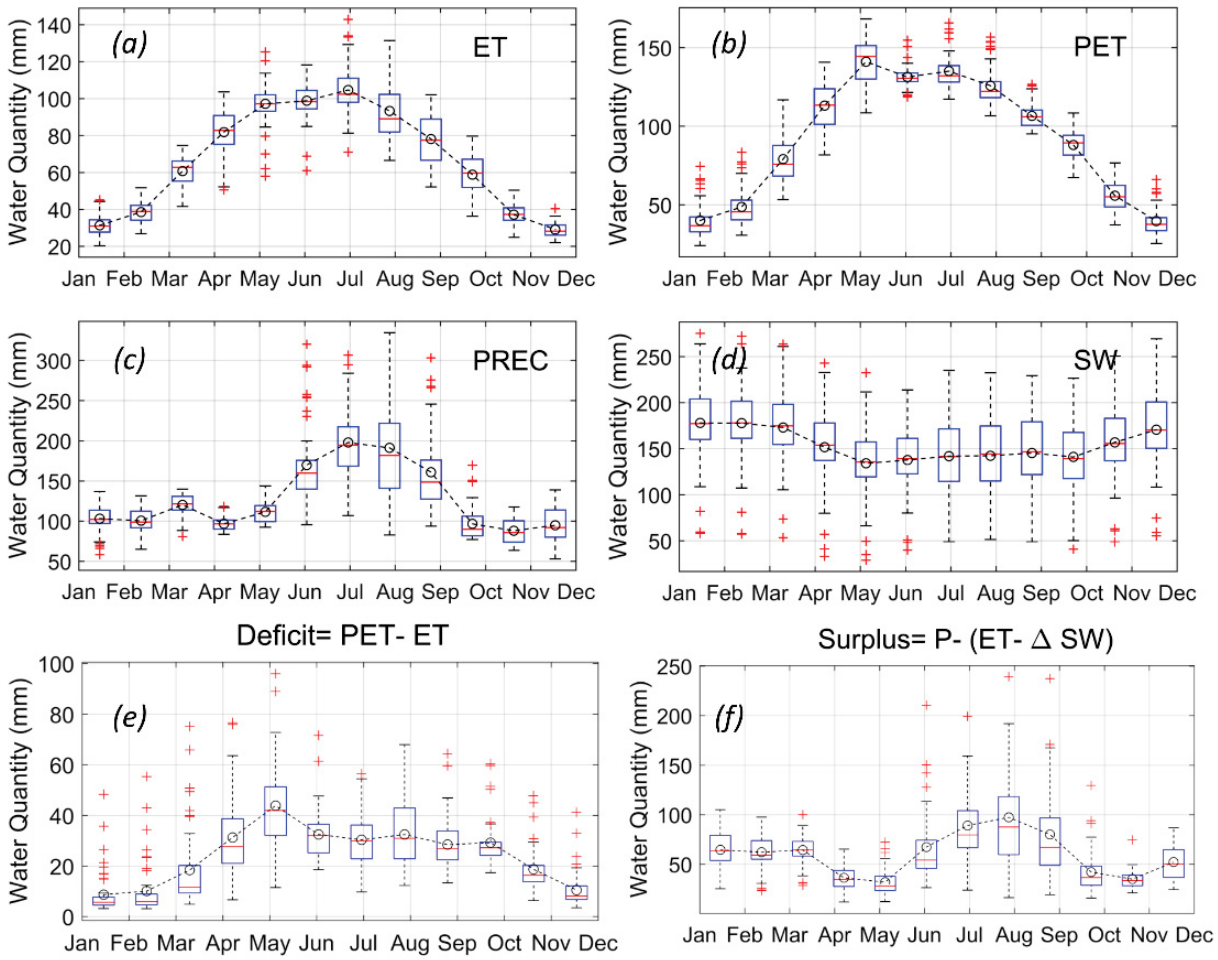

Figure 3-14: (a)- (d) Box plots for the monthly water budget components for the 50 watersheds in the study area (e-f) Box plots for monthly water deficit and surplus for the 50 watersheds.

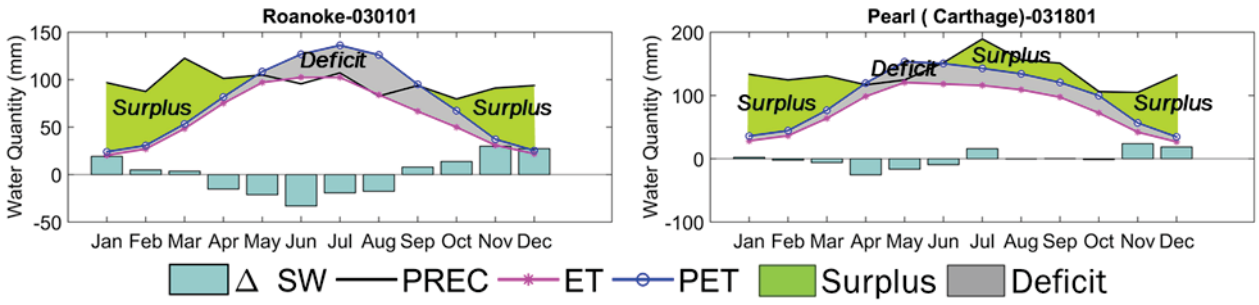

Figure 3-15: Monthly water budget components for the Roanoke and Pearl River watersheds. Water surplus and deficit conditions are shown with green and gray shade, respectively.

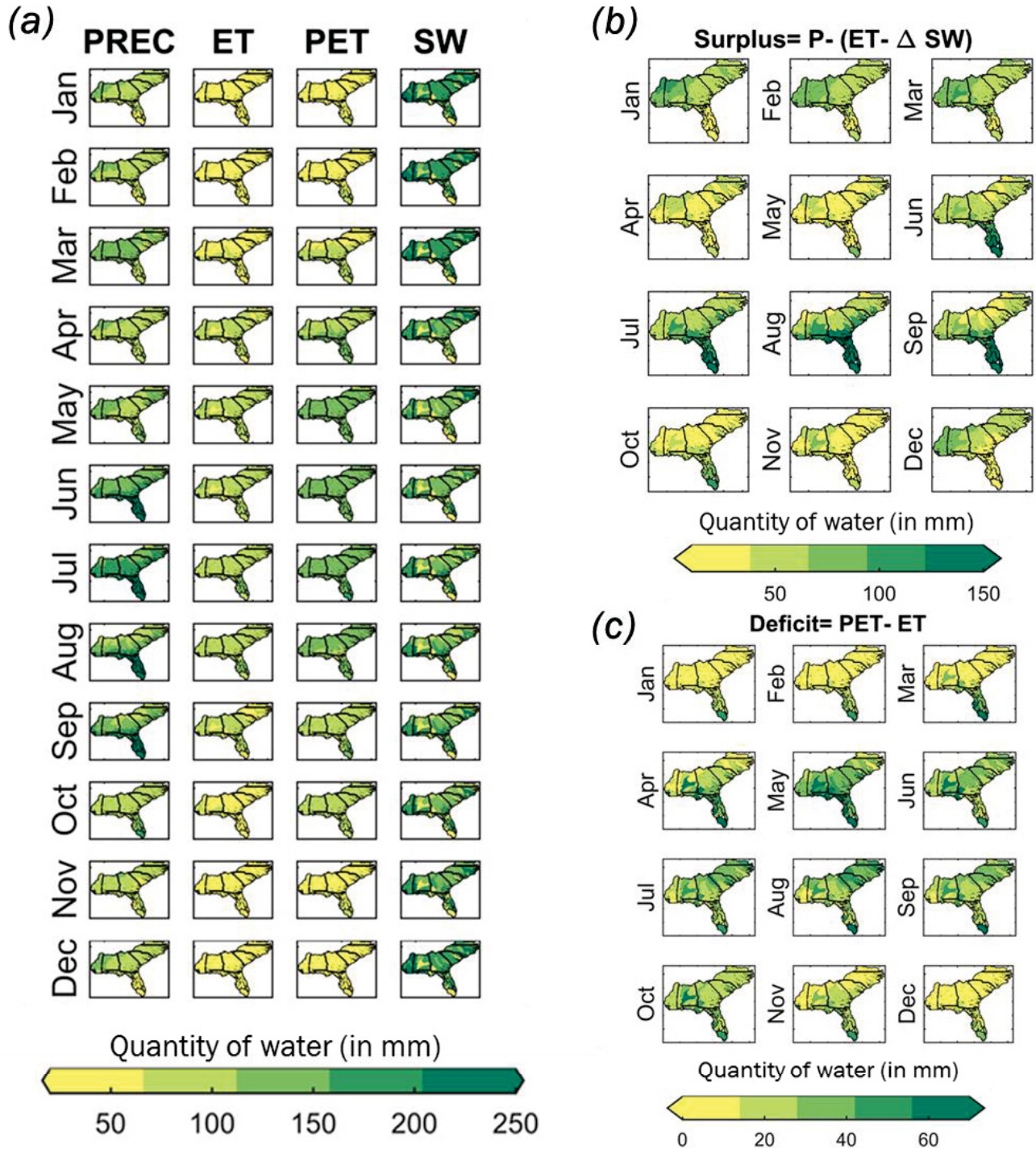

Figure 3-16: Spatial representation of the monthly Water (a) budget (b) surplus and (c) deficit for the SAG region. Deeper shades of green represent higher quantity of water.

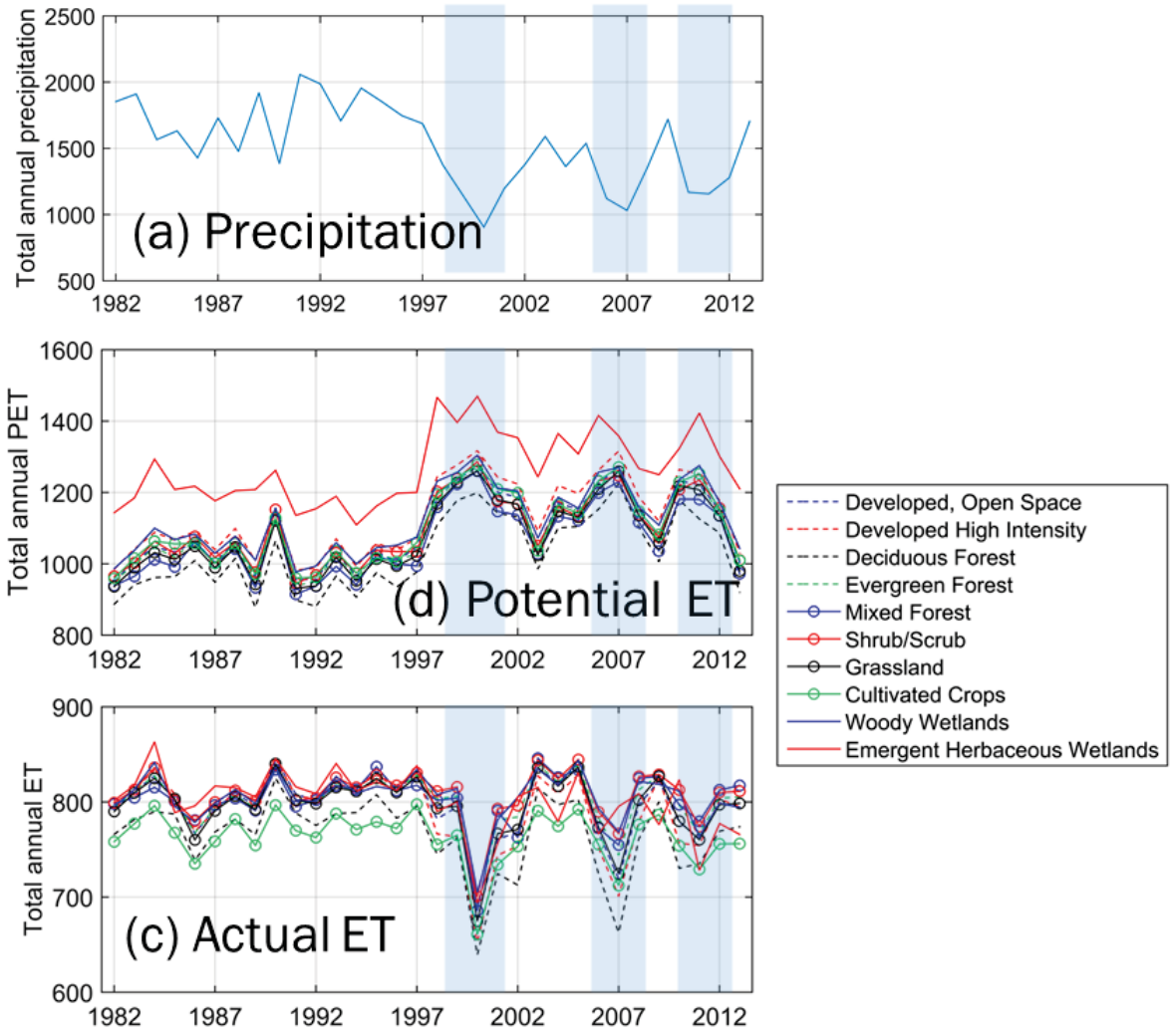

Figure 3-17: Area averaged total annual values for (a) Precipitation, (b) Soil water content, for the entire SAG region and, Area averaged total annual values for (c) Actual ET and (d) Potential ET (PET) based on the land use type. Light blue shade indicates severe drought years.

ET can display significant spatial variability based on vegetation (canopy, vegetation type), topography, local environmental conditions, water supply etc. (Liu et al., 2010; Zhang et al., 2001; Zhu et al., 2010). Hence, an analysis is carried out to highlight this variability in ET and PET estimates from the SWAT models based on the land use. Figure 3-17 provides a comparison of the actual ET and PET values (annual sum) averaged over the land use type as defined by NLCD,

2011. There is clear distinction in the PET and ET values for the different land use types. While the energy and water rich area have higher PET, ET is seen to be highest over the water bodies and wetlands due to abundance of water, closely followed by barren land, shrubs and grass lands. ET and PET follow a complimentary relationship due to the land–atmosphere feedback mechanism which is well studied in literature (Huntington et al., 2011; Jaksa et al., 2013), where PET decreases with the available moisture in the near-surface boundary layer because of increases in actual ET and was first proposed by Bouchet (1963). The complimentary relationship between the SWAT simulated ET and PET values (annual total) for various land-use types is shown in Figure 3-18. The effect of land use is evident from Figure 3-18 where while most land types show good agreement with the complimentary relationship, wetlands and cultivated land types show relatively lower agreement to the complimentary relationship between PET and ET. Due to saturated soil conditions, ET tends to have low variability over seasons and hence the convergence of PET and ET doesn't take place. Similarly, the effect of anthropogenic activities can be seen on PET- ET partitioning in developed regions while forested areas show better convergence of PET and ET.

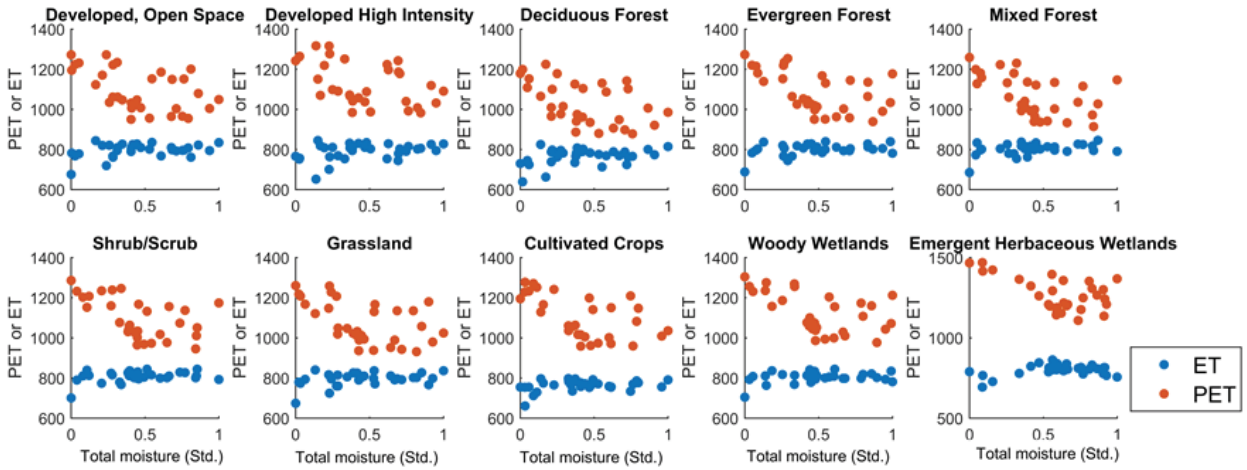

Figure 3-18: Complimentary relationship between ET act and PET based on total annual values for various land use classes.

7.2. Hydrological forecasts for South-Atlantic Gulf region using CFSv2 coupled SWAT models

Figure 3-19 shows the area-averaged values of PREC, ET, PET and SW using CFSv2 coupled SWAT models from January 2014 through December 2017. The effect of the drought in the region can be clearly observed from Figure 3-19 for the year 2016 where high PET, low soil moisture and precipitation lead to severe drought in the SEUS. A similar condition is expected to be observed in July and August' 2017 with relief due to forecasted precipitation in the region in later part of the year. Spatial maps of the forecasted values of PREC, PET, ET and SW is provided in Figure 3-20. The spatial variability in the hydrologic variables is evident from Figure 3-20 which is strongly influenced by seasonality and hydroclimatology.

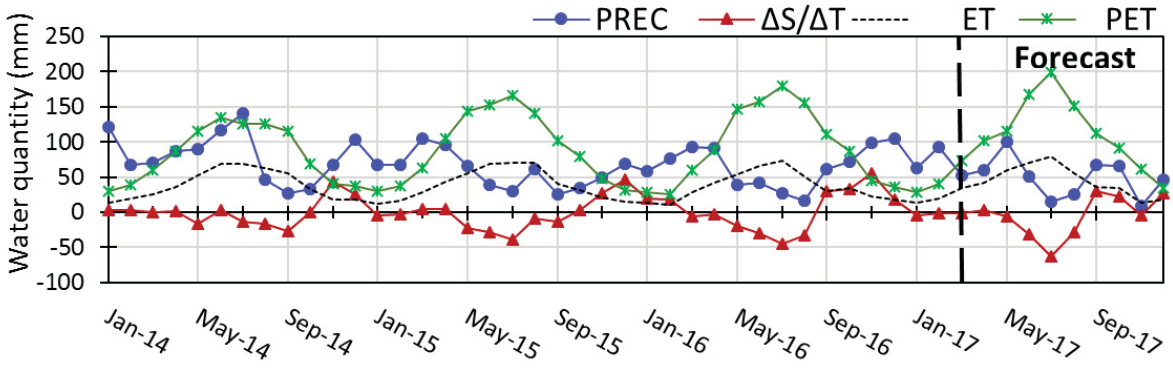

Figure 3-19: Area averaged values of mean monthly Precipitation (PREC), Actual Evaporation (ET), Potential Evapotranspiration (PET) and change in soil water storage ($\Delta S/\Delta T$) for the SAG region.

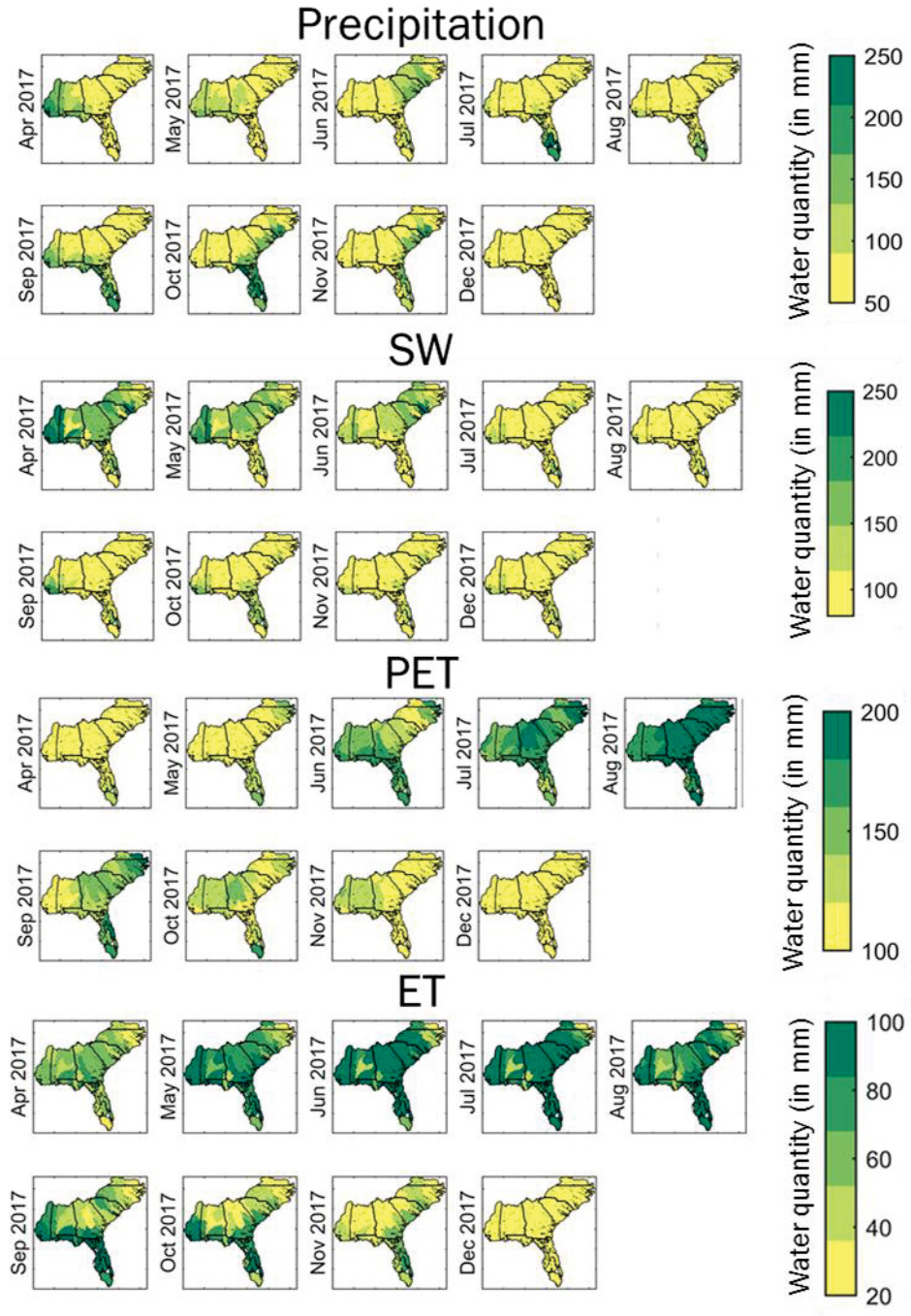

Figure 3-20: Spatial plots of forecasted monthly average values of Precipitation (PREC), Actual Evapotranspiration (ET), Potential Evapotranspiration (PET) and Soil water storage (SW) for the SAG region.

7.3.Model uncertainty

Model uncertainties can be a result of measurement errors associated with the model inputs (DEM, Land use classification), from model structural setup due to assumptions and simplification, and from approximation in determining parameters (Wu, 2016; Yang et al., 2008). Parameter uncertainty, among other sources, is highly likely because of unavailability of the measured parameters (e.g. soil hydraulic properties and basin characteristics etc.). Calibrating models for best parameters may also have issues like equifinality (Beven and Freer, 2001) (different parameter sets resulting in similar model results), due to interactions and interrelationships between the parameters. The issue of equifinality and parametric uncertainty in SWAT models is well discussed in literature (Abbaspour, 2011; Fu et al., 2015; Moreda et al., 2006). Though this paper provides the foundation of linking watershed-scale hydrological modeling with short-term seasonal weather products like CFSv2, the assessment of the modeling efficiency for multiple leads time remains to be the subject of further research. Zhang et al. (2017) tested the efficiency of VIC models initialized with satellite-aided monitoring (MONIT), CFSv2 and ensemble streamflow prediction (ESP) and evaluated the performance of soil moisture forecast skill and observed that the uncertainty in the soil moisture forecast is mostly controlled by initial conditions at the first month and that uncertainties in the CFSv2 climate forecasts have the largest contribution to SM forecast errors at longer lead times. Furthermore, seasonality and hydroclimatological variations have significant impact on the modeling performance of both SWAT and CFSv2 models. In other words, the hydrological predictions using SWAT-CFSv2 may be more skillful in some seasons compared to others due to combined influence of teleconnections with large scale climatic drivers which may lead to a more predictable influence on the water

budget of the study area (hurricanes and high precipitation or alternatively, increased temperatures and reduced precipitation etc.).

8. Conclusion

This study provides a high-resolution retrospective simulation of hydrologic variables for 50 watersheds in the South-Atlantic Gulf region of the Southeastern US by implementing SWAT models for each watershed at HUC-12 resolution. Also, the study provides a framework for near real-time forecasting of hydrologic variables in the study area by coupling SWAT models with meteorological drivers from CFSv2 climate forecast models with a lead time of 9 months. The models are calibrated using SUFI-2 algorithm module in SWAT-CUP. Retrospective data for January 1982 through December 2013 is obtained from CFSR dataset. CFSv2 coupled SWAT models provide hydrologic outputs corresponding to first model output of CFS models from January 2014 through March 2017 and 9 months forecasted values through December 2017. The results indicate that the models are effective in capturing the hydrologic variability in the implemented watershed in terms of high accuracy in simulating streamflow discharge for 50 outlet points and high correlation with *in-situ* observed soil moisture dataset from 9 stations across the region for both the surface, and the total rooting depth soil profiles. The study provides an important platform in understanding water balance of the watersheds using high resolution simulations, thus incorporating sub-watershed scale variability in the understanding of the underlying governing processes. Evaluation of the various water budget components for the region obtained from the SWAT- CFSv2 coupled models are observed to reflect on the recent drought conditions in the SEUS (Mid-2016). The forecasted state of hydrology using the calibrated SWAT-CFSv2 coupled models for 9 months (through December 2017) indicate mild water deficit conditions across the study region. The salient features of this study are:

1. This is the first application of HUC-12 resolution sub-watershed scale seasonal forecasting of hydrologic variables using CFSv2 coupled SWAT models.
2. Simulation of soil moisture for total rooting depth and surface soil moisture provides flexibility for use in diverse applications.
3. The simulated dataset provides a very useful platform for other varied applications like drought monitoring and forecasting, flood/ forest fire risk assessment and other agricultural and water resources related applications.

9. Resources

To facilitate reproducibility of this study and relevant data can be accessed through the following links:

1. Watershed boundaries (NHD plus): http://www.horizon-systems.com/nhdplus/NHDPlusV1_03.php
2. 100 m elevation dataset (USGS): https://catalog.data.gov/dataset/100-meter-resolution-elevation-of-the-conterminous-united-states-direct-download
3. Land use/ cover data: National Land Cover Database 2011 https://www.mrlc.gov/nlcd2011.php
4. Weather data: National Centers for Environmental Prediction (NCEP) Climate Forecast System Reanalysis (CFSR) data (Dile and Srinivasan, 2014; Fuka et al., 2013)
5. CFSv2 dataset: https://nomads.ncdc.noaa.gov/modeldata/cfsv2_forecast_ts_9mon/
6. U.S. Climate reference network (USCRN) *in-situ* soil moisture data: ftp://ftp.ncdc.noaa.gov/pub/data/uscrn/products/soilsip01/

Chapter 4 :
Retrospective drought analysis using SWAT-simulated hydrologic variables and implementation of SWAT-CFSv2 coupled models for near-real time seasonal drought forecasting.

Key points:

a) Sub-watershed scale retrospective drought analysis at HUC-12 resolution for SEUS from 1982- 2013.

b) Near-real time monitoring and 9-month lead drought forecasting using CFSv2 coupled SWAT models.

c) Stratified approach of drought severity assessment using multi-layer soil moisture.

d) Comparative analysis of several water budget components against surface and total rooting depth soil moisture in capturing drought onset and persistence.

1. Abstract

This study proposes a stratified approach of drought severity assessment and forecasting with a lead time of 9 months using weekly percentiles of surface and total rooting depth soil moisture (SM) for South-Atlantic Gulf (SAG) region of the Southeastern US (SEUS). Hydrologic variables for this analysis are obtained by implementing SWAT models for 50 watersheds in the region, at 12- digit Hydrologic Unit Code (HUC-12) resolution. SWAT models are calibrated using the observed streamflow dataset and daily retrospective model outputs for SM are obtained from January 1982 through December. Near-real time simulation (January 2014 through mid-March 2017) and forecasting (mid-March through December 2017) of high resolution hydrologic variables at sub-watershed scale (HUC-12) are obtained by pairing calibrated SWAT models with meteorological drivers (precipitation and temperature) from Coupled forecast system model version-2 (CFSv2) seasonal climate forecast models. Estimated drought severity using monthly percentiles of hydrologic variables from the calibrated SWAT models for the retrospective period is compared with various long-term (PDSI, PHDI, SPI-9, SPI-12 and SPI-24) and the short-term (Palmer Z index, SPI-1 and SPI-6) drought indices provided for the 53 climate regions in the SAG region. The results show that the simulated soil moisture percentiles show high (>60%) Index of Agreement (IOA) with PDSI with low (<10%) False Alarm (FA) percentage. High correlation is seen between the total column SM based percentiles with PDSI, PHDI, and other long-term drought indices (SPI-6, -9, and, -12) while surface soil moisture corresponded strongly with short term indices like ZNDX and SPI-1 and with other indices at long term temporal aggregations. IOA is observed to be very high (~ 80-90 %) for near-real time SM percentiles from SWAT-CFSv2 coupled models for (January 2014- March 2017). However, the accuracy of drought severity estimation using the proposed stratified soil moisture approach varies from watershed-to-

watershed based on the accuracy of calibration for the respective watershed. To assess the spatial association between the estimated drought severity using stratified SM percentiles and actual drought conditions, a comparison is made with the weekly drought severity maps provided by US drought monitor for three time periods i.e. 2000 through 2002, 2006 through 2009 and 2011 through 2012.

Key words: Soil moisture, SWAT, CFSv2, drought, Southeastern US

2. Introduction

Droughts produce a complex set of impacts that span many sectors of the economy and reach well beyond the area experiencing the drought. These calamities are the result of climate variations that infrequently occur in vast geographic areas without any specific border (Keshavarz et al., 2014; Mishra et al., 2009; Zou et al., 2017). The impact of drought manifests in all components of the hydrologic budget, namely, in water supply (precipitation), storage (soil moisture, snowpack, groundwater, and surface water), and exchange or flux (evapotranspiration, snowmelt, drainage/recharge, runoff, and streamflow) (Anderson et al., 2013). In the wake of warming up of climate, the likelihood of occurrence of severe droughts with longer durations in the future is expected to rise significantly in several parts of the world (Dai, 2011; Kundzewicz et al., 2010; Peterson et al., 2012; Trenberth and Fasullo, 2012).

McEvoy (2015) reported that the severity of the recent droughts in US has been accentuated by high temperatures and evaporative demand. With increasing human population, and associated demand for freshwater resources and food production, the global food security has come under severe risk (Mu et al., 2013). The Southeastern US (SEUS) has experienced widespread droughts three times within a span of 15 years since early 2000 and nearly 40% of the region is under

moderate to exceptional drought conditions as of early 2017. Several studies have expressed concerns over increasing drought vulnerability of the region owning to continued growth and subsequent industrial, agricultural and metropolitan demand throughout the southeast (Manuel, 2008; Pederson et al., 2012; Seager et al., 2009) and suggest that the threat of water-related conflict in the region has potential to grow more intense in the coming decades.

As the frequency of future droughts is expected to increase, a reliable hydrologic forecast for a region has a significant role in the efficient planning of available water resources (Madadgar and Moradkhani, 2014). Utilizing information from seasonal climate forecast and long-term climate prediction has always been of great interest to improve drought preparedness and mitigation (Hansen, 2005). Dynamical seasonal forecasting systems that are based on coupled atmosphere-ocean-land general circulation models (CGCMs) have been widely used for drought forecasting in recent years (Dutra et al., 2013; Ma et al., 2015). Seasonal climate forecasts are useful in improving farmers' ability for drought mitigation, particularly in rain-fed systems (Wetterhall et al., 2015). Skillful prediction of the field moisture availability is important to decide crop type, resource use, and crop insurance and contract renewals (Shafiee-Jood et al., 2014). However, only less than 30% of the global drought onsets can be detected by climate forecast models and drought forecast skill tends to be limited, especially over the regions with less impact from El Niño–Southern Oscillation (ENSO) (Ma et al., 2015; Yuan and Wood, 2013). Several studies have highlighted the applicability of climate forecast system reforecast and reanalysis (Saha et al., 2010) products in drought monitoring and prediction, seasonal soil moisture estimation and understanding land-surface interaction (Dirmeyer, 2013; Mace et al., 2015; McEvoy et al., 2016b; Mo et al., 2011; Mo et al., 2012b; Roundy et al., 2014).

In recent decades, use of drought matrices based on precipitation and temperature had been a common practice. The two most commonly used drought indices are the Palmer drought severity index (Palmer, 1965), and the Standardized Precipitation Index (McKee et al., 1993). While PDSI requires temperature and precipitation data for drought severity assessment, SPI uses precipitation data only. These matrices have limitations at short time scales and do not account for the effects of other important meteorological and radiative forcings such as specific humidity and downwelling shortwave radiation (McEvoy et al., 2016a). Soil moisture has significant impact on important meteorological phenomena in the surface and atmospheric boundary layer, including the development of mesoscale circulations between land surface patches with differing soil moisture conditions, the development of deep convection, and the growth and sustainment of large-scale interannual variations such as droughts (Hain et al., 2011). Soil moisture modulates the atmospheric surface energy balance and hence has a significant impact on the vertical distribution of turbulent heat fluxes, as well as the boundary layer structure, and, is a pivotal element in the hydrological process of converting precipitation into runoff and groundwater storage (Alapaty et al., 1997).

Many recent studies have established the usefulness of soil moisture anomalies for characterizing drought onset and demise (Hunt et al., 2009). Sehgal et al. (2017) proposed a stratified drought analysis using soil moisture of multiple layers from two land surface models and demonstrated that soil moisture based indices show high accuracy in capturing drought onset and propagation. Mozny et al. (2012) used *in-situ* soil moisture dataset for drought monitoring in the Czech Republic using a Soil Moisture Index (SMI) and found soil moisture based drought index to be useful in rapid-onset drought monitoring. Ford et al. (2015) used *in-situ* soil moisture observations for developing a flash drought early warning framework for Oklahoma. Sims and

Raman (2002) established strong interrelationship of two drought indices: Palmer Drought Severity Index (PDSI) and Standardized Precipitation Index (SPI) with soil moisture for North Carolina.

Accurate soil moisture simulations are very important for reliable drought severity estimations. The variability in soil moisture, accentuated with seasonal variations and influence of hydroclimatology, makes it challenging to accurately estimate droughts using soil moisture. Furthermore, variability in watershed characteristics also influences the interrelationship between drought and its manifestation in the water balance of the watershed. Also, a lot of emphasis is given on retrospective drought assessments using simulated dataset, whereas, the forecasting products often miss the watershed and sub-watershed scale variability in the hydrologic variables. This study uses high resolution water balance components from SWAT models implemented at HUC-12 resolution using global scale, short term meteorological forecasts from CFSv2 for near-real time drought monitoring, and forecasting with a lead time of 9 months for 50 watersheds comprising the South-Atlantic Gulf region of Southeastern US.

The objectives of this study are as follows:

a) To implement a stratified drought analysis approach for drought severity estimation using the top soil layer for analyzing the transient and low intensity droughts, and total column soil moisture for long term, severe droughts, using sub-watershed scale (at HUC-12 resolution) soil moisture dataset obtained by implementing SWAT models for 50 watersheds across the South-Atlantic gulf region of the Southeastern US.
b) To carry out retrospective drought analysis for the SAG region with a focus on three recent drought occurrences in the year 2000- 02, 2006- 09 and 2011-13 using the proposed layer-wise approach.

c) To develop a real- time drought forecasting framework using high resolution SWAT based simulated soil moisture, initialized using climate drivers from CFSv2, with a lead time of up to 9 months at a weekly time step.

3. Study Area

3.1. Study area

This study is focused on the South Atlantic-Gulf (SAG) region in the Southeastern US which includes Florida and South Carolina, and parts of Alabama, Georgia, Louisiana, Mississippi, North Carolina, Tennessee, and Virginia (USGS, 2017). The region is listed with a 2-digit Hydrologic Unit Code (HUC) of 03 and consists of 18 sub-regions, each listed with the 4-digit HUC codes ranging from 0301 through 0318. Each HUC-4 basin is further divided into smaller watersheds for this study, totaling 50 for the entire SAG region (Figure 3-1), each of which is modeled using SWAT to delineate sub-watersheds matching the HUC12 resolution as provided by the National Hydrology Dataset plus (NHD+). Table 4-1 provides the complete list of the 18 basins in the SAG region, each referred to by its HUC- 4 identifier with list and name of the sub-watersheds with the outlet U.S. Geological Survey (USGS) stations. Note that the watershed numbers are provided by the authors only for easy referencing and identification of these watersheds in the study and not to be confused with the watersheds at HUC-6 which are larger than these watersheds in most cases.

The northern part of the study region is bounded by Appalachia, and is predominantly forested. Wetlands are common on the southern part of the study region. There is a gradient in the average annual rainfall in the region where watersheds in Virginia, North and South Carolina receive less rainfall (1100-1130 mm) compared to Alabama, Mississippi. Watersheds in Florida and parts of Georgia receive the highest rainfall in the region with total annual precipitation of upto ~2000 mm

for some watersheds. Florida and parts of Alabama and Georgia, typically have higher mean annual temperatures compared to other regions with lows as high as 2.3°C and highs as high as 39°C for some watersheds due to humid subtropical climate. Climatology of the region is provided in Table 4-2.

Figure 4-1: Map showing the location of the study area. The watersheds in the South Atlantic-Gulf (SAG) region are highlighted in grey shade.

Table 4-1: List of the 18 basins in the South Atlantic- Gulf region identified with 4-digit Hydrologic Unit Code with name and a 6-digit identification number (not to be confused with HUC-6) for the constituent watersheds, and, respective outlet USGS stations.

Basin	Watershed	River/ basin	Basin	Watershed	River/ basin
0301	030101	Roanoke	0309	030902	Caloosahatchee
	030102	Dan	0310	031001	Peace
	030103	Nottoway		031002	Alafia
0302	030201	Tar		031003	Withlacoochee
	030202	Neuse	0311	031101	Suwannee
0303	030301	Lumber		031102	Alapaha
	030302	Black	0312	031201	Ochlockonee
	030303	NE Cape fear	0313	031301	Chattahoochee
0304	030401	Pee Dee		031302	Flint
	030402	Lumber		031303	Apalachicola
	030403	Lynches	0314	031401	Yellow
0305	030501	Catawba		031402	Choctawhatchee
	030502	Congaree		031403	Conecuh
	030503	Edisto	0315	031501	Coosa (Rome)
0306	030601	Savannah		031502	Coosa (Childersburg)
	030602	Barrier Creek		031503	Alabama
	030603	Ogeechee	0316	031601	Noxubee
	030604	Canoochee		031602	Black warrior
0307	030701	Oconee		031603	Tombigbee
	030702	Ocmulgee	0317	031701	Chickasawhay
	030703	Ohoopee		031702	Tallahala
	030704	Satilla		031703	Red Cr.
0308	030801	St. Johns (Geneva)	0318	031801	Pearl (Carthage)
	030802	St. Johns (Buffalo bluff)		031802	Pearl (Monticello)
0309	030901	Arbuckle Cr.		031803	Pearl (Bogalusa)

Table 4-2: Climatology (Total annual precipitation, Maximum and minimum annual temperatures) of 50 watersheds based on 1979- 2013 data.

Basin	Watershed	PREC (mm)	Tmin (°C)	Tmax (°C)
0301	30101	1156.8	-14.0	37.9
	30102	1202.5	-12.2	38.7
	30103	1295.6	-10.4	38.1
0302	30201	1357.3	-10.0	38.7
	30202	1443.1	-9.3	38.3
0303	30301	1336.7	-10.0	38.9
	30302	1458.4	-9.6	39.6
	30303	1577.9	-8.5	39.4
0304	30401	1268.5	-10.9	38.7
	30402	1465.8	-8.3	39.4
	30403	1437.4	-7.9	40.1
0305	30501	1307.8	-11.0	38.2
	30502	1462.2	-6.0	40.1
	30503	1298.2	-9.0	39.3
0306	30601	1338.9	-8.7	39.2
	30602	1399.7	-6.0	40.1
	30603	1351.8	-6.8	40.3
	30604	1487.4	-5.5	40.0
0307	30701	1367.3	-8.1	39.8
	30702	1389.0	-7.6	39.7
	30703	1459.8	-6.0	40.0
	30704	1576.1	-4.7	39.8
0308	30801	1809.9	-0.5	37.8
	30802	1732.7	-2.3	38.4
0309	30901	1916.3	0.6	38.4
	30902	2013.3	2.3	36.5

Basin	Watershed	PREC (mm)	Tmin (°C)	Tmax (°C)
0310	31001	1844.0	-0.7	39.3
	31002	1693.3	0.4	37.1
	31003	1728.6	-2.2	38.8
0311	31101	1744.1	-4.1	39.5
	31102	1584.2	-5.2	39.6
0312	31201	1704.7	-7.1	39.0
0313	31301	1470.1	-9.1	38.3
	31302	1446.2	-7.4	39.5
	31303	1565.2	-4.9	39.2
0314	31401	1653.6	-4.9	37.8
	31402	1587.8	-5.8	40.0
	31403	1599.0	-7.1	39.8
0315	31501	1458.8	-11.3	37.8
	31502	1487.6	-9.6	38.6
	31503	1547.7	-7.9	39.9
0316	31601	1563.4	-9.7	39.7
	31602	1546.3	-10.1	39.1
	31603	1622.7	-7.3	40.0
0317	31701	1615.4	-7.8	40.4
	31702	1617.7	-7.4	40.5
	31703	1718.9	-6.0	39.8
0318	31801	1621.3	-8.9	39.9
	31802	1626.8	-7.7	40.0
	31803	1648.8	-6.5	40.2

4. Methodology

4.1. Brief description of SWAT models

SWAT is a comprehensive, semi-distributed, continuous-time, processed-based model (Arnold et al., 2012; Gassman et al., 2007; Neitsch et al., 2011) initially developed to model the impacts of management practices on hydrologic cycle, plant growth, and water quality in medium to large basins (Jin and Sridhar, 2012). SWAT simulations incorporates weather, hydrology, sedimentation, soil temperature, plant growth, nutrients, pesticides and land management (Arnold et al., 1998). The model uses weather (precipitation, radiation and temperature), elevation, soil,

land cover/ use data to simulate surface and subsurface hydrology and various chemical, biological and sediment fluxes. Hydrologic cycle simulations by SWAT are based on water balance concept. SWAT is an open source code simulation model and has been extensively used in hydrological modeling community across the globe with applications in studies ranging from catchment to continental scales (Abbaspour et al., 2015).

The basic drivers for this model are the U.S. Geological Survey (USGS)- derived Digital Elevation Model (DEM), STATSGO soil layer and land use/ cover data from National Land Cover Data (NLCD) 20011 (Homer et al., 2015). Weather data (Precipitation and temperature) is obtained from the National Centers for Environmental Prediction (NCEP) Climate Forecast System Reanalysis (CFSR) data (Dile and Srinivasan, 2014; Fuka et al., 2013). One USGS station for each watershed is chosen for calibrating and validating the streamflow generated by the SWAT models.

SWAT models are calibrated for a period of 2003 through 2010 with three years of warm-up period (2000 through 2002) and are validated for a period of 2011 through 2013. The ArcSWAT 2010 interface is used to setup and parameterize the model. Sequential Uncertainty Fitting-2 algorithm (Abbaspour et al., 1997; Abbaspour et al., 2004; Abbaspour et al., 2015) is used to calibrate model parameters for each watershed using SWAT-CUP (calibration/uncertainty or sensitivity program) interface for SWAT. A set of 24 parameters are chosen for calibration to address various hydrologic components of watershed like surface runoff (Curve number, soil and plant evaporation, surface runoff and Manning's coefficient, and available soil water capacity etc.), baseflow (Groundwater "revap", aquifer – soil interaction, depth of water in the shallow aquifer, time for water leaving the root zone to reach the shallow aquifer, deep aquifer percolation), storm water (Channel hydraulic conductivity, stormflow lag time etc.), snow (snowmelt rate, snow

temperature etc.) etc. The choice and effect of these parameters are very well documented in SWAT literature (Abbaspour et al., 2015; Arnold et al., 2012; Feyereisen et al., 2007; Jin and Sridhar, 2012; Liu et al., 2008; Sommerlot et al., 2016; Uniyal et al., 2015; Van Liew et al., 2005; Wang et al., 2008) and the selected parameters are consistent with the aforementioned studies. For detailed description of the watershed models, model calibration and validation for the SWAT models used in this study for obtaining various hydrologic variables at HUC-12 resolution, the readers are referred to Sehgal and Sridhar (2017).

The calibrated models are then back-run for retrospective period till 1979 with three years of model spin-up period, thus providing continuous daily data of hydrologic variables from January' 1982 through December' 2013.

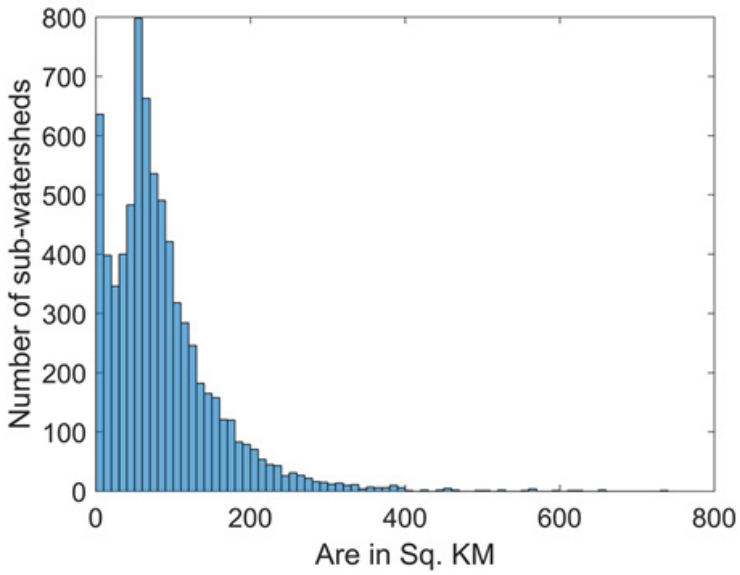

Figure 4-2: Modeled and actual NHD+ HUC-12 watersheds. Against a total of 7453 sub-watersheds at HUC-12 resolution (NHD+), the models delineated a total of 7391 to match with high spatial resolution

4.2. Coupling SWAT models with CFSv2 data

CFSR has been extended as an operational, real-time product into the future which provides estimates of the atmospheric variables with a lead time of nine months and are initialized at multiple times a day, and, different days of a month (Table 4-3). Figure 4-3 provides a schematic of data assimilation for the study. Precipitation and temperature time series is obtained from CFSv2 data from 1st April 2011 through 19th Dec 2017 by using the first output of CFSv2 models from 1st April 2011 through 12th March 2017 and 9-month forecast data is then obtained from the latest initialization (12th March 2017 in this study). Figure 3-4 provides a schematic of data assimilation for the study. The red ellipse highlights the model run for each initialization which is used for SWAT model implementation with a total number of *K* initializations from 1st April through 12th Match 2017.

Table 4-3: CFSv2 monthly ensembles with respective initial day of the month for four members initialized at 00Z, 06Z, 12Z, and 18Z. (McEvoy, 2015)

Initialization Month	**Total Members**	**Initialization Days**
January	28	1, 6, 11, 16, 21, 26, 31
February	20	5, 10, 15, 20, 25
March	24	2, 7, 12, 17, 22, 27
April	24	1, 6, 11, 16, 21, 26
May	28	1, 6, 11, 16, 21, 26, 31
June	24	5, 10, 15, 20, 25, 30
July	24	5, 10, 15, 20, 25, 30
August	24	4, 9, 14, 19, 24, 29
September	24	3, 8, 13, 18, 23, 28
October	24	3, 8, 13, 18, 23, 28
November	24	2, 7, 12, 17, 22, 27
December	24	2, 7, 12, 17, 22, 27

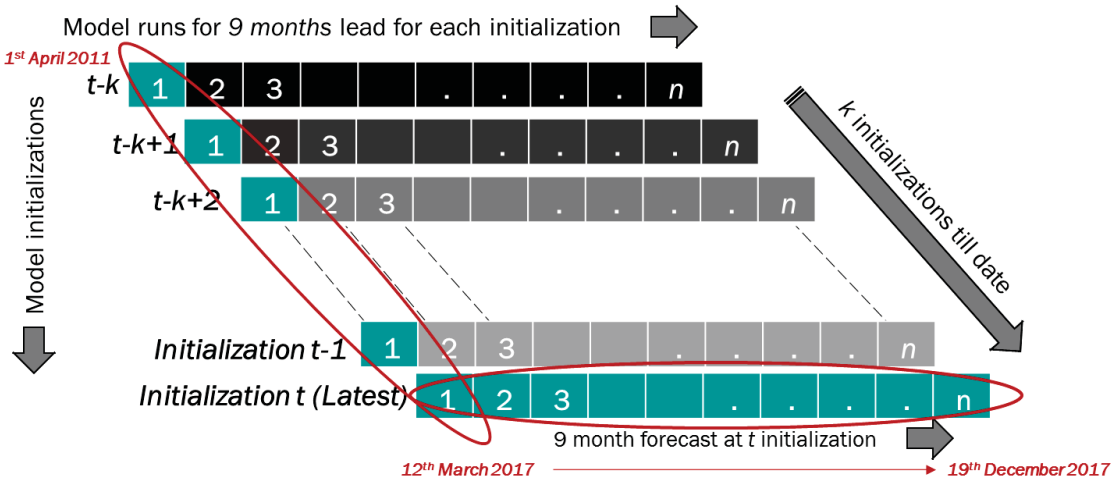

Figure 4-3 : Data assimilation scheme for precipitation and temperature from CFSv2 dataset.

The calibrated SWAT models (Sehgal and Sridhar, 2017) are then coupled with CFSv2 drivers from April- 2011 through December 2017 with a warm-up period of 3 years thus providing simulation outputs from Jan- 2014 through December 2017. Combining the retrospective model simulations from CFSR coupled SWAT models and the CFSv2 coupled SWAT models, a seamless daily simulation outputs are obtained from January 1982 through December 2017. A schematic of the entire model setup is provided in Figure 4-4.

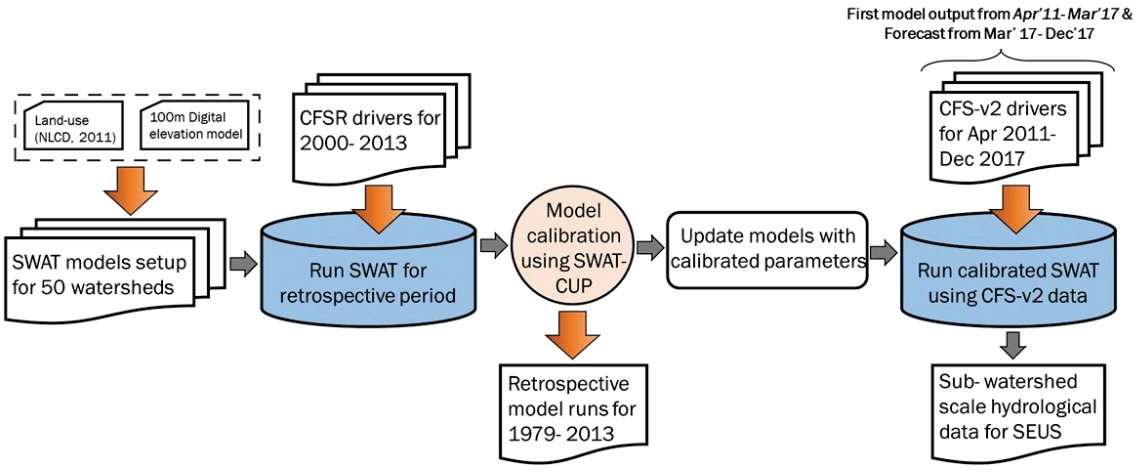

Figure 4-4: Schematic for conceptual framework of forecasting hydrologic variables using CFSv2 dataset in conjunction with SWAT models for the South-Atlantic Gulf region.

4.3. Capturing variability in soil moisture using appropriate distribution function

This study uses soil moisture from two soil layers namely surface layer (typically extending up to a few centimeters from the surface) and the total rooting depth (can extend up to around 2.5 meters). Soil moisture from these two profiles have very distinct behavior in terms of the persistence and hence their relative response to drought. Figure 4-5(a) provides the map of spatially varying soil moisture profiles for the two layers. Figure 4-5(b) provides the persistence (Delworth and Manabe, 1988; Trenberth, 1984), in weeks, of soil moisture from each sub-watershed at HUC-12 for the SAG region. It is evident that along with a difference in the response of the two layers in terms of their persistence, there is a significant spatial variability in the persistence of each layer across the study region. It can be observed that although the persistence values vary spatially for the two layers, the values for the surface soil moisture is less than 5 weeks for most of the study area. Total column soil moisture shows higher persistence values (>15 weeks) for most parts of the SAG region. While surface soil interacts with wind, solar radiation and several other transient weather patterns and provide a platform for the soil-atmospheric interaction, deeper strata interact with the groundwater and are pivotal in surface-groundwater interaction. These factors, when combined with s significant heterogeneity in the watershed characteristics in terms of soil type, vegetation and land use, lead to high spatial variability in the soil moisture from the surface and total column soil moisture.

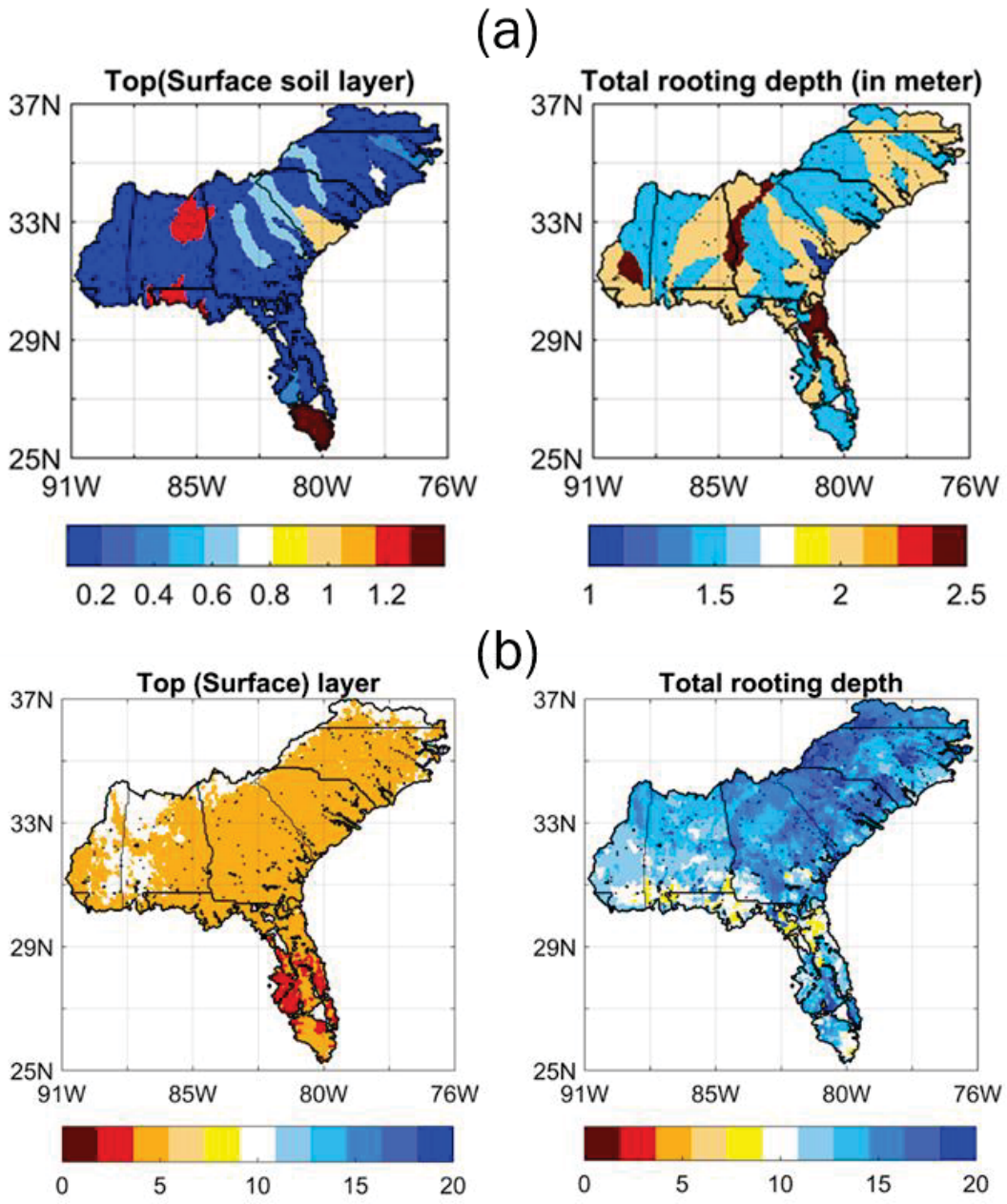

Figure 4-5: (a) Spatially varying profile (in meters) of the Top (surface) and total rooting depth soil column across the SAG region. (b) Persistence (in weeks) of the weekly surface and total column soil moisture. (Persistence of soil moisture is defined as the lag time at which the autocorrelation of the time series of soil moisture decays to $^{1}/_{e}$ (Delworth and Manabe, 1988; Trenberth, 1984))

Daily soil moisture data is obtained for each sub-watershed (at HUC-12 resolution) for a period of January 1982 through December 2013 and averaged over each week. Severity assessment of drought is considered with reference to their historical frequency of occurrence for the location and time of year in question in accordance with Svoboda et al. (2002). A discretized approach is employed in this study to select the suitable distribution function for capturing the soil moisture variability in drought assessment, with a flexibility to account for the seasonal and sub-seasonal, geographic and inter-layer variability at a sub-watershed scale. This study uses a selection of four distribution functions namely *normal*, *gamma*, *log-normal* and e*xtreme value* to capture soil moisture variability for each layer for each calendar week. The fit of the distribution for the respective week and layer, is assessed using the loglikelihood of the distribution function. The best distribution function for estimating the variance in weekly soil moisture is selected based on the loglikelihood of the distribution fit from the dataset. The distribution function with lowest loglikelihood for every week is selected to fit the distribution on the soil moisture data of the respective week and later calculations of cumulative distribution function and hence percentile estimation for that week of the watershed. Figure 4-6 provides the comparison of loglikelihood values for the four distribution functions for soil moisture data for each calendar week, averaged over entire watershed for Roanoke, Satilla, Coosa and Pearl watersheds. It can be observed that the best choice distribution function changes from week-to-week, and, watershed to watershed, which is effectively accounted in the proposed discretized approach of selection of distribution function for estimating weekly soil moisture percentiles.

Figure 4-7 provides a comparison between the distribution of soil moisture for the first week of April and December for Roanoke watershed. It can be observed that while for April, the variability in the soil moisture is low, all distribution functions were very close to each other in

terms of the shape of the PDF and CDF. The extreme value distribution shows a surge in density around 170 mm due to heightened response to the high values (18 in count) in 170-180 mm range, compared to other distributions. However, with greater variance in the data for December (due to stronger dependence of advective winter precipitation on polar winds, which itself has high variability due to hydroclimatic influence), the choice of distribution function can be seen to have significant impact on the shape of the CDF and effects the percentile estimates of the soil moisture for the respective weeks. Figure 4-8 provides a schematic for the weekly percentile calculation scheme used in this study.

Table 4-4: Classification of drought based on layer-wise soil moisture percentiles proposed in this study

Layer-wise classification of drought severity				
Soil Moisture Percentile	Interpretation	USDM classification	Top layer	Total column
Normal	Normal	D0	D0	D0
Less than 30	Abnormally dry	D1	D1	D1
Less than 20	Moderate drought	D2	D1	D2
Less than 10	Severe drought	D3	D2	D3
Less than 5	Extreme drought	D4	D2	D4
Less than 2	Exceptional drought	D5	D3	D5

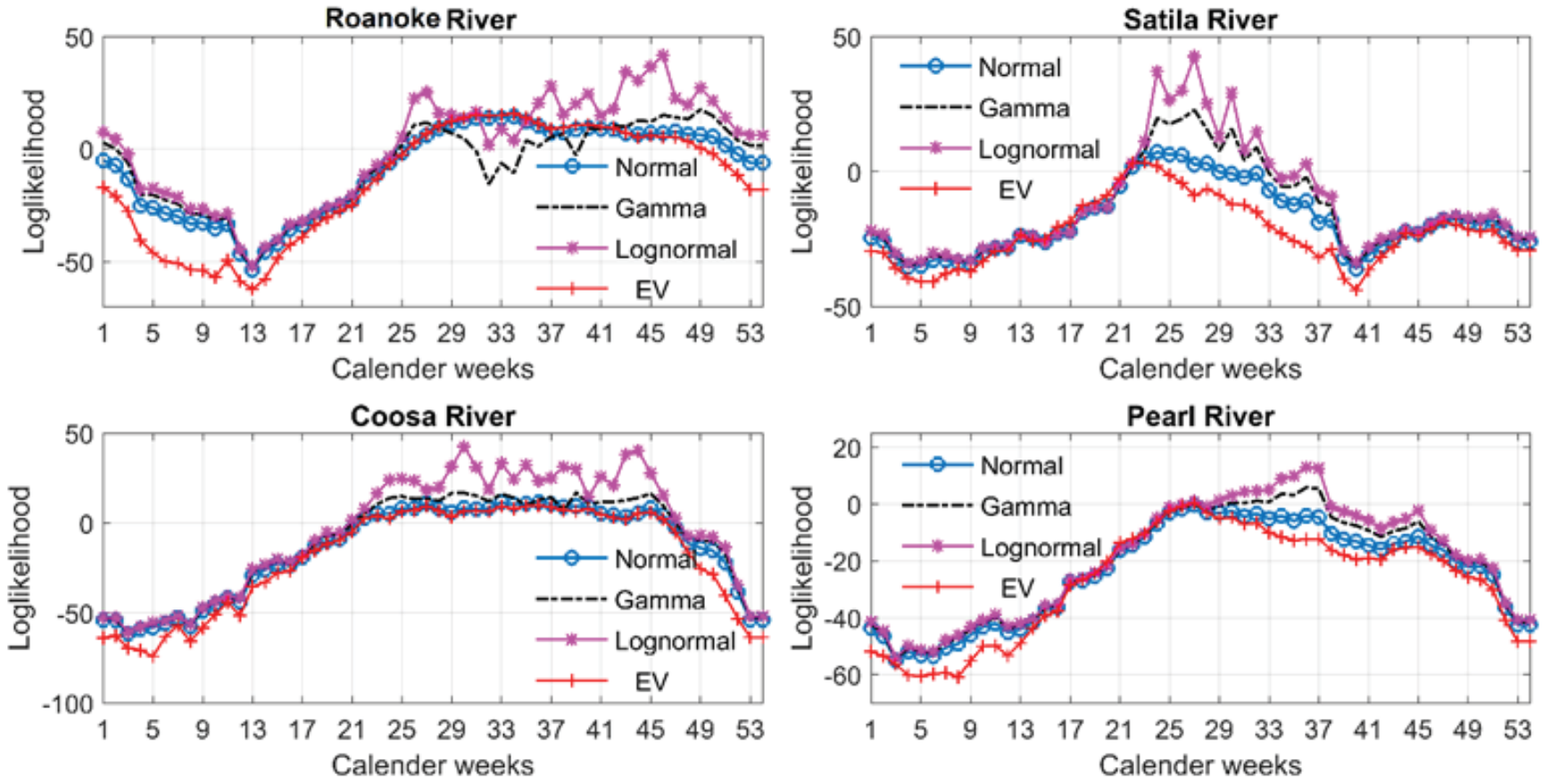

Figure 4-6: Loglikelihood for week-wise fit of four distribution functions i.e. Normal, Gamma, Lognormal and Extreme Value for Roanoke, Satilla, Coosa and Pearl River watersheds.

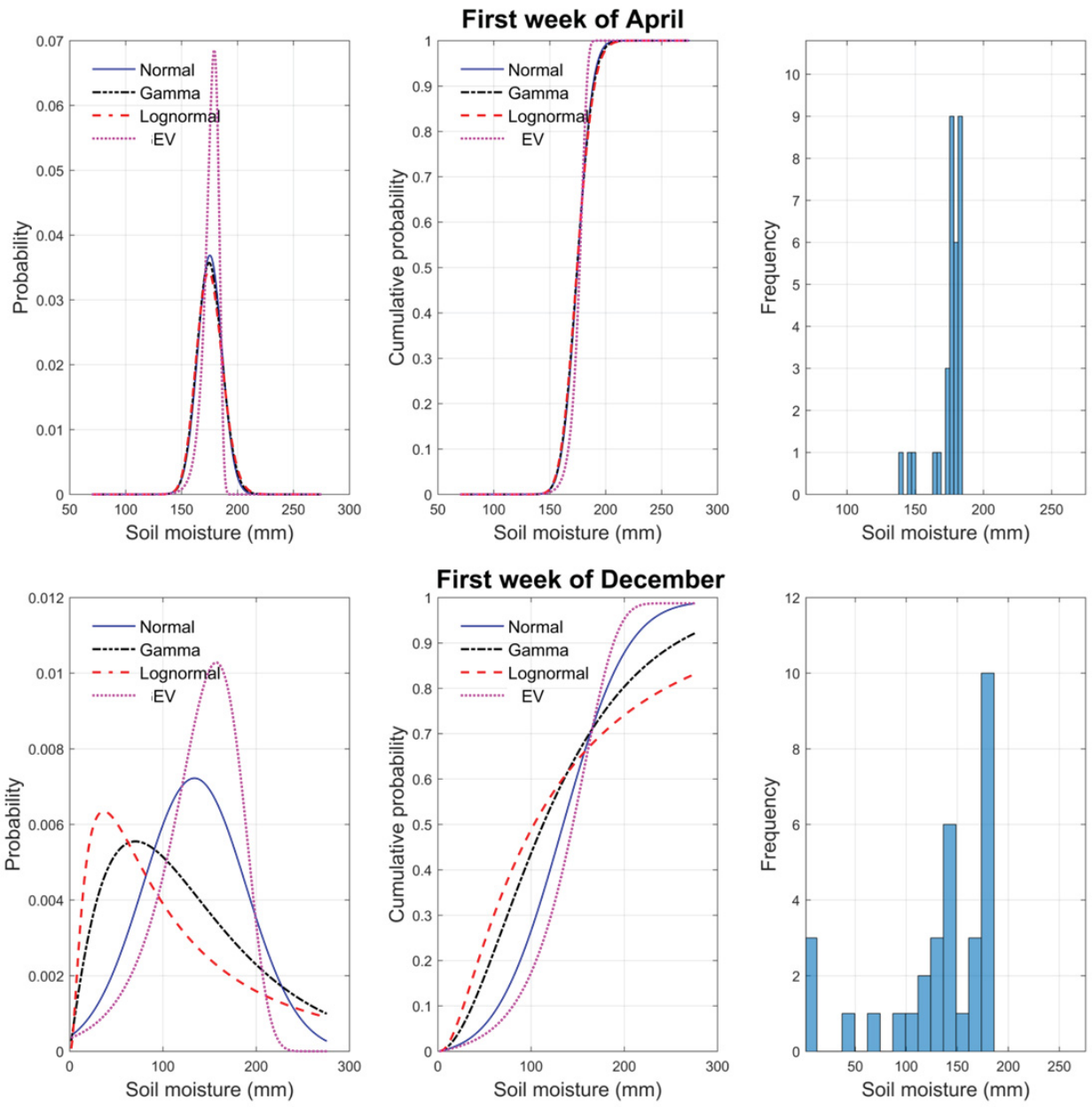

Figure 4-7: Comparison of the probability density function, cumulative density function and histogram for soil moisture for first week of April and December for Roanoke watershed.

4.4. Estimating soil moisture percentiles

The estimated drought severity is tested against the drought severity assessment provided by the US drought monitor (USDM). USDM provides a comprehensive drought assessment of current

drought conditions for the US and provides a useful reference for the socio- economic and agricultural management purposes at a weekly time step (Wang et al., 2009). USDM drought assessment maps are popularly used for validating the drought assessment from various research products. The USDM classification of drought severity based on soil moisture percentile is given in Table 4-4.

In the proposed approach, the drought classification is carried out for each layer using the classification provided in Table 4-4 and drought severity classification from the two layers is compared. The severity classification for the surface and the total column soil moisture can be observed to be different. While surface soil moisture is used only to capture transient drought conditions, severe and long-term droughts are captured using soil moisture percentiles from total column soil moisture. Previously, (Sehgal et al., 2017) proposed a stratified approach of drought severity assessment from multiple soil layers. This study follows Sehgal et al. (2017) in assigning the relative severity class to percentiles of moisture from different layers and use top surface percentiles to identify droughts in D0-D3 category while only total column soil moisture is used to identify D0 to D4 (all classes) droughts. The highest value among the two layers is then selected as the drought severity for the sub-watershed. To illustrate, if we assume the moisture percentile for both layers for a sub-watershed is observed between 5^{th} and 2^{nd} percentile, then the drought severity is classified to be D4 (Extreme drought), however, if top surface soil moisture percentile is less than 30^{th} percentile while total column soil moisture percentile is still above 30^{th} percentile, then the drought severity is assessed to be D1(Abnormally dry).

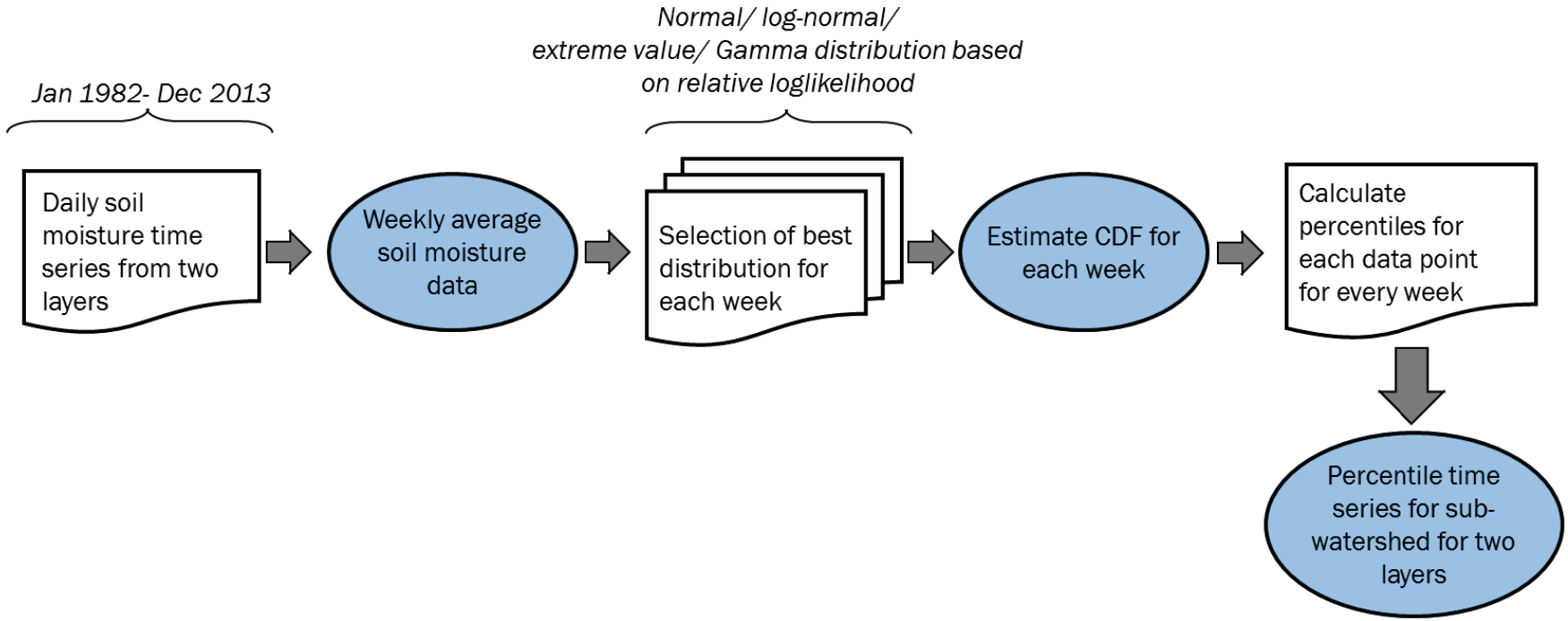

Figure 4-8: Schematic for soil moisture percentile calculation at sub-watershed scale

5. Results

5.1. Severity classification and aggregation of soil moisture percentile

Suitable aggregation (cumulative value over the period) of soil moisture is important to characterize drought on a range of timescales. Several drought indices like Standardized Precipitation Index (SPI) are defined at various timescales to capture long and short-term anomalies. Since the persistence of the surface and the total column soil moisture vary significantly, suitable aggregation of soil moisture from the two layers will be of importance to capture various forms of droughts (transient or long term; meteorological or hydrological etc.) in the proposed stratified approach. Shorter temporal aggregation of soil moisture data preserves transient changes in soil moisture while longer aggregation of data smoothens out the percentiles and represent only long-term variations in the data. This study evaluated aggregation of soil moisture to a range of timescales (4-, 8-, 12- 16- and 20 weeks) to select the best aggregation for characterizing drought using a combination of surface and total column soil moisture. Three recent droughts are considered in evaluating the suitability of various aggregations in capturing both transient and long-term drought characteristics effectively at a sub-watershed scale. Chronology of the selected droughts is: 2000 through 2002, 2006 through 2009 and 2011 through 2012.

Figure 4-9 provides soil moisture percentiles for Pearl River for the three selected drought periods. It can be observed from Figure 4-9 that soil moisture percentile for both surface and total column soil moisture is less than 30% (signifying drought conditions), for most part of the three drought periods. The effect of different aggregations is evident where higher aggregations (12 and 20 weeks) possess higher persistence and often respond to long term conditions in soil moisture change with a longer lag. Also, different response of top surface and total column soil moisture to short term moisture conditions is evident. For example, from December 2001 through July 2011,

surface soil moisture percentiles show three distinct peaks with moisture falling low in the months of February 2011 and May 2011. However, corresponding percentiles from total column soil moisture do not reflect these transient changes.

To preserve both short and long-term drought signals, a combination of surface and total column soil moisture aggregation of 4 weeks for the top surface soil moisture and 8 weeks for total column soil moisture is found to be appropriate. Figure 4-10 provides a comparison of the severity-area plots built using 4- and 8- weeks of aggregation of area averaged surface and total column soil moisture for the SAG region for the period of January 2000 through December 2013. For the comparison, severity classes for both, total column and the surface soil moisture, are kept consistent with the USDM (D0- D4). Transient nature of the surface soil moisture is evident from Figure 4-10. It can be observed that the total column soil moisture has better association with the USDM severity-area plots compared to the surface soil moisture. Compared to total column soil moisture, surface soil moisture drought severity fluctuates within a period of 1- months which corresponds with the persistence of the soil moisture for the surface layer. This indicates that inclusion of surface soil moisture percentiles in drought severity estimation will be helpful in identifying regions with still emerging drought conditions. Figure 4-11 provides a comparison of the percentiles of the total column soil moisture (aggregated to 8-weeks) and the surface soil moisture data (aggregated to 4-weeks) averaged over entire SAG. The two percentile time series have low correlation of 0.43 primarily because of the transient nature of the surface soil moisture percentiles.

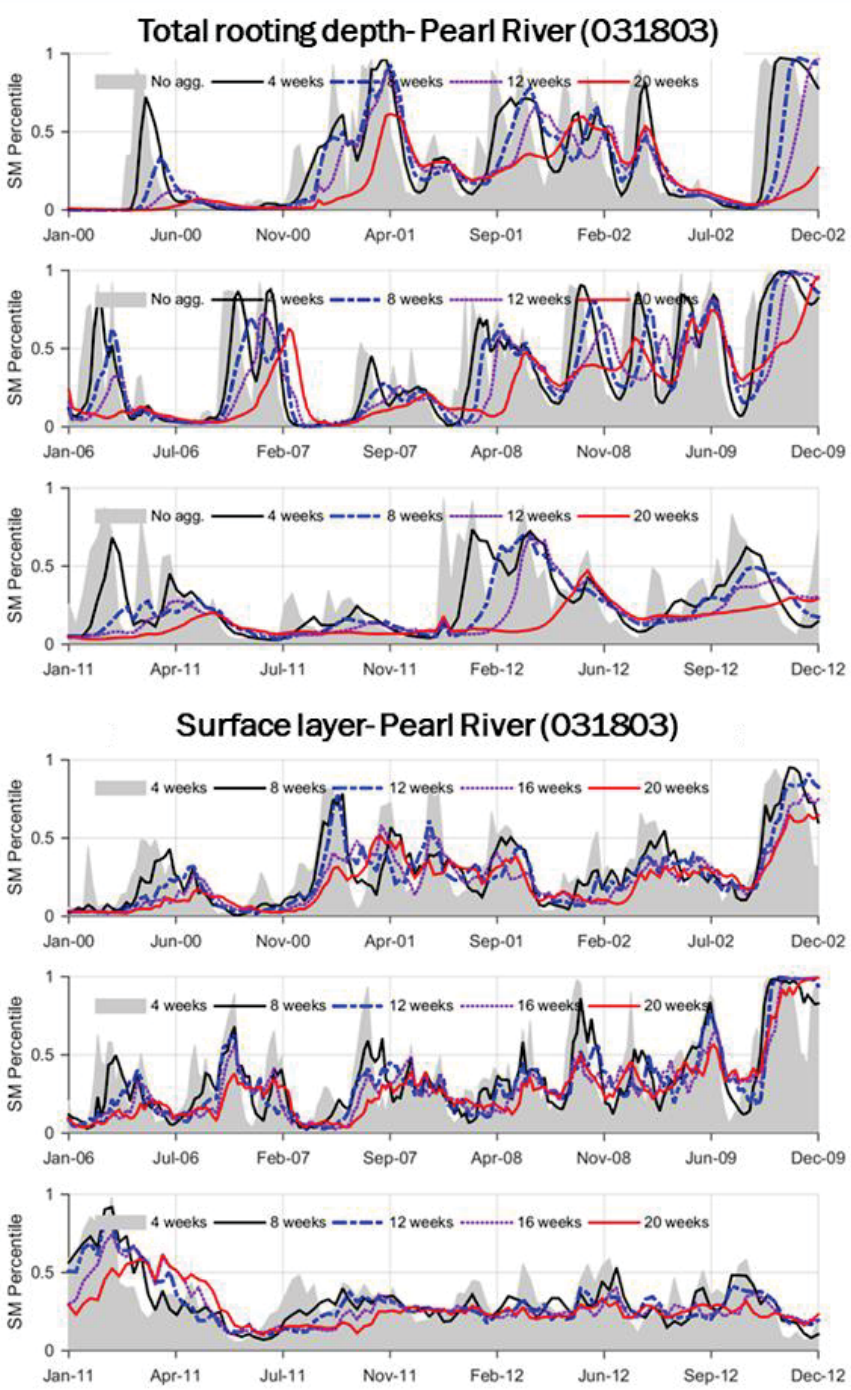

Figure 4-9: Comparison of percentiles of the total rooting depth and the surface soil moisture with 4-, 8-, 12-, 16- and 24- weeks aggregation for the three selected drought periods for Pearl watershed.

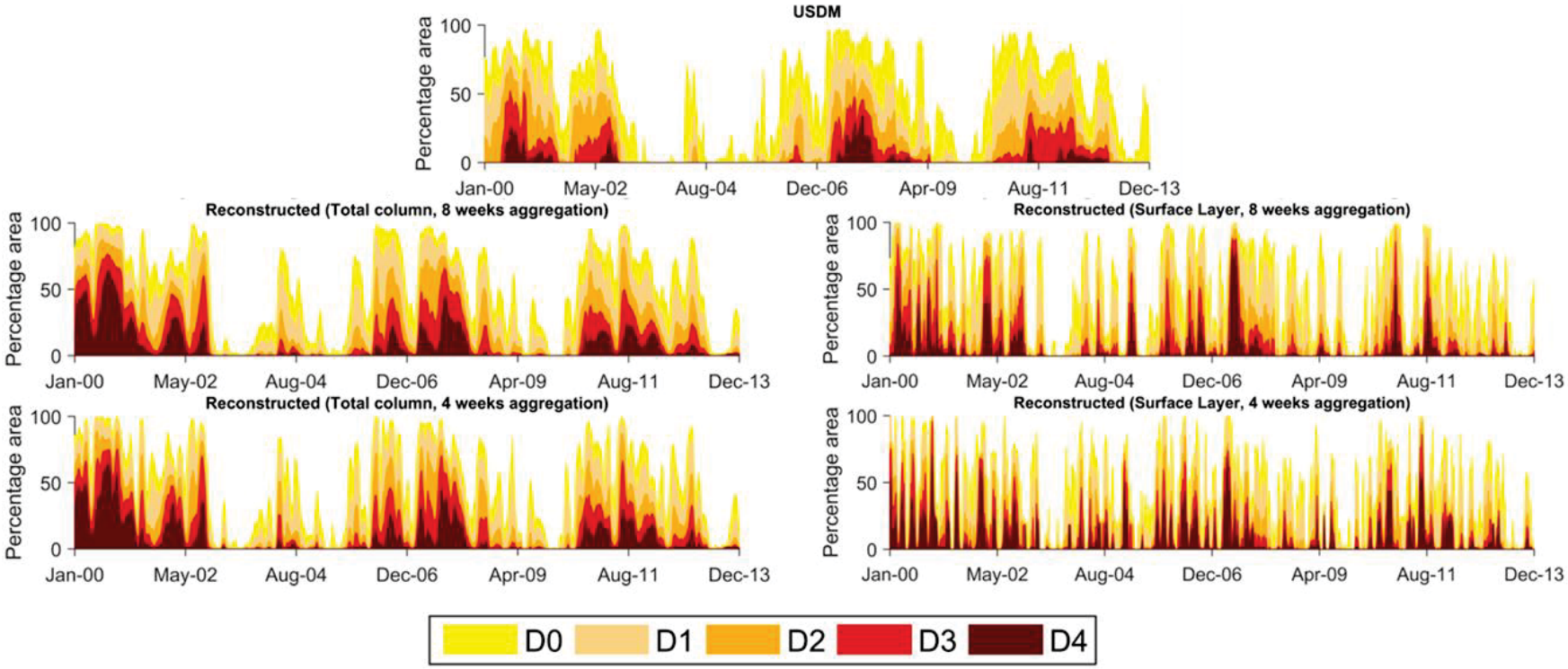

Figure 4-10: Comparison of the severity-area plots for the South-Atlantic Gulf region using Total column and Surface layer soil moisture for 4- and 8-weeks aggregation with the severity-area plot by U.S. drought monitor for the corresponding period. Note that the selected period covers three recent drought periods under focus in this study: Jan' 2000- Dec' 02, Jan' 06- Dec' 09, and, Jan'11-Dec'12.

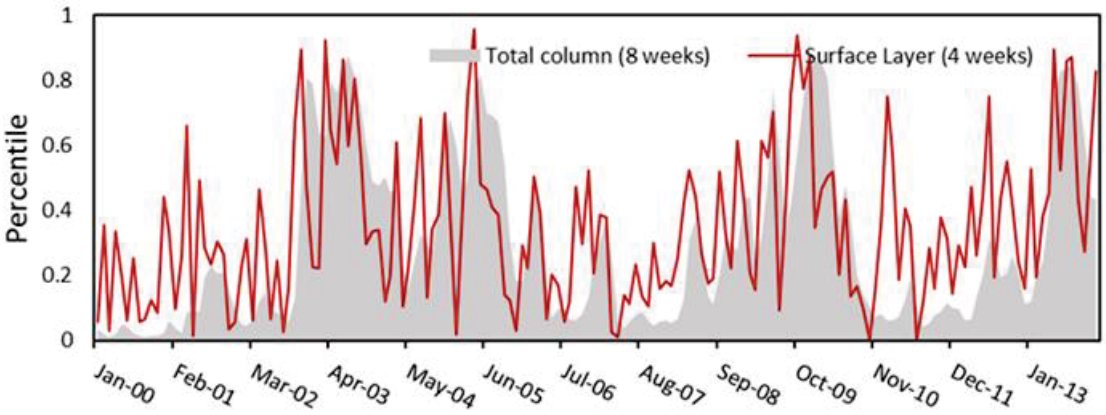

Figure 4-11: comparison of the percentiles of total column soil moisture aggregated to 8-weeks and surface soil moisture data aggregated to 4-weeks averaged over entire SAG.

5.2. Reconstructed drought severity and performance evaluation

To ascertain the accuracy of the proposed drought assessment approach, the reconstructed drought maps are compared with the respective USDM drought severity maps. Figure 4-12 provides a comparison of the reconstructed and USDM drought severity maps for two drought periods, February- August 2007, and, May through November 2011. It can be observed from Figure 4-12 that the reconstructed drought maps generally predate drought compared to its USDM counterpart, especially during the onset of drought. However, the proposed approach also retains drought persistence longer than the USDM maps owning to the influence of the total column soil moisture with long aggregation (8-weeks). The reconstructed drought maps corresponded well in identifying the area under drought stress. However, overestimation of drought stress can be seen for some of the regions especially in the northeast part of the study area. A possible reason for the disagreement is the independent parameterization of each watershed for SWAT model calibration which leads to difference in the sensitivity of the watersheds to droughts impacted by hydrologic conditions including soil moisture, evapotranspiration and runoff.

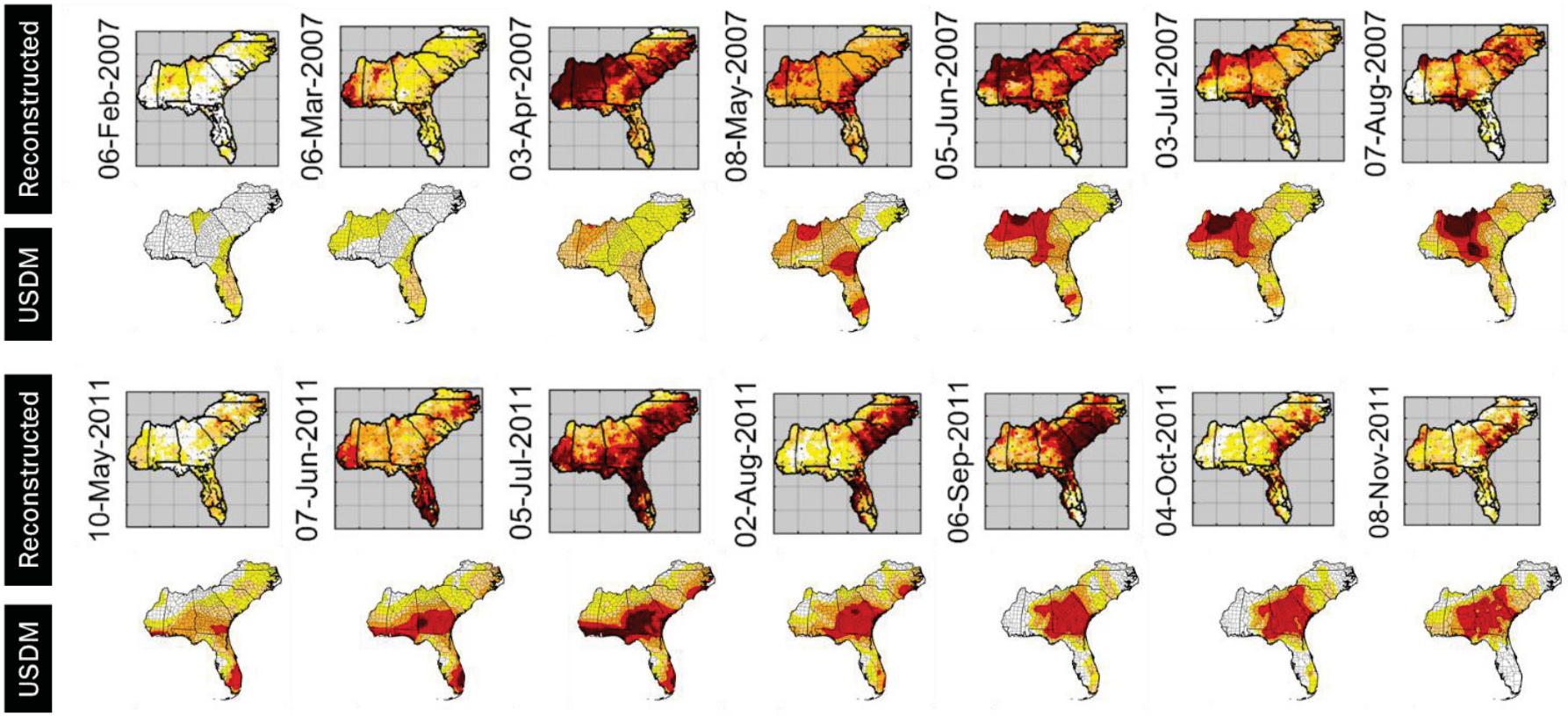

Figure 4-12: Drought severity maps for South-Atlantic Gulf region using the proposed stratified approach compared with the US drought monitor severity maps for the first week of the month for a period of February- August' 2007, and, May through November' 2011.

5.3. Comparison with PDSI, PHDI, Palmer Z index and SPI-1, 6, 9 and 12

The soil moisture percentiles for the total column and the surface soil moisture with multiple aggregations are compared with several other drought indices provided by NOAA's National Climatic Data Center (NCDC) repository for 53 climatic divisions in the SAG region. In order to obtain corresponding values from weekly soil moisture percentiles, the weekly values are averaged for the respective month and a time series of soil moisture percentile is obtained. Eight drought indices namely Palmer Drought Severity Index (PDSI), Palmer Hydrological Drought Index (PHDI), Palmer Z Index (ZNDX), Standardized Precipitation Index (SPI) for 1, 6, 9, and 12 months are chosen for this study. The indices have been selected to facilitate a representation of a diverse set of drought scenarios. While indices like PHDI, PDSI, and SPI-12 relate to the long-term droughts, ZNDX, SPI-1 and SPI-6 indicate relatively short-term drought predictability. While PDSI accounts for drought-inducing circulation patterns, PHDI is used to quantify the hydrological effects of drought. PDSI, PHDI, and ZNDX are water balance indices (consider water supply, demand and loss through precipitation, evapotranspiration and runoff respectively), the Standardized Precipitation Index (SPI) is a probability index and relates to precipitation only (Sehgal et al., 2017). For a given month, each point in a climatic division is assumed to have the same value for a drought index. Detailed information on the difference between these drought indices can be obtained from Mishra and Singh (2010).

Figure 4-13 provides correlation between PDSI, PHDI, Palmer Z index, SPI-1, SPI-6, SPI-9 and SPI-12 with monthly percentiles of the area averaged total column and surface soil moisture aggregated at 4-, 8-, 24-, 36-, 52- weeks, and without any aggregation for the SAG region. It can be observed from Figure 4-13 that the total column soil moisture percentile has higher correlation with long-term drought indices (PDSI, PHDI, SPI-6, SPI- 9 and SPI-12) while surface soil

moisture percentiles have higher correlation with palmer Z-index and SPI-1 when no aggregation is used. Increase in aggregation leads to small increase in correlation value of total column soil moisture with PDSI, PHDI, SPI-6,9 and 12 while the correlation decreases with Z index and SPI-1 with increasing aggregation of total column soil moisture. However, for surface soil moisture, increasing aggregation leads to increase in correlation of soil moisture percentiles with the long-term drought indices, with the highest correlations beyond 24-weeks of aggregation. Due to shorter response time of Z-index and SPI-1, increasing aggregation has adverse effect on the correlation with Z- index and SPI-1 of soil moisture percentiles of both layers.

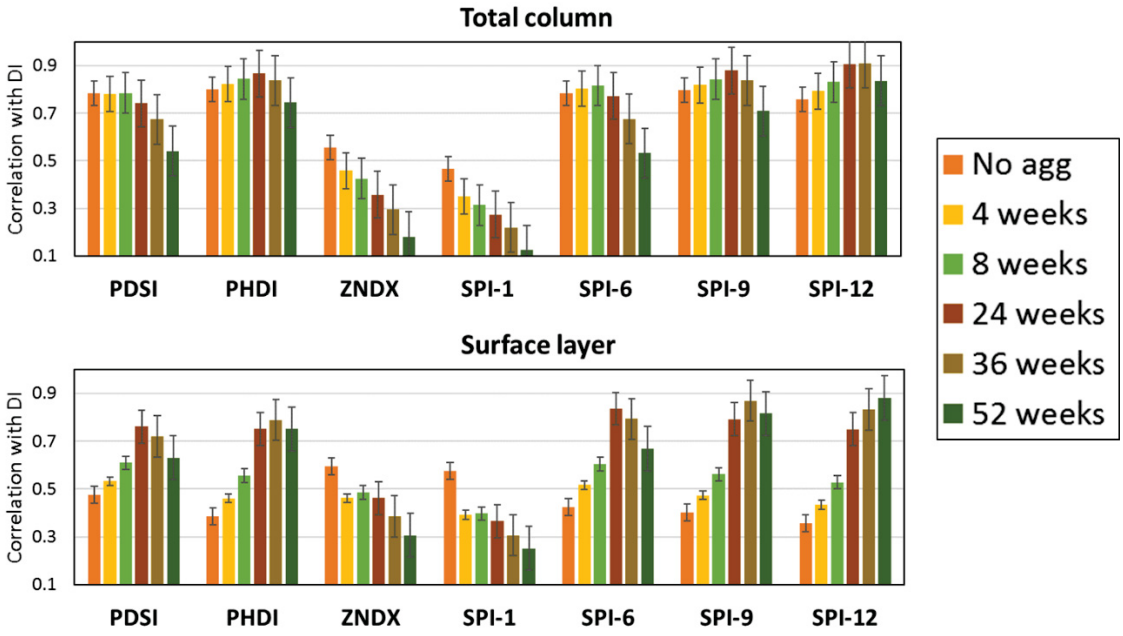

Figure 4-13: Correlation of percentiles of area averaged total column soil moisture (top) and surface soil moisture (bottom) with different aggregations with PDSI, PHDI, Palmer Z index, SPI-1, SPI-6, SPI-9 and SPI-12 for a period of 2000 through 2013.

A comparison of the values of PHDI, SPI-6, and Z index and SPI-1 with the total column and surface soil moisture percentiles for a period of January 2000 through December 2013 is

provided in Figure 4-14. Climate division-wise scatter plots of PDSI with monthly percentile of total column soil moisture with 8-weeks of aggregation for all 53 climate divisions in the study region for a period of 2000 through 2013 is provided in Figure 4-15. The R^2 values for the straight line fit between PDSI and soil moisture percentiles is also provided in the scatter plots of the respective climate division. From Figure 4-14 and Figure 4-15, it can be observed that the soil moisture percentiles obtained from the SWAT models are able to capture the drought in the study region. Climate division-wise evaluation of the goodness of linear fit indicates strong variations in the PDSI predictability for different climate divisions, due to a combination of factors like local climate, land use, vegetation, soil type etc. along with the model uncertainty in modeling soil moisture for the watersheds in the climate division.

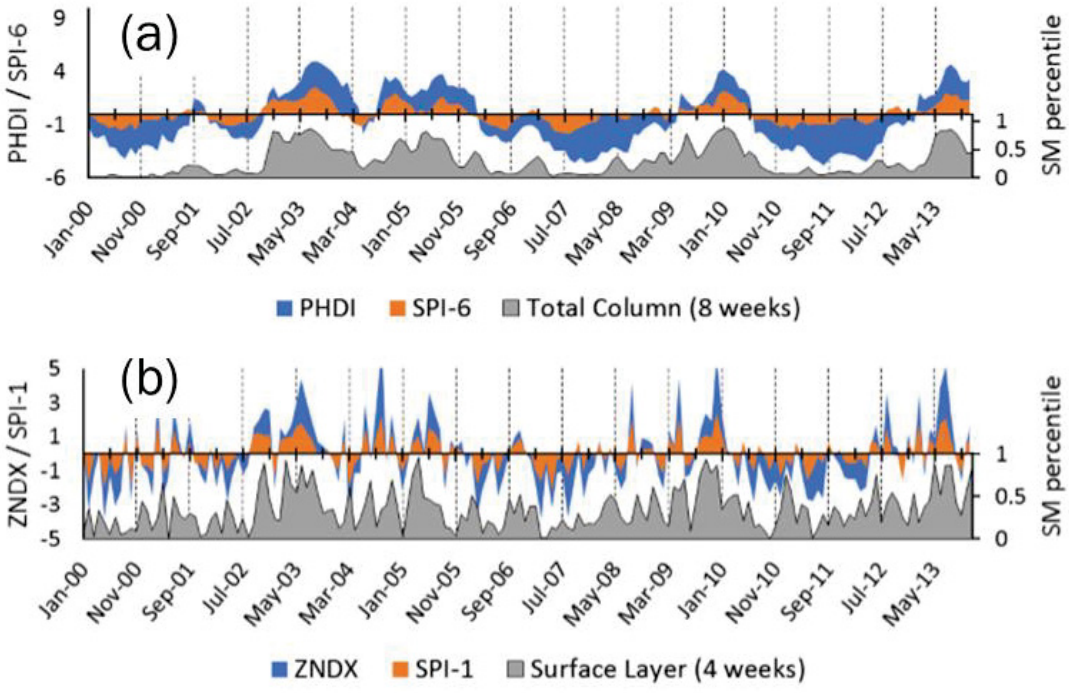

Figure 4-14: Comparison of (a) 8 weeks aggregated total column soil moisture percentile with PHDI and SPI-6 (b) 4 weeks aggregated surface soil moisture percentile with palmer Z- index and SPI-1 for a period of 2000 through 2013.

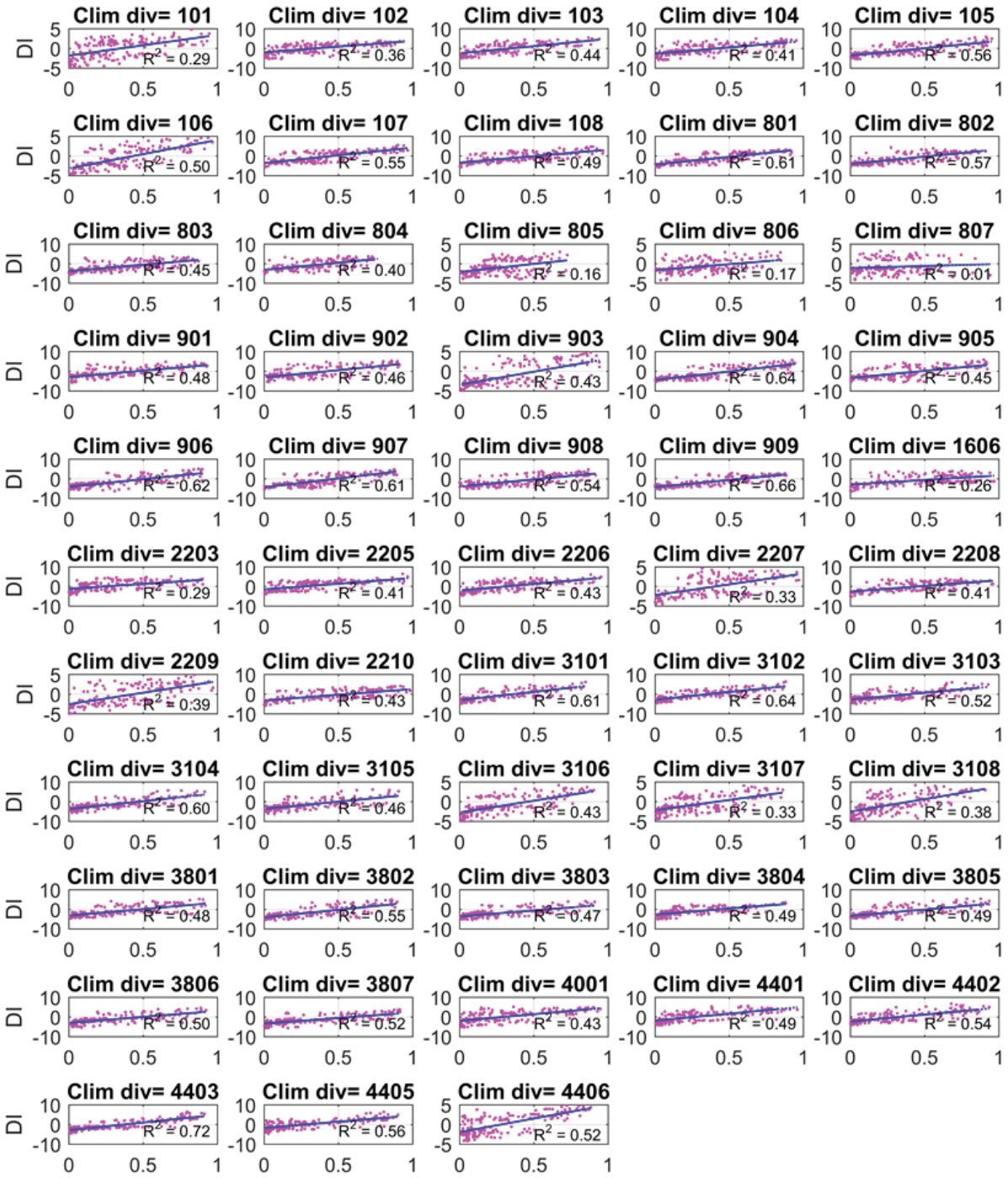

Figure 4-15: Scatter plots of monthly percentile of total column soil moisture aggregated to 8 weeks with PDSI for all 53 climate divisions in the South-Atlantic Gulf region for a period of 2000 through 2013.

Three performance matrices are used in this study to quantify the agreement between PDSI and total column soil moisture percentile (8-weeks aggregation) at watershed scale for different multiple severity conditions. The matrices are:

a) *Index of agreement (IOA):*

Number of months soil moisture percentiles correctly captured drought severity per total months the watershed experienced drought of a given severity.

b) *Drought prediction failure (DPF):*

Number of months soil moisture percentiles failed to capture drought severity per total month the watershed experienced drought of a given severity.

c) *False alarm (FA):*

Number of months soil moisture percentiles reported drought in the absence of actual drought per total number of months evaluated.

Note that IOA and DM are complimentary to each other and adds up to 100%. FA is calculated based on 384-month climatology (January 1982- December 2013).

Figure 4-16 shows the IOA, DPF, FA assessment for four drought severities namely, mild (PDSI <1 and soil moisture percentile < 0.3), Moderate (PDSI <2 and soil moisture percentile < 0.2), severe (PDSI <3 and soil moisture percentile < 0.1) and exceptional (PDSI <4 and soil moisture percentile < 0.05). Categorization of these indices based on drought severity classes helps in understanding the relative accuracy of soil moisture percentiles in capturing PDSI of a given severity range. For example, IOA for mild drought gives the agreement values between PDSI and soil moisture percentile when both PDSI and the soil moisture percentile classified drought

severity under mild category for the respective month. It can be seen from Figure 4-16 that IOA between PDSI and total column soil moisture percentiles (aggregated to 8 weeks) varies among watersheds and severity classification. Overall, IOA is seen to be above 50% for majority watersheds for Mild and Moderate droughts. However, IOA is high for the watersheds in Mississippi and Alabama states. While for some of the watersheds especially in the tip of Florida peninsula (watersheds 20-30) the IOA is seen to fall low. This is because of differences in the accuracy of SWAT models for the respective watersheds. Watersheds with a relatively low accuracy while calibrating the SWAT model are expected to show higher disagreement (DPF) with PDSI for the respective watershed. Also, IOA values are lower for most watersheds compared to respective values for lower severity values. This can be attributed to the observation that for most watersheds, low soil moisture percentiles predate PDSI values with similar drought severity. This is more noticeable in higher severity values. Overall, FA can be observed to be less than 15 percent of total climatology (384 months) for all watersheds across drought severity values.

An illustration of DPF, IOA and FA is provided in Figure 4-17. It can be observed that low PDSI values are not reciprocated in retrospective soil moisture percentiles for 1992-1993 period (DM). Year 1998 and 2005 are depicted as drought hit by soil moisture percentile which do not find correspondence in the respective PDSI values (FA) whereas both drought matrices capture severe drought in 2000, 2007 and 2013 (Agreement).

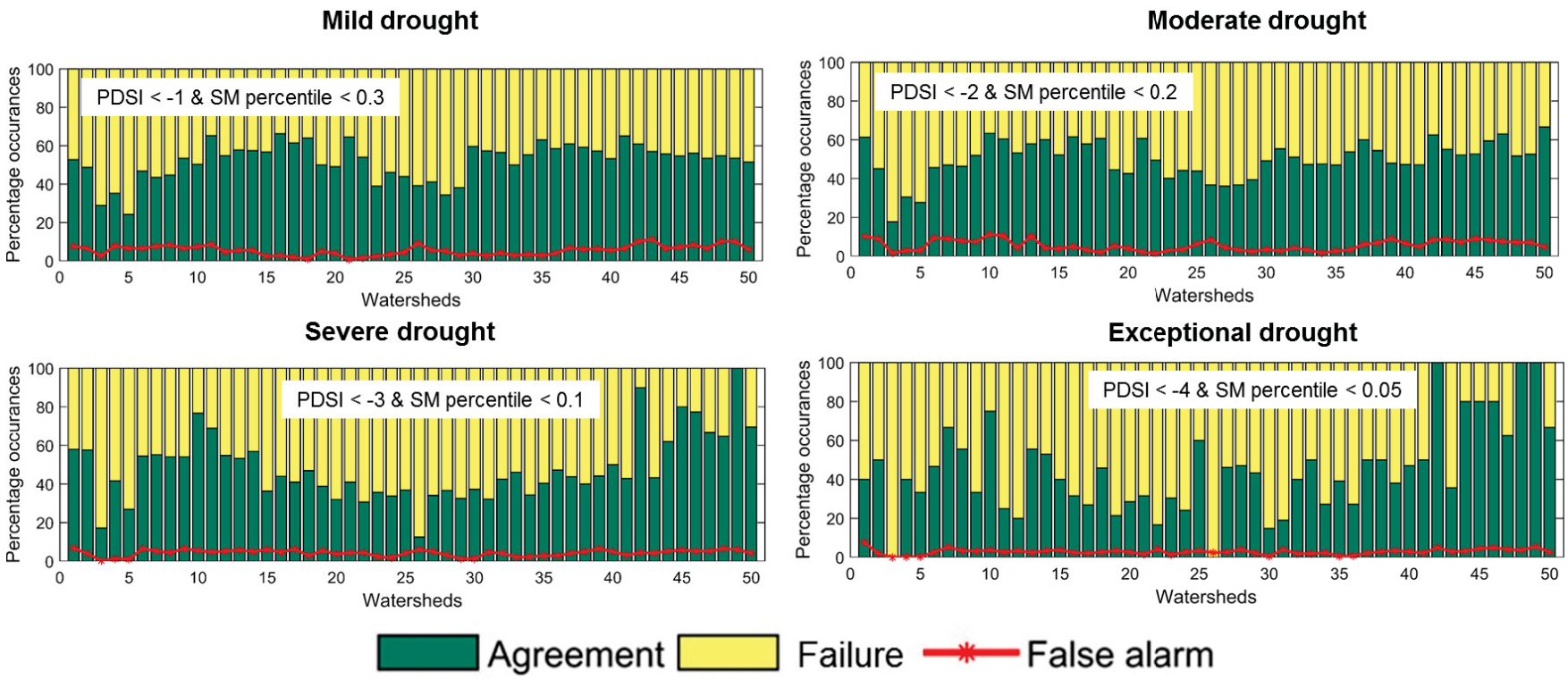

Figure 4-16: For all 50 watersheds: Index of Agreement (IOA), Drought prediction failure (DPF) and False Alarm (FA) between PDSI and total column soil moisture (aggregated to 8 weeks) for four drought categories namely Mild, moderate, severe and Exceptional based on January 1982 through December 2013 climatology.

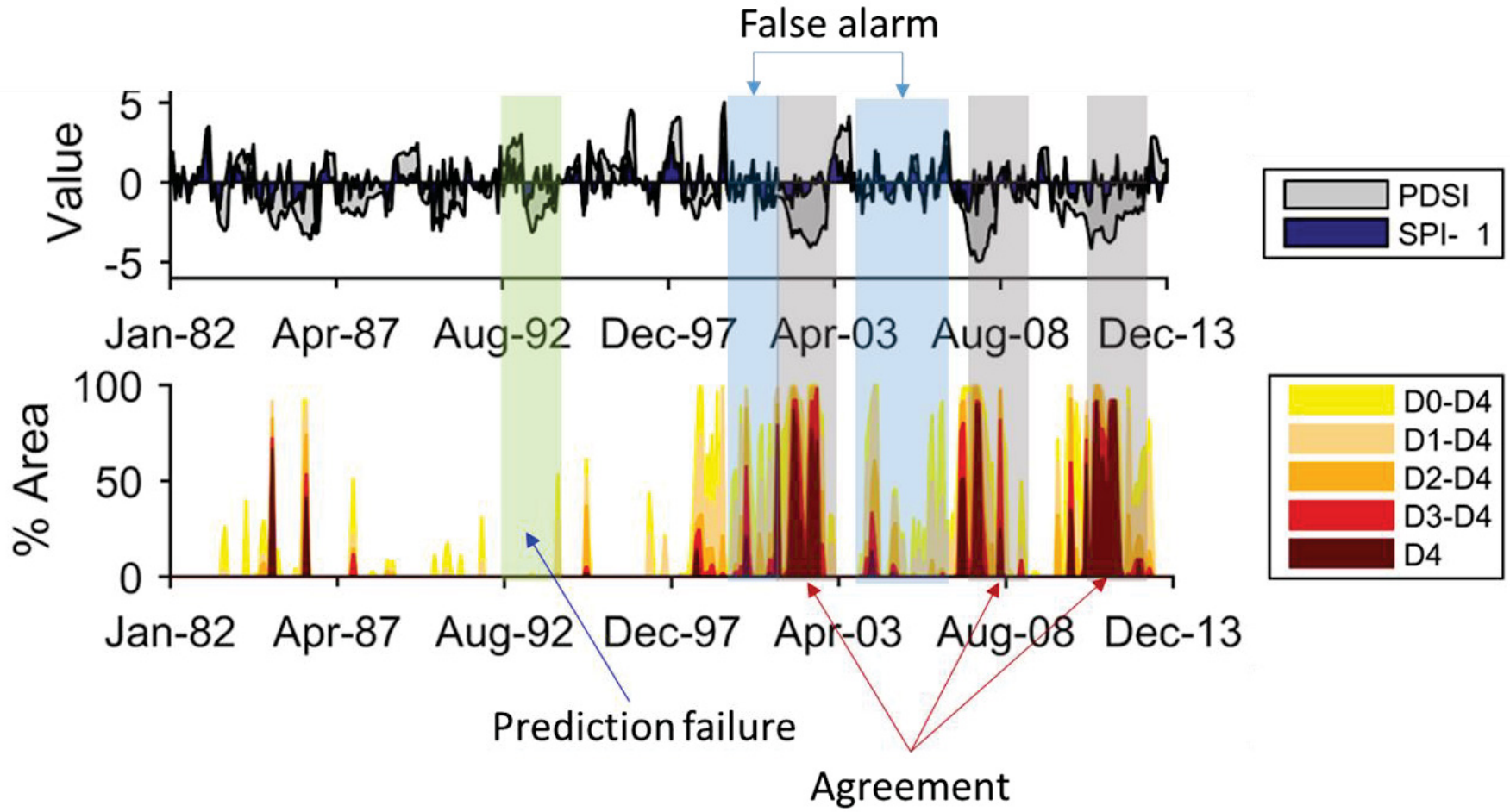

Figure 4-17: Illustration of agreement, false alarm and drought prediction failure (PDSI) conditions using total column soil moisture aggregated to 8 weeks from January 1982 through December 2013 for a selected watershed.

The focus of the analysis is also expanded to other hydrologic variables namely potential evapotranspiration (PET), actual evapotranspiration (ET) and precipitation to evaluate the relative correlation of the percentiles of these variables and the soil moisture from two soil layers with namely PDSI, PHDI, SPI-9, SPI-6, SPI-1 and Palmer Z index (ZNDX) for a period of 1982 through 2013. Spatial maps of correlation between the hydrologic variables and drought indices is provided in Figure 4-18. It can be observed from Figure 4-18 that soil moisture percentiles for total column soil moisture have high correlation (>0.6) with PDSI, PHDI SPI-12, -9 and -6 compared to other hydrologic variables across the region. Precipitation shows better correlation with SPI-1 and Palmer Z-index compared to other drought indices with correlation values over 0.7 in most regions. Potential evapotranspiration seconds precipitation in correlation with SPI-1 and Palmer Z- index with correlation values in the range of 0.4- 0.5. It should be noted that these values are higher than the correlation of surface soil moisture with the respective indices which remain in the range of 0.3- 0.4.

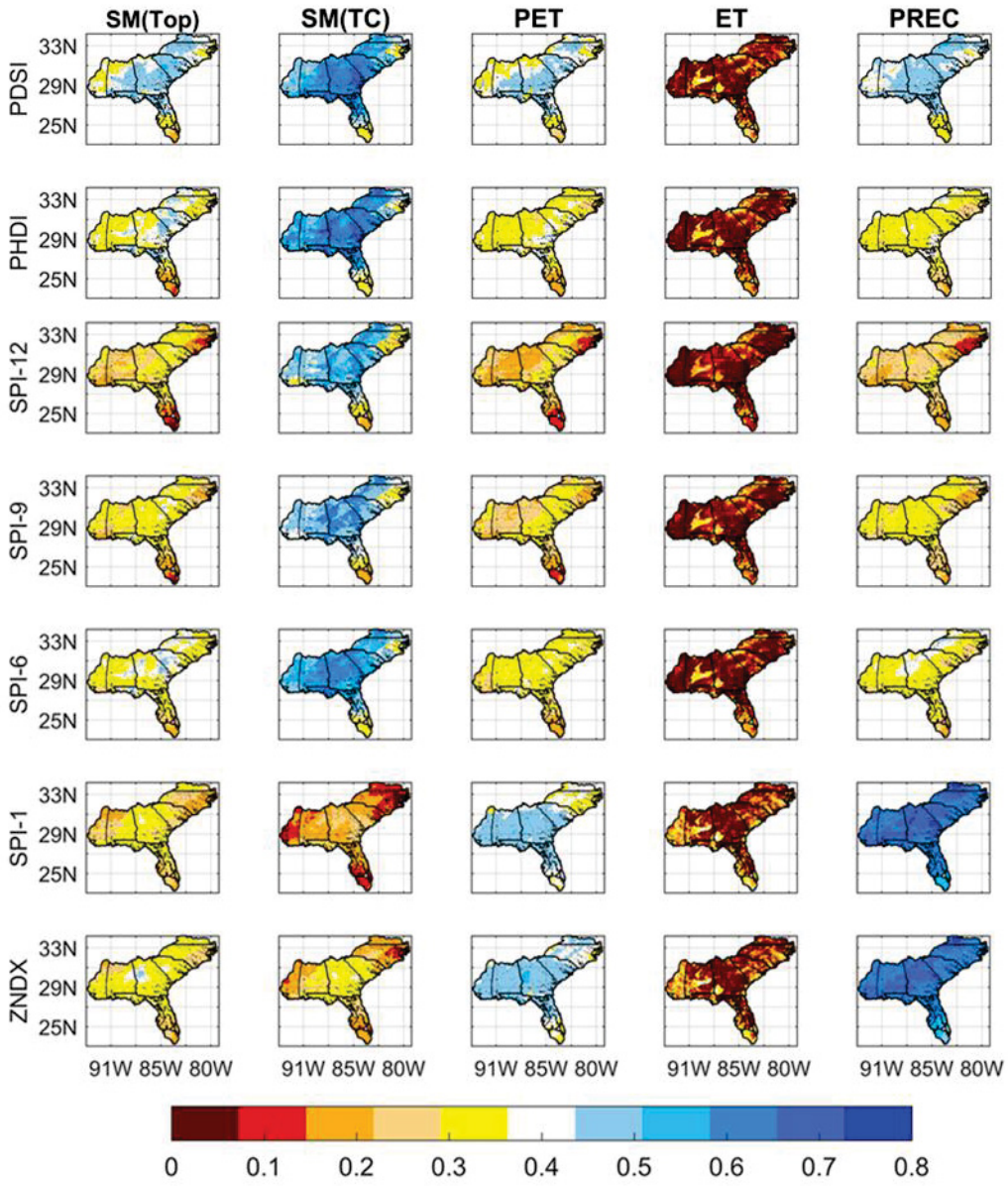

Figure 4-18: Correlation of monthly percentiles of (a) surface soil moisture (SM(Top)) (b) total column soil moisture (SM(TC)) (c) Potential evapotranspiration (PET) (d) Actual evapotranspiration (ET) and (e) precipitation (PREC) with eight drought indices namely PDSI, PHDI, SPI-9 , SPI-6, SPI-1 and Palmer Z index (ZNDX) for a period of 1982 through 2013.

5.4. Drought assessment and forecasting using SWAT-CFS v2 couple model outputs

After having established the accuracy of the proposed stratified approach for retrospective drought analysis using SWAT generated sub-watershed scale (HUC-12 resolution) soil moisture dataset, the approach is expanded to forecast drought severity for 9-months lead time using SWT-CFSv2 coupled hybrid models. SWAT-CFSv2 hybrid models provide hydrologic variables from January 2014 through March 2017 in near- time while the forecasted values are available for 9-months lead, through third week of December' 2017. Soil moisture percentiles are calculated in the same method as described in previous sections.

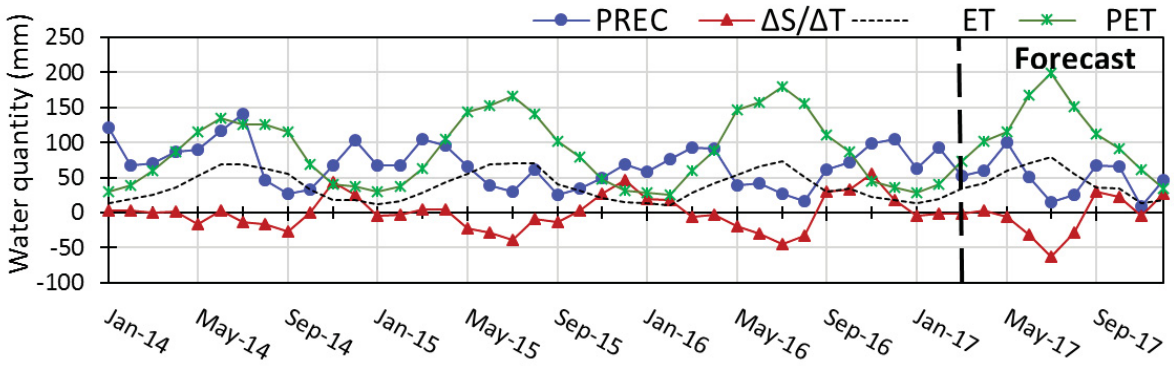

Figure 4-19: Area averaged values of mean monthly Precipitation (PREC), Actual Evaporation (ET), Potential Evapotranspiration (PET) and change in soil water storage ($\Delta S/\Delta T$) for the study region using SWAT- CFSv2 coupled models. The red line demarcates the SWAT-CFSv2 model warm-up (January 2014 through March 12th, 2017) from model forecast period (March through December 2017). The blue share highlights dry conditions in June- October 2016 and forecasted dry condition in April- September' 2017.

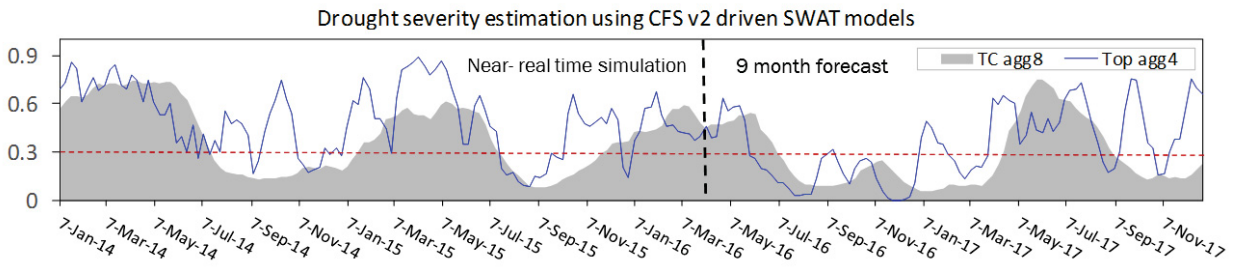

Figure 4-20: Weekly percentiles of the area averaged soil moisture for SAG region using 8- weeks aggregated total column soil moisture (shaded in gray) and 4-weeks aggregated surface soil moisture.

Figure 4-19 provides the time series of PREC, $\Delta S/\Delta T$, PET and ET for January 2014 through December 2017 using SWAT- CFS v2 coupled models. It can be seen from Figure 4-19 that the SWAT-CFSv2 coupled models are able to capture a recent drought in the region in 2016. The period of June through October 2016 is seen to have low soil moisture and precipitation while above normal PET and ET. Time series of weekly soil moisture percentiles from the top and total column soil moisture from SWAT-CFSv2 coupled models is provided in Figure 4-20 for a period of Jan 2014 through Dec 2017. For performance evaluation of near-real time drought severity maps from the models, Figure 4-21 provides a comparison of SPI-1 and PDSI for the SAG region with soil moisture percentiles aggregated to 4- and 8- weeks from surface and total column respectively. It can be observed from Figure 4-21 that the soil moisture percentiles obtained from SWAT-CFSv2 models are able to capture the 2016 drought in the region. The strength of agreement is more between PDSI and total column soil moisture percentile as seen in previous analysis as well. While there are inter- layer and inter basin variations in drought predictability, the models are, overall, able to reflect on the drought conditions in the region. Figure 4-22 provides IOA, FA and DM values between PDSI and total column soil moisture from SWAT-CFSv2 coupled model (aggregated to 8 weeks) for a period of January' 2014 through March' 2017. Results indicate that

high IOA exists between the PDSI and estimated drought severity. For majority watersheds, IOA is found to be greater than 60%. Some of the watersheds did not experience any drought in a particular severity class in the period of evaluation and hence no IOA or DM values are assigned to such watersheds (For example 1-10 watersheds in severe drought category). The IOA values can be seen to increase with increasing severity class indicating that the simulated soil moisture percentiles are very effective in capturing Severe and Extreme drought in near-real time mode using SWAT-CFSv2 model outputs. However, a higher number of FA is observed especially for the mild and moderate drought categories due to *(i)* higher sensitivity of soil moisture percentiles to transient droughts for these watersheds, and *(ii)* a smaller period of evaluation (39 months) leading to high percentage of FA with relatively less number of actual FA months.

Concurrent values of the USDM drought maps for the region with respective weekly maps generated using SWAT-CFSv2 model soil moisture percentiles in forecast mode for 12 weeks is shown in Figure 4-23 for a period of 21st March' 2017 through 6th July' 2017. The USDM and simulated drought severity maps have a high degree of spatial association for 1st month (21st March- 18th April). However, the disagreement between the USDM and simulated drought increases with increasing lead time of forecast. This can be directly linked to increasing uncertainty in the meteorological drivers from CFSv2 model with increasing lead time. Assessment of uncertainty in CFSv2 meteorological data for increasing lead time in a topic of further research and can be used to assign an accuracy score to simulated drought maps with increasing lead times.

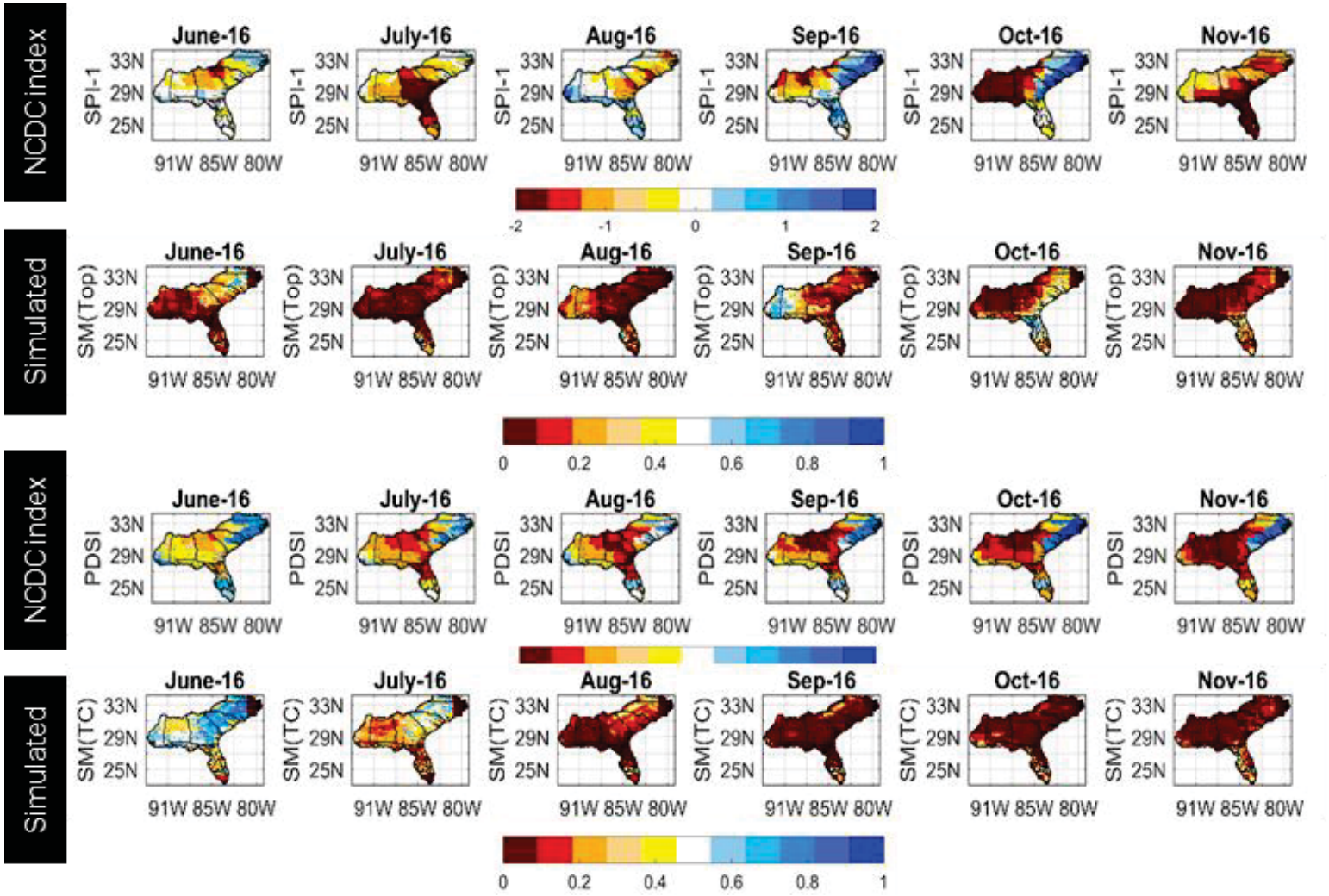

Figure 4-21: Comparison of SPI-1 and PDSI with monthly percentiles of (a) surface soil moisture (b) total column soil moisture obtained from SWAT-CFSv2 coupled models in near-real time for a period of June through November 2016.

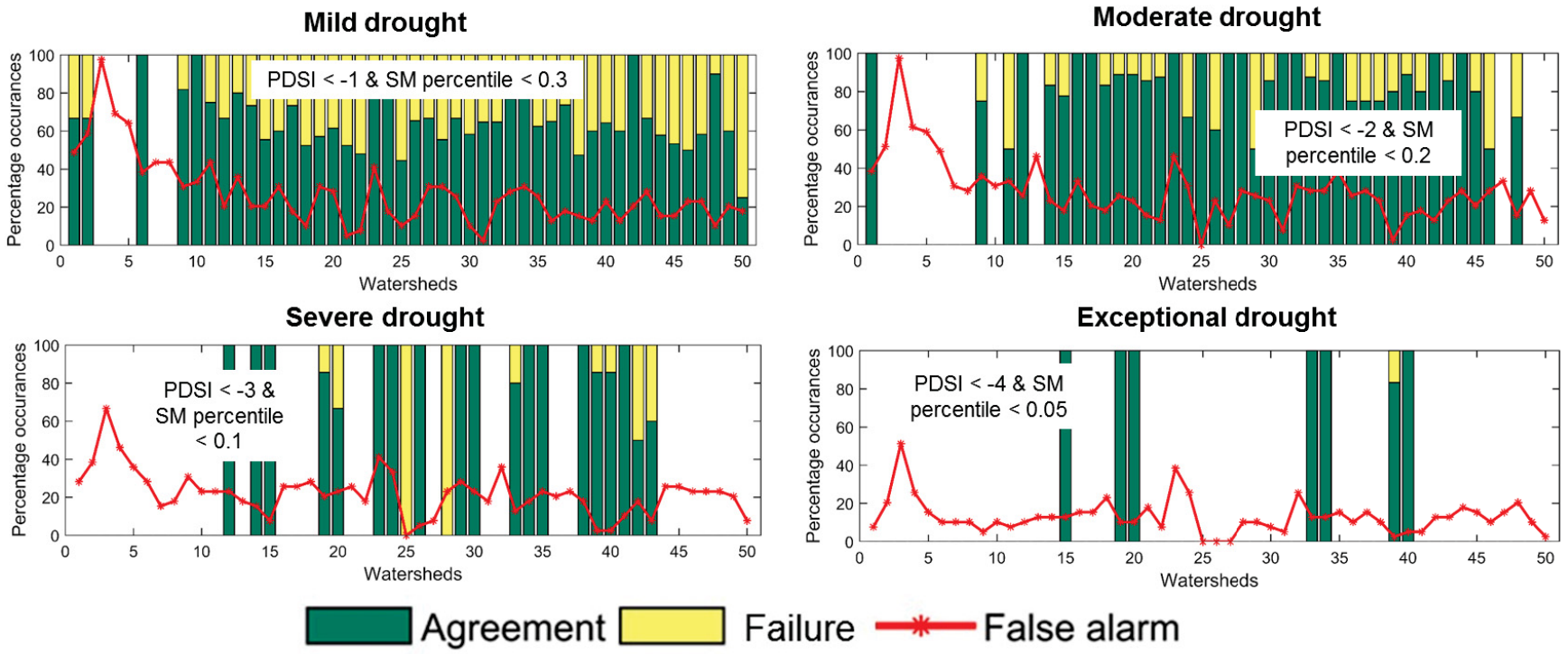

Figure 4-22: Same as figure 16, but using SWAT-CFSv2 coupled model outputs in near- real time mode for Jan 2014- March 2017 period.

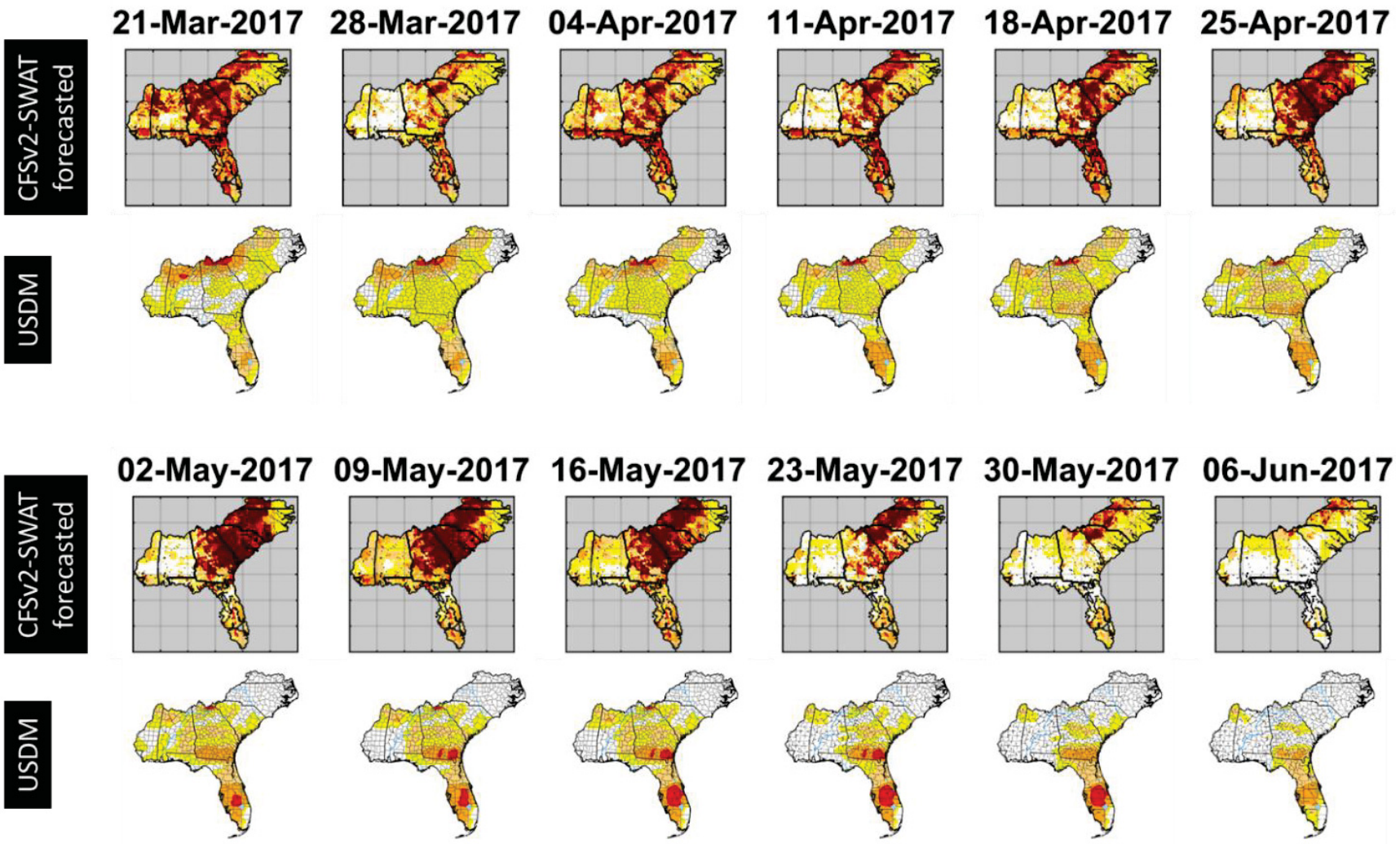

Figure 4-23: Comparison of the USDM and simulated drought severity maps using SWAT-CFSv2 coupled models in the forecast mode from 21st March' 2017 through 6th June 2017.

Conditions similar to June- October 2016 are forecasted to occur in Mid of 2017 leading to drought conditions in the region. Figure 4-25 shows the drought severity map for the SAG region showing forecasted drought conditions from April through December 2017. While precipitation of the range of 100 mm in most part of the region is expected to provide relief from drought conditions, moisture deficit during late July and August is forecasted to contribute to building up of dry conditions in Alabama, Georgia, most parts of Florida and parts of Louisiana.

Dry and hot conditions in the later part of 2016 contributed to forest fire in several parts of North and South Carolina, Tennessee, Georgia during this period. Figure 4-24 provides a comparison of the estimated drought severity using the SWAT-CFSv2 coupled model outputs, and incidences of forest fire in the Tennessee-North Carolina region during November 2016 as recorded by the Moderate Resolution Imaging Spectroradiometer (MODIS) aboard the Aqua satellite. Due to persistent drought conditions in the region, several instances of forest fires were recorded during the time. Strong agreements between droughts and forest fire in the region can be observed from Figure 4-24 thus establishing the scope of the proposed real-time drought monitoring approach for a range of applications including estimating the risk of forest fires.

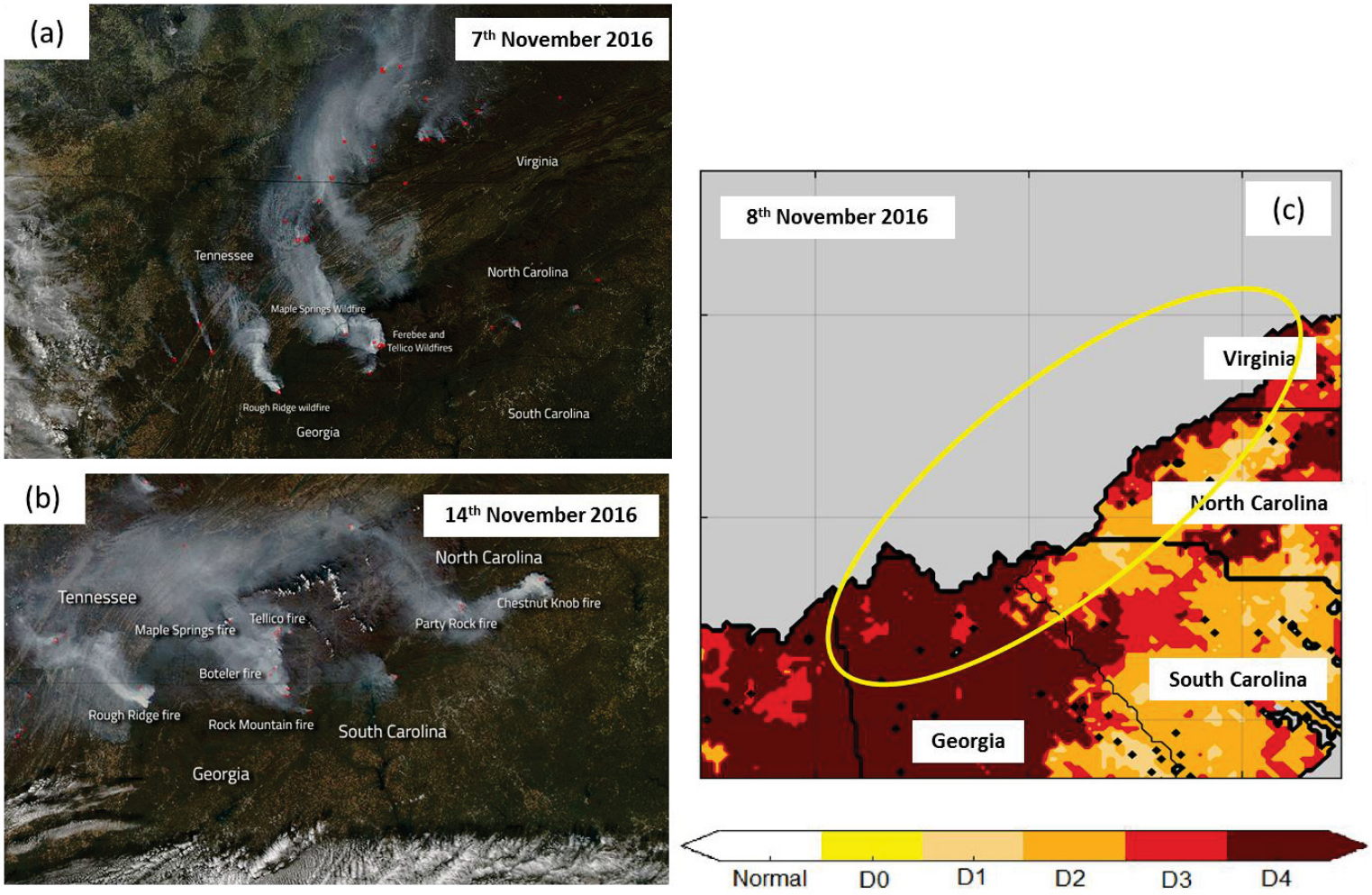

Figure 4-24: (a) and (b) Forest fires in the Tennessee-North Carolina region during 7th and 14th of November, respectively. (c) Estimated drought severity in the region using the SWAT-CFSv2 hybrid models for November 8th. The remote sensing images are captured by the Moderate Resolution Imaging Spectroradiometer (MODIS) aboard the Aqua satellite.

6. Discussion

A layer- wise perspective is imperative to completely represent the water transport dynamics in the soil column in the event of drought. While, drier conditions in the near surface soil layer may indicate short-term meteorological drought, it may not be a good measure of agricultural drought if the root zone soil is relatively wet. Deficit soil moisture storage in the total soil column may be indicative of hydrological drought but a single storm may replenish root zone soil moisture enough to relieve agricultural drought, yet hydrological drought could inflict the region over a season (Sheffield et al., 2004b). Deeper layers represent the water availability for plant uptake, aquifer recharge, and, baseflow to streams, whereas, the near- surface soil moisture indirectly indicates the dryness of the deposited plant litter which may indicate susceptibility to other natural hazards like wildfire, essentially, aggravating drought conditions. A detailed study on the dynamics of soil moisture can be found in D'Odorico et al. (2000).

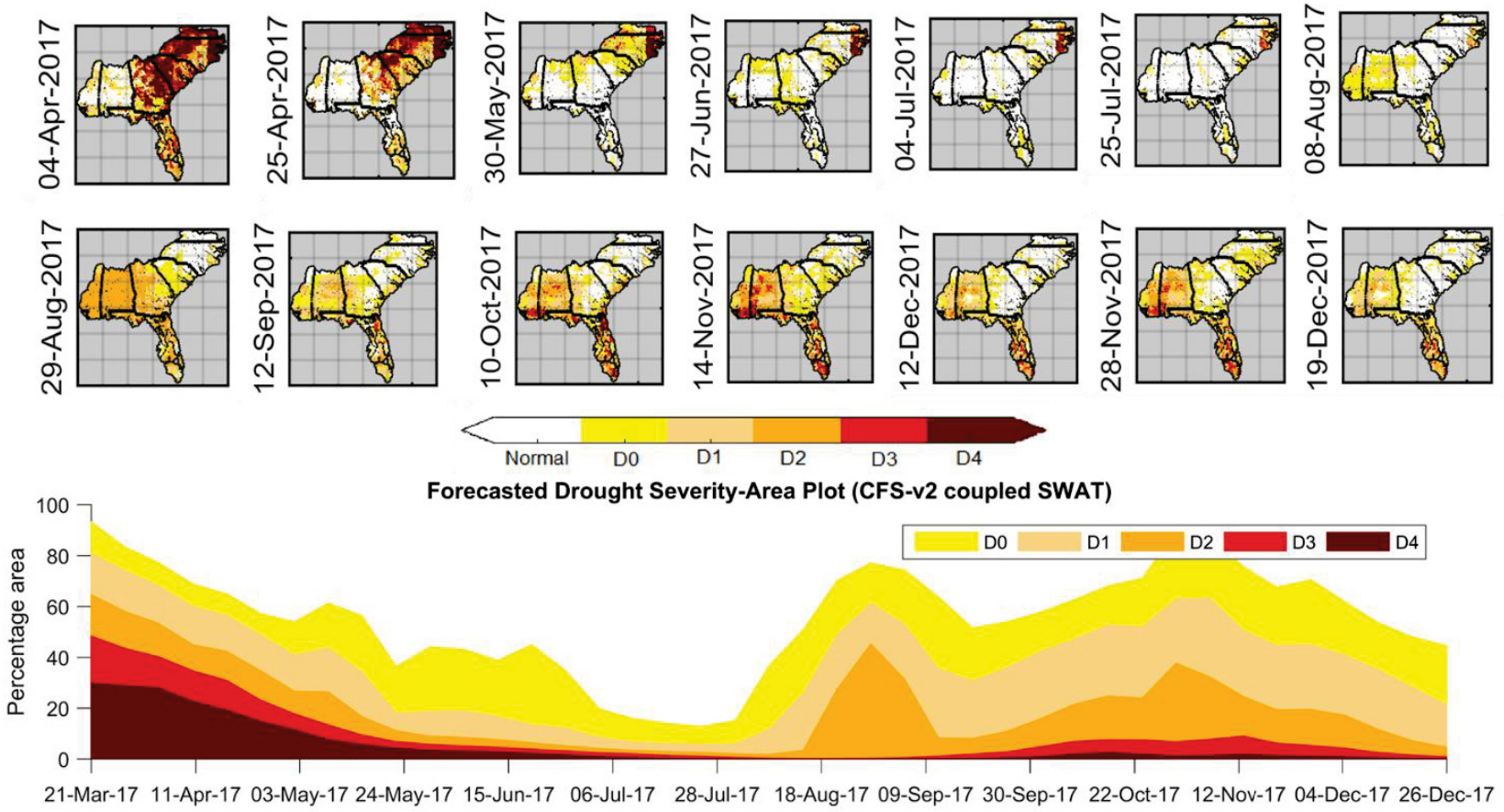

Figure 4-25: (Top) Drought severity maps for the South-Atlantic Gulf region using the stratified soil moisture percentile approach using SWAT-CFSv2 coupled soil moisture percentiles for top and total column soil profiles (Bottom) Drought severity-area plot for the forecast period (Third week of march through third week of December' 2017 using SWAT-CFSv2 coupled model soil moisture percentiles.

The variability in soil moisture can be effected by scale (spatial and temporal), season and hydroclimatology of the study region, and can significantly alter the choice of the distributions to estimate the variability in the data. Seasonal and geographical variations in soil moisture variability can be attributed to a combination of factors like hydroclimatology (precipitation, evapotranspiration, transpiration), surface characteristics (soil texture, topography, vegetation, land use and land surface properties, drainage etc.) and infiltration-runoff processes of the study region (Famiglietti et al., 2008; Kim and Barros, 2002; Oldak et al., 2002; Peters-Lidard and Pan, 2002; Teuling and Troch, 2005).

Ignoring the heterogeneity at sub-watershed scale may lead to a substantial bias in simulated surface water and energy fluxes (Crow and Wood, 2002; Famiglietti and Wood, 1995), infiltration and surface runoff (Famiglietti et al., 2008). In order to reduce this error, the heterogeneity of soil moisture at finer scales is often parameterized using the soil moisture variance and assuming a certain type of probability density function (PDF) (Famiglietti et al., 2008). Characterizing soil moisture variability using a probability density function (PDF) is an important task in translating soil moisture values to their respective percentiles, however, there is a considerable difference in the choice of distribution functions employed by various studies to capture soil moisture variability (simulated or field observed). In previous studies, normal (Kim et al., 2015), lognormal (Li and Avissar, 1994; Sivapalan and Wood, 1986), gamma (Entekhabi and Eagleson, 1989; Famiglietti and Wood, 1994), extreme value (Brabson et al., 2005) distributions, among others, have been effectively used to estimate the variability in soil moisture data. Kernel density plots for the daily total-column soil moisture data for the 50 watershed is shown in Figure 4-26 to highlight the spatial variability in the distribution of soil moisture for the study area.

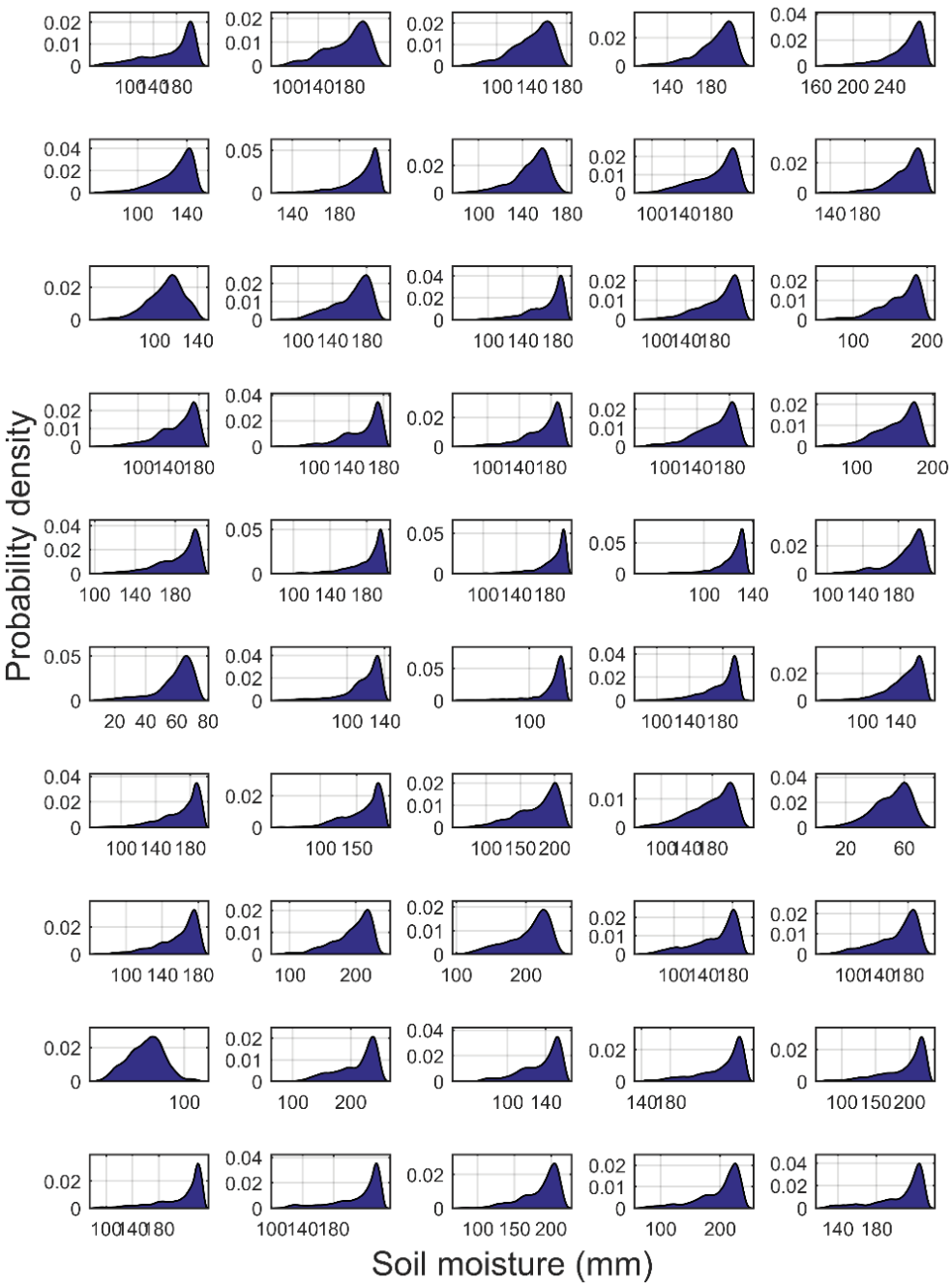

Figure 4-26: Kernel density plots of the averaged soil moisture data for each sub-watershed.

Figure 4-27 provides a comparison of the histograms of the week- wise soil moisture for two distinct periods i.e. April (Week 15) and August (Week 35) to highlight the difference in the distribution of soil moisture for the respective weeks. While mean soil moisture for Roanoke,

Satilla and Pearl sub-watersheds is higher for April, soil moisture shows lower mean and higher variance for the months of August. Similar observation can be made for Satilla River with an exception that the mean soil moisture for August is higher compared to April. These variations are primarily driven by seasonal hydroclimatology of the respective watershed. Since this study provides drought severity maps at a weekly time-step, selection of suitable distribution function to capture the variability in soil moisture for each week becomes important for effective drought severity estimation at sub-watershed scale.

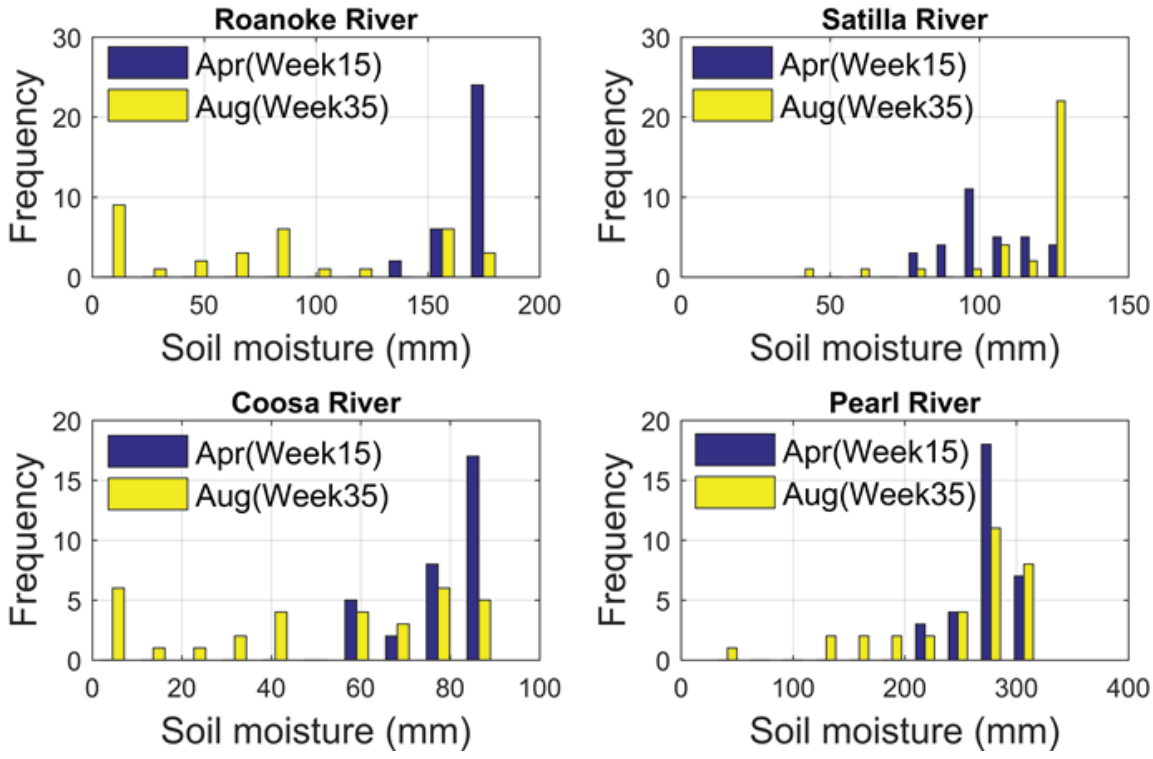

Figure 4-27: Histogram of the total column soil moisture data for 15th and 35th calendar week for four watersheds. Note the difference in the shape and spread of the histograms for the two selected weeks for the watersheds.

The interplay of the mean and variance of the soil moisture time series for different part of a year is important in selecting the right distribution function to effectively capture soil moisture variability. An analysis is carried out in this study to study the relationship between the mean and variance of soil moisture for each calendar week for the 50 watersheds which in turn, reflects on the choice of the distribution function to estimate soil moisture variability at watershed scale. The mean and variance for each week is calculated using the historic simulation (January 1982-December 2013) and later divided by the maximum value for each watershed in order to obtain a comparable range of values across different watersheds. Two distinct phases in the relationship between the mean and variance of week- wise soil moisture is observed (Figure 4-28):

a) *Increase in mean soil moisture with decreasing variance*:

This part of the year is marked by increasing mean soil moisture with subsequent weeks whereas the variance in soil moisture is seen to decrease. Empirical fit to this phase shows that an exponential curve can be used to satisfactorily explain the process where the variance in soil moisture for the week is a factor of mean soil moisture through the following relationship:

$$Variance = a' e^{-\acute{b}`(Mean)} \quad (2)$$

Where $a`$ and $b`$ are constants.

b) *Decrease in mean soil moisture with increasing variance*:

This is a complimentary process to *(a)* where the mean soil moisture decreases whereas the variance in soil moisture increases over the weeks. Empirical fir to the data reveals that the interrelationship between variance and mean of soil moisture follows a second- order polynomial function as follows:

$$Variance = aMean^2 + bMean + c \quad (3)$$

Where *a, b* and *c* are constants for the respective sub-watershed.

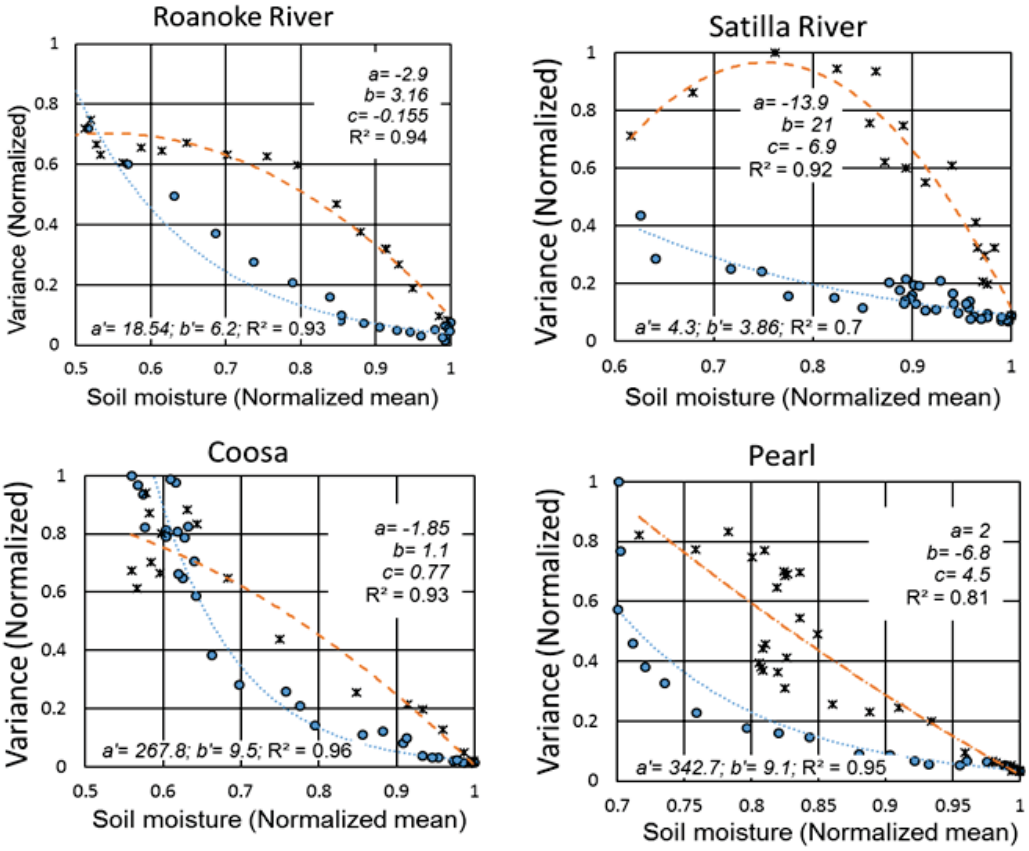

Figure 4-28: Relationship between mean and variance of soil moisture for each calendar week for Roanoke, Satilla, Coosa and Pearl River watersheds. The coefficients and R^2 of empirical fit to the watershed scale mean and variance of soil moisture for all calendar weeks of a year is provided in the plots.

However, the proposed approach of weekly (or monthly) percentile estimation has certain limitations The proposed approach for drought severity assessment using weekly (or monthly) percentiles is developed in a time independent way, which means, that the drought severity is estimated for the current month and hence compromise on maintaining the continuity during

month-to-month transitions and doesn't account for the contribution of the additional soil moisture for hydrologic processes in the next time step.

Though this paper provides the foundation of linking watershed-scale hydrological modeling with short-term seasonal weather products like CFSv2, the assessment of the modeling efficiency for multiple leads time remains to be the subject of further research. Zhang et al. (2017) tested the efficiency of VIC models initialized with satellite-aided monitoring (MONIT), CFSv2 and ensemble streamflow prediction (ESP) and evaluated the performance of soil moisture forecast skill and observed that the uncertainty in the soil moisture forecast is mostly controlled by initial conditions at the first month and that uncertainties in the CFSv2 climate forecasts have the largest contribution to SM forecast errors at longer lead times.

While the climatology and dataset for the USDM and this study are not the same, the USDM involves many other factors like county-level information on drought, reservoir levels, snowpack and groundwater which may lead to different interpretation of drought at local scales. However, the proposed representation of drought severity is directly comparable to the USDM maps, which are popular benchmarks for drought analysis, making it easier for the policy makers in taking decisions based on evolving hydrometeorological conditions.

6.1. Comparison with empirical approach of severity estimation: EDDI vs PET percentiles

Many studies have demonstrated the application of empirical plotting positions for percentile calculations of hydrological variables (and hence, drought severity assessment) for e.g. Tukey plotting position (Hobbins et al., 2016; Wilks, 2011), Gringorten plotting position (AghaKouchak et al., 2014; Gringorten, 1963; Kang and Sridhar, 2017), Weibull plotting position (Makkonen,

2006; Wang et al., 2009) etc. To highlight the effectiveness of the proposed discretized approach of selection of distribution functions for severity estimation (to account for seasonal and geographical variability), a comparison in made between the monthly percentiles of PET and an evaporative demand deficit index (EDDI) using Tukey plotting position for obtaining percentiles of PET as proposed by Hobbins et al. (2016). Figure 4-29 provides a comparison between severity estimated using the two approaches. Figure 4-29 (a) provides a correlation between EDDI and PET percentiles calculated for the entire study region (all HUC-12 sub-watersheds). It can be observed that the overall correlation between the two approaches is very high for all the regions (>95%). However, the correlation values are comparatively low for southern Florida watersheds compared to other regions. A comparison of the normalized time series of PET percentiles using the proposed and the empirical approach is provided in Figure 4-29 (b), for a selected location in Southern Alabama show that severity estimates for the extreme values differ for the two approaches. While the two approaches conform with each other for the most and the least severe occurrences (Normalized values of 0 and 1), there is an overestimation of the drought severity using the proposed percentile calculation approach. This is observable from the drought severity-area plots for 2000 - 2013 period for the SAG region as provided in Figure 4-30 and Figure 4-31. It can be seen from Figure 4-30 that, while PET percentiles are able to reflect on the transient drought conditions in the region, the severity of drought is overestimated compared to the empirical approach. In comparison to the USDM severity-area maps, both estimates of drought severity can be seen to be highly transient in nature and highlights the need of aggregation of PET values to longer temporal scales as done for the soil moisture dataset in the previous analysis (Figure 4-10). Figure 4-31 compares the area under different drought categories classified using the proposed and the empirical approach. It can be seen that the severity values of PET are underestimated using the

empirical approach, whereas the proposed approach is observed to provide a more conservative estimate of drought severity. The empirical approach of percentile calculation is based on the retrospective dataset and is strongly influenced by the bimodality of the data (Figure 4-26). This leads to a higher density of values in the mid-severity classes. However, in the parametric distributions, the severity classes are influenced by the mean values of the dataset and lower density is assigned to the extreme values. This leads to higher sensitivity of the distribution to severe values compared to the empirical approach. The proposed parametric approach of severity estimation is desirable in the forecasting applications in non-stationary climate where the future values may have significant effect on the kernel density of the dataset compared to the historically observed values. A comparison of the drought maps from the two approaches with the USDM maps for some selected months are provided in Figure 4-32. A clear disagreement between the two approaches of severity estimation is evident. It can be observed from Figure 4-32 that the oversensitivity of the proposed severity estimation approach to drought conditions is not spatially dependent and there is a systematic bias in severity assessment irrespective of spatial locations.

Also, it can be seen from Figure 4-29 (c) that the cumulative density function of EDDI is pixelated compared to PET percentiles calculated using the proposed approach. Because of relatively low sample size (~32, corresponding to 1982-2013) for each month in calculating percentiles using the empirical approach, the PET values are classified into 32 percentile classes. However, in the proposed approach, the sample severity space is divided into much larger (1000 in this study) classes which leads to a smoother ECDF of the PET percentiles compared to EDDI.

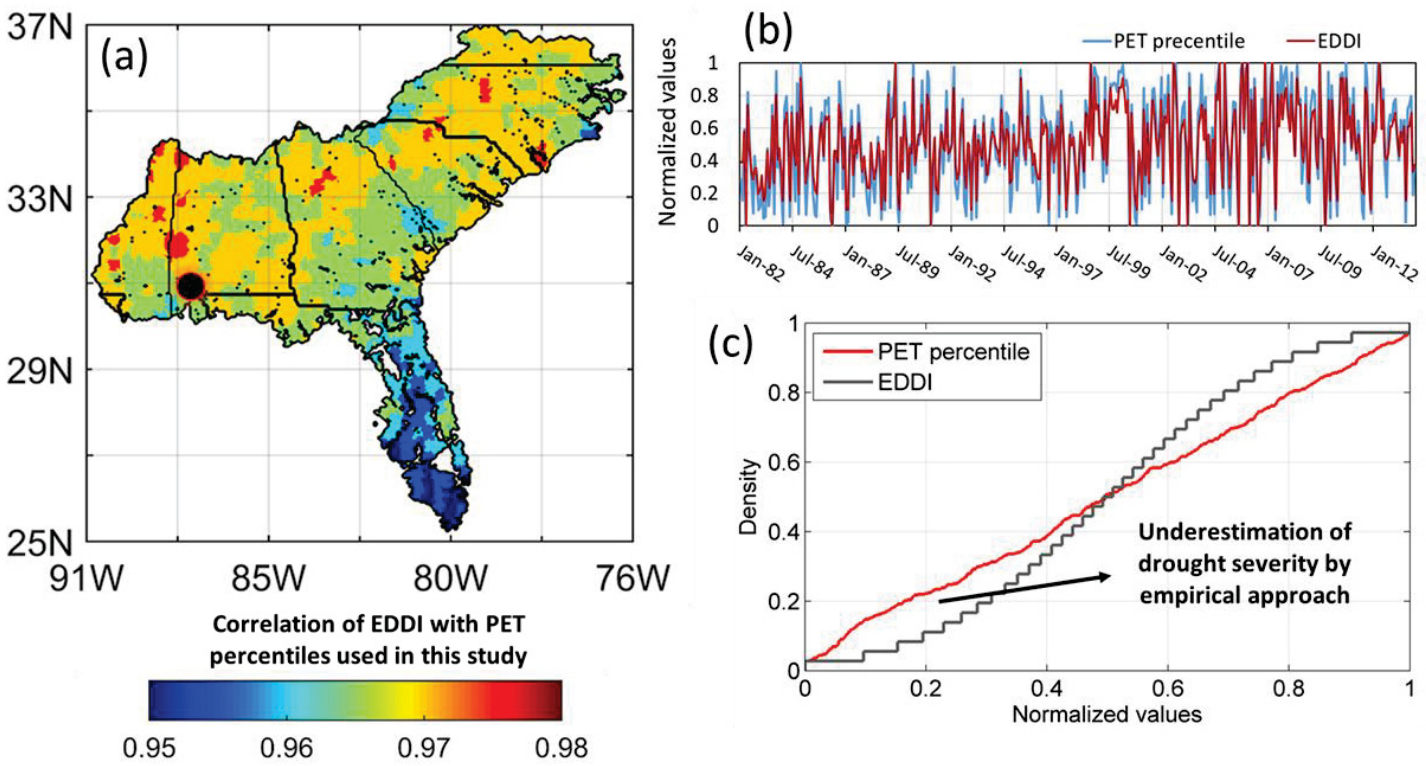

Figure 4-29: (a) Correlation between EDDI (empirical approach for severity estimation as proposed by Hobbins et al. (2016) and PET percentiles for the study region. The black dot in South Alabama marks the location selected for comparing EDDI and PET percentiles (b) Comparison of PET percentiles and the EDDI time series for Jan 1982 through December 2013 for the selected location (c) Comparison of the empirical cumulative density function (ECDF) of the normalized values of EDDI and the PET percentiles for the selected location.

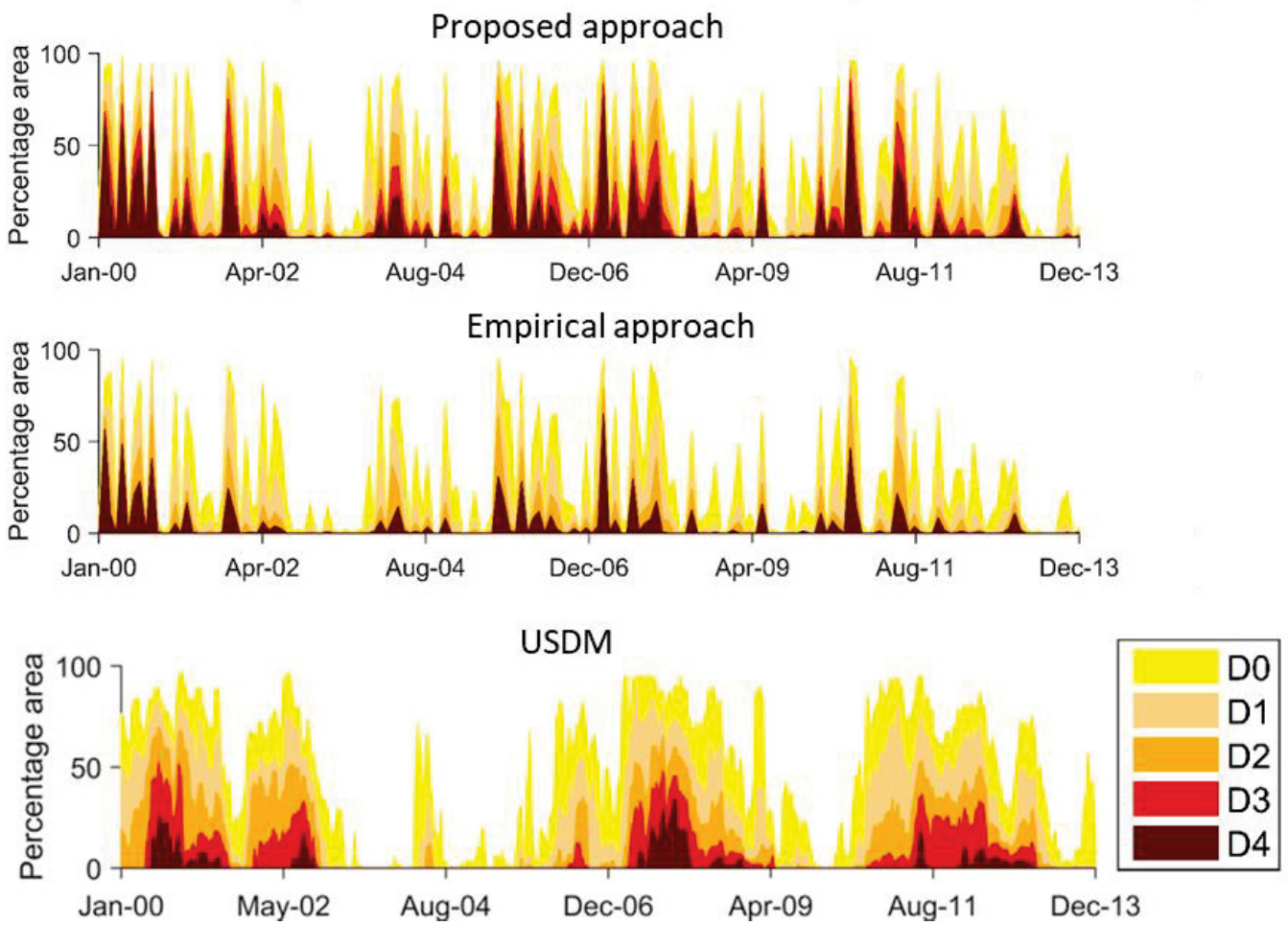

Figure 4-30: Comparison of drought severity-area plots for the South-Atlantic Gulf region using percentiles of the SWAT model-generated PET using the proposed approach (Top), empirical approach as proposed by Hobbins et al. (2016) (Middle) and USDM (Bottom).

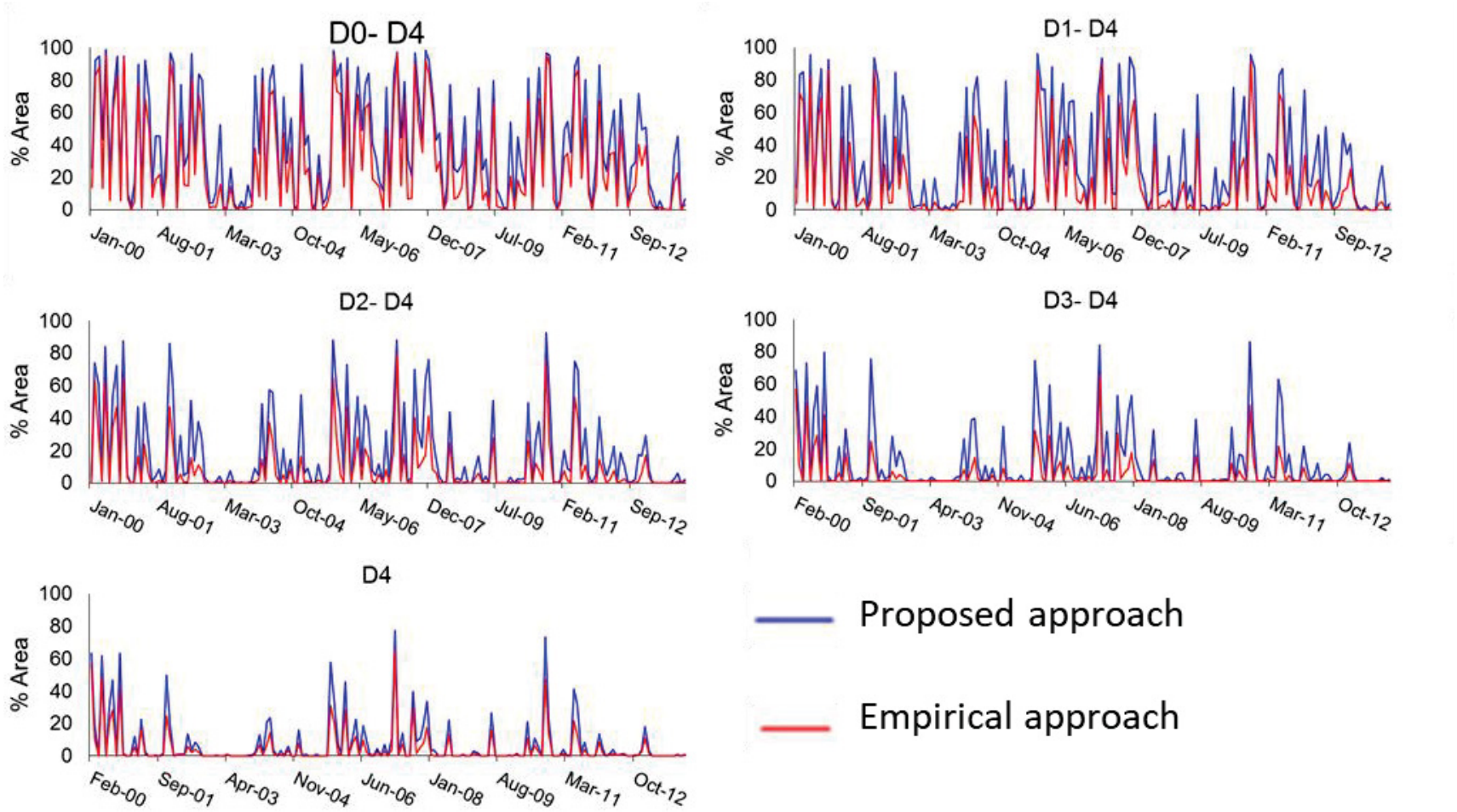

Figure 4-31: Comparison of area under drought for various drought severity categories using the proposed and empirical approach for drought severity classification during January 2000- December 2013 for the South-Atlantic Gulf region.

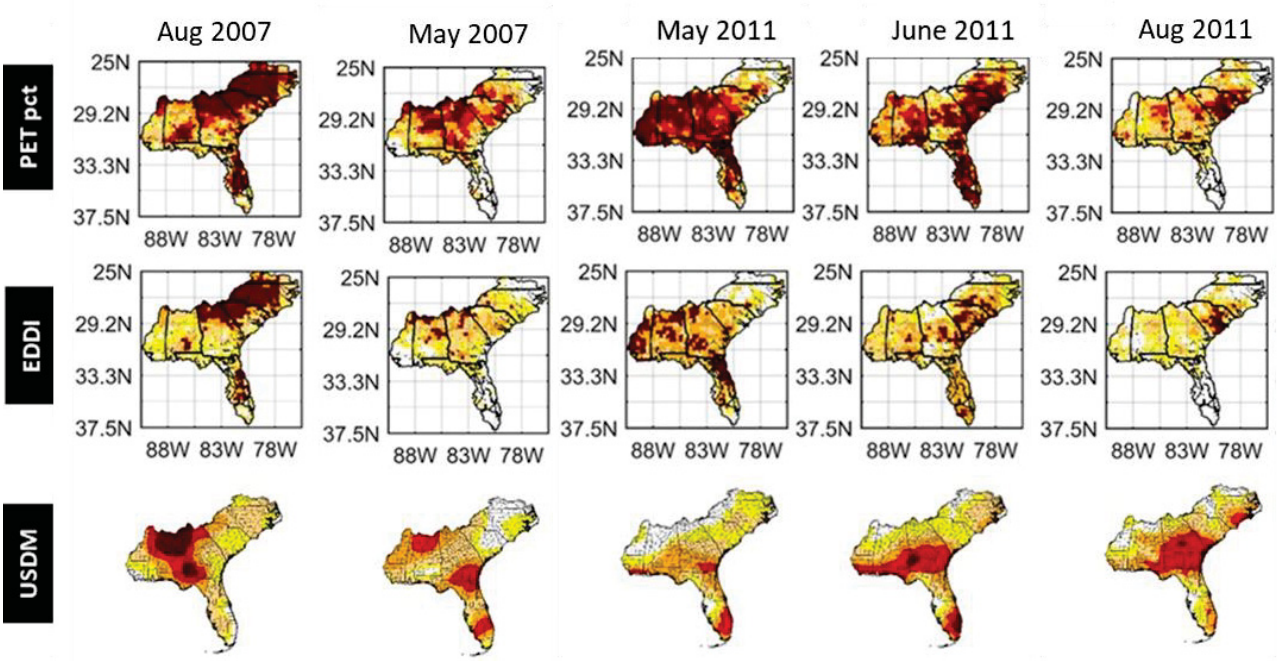

Figure 4-32: Comparison of drought maps generated using the proposed PET percentile calculation approach and empirical approach for severity estimation, with the USDM drought maps for some selected months.

It is to be noted that both, EDDI and PET percentiles are calculated from the outputs from the SWAT models at sub-watershed scale for comparison between the two approached of percentiles estimation. However, Hobbins et al. (2016) uses the North American Land Data Assimilation System phase-2 (NLDAS-2; Xia et al. (2014b)) forcings and apply the ASCE Standardized Reference ET formulation (Walter et al., 2000) for calculating the evaporative demand.

6.2. Soil moisture-based drought severity estimation and the general perception of drought

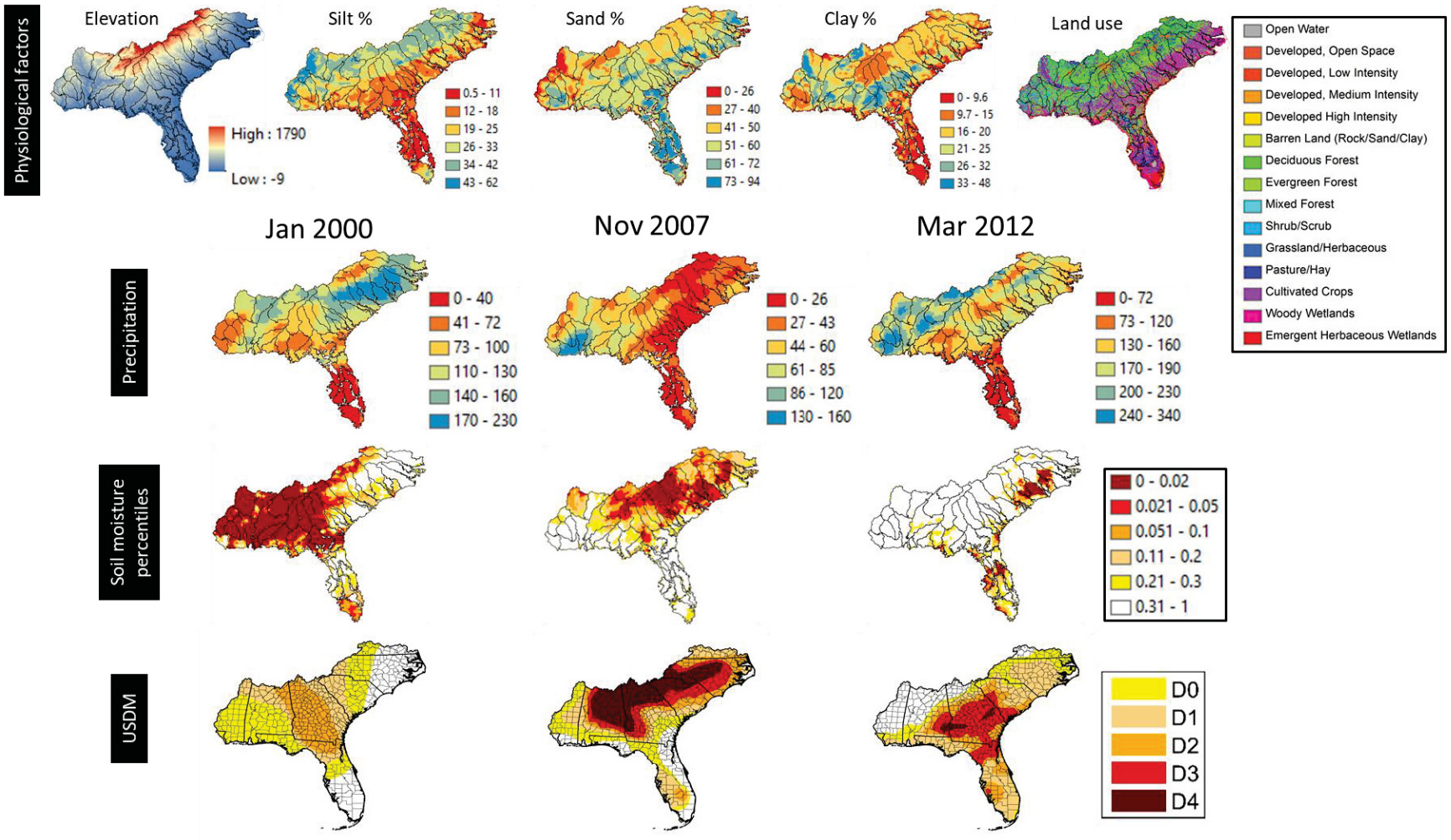

Figure 4-33: Spatial representation of several physiological factors Elevation, Soil composition (Silt, sand and clay percentage) and land use compared with monthly precipitation (in mm) , monthly soil moisture percentile and concurrent USDM maps for January 2000, November 2007 and March 2012.

In this study, the water deficit, and thus the drought conditions, are estimated by calculating the deviation of the natural conditions of soil moisture from the historic normal values for the respective month or week. However, these extremes may be exasperated by several anthropologic interventions. The difference in the hydrologic/soil moisture/meteorological extremes and the people's perception of drought can be linked to availability of water for several applications like public water demand, agricultural practices, industrial utilities, recreation etc. Hence, similar meteorological conditions in one watershed, may trigger a different perception of drought in that region compared to another watershed with different geographic conditions, public water needs and/or agricultural applications etc. Figure 4-33 provides several physiological factors like elevation, soil composition (Silt, sand and clay percentage) and land use for the SAG region and a comparison is made between monthly precipitation, total rooting depth soil moisture percentile and USDM maps for three months i.e. January 2000, November 2007 and March 2012. It can be seen from Figure 4-33 that while there is a strong relationship between precipitation and soil moisture percentiles, the meteorological extremes (wet or dry soil) may not necessarily translate to the same perceived drought category (represented by the USDM maps).

7. Conclusion

This study provides a retrospective drought analysis and a near- real time drought forecasting framework using simulated hydrological variables by SWAT- CFSv2 coupled models for the South-Atlantic Gulf region of the Southeastern US. Retrospective analysis is carried out for a period of 1982 through March 2017 and drought forecasts are provided for a period of March through December 2017 at a weekly time step. The study uses a stratified approach to capture drought onset and persistence using surface soil moisture to characterize low-intensity droughts and total rooting depth soil moisture to capture persistence and severity of severe droughts.

Accuracy of the proposed approach is established by comparing the simulated drought maps with those of US drought monitor and other drought indicators provided by NCDC (PDSI, PHDI, Palmer Z index and SPI-1, 6, 9, and 12) for the region. The study finds that the soil moisture percentiles for total rooting depth and surface soil moisture with various aggregations are in good agreement with other long and short-term drought indices provided by NCDC. A comparison of the correlation of monthly percentiles of the simulated stratified soil moisture, evapotranspiration, potential evapotranspiration and precipitation with NCDC drought indices is also provided in this study. The important observations of this study are as follows:

a) Proposed stratified approach is a useful tool in capturing drought onset and persistence where surface layer soil moisture can reflect on transient drought conditions while total rooting depth soil moisture captures the persistence and severity of severe droughts.
b) Variability in soil moisture varied spatially and seasonally which demands a dynamic approach in selecting distribution function for capturing soil moisture dynamics.
c) Aggregation of soil moisture data to several weeks has strong influence on the correlation of soil moisture to PDSI, PHDI and Z index, and, SPI-1, 6, 9, and 12. The correlation of the soil moisture percentiles with these indices varies spatially due to the influence of vegetation, land use, hydroclimatology etc.
d) Comparison of correlation of monthly soil moisture percentiles with PDSI, PHDI and Z index, and, SPI-1, 6, 9, and 12 against that with other hydrologic variables namely PET, ET, PREC shows that PET and PREC show higher correlation with short term drought indices while soil moisture based indices displayed highest correlation with long- term drought indices compared to other hydrologic variables.

e) Drought severity assessment using soil moisture from SWAT- CFS v2 coupled models at HUC-12 resolution shows that the models are able to capture the most recent drought of 2016 in the region. A forecast of 9 months lead time is also provided for the region using the forecasts from SWAT- CFSv2 coupled models.

Chapter 5 :
Effect of hydroclimatological teleconnections on the watershed-scale drought predictability in the Southeastern US

Key points:

a) Watershed-wise identification of teleconnections between hydroclimatic indices and water balance components of 50 watersheds in the SEUS.

b) Evaluations of the combined effect of seasonality and hydroclimatology on drought predictability in the region.

c) Spatial evaluation of the effect of hydroclimatology on short-term (SPI-1) and long-term (PDSI) drought predictability in the SEUS.

1. Abstract

Large-scale atmospheric circulation patterns have strong influence on hydrologic variability in the Southeastern U.S (SEUS). These hydroclimatic indices are often liked with extreme climatic conditions in the region, thus leading to water surplus, or deficit conditions. This study provides an assessment of the watershed scale influence of hydroclimatological teleconnections in the context of drought predictability. The interrelationship between several hydroclimatic indices (HCIs) is assessed with the monthly percentiles of soil water storage (SW), precipitation (PCP), surface runoff (SURQ) and potential evapotranspiration (PET) for 50 watersheds in the South-Atlantic Gulf region of the SEUS. The hydrologic variables are simulated by implementing SWAT models for each watershed at HUC-12 resolution for a period of January 1982 through December 2013. The study highlights strong correlation between the hydroclimatological indices (HCIs) and watershed-scale hydrologic variables. The study provides important insights on the effect of seasonality and the dynamics of water balance components on the predictability of drought at watershed-scale. Among all hydrologic variables evaluated, soil moisture shows stronger relationship to hydrologic variability with the HCIs compared to PCP, SW and SURQ. The interrelationship between watershed hydrology and hydroclimatology is found to be stronger during fall (September- November) and winter months (December- February) with R^2 between SW and PCP with the HCIs as high as 60% for some watersheds especially in the Carolinas, Georgia and parts of Florida. Simulated SW corresponds strongly with Palmer drought severity index (PDSI) in terms of its response to HCIs with high Index of Agreement (IOA) with HCIs in most of the watersheds (>60%), indicating that SW can be an effective predictor of drought in the region using various HCIs. It is observed that, while large scale approach highlights the overall influence of HCIs on the climatology of the study region, there remains a strong inter-watershed

variability in terms of response to these hydroclimatic teleconnections. Overall, the strength of the interrelationship between the HCIs and hydrologic variables is found to be stronger in Carolinas, parts of Georgia and Florida, compared to the watersheds in Virginia, Mississippi and parts of Alabama.

Key words: Hydroclimatology, drought predictability, teleconnections, ENSO, PDSI, SWAT, Southeastern US

2. Introduction

Droughts are a recurring, worldwide phenomenon, with spatial and temporal characteristics varying significantly from region to region (Tallaksen and Van Lanen, 2004). The impact of drought manifests in all components of the hydrologic budget, namely, in water supply (precipitation), storage (soil moisture, snowpack, groundwater, and surface water), and exchange or flux (evapotranspiration, snowmelt, drainage/recharge, runoff, and streamflow) (Anderson et al., 2013). A prolonged lack of precipitation (meteorological drought) can propagate through the hydrological system and affect soil moisture, resulting in soil moisture drought, as well as groundwater and discharge, resulting in hydrological drought (Mishra and Singh, 2010; Tallaksen and Van Lanen, 2004; Van Loon and Van Lanen, 2012). Efficient water resource management requires an understanding of the effects of natural climate variability, particularly in the context of increasing climate uncertainties (Rathinasamy et al., 2017). The SEUS has experienced widespread droughts three times within a span of 15 years since early 2000 and nearly 40% of the region is under moderate to exceptional drought conditions as of early 2017. Several studies have expressed concerns over increasing drought vulnerability of the region owning to continued growth and subsequent industrial, agricultural and metropolitan demand throughout the southeast

(Manuel, 2008; Pederson et al., 2012; Seager et al., 2009) and suggest that the threat of water-related conflict in the region has potential to grow more intense in the coming decades.

Hydrologic variability in the SEUS in terms of precipitation and streamflow can be partly explained by the phase of various hydroclimatological teleconnections (Engström and Waylen, 2017a; Kahya and Dracup, 1993; Labosier and Quiring, 2013). Previously, Labosier and Quiring (2013) reviewed the hydroclimatology of the SEUS and concluded that the region is strongly impacted by El Niño/Southern Oscillation (ENSO), the Pacific North American (PNA) pattern, the Bermuda High, and tropical cyclones. El Niño-Southern Oscillation, the North Atlantic Oscillation and Pacific North American Pattern, all found to significantly change seasonal precipitation and runoff in the SEUS (Engström and Waylen, 2017a). Nag et al. (2014) evaluated the ENSO teleconnections on winter hydrology of the SEUS. Engström and Waylen (2017b) reported that the Atlantic Multidecadal Oscillation and El Niño-Southern Oscillation are the main atmospheric drivers of precipitation and runoff variability in the region, and operate at a lag of several months. The study further observed that the hydroclimatic influence is strongest in fall through spring. The Arctic Oscillation, North Atlantic Oscillation, and Pacific-North American patterns were found to vary on shorter-term bases while displaying a significant and temporally sporadic influence. Katz et al. (2003) observed that the Bermuda High (a subtropical Atlantic circulation feature) has a high contemporaneous correlation with seasonal mean temperature and total precipitation in the SEUS. Sen (2012) examined streamflow variability in the Southern Appalachian region of the Southeastern US and observed strong interrelationship with Pacific North American (PNA) teleconnection pattern.

Dracup and Kahya (1994) evaluated the interrelationship between streamflow variability and ENSO across US. Khong et al. (2015) reported a significant interannual variability in the soil

moisture and attributed about 20% of the variance in soil moisture to El Niño-Southern Oscillation (ENSO) for Iowa state (U.S). Schmidt et al. (2001) analyzed to ENSO-related climatic patterns and observed strong responses on seasonal rainfall and river discharge in Florida in the Southeastern U.S, especially during winter season. Several other studies have evaluated the relationship between the cold phase of ENSO and winter precipitation in the southeast U.S (Ropelewski and Halpert, 1986; Tootle et al., 2009; Wang and Kumar, 2015; Wang and Ting, 2000; Wilhite et al., 1987). It is evident from the discussion so far that hydrology in the SEUS is well knit with large scale hydroclimatic teleconnections. However, impact assessment of these large-scale hydroclimatological teleconnections on watershed-scale hydrology in the context of drought needs more attention from local water management and drought mitigation point-of-view.

While droughts are recurrent features of the natural system, driven by climate and weather patterns, these climatic extremes are moderated by basin characteristics, which may also be exacerbated or alleviated by anthropogenic activities (Garner et al., 2015). Several catchment scale processes associated with droughts like combination of meteorological droughts into a long-term hydrological drought (pooling); attenuation of meteorological droughts in groundwater storage; a lag between the meteorological, soil moisture, and hydrological drought; lengthening of droughts while drought characteristics change from meteorological to soil moisture to hydrological drought; are controlled by both catchment characteristics and climate (Van Loon and Van Lanen, 2012). The characteristics of meteorological anomalies leading to droughts vary spatially (between climatic regions) and temporally (between seasons) and interact with the physical characteristics of the catchment (e.g. area, soils, geology and land use) that govern basin water storage and transfer processes to determine river flow response (Garner et al., 2015; Van Loon and Van Lanen, 2012). Hence a catchment/watershed scale understanding of drought dynamics becomes critical in the

context of drought predictability and an inclusive drought impact assessment. Several studies have previously linked droughts in river basins in SEUS to hydroclimatic teleconnections. Previously, Twine et al. (2005) evaluated climate, surface water balance, and river hydrology within the Mississippi River basin. Guetter and Georgakakos (1996) studied the response of seasonal streamflow to El Niño and La Niña in the Iowa River basin. Mitra (2014) evaluated induced droughts and irrigation pumpage on groundwater levels and groundwater budget components of the Upper Floridan Aquifer (UFA) in the lower Apalachicola-Chattahoochee-Flint (ACF) River Basin in the SEUS.

This study provides an assessment of drought predictability under the influence of large scale hydroclimatic anomalies for 50 watersheds in the SEUS. The interrelationship between 10 hydroclimatic indices namely, MEI (Multivariate ENSO index), Nino 1+2 (Extreme Eastern Tropical Pacific SST), Nina 4 (Central Tropical Pacific SST), Nina 3.4 (East Central Tropical Pacific SST), PDO (Pacific decadal oscillation), BEST (Bivariate ENSO Timeseries), ONI (Oceanic Nino Index), TNI (Trans Nino index), WHWP (Western Hemisphere warm pool) and TSA (tropical Southern Atlantic Index) is assessed with soil water storage (SW), precipitation (PCP), surface runoff (SURQ) and Potential Evapotranspiration (PET) at watershed scale in the context of drought. These indices represent anomalies pertaining to sea surface temperature and other meteorological conditions like sea-level pressure, zonal and meridional components of the surface wind etc. from various regions in Pacific and Atlantic oceans. The study provides assessment of a watershed-scale interrelationship between these HCIs with the water balance components and the variability of this relationship across seasons. The study evaluates the applicability of these HCI as a predictor of drought at watershed scale for the study region.

The objectives of this study are as follows:

a) To evaluate the response of four water budget components namely SW, PCP, PET and SURQ to various HCIs for 50 watersheds in the SEUS.
b) To assess the link between hydroclimatology and drought predictability in terms of different water budget components at the watershed scale.
c) To compare the drought predictability scores obtained from simulated water budget components with existing drought indices like 1-month standard precipitation index (SPI-1) and Palmer drought severity index (PDSI) to understand the interrelationship between the long-term and short-term drought predictability to hydroclimatology.
d) To highlight the spatial variability in the association between watershed scale hydrology and climatic indices for the SEUS.

3. Study area and dataset

3.1.Study area

This study is focused on the South-Atlantic Gulf (SAG) region in the SEUS. The geographic area of the SAG region includes all of Florida and South Carolina, and parts of Alabama, Georgia, Louisiana, Mississippi, North Carolina, Tennessee, and Virginia (USGS, 2017). The South-Atlantic Gulf region spans over 724,326 square kilometers. The northern part of the study region is bounded by the Appalachia, and is predominantly forested. Wetlands are common on the southern part of the study region. The elevation decreases from north to south from over 1700 m to sea level elevation at the coasts. SAG is listed with a 2-digit Hydrologic Unit Code (HUC) of 03 and consists of 18 sub-regions, each listed with the 4-digit HUC codes ranging from 0301 through 0318. Each HUC-4 basin is further divided into smaller watersheds for this study, totaling 50 for the entire SAG region (Figure 5-1), each of which is modeled using SWAT to delineate sub-watersheds matching the HUC12 resolution as provided by National Hydrology Dataset plus

(NHD+). Table 5-1 provides the complete list of the 18 basins in the SAG region, each referred to by its HUC-4 identifier with list and name of the sub-watersheds with the outlet U.S. Geological Survey (USGS) stations. Note that the watershed numbers are provided by the authors only for easy referencing and identification of these watersheds in the study and not to be confused with the watersheds at HUC-6 which are larger than these watersheds in most cases.

3.2. High resolution hydrologic modeling using SWAT at HUC-12 resolution

SWAT (Soil and Water assessment tool) models are implemented for 50 watersheds at HUC-12 resolution for the entire study area to obtain high resolution hydrologic variables to be used in this study for the analysis. Total column soil water storage (SW), precipitation (PCP), potential evapotranspiration (PET) and surface runoff (SURQ) from the models are used to represent watershed scale hydrology. SWAT models are calibrated for a period of 2003 through 2010 with three years of warm-up period (2000 through 2002) and are validated for a period of 2011 through 2013. The calibrated models are then back-run for retrospective period till 1979 with three years of model spin-up period, thus providing continuous daily data of hydrologic variables from January' 1982 through December' 2013. The ArcSWAT 2010 interface is used to setup and parameterize the model. Sequential Uncertainty Fitting-2 algorithm (Abbaspour et al., 1997; Abbaspour et al., 2004; Abbaspour et al., 2015) is used to calibrate model parameters for each watershed using SWAT-CUP (calibration/uncertainty or sensitivity program) interface for SWAT. For detailed description of the watershed models, model calibration and validation for the SWAT models used in this study for obtaining hydrologic variables at HUC-12 resolution, the readers are referred to Sehgal and Sridhar (2017).

3.3.Hydroclimatic indices (HCIs)

Anomalies and internal variation in the coupled ocean-atmospheric-land systems are strongly related to climatic extremes across the world thus serving as the natural drivers of droughts. The hydroclimatological variability ranges from interannual to decadal timescale and can significant impact the climate across the globe. Anomalies at the ocean surface interact with the overlying atmosphere to alter the transport of soil moisture across the globe by intensifying local convection, shifting storm tract and bringing hurricanes and droughts across globe (Sheffield and Wood, 2012). Following HCIs are evaluated in this study for the relationship with drought in the SEUS:

a) Multivariate ENSO index (MEI): MEI is calculated as the first unrotated Principal Component (PC) of sea-level pressure (P), zonal (U) and meridional (V) components of the surface wind, sea surface temperature (SST), surface air temperature (A), and total cloudiness fraction of the sky (C) observed over the tropical Pacific. The MEI is computed separately for each of twelve sliding bi-monthly seasons (Wolter and Timlin, 1998; Wolter and Timlin, 2011).
b) Nino 1+2: is the Extreme Eastern Tropical Pacific (0-10S, 90W-80W) SST.
c) Nina 4: Central Tropical Pacific (5N-5S, 160E-150W) SST.
d) Nina 3.4: East Central Tropical Pacific (5N-5S, 170-120W) SST.
e) PDO (Pacific decadal oscillation): is the leading PC of monthly SST anomalies in the North Pacific Ocean (Mantua et al., 1997; Zang et al., 1997).
f) BEST (Bivariate ENSO Timeseries): Combination of standardized SOI (Southern Oscillation Index) and a standardized Nino3.4 SST (Smith and Sardeshmukh, 2000).
g) ONI (Oceanic Nino Index): Three month running mean of NOAA ERSST.V4 SST anomalies in the Nino 3.4 region (5N-5S, 120-170W), based on changing base period

which consist of multiple centered 30-year base periods (Huang et al., 2015). These 30-year base periods are used to calculate the anomalies for successive 5-year periods in the historical record.

h) TNI (Trans Nino index): is a measure of El Niño evolution (Trenberth and Stepaniak, 2001). TNI is calculated using the standardized Nino 12 minus the Niño 4 with a 5-month running mean applied which is then standardized using the 1950-1979 period.

i) WHWP (Western Hemisphere warm pool): is the monthly anomaly of the ocean surface area warmer than 28.5ºC in the Atlantic and eastern North Pacific(Wang and Enfield, 2001).

j) TSA (tropical Southern Atlantic Index): is the anomaly of the average of the monthly SST from 0-20S and 10E-30W (Enfield et al., 1999).

These indices are obtained from National Oceanic and Atmospheric Administration (NOAA) webpage by accessing the following link: *https://www.esrl.noaa.gov/psd/data/climateindices/list/*. The data for HCIs is obtained for a period of December 1981 through December 2013. Selection of these hydroclimatic indices is made from a larger set of 35 indices and only the variables which showed high correlation with hydrologic variables across all watersheds are selected for further evaluation (List and selection criteria provided in Appendix).

3.4.Drought indices (DIs)

Two doughty indices namely monthly Palmer Drought Severity Index (PDSI) and 1-month standardized precipitation index (SPI-1) are used in this study for comparison with the percentiles of the four hydrologic variables. PDSI and SPI-1 are obtained from the NOAA's National Climatic Data Center (NCDC– NOAA) repository for 53 climatic divisions in the SEUS. PDSI is a water balance index (consider water supply, demand and loss through precipitation, evapotranspiration

and runoff respectively) and relates to long-term droughts accounts for drought-inducing circulation patterns. SPI-1 is a probability index and relates to precipitation only. For a given month each point in climatic division is assumed to have the same value for a drought index. Detailed information on and difference between these drought indices can be obtained from Mishra and Singh (2010). A time series of area averaged PDSI with PDO and MEI for South-Atlantic Gulf (SAG) region from January 1950 through December 2013 is provided in Figure 5-2.

Figure 5-1: Map showing the location of the study area. The watersheds in the South-Atlantic Gulf (SAG) region are highlighted in grey shade.

4. Methodology

4.1.Percentile calculation of PREC, SW, PET and SURQ

Daily data for PREC, SW, SURQ, PET is obtained for each sub-watershed (at HUC-12 resolution) for a period of January 1982 through December 2013. To generate the representative

numbers at monthly resolution, the data for PER, PCP, QURQ is aggregated for each month, while SW data is averaged for the respective period to get monthly total and monthly mean respectively. Selection of the distribution function to quantify the variability in the data for each month is done by comparing the loglikelihood values of the distribution fit for the four distribution functions namely, *Normal*, *Gamma*, *Log-Normal* and *Extremevalue*. The CDF from the best fit distribution is then used to calculate the monthly percentiles of the data (January 1982 through December 2013). Monthly percentiles of the hydrologic variables are calculated to quantify drought severity based on the respective values at monthly time step based on the 32-year climatology. The monthly percentiles (indicative of drought severity based on respective hydrologic water budget component) are calculated with reference to their historical frequency of occurrence for the location and time of year in question. For more details on percentile calculation methodology used in this study, the readers are referred to (Sehgal and Sridhar, 2017).

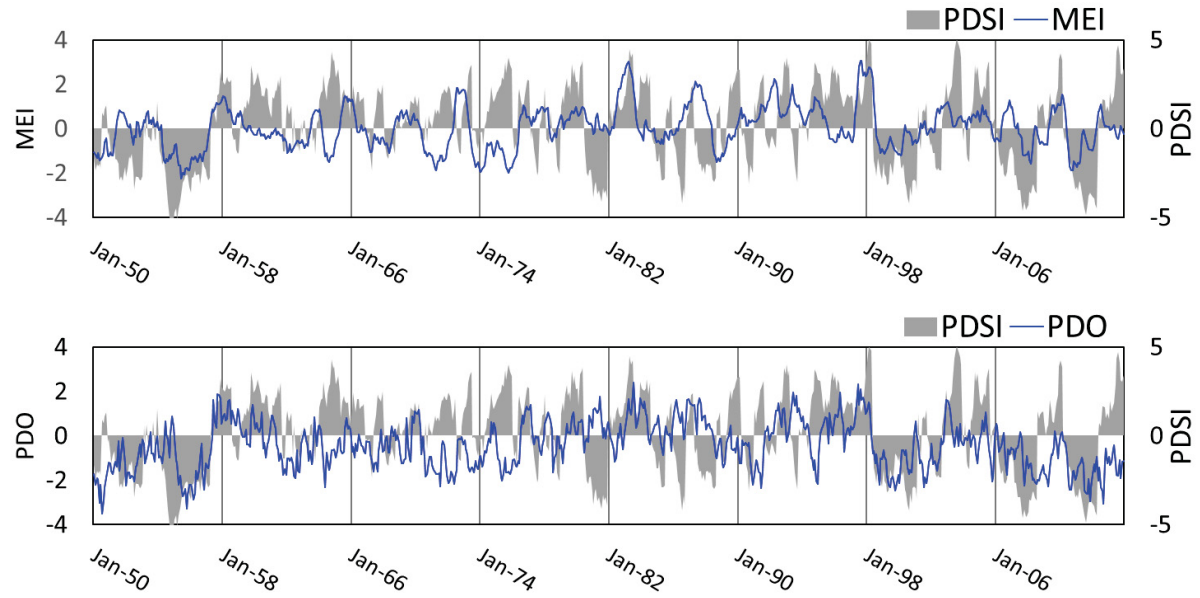

Figure 5-2: Pacific decadal oscillation (PDO) and Multivariate ENSO index (MEI) with Palmer drought severity index (PDSI) time series for South-Atlantic Gulf (SAG) region from January' 1950 through December' 2013.

Table 5-1: List of the 18 basins in the South-Atlantic Gulf region identified with 4- digit Hydrologic Unit Code with name and a 6- digit identification number (not to be confused with HUC-6) for the constituent watersheds, and, respective outlet USGS stations.

Basin	USGS stn.	Watershed	River/ basin	Basin	USGS stn.	Watershed	River/ basin
0301	02066000	030101	Roanoke	0309	02292900	030902	Caloosahatchee
	02075500	030102	Dan	0310	02296750	031001	Peace
	02047000	030103	Nottoway		02301500	031002	Alafia
0302	02084000	030201	Tar		02313000	031003	Withlacoochee
	02091814	030202	Neuse	0311	02323500	031101	Suwannee
0303	02134500	030301	Lumber		02317500	031102	Alapaha
	02106500	030302	Black	0312	02330150	031201	Ochlockonee
	02108000	030303	NE Cape fear	0313	02338000	031301	Chattahoochee
0304	02129000	030401	Pee Dee		02350512	031302	Flint
	02134500	030402	Lumber		02358700	031303	Apalachicola
	02132000	030403	Lynches	0314	02369600	031401	Yellow
0305	02147020	030501	Catawba		02366500	031402	Choctawhatchee
	02169500	030502	Congaree		02374250	031403	Conecuh
	02175000	030503	Edisto	0315	02397000	031501	Coosa (Rome)
0306	02197000	030601	Savannah		02407000	031502	Coosa (Childersburg)
	02198000	030602	Barrier Creek		02428400	031503	Alabama
	02202500	030603	Ogeechee	0316	02448500	031601	Noxubee
	02203000	030604	Canoochee		02466030	031602	Black warrior
0307	02223500	030701	Oconee		02469761	031603	Tombigbee
	02215000	030702	Ocmulgee	0317	02478500	031701	Chickasawhay
	02225500	030703	Ohoopee		02474500	031702	Tallahala
	02228000	030704	Satilla		02479300	031703	Red Cr.
0308	02234000	030801	St. Johns (Geneva)	0318	02482550	031801	Pearl (Carthage)
	02244040	030802	St. Johns (Buffalo bluff)		02488500	031802	Pearl (Monticello)
0309	02270500	030901	Arbuckle Cr.		02489500	031803	Pearl (Bogalusa)

4.2.Matrices for assessing interrelationship between percentiles of hydrologic variables and HCIs

This study uses three statistical indices for quantifying the relative strength of agreement between HCI and the percentiles of various hydrologic variables. Correlation coefficient is used to find the strength of the interrelationship between the hydrologic variables and HCI. Drought predictability is measured in terms of the R^2 of the least square linear model fit between the percentiles of hydrologic variables (PHV) and the HCIs. A new index termed as Index of relative cooccurrence (IOC-r) is defined as:

$$IOC\text{-}r = \frac{Num.of\ months\ PHV\ is\ lower\ than\ severity\ threshold\ while\ strong\ HCI\ in\ place}{Total\ number\ of\ months\ PHV\ is\ lesser\ than\ severity\ threshold}$$

IOC-r shows how many occurrences of drought occurred (months) while strong hydroclimatic anomaly was in place compared to total occurrences of drought categorized by the PHV.

5. Results and discussion

5.1. Correlation between PHVs and HCIs

Correlation analysis is carried out between the percentiles of the four hydrologic variables and ten HCIs to assess the strength of the mutual interrelationship. SW, PET, SURQ are obtained at HUC-12 resolution by implementing calibrated SWAT models for each watershed in the region (total 50). Precipitation data is obtained from the National Centers for Environmental Prediction (NCEP) Climate Forecast System Reanalysis (CFSR) stations in the study area. A total of 1070 weather stations are available in the region and the data is spatially interpolated for comparable analysis between precipitation and other hydrologic variables.

Figure 5-3 provides a summary of the correlation between the ten HCI and four hydrologic variables for all 50 watersheds in the study region. It can be observed that SW, PCP and SURQ display high positive correlation with MEI, Nino 4, Nino 3.4, PDO, BEST and ONI, whereas negative correlation is observed for TNI, WHWP and TSA. The variability in the correlation values for each variable with the HCIs is evident from the figures. The mean values of correlation of SW with the HCIs are higher in magnitude for all indices. The complimentary behavior of PET compared to other hydrologic variables is also evident from Figure 5-3. PCP and SURQ show a very similar mean correlation with the HCI except for Nino 1+2 where SURQ shows slightly higher magnitude of correlation. PET shows higher correlation with PDO and BEST than PCP and

SURQ. A detailed list of correlation values of SW, PET, SURQ and PCP is provided in the Appendix.

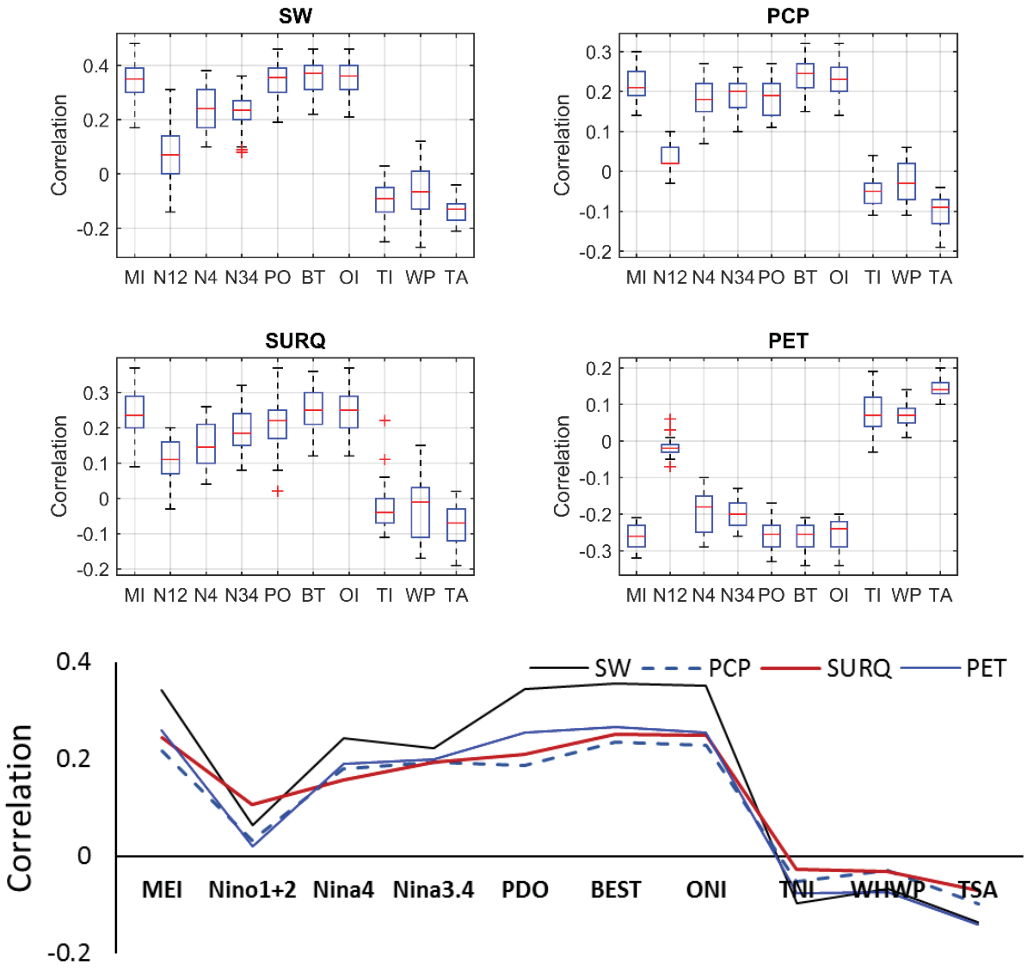

Figure 5-3: (a) Box plots (Top two rows) of correlation for 50 watersheds with monthly percentiles of soil water (SW), precipitation (PCP), surface runoff (SURQ) and potential evapotranspiration (PET) per hydroclimatic index (HCI). The name of the HCIs are indicated in short in the figure with the following abbreviations: MI= MEI, N12=Nino 1+2, N4= Nino4, N34= Nino 3.4, PO= PDO, BT= BEST, OI= ONI, TI=TNI, WP=WHWP, TA= TSA. (Bottom row) Line plots of average correlation of percentiles of hydrologic variables (PHV) with HCI across 50 watersheds.

5.2. Influence of seasonality on the interrelationship between PHVs and HCIs

The interrelationship between the HCIs and hydrology in the SEUS is strongly influenced by seasonality. Figure 5-4 shows the R^2 between the seasonal average of PHVs and HCIs for four seasons namely December-February (DJF), March-May (MAM), June-August (JJA) and September-November (SON). Furthermore, since the effect of hydroclimatology generally manifests with some delay (lag) the seasonal-wise R^2 values are evaluated for no lag (concurrent month), 1-month lag and 2-months lags period where the time series of HCIs from antecedent months are averaged for the analysis. For e.g., 1-month lag of DJF season corresponds to the average HCIs of November-January months.

The interplay of seasonality on the correlation of PHVs with the HCIs can be observed from Figure 5-4. It is to be noted that the R^2 values of PCP and SURQ with the HCIs resemble each other irrespective of the season. The R^2 of SW with the HCIs can be observed to be the highest among other variables across all seasons with an exception of a few combinations of season and HCIs. PET displays an interesting variability in terms of its response to the HCIs across different seasons. MAM season marks heightened evaporative demand due to increasing temperatures and low precipitation leading to low water surplus conditions in the region. This makes PET a dominating component in the water budget of the region. However, with precipitation in the subsequent months, PCP, SW and SURQ dominate over PET (Figure 5-5). Again, due to decreasing variability in SURQ and low precipitation, PET again displays stronger interrelationship with the HCIs. It is interesting to note that since SW acts as a link between the energy driven and moisture driven components of the water budget, SW sustains stronger interrelationship with the HCIs across throughout the year compared to other hydrologic variables. Also, since 1-month lag between the HCIs and the PHVs represents the relative trend and

magnitude of the inter-relationship between different variables across seasons, further analysis uses 1 month lag between the HCIs and PHVs.

Figure 5-6 and Figure 5-7 provide a spatial representation of the variability in the interrelationship between the PHVs and HCIs. SW, SURQ and PET are obtained from the implementation of calibrated SWAT models at HUC-12 resolution whereas PCP is obtained by spatially interpolating precipitation data from 1070 stations from CFSRR data. It can be observed from Figure 5-6 that SW displays stronger interrelationship with BEST, ONI, MEI Nina 3.4 and Nina 4 for DJF. While for JJA and SON, strongest R^2 is observed for PDO for most past of the region. MAM season SW is primarily impacted by BEST; however, the strength of the relationship is weaker compared to other seasons. Similar observations can be seen for PCP. However, the magnitude and the geographic regions having strongest R^2 with HCIs are different as compared to that of SW. On comparing Figure 5-6 and Figure 5-7, it can be observed that SURQ and PCP are similar both in the magnitude and the spatial pattern in the interrelationship between these variables and the HCIs. PET can be seen to have highest R^2 with PDO and WHWP for SON. BEST and MEI impacts PET in DJF months, however the influence is restricted to the southern parts, esp. in the Floridan peninsula. A clear influence of the soil characteristics and topography on the interrelationship of the HCIs with PHVs can be seen in Figure 5-6 and Figure 5-7. Hydrologic variables in the Appalachia mountain region (Virginia and Carolinas) have a very distinct relationship with the HCIs compared to Florida and most part of Alabama and Georgia due to distinctively different land type, and climatic conditions. Watershed-wise correlation values between SW, PCP, SURQ and PET with the HCIs for each season are summarized in the form of a table in the Appendix.

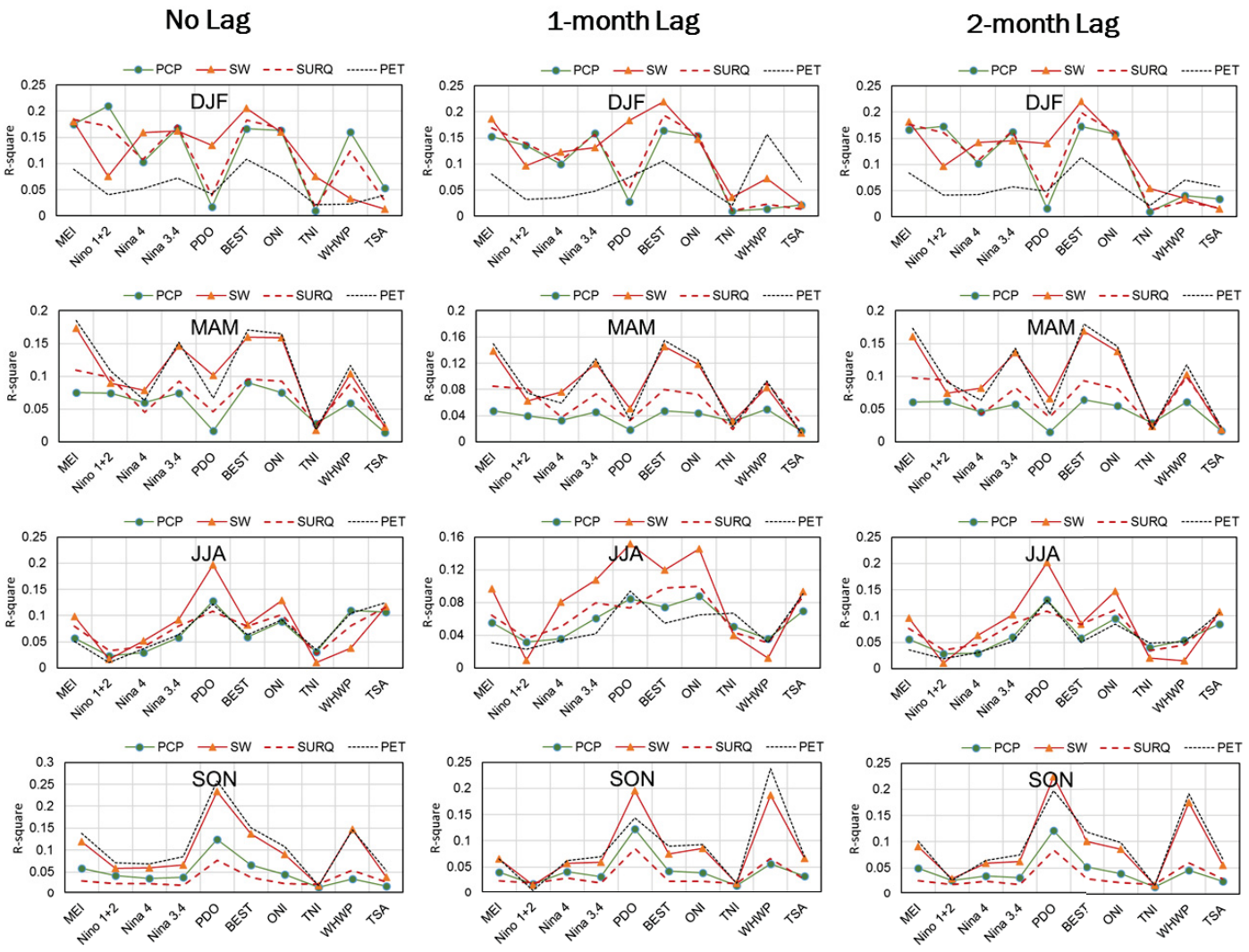

Figure 5-4: Season-wise R-square (R^2) of monthly percentiles of four hydrologic variables with 10 hydroclimatic indices averaged over entire study area.

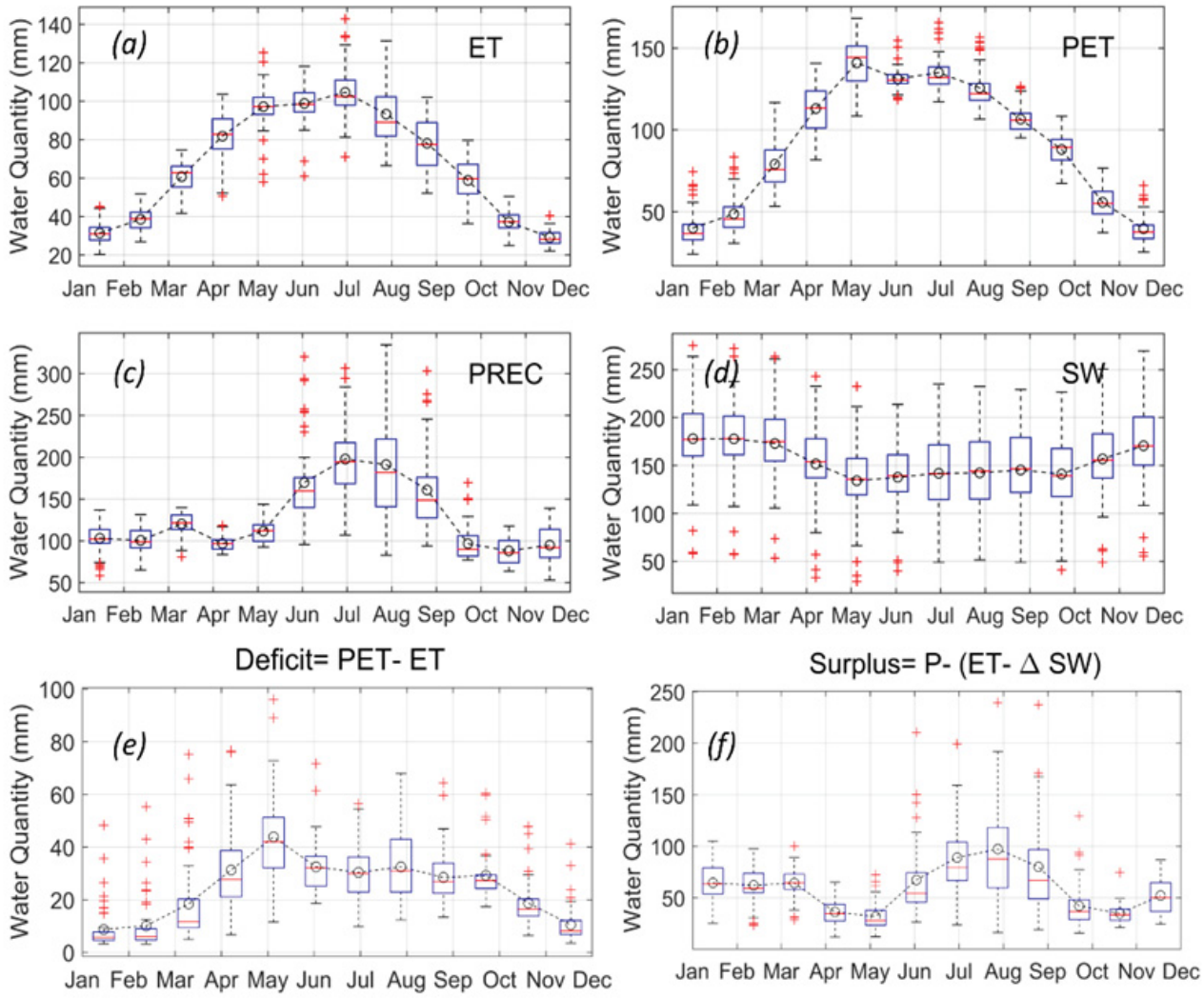

Figure 5-5: Water budget of the study region (Sehgal and Sridhar, 2017). The box plot for each month represent the values from all 50 watersheds.

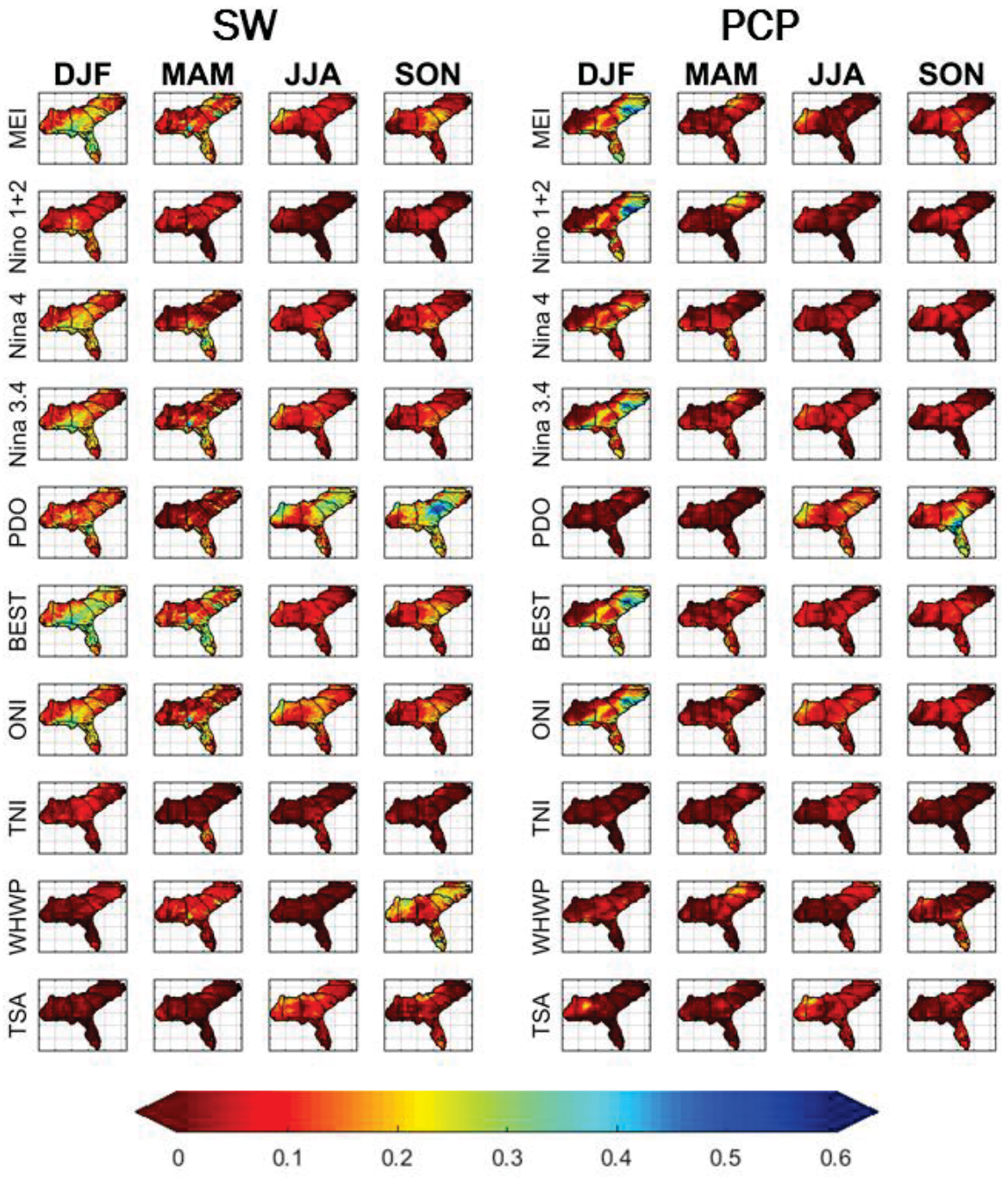

Figure 5-6: Spatial representation of the season-wise R-square (R^2) of monthly percentiles of simulated soil water (SW) at HUC-12 resolution, and interpolated precipitation (PCP) from 1070 weather stations with 10 hydroclimatic indices. Blue indicate high R^2 whereas red indicates low values of R^2.

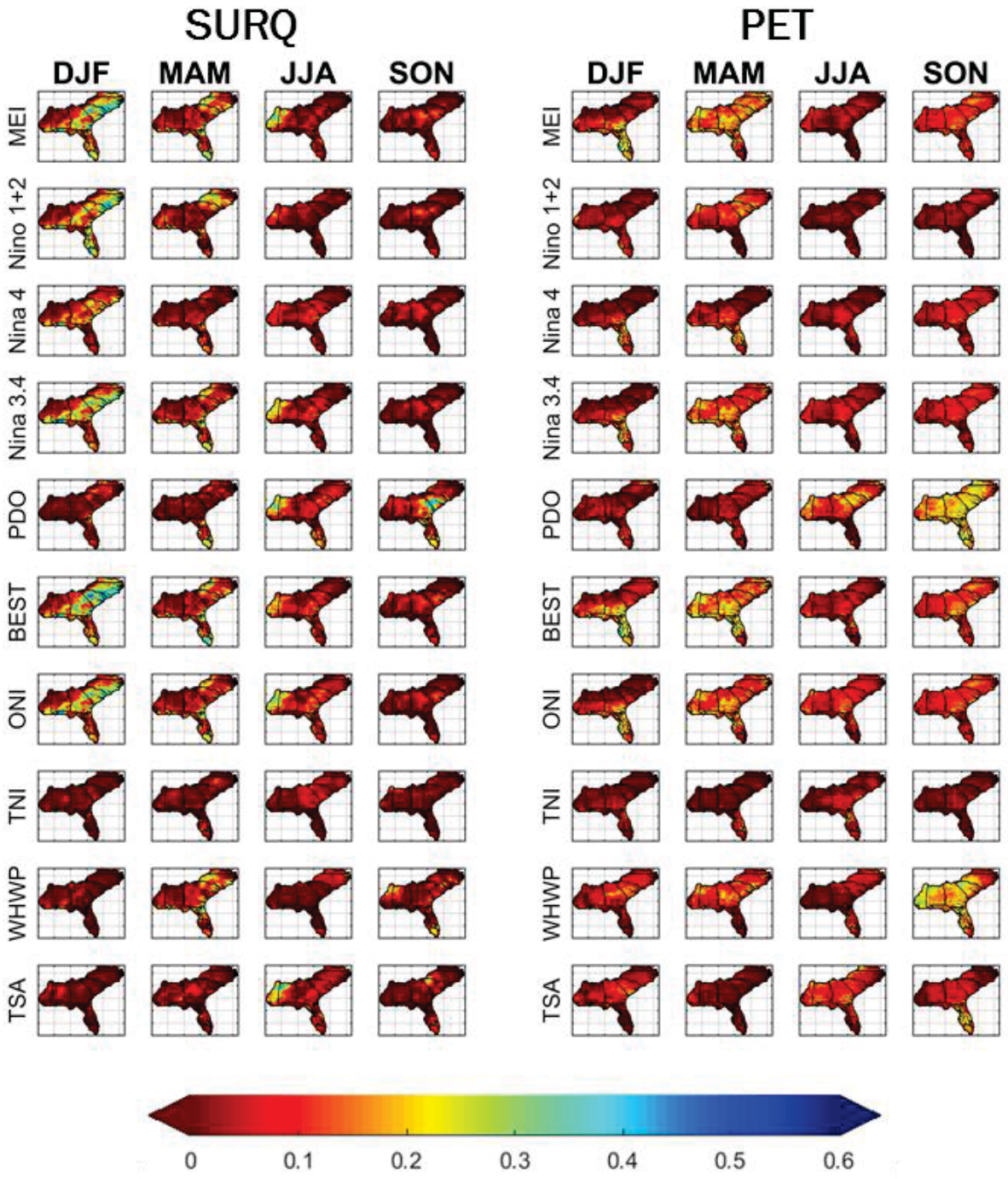

Figure 5-7: Spatial representation of the season-wise R-square (R^2) of monthly percentiles of simulated surface runoff (SURQ) and potential evapotranspiration (PET) at HUC-12 resolution with 10 hydroclimatic indices. Blue indicate high R^2 whereas red indicates low values of R^2.

5.3. Using PDSI and SPI-1 for comparison with the simulated hydrologic variables w.r.t. the interrelationship with the HCIs

To compare the interpretations about the strength of interrelationship between the PHVs and HCIs for multiple seasons, the analysis is extended to PDSI and SPI-1 for comparison. It can be observed form Figure 5-8 that PCP and SPI-1 have strong similarity in terms of their response to HCIs especially in JJF, MAM and SON months. Although SPI-1 shows higher value of R^2 with Nino 1+2 and TNI compared to PCP, the values are less than 0.1 (very low). PDSI can be observed to show highest correlation with the HCIs compared to all PHVs and SPI-1 for DJF and MAM seasons. However, SW shows equally high R^2 with most of the HCIs for DJF while being able to retain the relative sensitivity to the HCIs like PDSI, yet with a smaller magnitude. Overall, SW can be seen to be the variable of choice to retain the sensitivity to the HCIs across year compared to other hydrologic variables. Figure 5-9 provides a spatial representation of the R^2 values between the HCIs and the selected drought indicators. It can be observed that the two drought indices vary significantly in terms of the spatial values of R^2 with the HCIs for the four seasons. Since SPI-1 is influenced by variability in precipitation only, R^2 for DJF is seen to be high in Virginia, Carolinas and Southern tip of Florida which receive significant precipitation in winter months. In contrast, PDSI has higher predictability in DJF and MAM especially in the Alabama, Georgia and Florida region, most of which have higher variability in river discharge and soil moisture during this period.

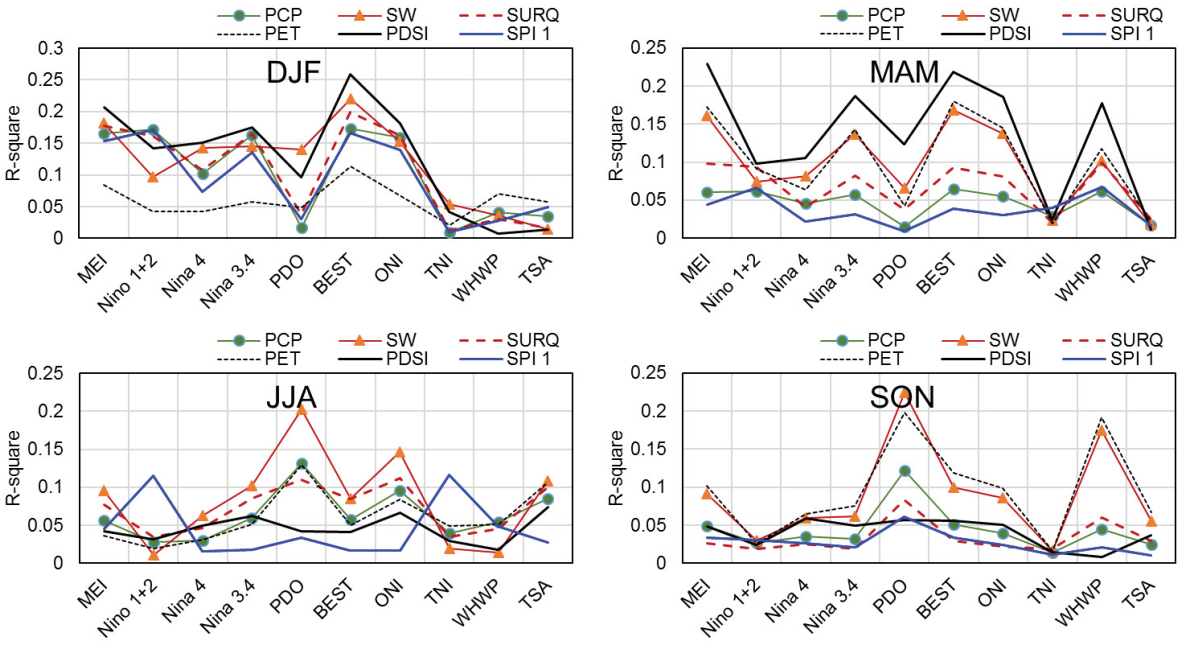

Figure 5-8: Comparison of the area averaged R^2 over South-Atlantic Gulf region between PHVs, PDSI and SPI-1 with the HCIs for four seasons.

Figure 5-10 provides the time series of the ten selected HCIs, values of PDSI and SPI-1 and severity-area plot based on the reconstructed drought assessment using the simulated soil moisture percentiles for Roanoke watershed. It can be observed that the drought indicators follow the trend of the hydroclimatic indices. The drought classification using the reconstructed soil moisture percentiles following Sehgal and Sridhar (2017), is consistent with the convention used by the U.S drought monitor. The study region has experienced three severe droughts in recent past (2000-2002, 2008-09, 20012-13) where most of the watersheds in the region were impacted. On observing Figure 5-10 and

Figure 5-11 (same as Figure 5-10, but for Satilla, Coosa and Pearl watersheds) it can be observed that under the same hydroclimatological conditions, the impact of drought was different across different watersheds. While Roanoke watershed had higher percentage of area under severe

drought category, Pearl river watershed, in comparison, experienced drought for a shorter period and lesser intensity. This variability in watershed scale drought severity is also evident in season-wise evaluation in Figure 5-12.

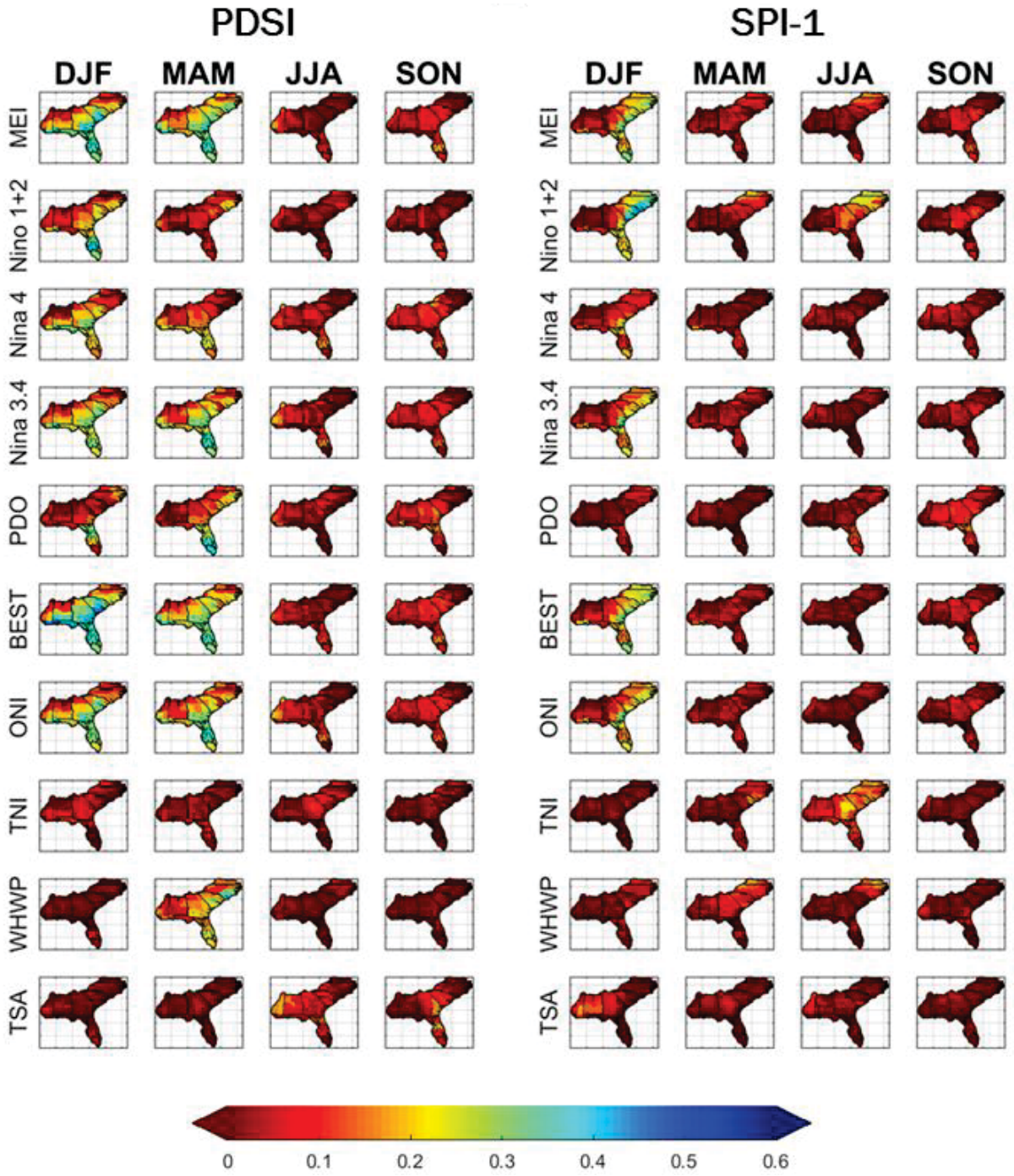

Figure 5-9: Spatial maps of the R^2 between the HCIs and PDSI, and, HCIs and SPI-1 for four seasons.

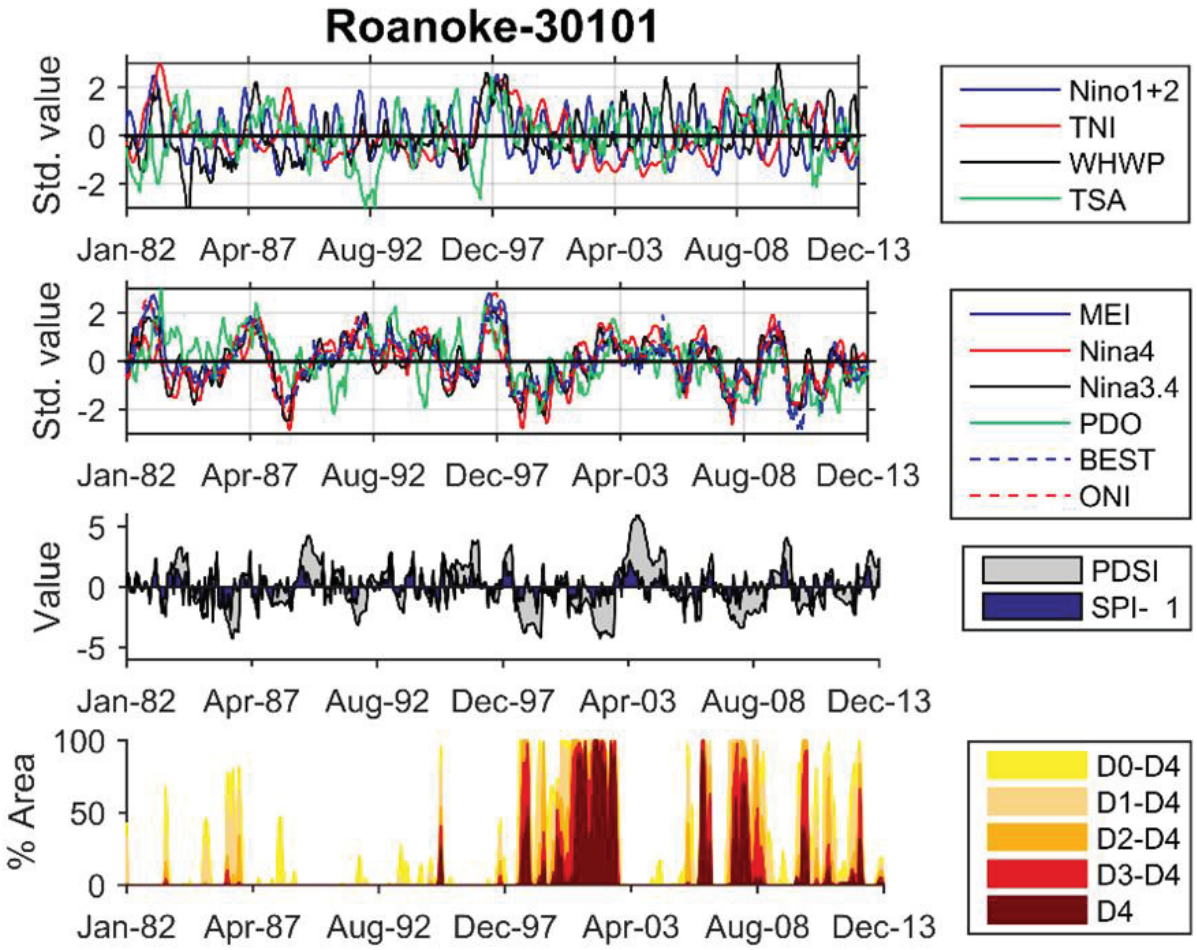

Figure 5-10: Comparison of the time series of the 10 HCIs, and, PDSI and SPI-1 for the Roanoke watershed, with the respective severity-area values for the watershed based on the reconstructed drought percentiles for January 1982 through December 2013. (D0- Abnormally dry, D1-Moderate drought, D2-Extreme drought, D4-Exceptional drought)

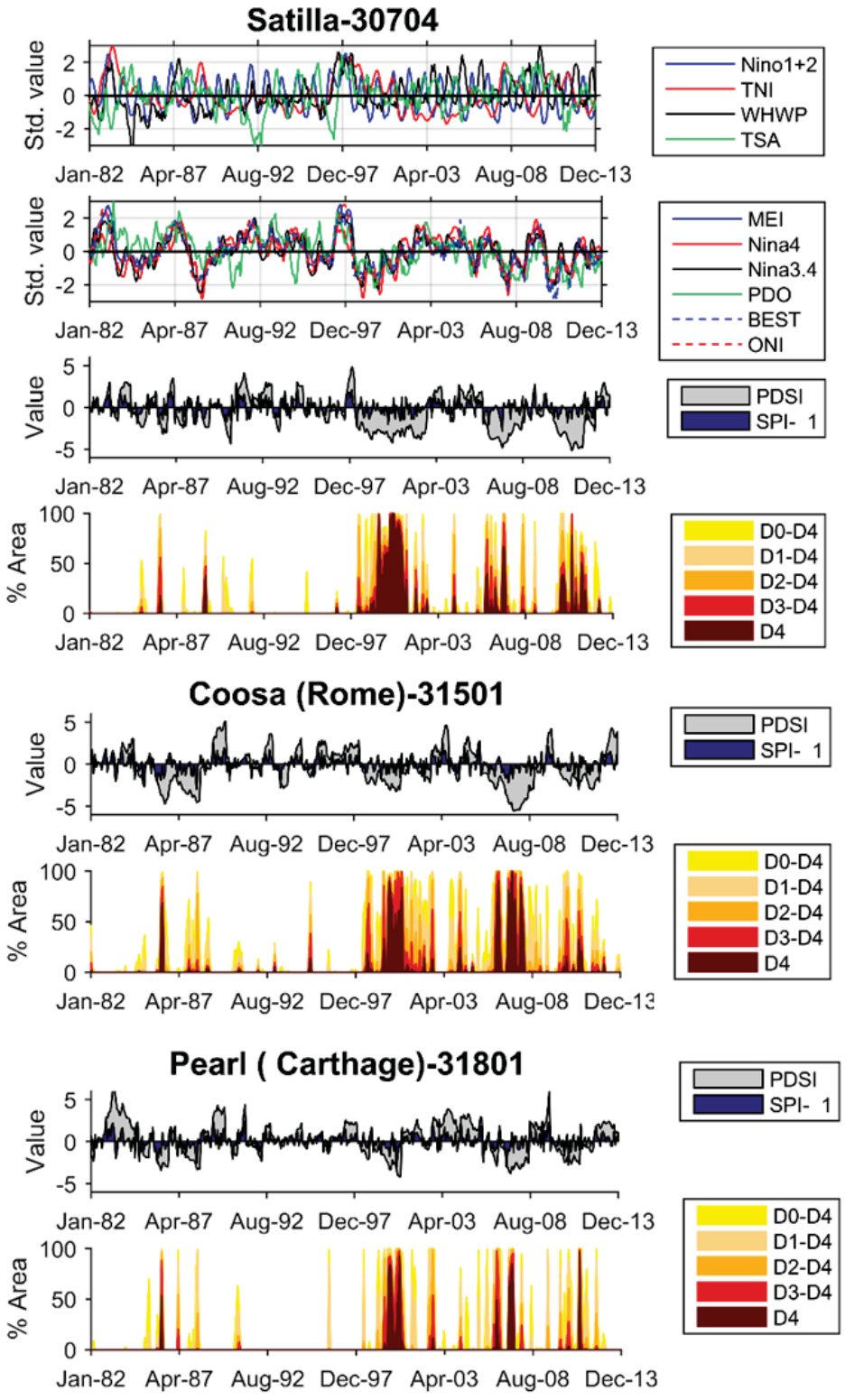

Figure 5-11: Same as Figure 9, for Satilla, Coosa and Pearl watersheds.

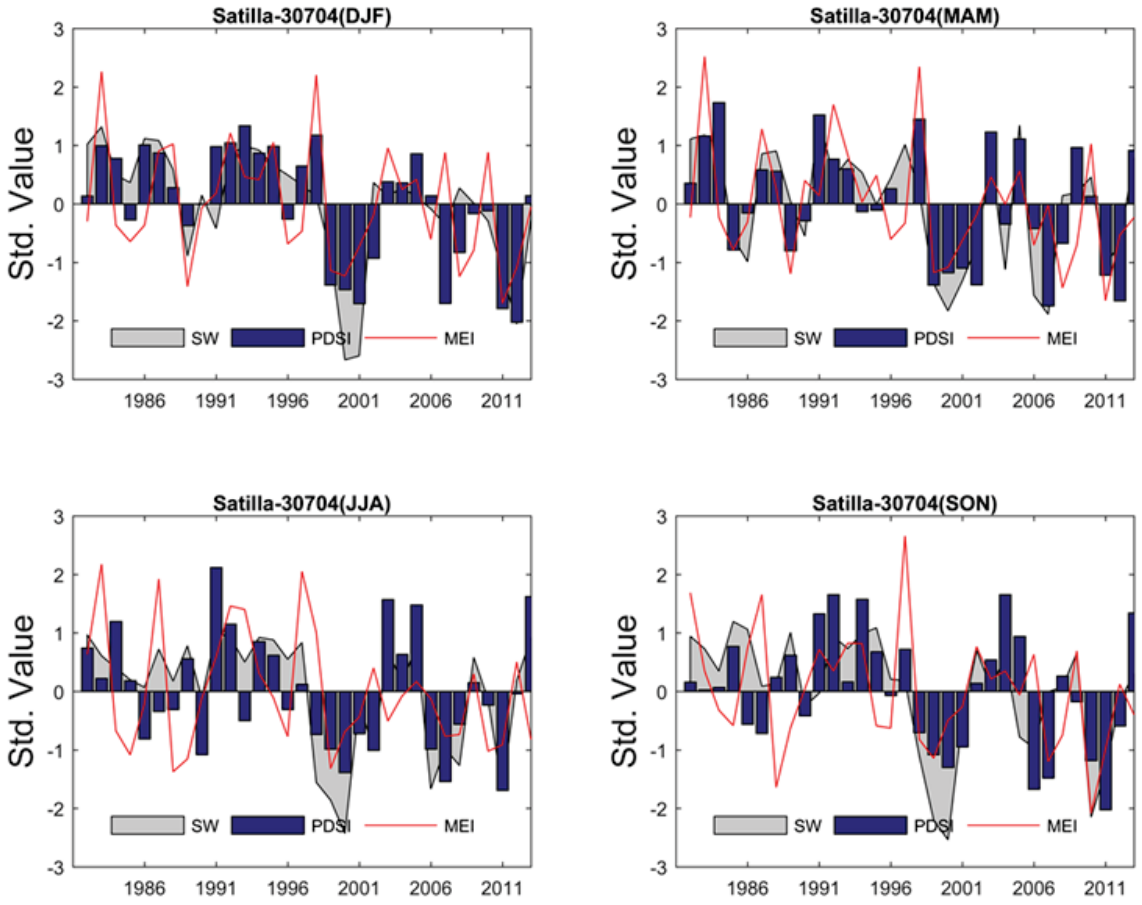

Figure 5-12: Comparison of season-wise values PDSI, SW percentiles (standardized to unit variance and zero mean) and MEI for Roanoke and Satilla watersheds.

5.4.Attributing drought occurrences to hydroclimatic extremes using IOC-r matrix

IOC-r is used to comprehensively test if the drought spell in the watershed coincided with hydroclimatological extremes for the same month compared to the total number of drought spells. This facilitated an event-by-event assessment of drought spells at watershed scale and link that to severities in the HCIs. The lower/ upper 30th percentiles are considered severely values in this analysis. Figure 5-13 provides a comparison of the IOC-r values for each watershed and HCI, and drought spell is characterized using soil water percentiles, PDSI and SPI-1. A IOC-r of 60 mean

that 60% of the total drought affected months for the watershed occurred during simultaneous high/low values of the HCI. The results of Figure 5-13 are summarized in the form of a boxplot in Figure 5-14. It can be observed that there is a strong inter-watershed variability in terms of the response of each basin to severe hydroclimatic anomalies. While some watersheds have high IOC-r with the HCIs (as high as 60-70 percent droughts can be attributed to hydroclimatology), other watersheds do not have strong relevance to hydroclimatic extremes in terms of drought. The response also varied from one HCI to other. Also, PDSI and SW percentiles have stronger relationship with the hydroclimatic abnormalities compared to SPI-1 for most of the indices except TSA, WHWP and TNI.

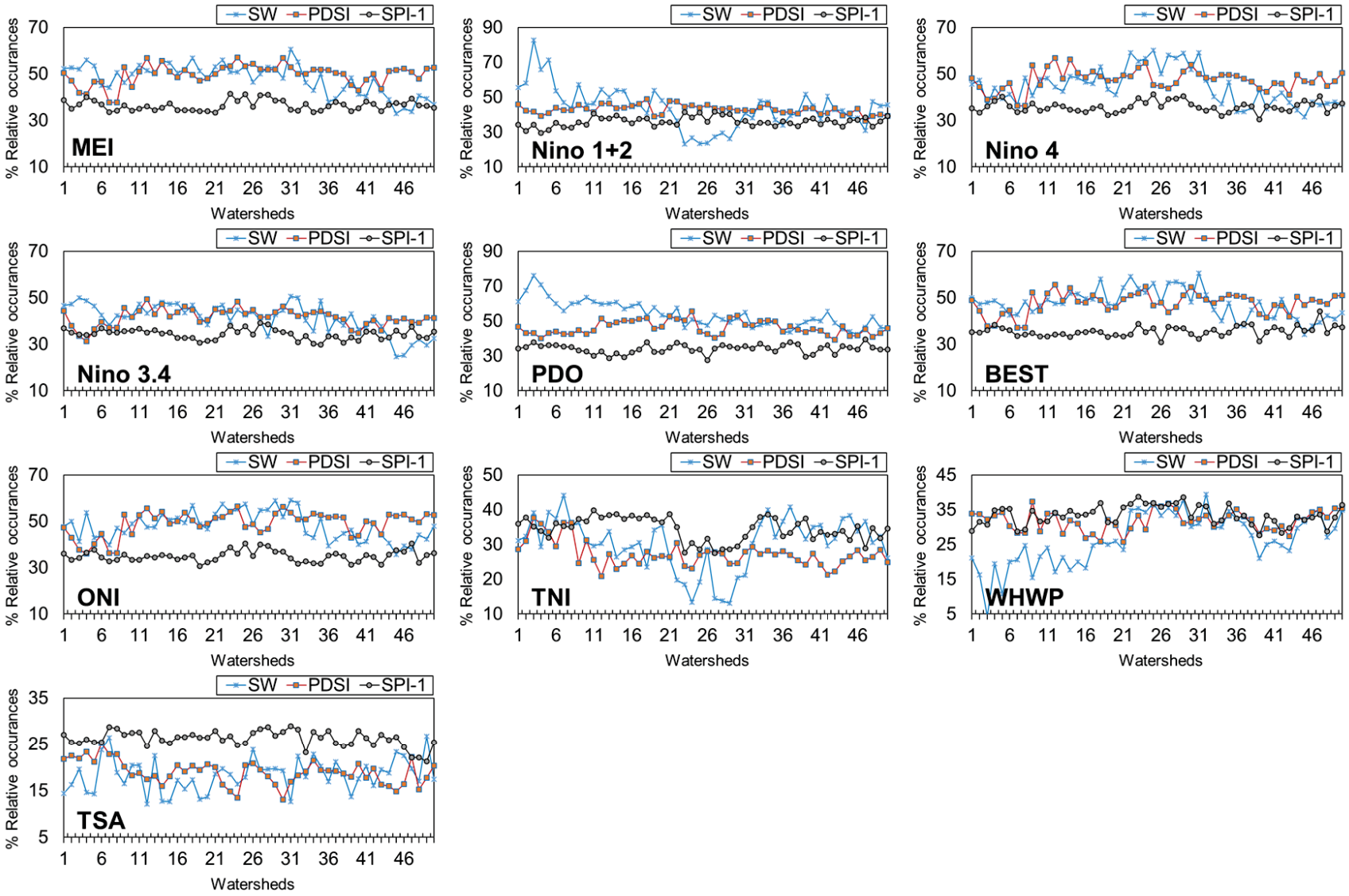

Figure 5-13: Comparison of the IOC-r of PDSI, SPI-1 and SW percentiles for 50 watersheds with 10 HCIs.

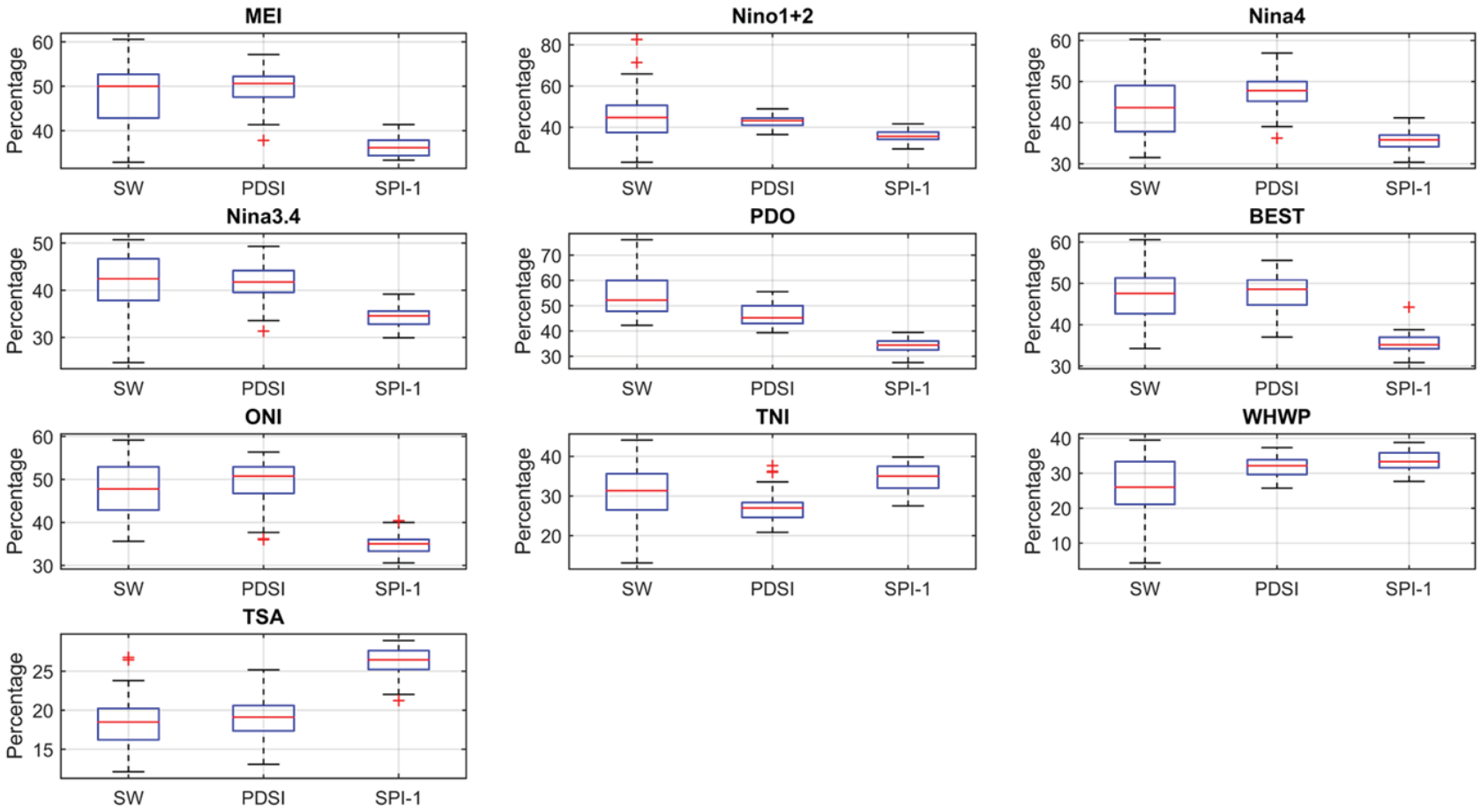

Figure 5-14: Boxplots to compare the IOC-r values of SW percentiles, PDSI and SPI-1 with 10 HCIs for all 50 watersheds.

5.5. Combined influence of seasonality and hydroclimatology on drought predictability

It is evident from the discussion so far that the relationship between hydrologic variables and HCIs is strongly influenced by seasonality. Similarly, the drought indices like PDSI are seen to have variability in the inter-relationship with the HCIs based on seasonality. Hence, to evaluate the combined influence of seasonality and hydroclimatology on drought predictability in the study area, an analysis is carried out to study the predictability score between PDSI and SW percentiles in the months corresponding to strong hydroclimatic anomalies. This study choses MEI as the index of choice for this analysis due to its strong and well documented influence on the precipitation variability in the SEUS. Predictability (R^2) of PDSI using monthly SW percentiles is evaluated for two phases of MEI i.e. warm (El Nino) and cold (La Nina). Figure 5-15 provides time series of MEI and area averaged PDSI and SW percentiles for the SAG region. It can be observed from Figure 5-15 that low values of PDSI and SM percentiles (dry conditions) correlate with strong La Nina while higher values of PDSI and SW percentiles (wet conditions) exist in the years with strong El Nino. The spatial maps of PDSI predictability skill using SW percentiles for the two phases of MEI are shown in Figure 5-16 based on 1982-2013 climatology. Strong seasonal variation on PDSI predictability using SW percentiles under La Nina and El Nino can be seen from Figure 5-16. Overall PDSI predictability is higher in the winter months for both phases of MEI. However, spatial variability in the predictability changes with seasons. Higher overall R^2 of PDSI predictability under El Nino from fall to spring can be attributed to above average precipitation in the SEUS which leads to positive PDSI values and higher SW percentiles. Strong influence of the subtropical jet stream in winter causes more clouds, rain, and severe weather causing cooler and wetter conditions in the SEUS, leading to higher R^2 between PDSI and SW percentiles. La Nina

is typically associated with above average temperatures in the SEUS which during summer months can accentuates the possibility of drought. Hence most parts of Florida and southern parts of North and South Carolina show very high R^2 with PDSI values for summer under La Nina conditions. These observations are consistent with several other studies (Livezey and Smith, 1999; Schmidt et al., 2001; Sittel, 1994) on the seasonal variations in the influence of cold and warm phases of ENSO on the weather conditions in the SEUS.

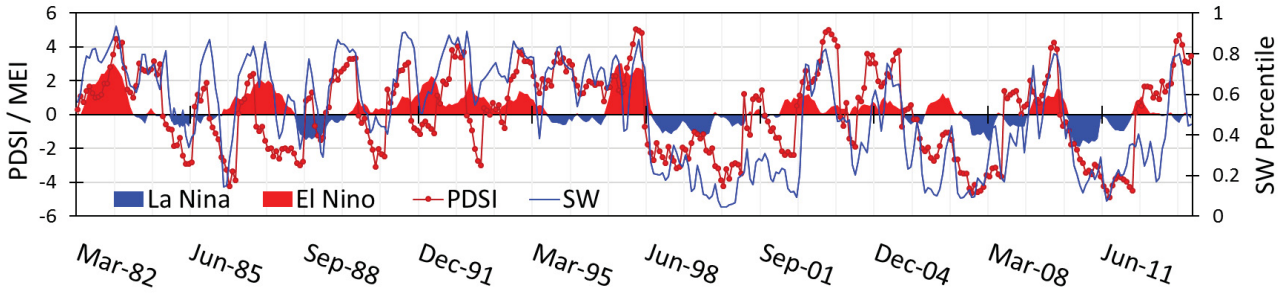

Figure 5-15: Time series area averaged PDSI and SW percentile with MEI from January 1982 through December 2013. Red portion of MEI represent positive (El Nino) and blue portion represent negative (La Nina) phase of MEI.

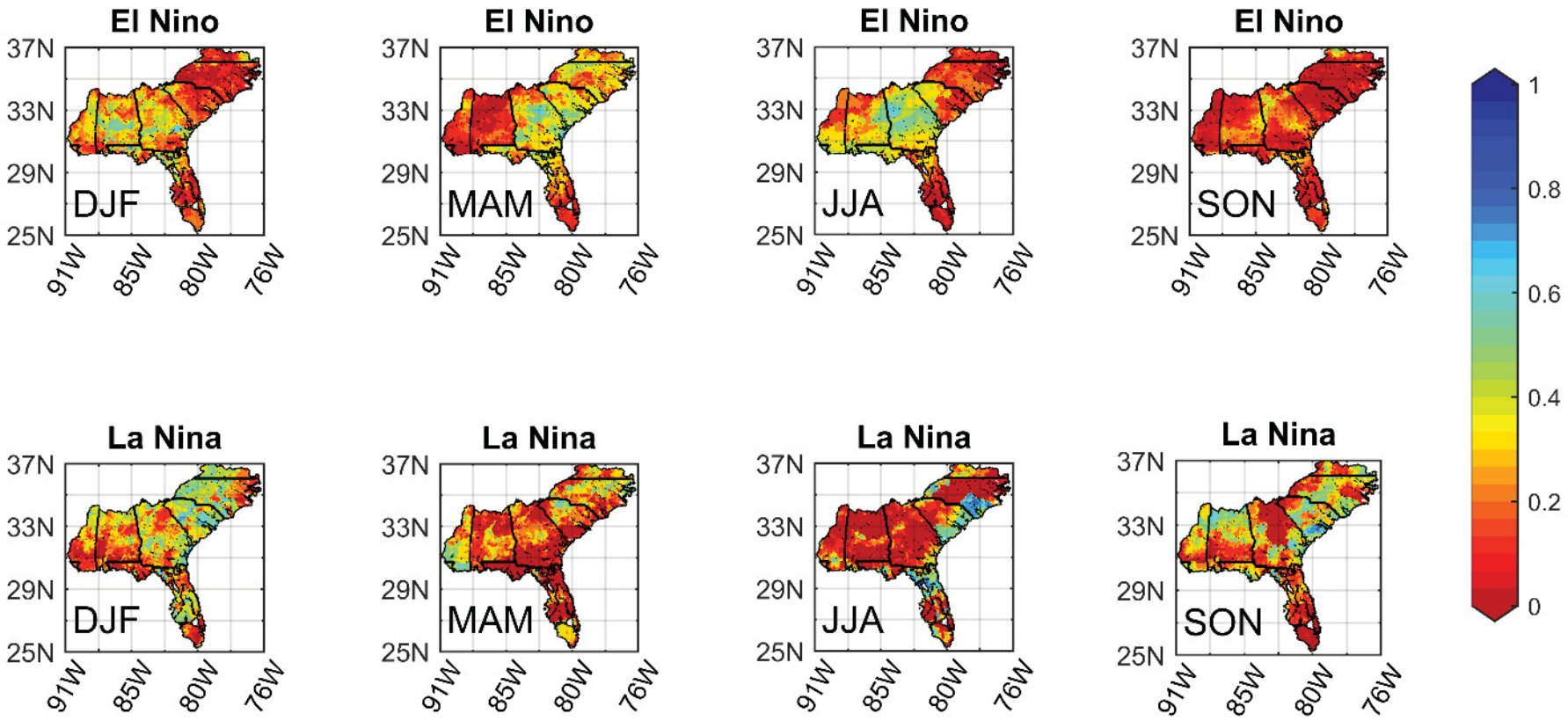

Figure 5-16: Spatial representation of predictability of PDSI using SW percentiles for December-January (Winter), March – May (Spring), June- August (Summer) and September -November (Fall) months based on January 1982 through December 2013 climatology for (Top) Positive (El Nino) and (Bottom) Negative (La Nina) phase of MEI.

6. Conclusion

This study provides a watershed scale assessment of drought predictability in the context of hydroclimatological teleconnections. Watershed scale water balance components are obtained by implementing calibrated SWAT model for 50 watersheds in the South-Atlantic Gulf of Southeastern U.S. for a period of January 1982 through 2013. Monthly percentiles of four hydrologic variables namely, soil water, surface runoff, potential evapotranspiration and precipitation are used to evaluate the relative strength of each of these variables in able to reflect drought conditions under strong hydroclimatological extremes. The study highlights the importance of watershed characteristics, influence of seasonality, and interplay of various water budget components in predictability of drought at watershed scale. Key findings of this study are as follows:

a) Drought predictability in the context of hydroclimatic extremes is strongly impacted by watershed characteristics. Watersheds in Florida and parts of Georgia, Alabama and Mississippi states are seen to show higher correlation with the hydroclimatic indices. MEI, PDO, BEST and ONI are observed to have higher correlation with various water balance components compared to other indices.
b) Seasonality has strong influence on the watershed scale response to hydroclimatology due to interplay of several water balance components. Winter and fall seasons show higher dependence on hydroclimatology compared to summer and spring months.
c) Precipitation and surface runoff offer comparatively lower values R^2 with hydroclimatic indices compared to soil water. Water deficit months see higher predictability of PET percentiles. Overall, SW based drought assessment has highest predictability using hydroclimatic indices across all seasons.

d) Drought months identified using soil moisture percentiles corresponded strongly with the low PDSI values for the respective months. Disagreement between SPI-1 and SW percentiles in drought identification is relatively high.

e) Predictability of PDSI using SW percentiles is observed to be very high >90% for summer season under La Nina condition. Overall, predictability of PDSI is observed to be high for winter across the study area. Spring season shows higher predictability of PDSI for Virginia and Carolinas. Drought predictability in summer under El Nino conditions is observed to be low.

Chapter 6 :
Conclusion

Soil moisture is important for understanding the onset, propagation, and recovery of droughts. However, in the absence of a long-term, *in- situ* soil moisture data for drought analysis a combination of two Land Surface Models (LSMs) namely, Noah and Mosaic, is developed for application in retrospective drought analysis for Contiguous United Stated (CONUS) using a multi-resolution regression, coupled with Bayesian Model Averaging models. A stratified correlation analysis between soil moisture and eight drought indices namely PDSI, PHDI, Z index, SPI- 1, 6, 9, 12 and 24 shows that shallow soil layers (0-10 cm and 10- 40 cm) respond to short-term drought occurrences with higher correlation whereas deeper layer (40- 100 cm) is more responsive to long-term droughts. Soil stratum differs significantly with respect to their persistence and so, possess a characteristic response to drought. A new drought classification based on stratified soil moisture percentiles is proposed and applied to reconstruct drought over CONUS for Apr- Dec 2011.

While large scale (continental) models are helpful in deriving useful interpretations about drought dynamics, especially their propagation and interrelationship with long-term climatic factors, a watershed-scale analysis is required to effectively and comprehensively characterize drought severity at a watershed scale. This understanding can have significant implications in catchment/watershed level water management practices for example:

a) Improving farmers' ability for drought mitigation, particularly in rain-fed systems.
b) Skillful prediction of the field moisture availability is important to decide crop type, resource use, and crop insurance and contract renewals.

c) *Drought water restrictions* at local/community level for example, prohibitions against wasteful practices such as watering lawns, hosing off sidewalks and driveways, or overwatering landscaping.

d) *Contamination in water bodies:* Preventing compounding of pollutants to unsafe levels in the local water bodies because of poor water quality, high temperatures and reduced water supplies due to severe drought stress.

e) *Wildlife management:* Water stress leads to reduced productivity for all wildlife species of wildlife. Foraging wildlife could potentially increase conflict between wild animals and humans.

f) *Recreational restrictions:* Reduced streamflow and reservoir storage could restrict freshwater fishing activities, restrictions on accessing hunting areas due to the danger of forest fire, availability of fewer game animals for harvest in next hunting seasons due to lower wildlife productivity. Regulations on recreational activities like white-water rafting, kayaking, or canoeing due to low instream flows and river water depths.

A high-resolution retrospective simulation of hydrologic variables for 50 watersheds in the South-Atlantic Gulf region of the Southeastern US, is performed by implementing SWAT models for each watershed at HUC-12 resolution to facilitate a watershed scale drought analysis, and its effect on several water balance components of the watershed. The study expands the scope of retrospective drought analysis to near real-time forecasting of drought by providing seasonal forecasts of hydrologic variables in the study area by coupling SWAT models with meteorological drivers from CFSv2 climate forecast models with a lead time of 9 months. Retrospective drought analysis is carried out for a period of 1982 through March 2017 drought forecasts are provided for a period of March through December 2017 at a weekly time step.

It is observed that the proposed stratified approach is a useful tool in capturing drought onset and persistence, where surface layer soil moisture can reflect on transient drought conditions while total rooting depth soil moisture captures the persistence and long-term severity of droughts at a sub-watershed scale. Significant spatial and seasonal variability in soil moisture is captured using a choice of several distribution functions which are dynamically chosen based on the best-fit criteria for each sub-watershed. The choice of distribution varied from week-to-week based on the interplay of mean and variance of soil moisture data.

Aggregation of soil moisture data to several weeks has a strong influence on the correlation of soil moisture to PDSI, PHDI and Z index, and, SPI-1, 6, 9, and 12. The correlation of soil moisture percentiles with these indices varies spatially due to the influence of vegetation, land use and hydroclimatology. The accuracy of the proposed approach is established by comparing the simulated drought maps with those of US drought monitor and other drought indicators provided by NCDC (PDSI, PHDI, Palmer Z index and SPI-1, 6, 9, and 12) for the region. The study finds that the soil moisture percentiles for the total and the surface soil moisture with various aggregations are in good agreement with other long and short-term drought indices provided by NCDC. Comparisons of the correlation of monthly percentiles of the simulated surface and total rooting depth soil moisture, evapotranspiration, potential evapotranspiration and precipitation with NCDC drought indices are also carried out. Real-time drought assessment using SWAT-CFSv2 coupled models at HUC-12 resolution shows that the models capture most recent drought of 2016 in the region. A forecast of 9 months lead time is also provided for the region using the forecasts from SWAT- CFSv2 coupled models.

A watershed scale evaluation of hydrologic variables with several hydroclimatological indices reflects strong teleconnections between the watershed-scale water balance components and large-

scale circulation patterns and sea surface temperature anomalies. Monthly percentiles of four hydrologic variables namely, soil water, surface runoff, potential evapotranspiration, and precipitation are used to evaluate the relative strength of each of these variables to reflect drought conditions under strong hydroclimatological extremes. It is observed that drought predictability in the context of hydroclimatic extremes is strongly impacted by watershed characteristics like soil type, land use, geography, topography, and climatology. Watersheds in Florida and parts of Georgia, Alabama and Mississippi states are seen to show a higher correlation with the hydroclimatic indices. MEI, PDO, BEST and ONI are observed to have a higher correlation with various water balance components compared to other indices.

It is observed that seasonality has a strong influence on the watershed-scale response to hydroclimatology due to dynamic interrelationship of several water balance components. Winter and fall seasons show higher dependence on hydroclimatology compared to summer and spring months. It is observed that drought months identified using soil moisture percentiles corresponded strongly with low PDSI values for the respective months. Predictability of PDSI using SW percentiles is observed to be very high >90% for summer season under La Nina condition. Overall, the predictability of PDSI is observed to be high for winter across the study area. Spring season shows higher predictability of PDSI for Virginia and Carolinas. Drought predictability in summer under El Nino conditions is observed to be low.

Appendix

A1. Pre-whitening of time series prior to correlation analysis between drought indices and soil moisture

Percentage of selected grid cells with respective model combination (i.e. *p* and *q* values) are plotted to evaluate best models for a generalized analysis. It is observed that ARIMA (*2,1,2*) is the most suitable model combination and hence, is used for pre-whitening the time series from each grid cell across CONUS. The bar plots for percentage of selected grid cells with suitable model combination for soil moisture (HSM) and drought indices in provided in Figure. A0-1. For details on ARIMA modeling, readers are referred to Box and Jenkins (1976).

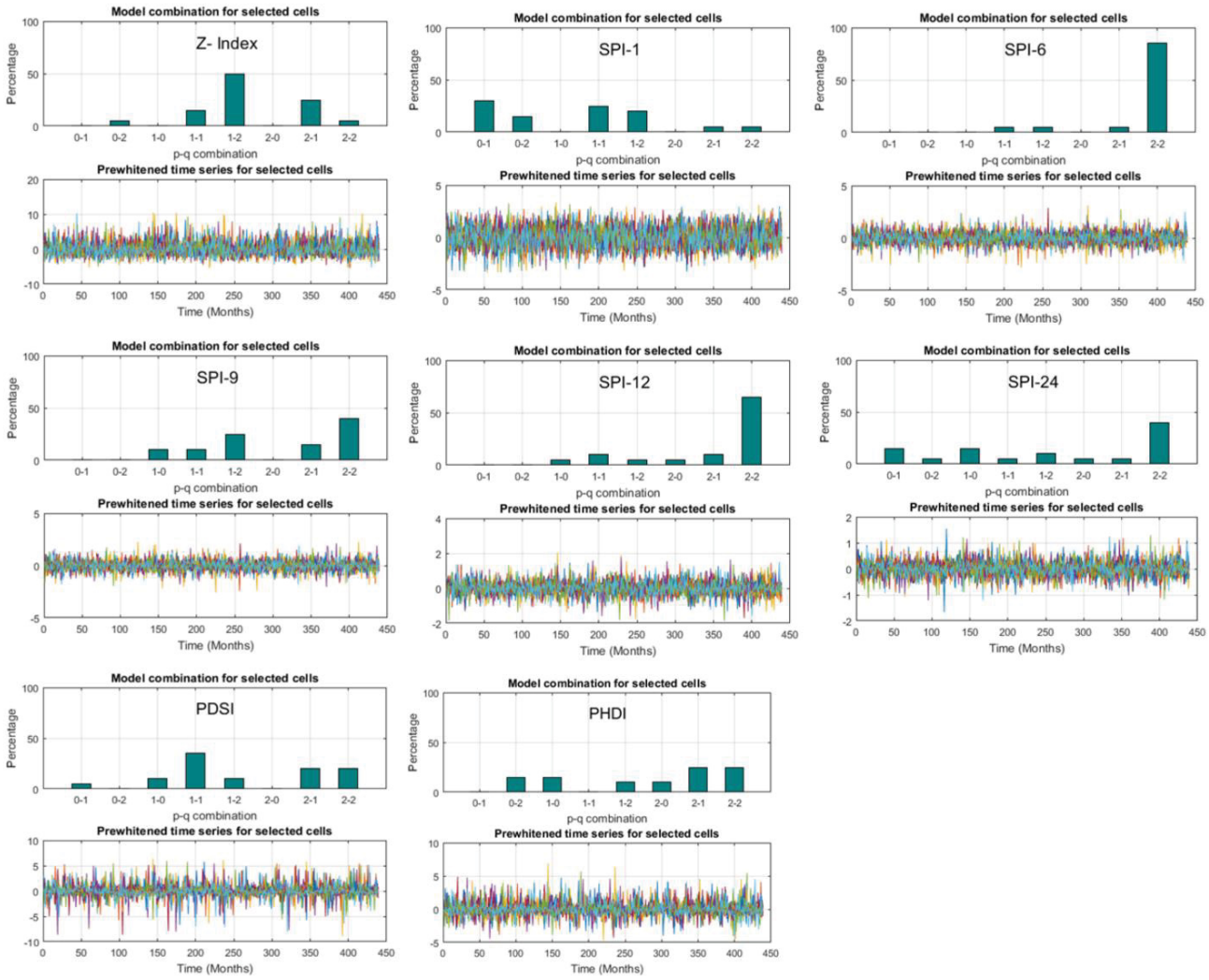

Figure. A0-1: Percentage of selected cells with best ARIMA (*p,1,q*) combination for soil moisture for all three layers (top row) and all drought indices considered in this study (second row and below). The pre-whitened time series are provided beneath the bar chart for the respective variable.

A2. Time series decomposition using DWT

Figure. A0-2 provides decomposed time series of *in- situ* soil moisture data, HSM, Noah and Mosaic dataset using db3 wavelet for comparison. It can be seen that the DWT is able to separate out the long-term trends in the time series pertaining to low frequency component of the signal from the rapidly varying (high frequency) transient components.

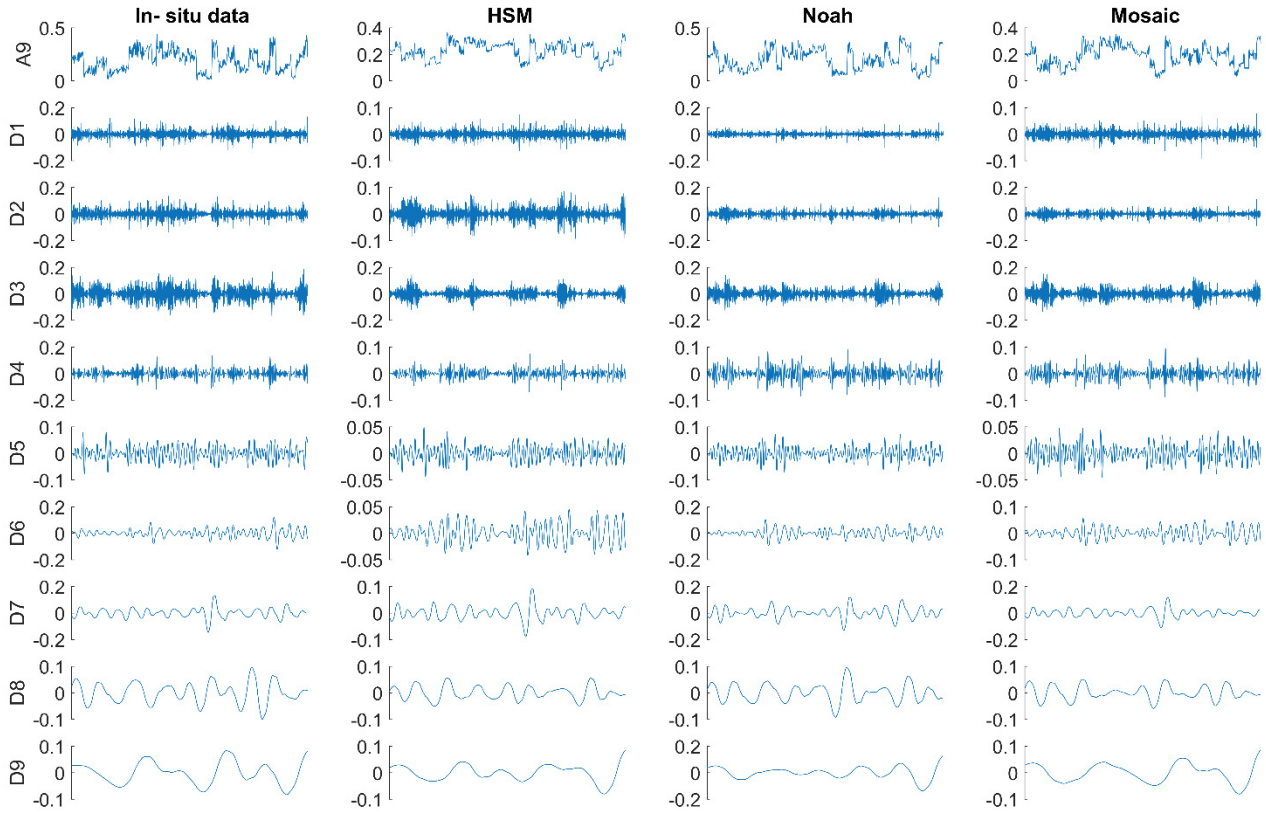

Figure. A0-2: Discrete Wavelet Components (or Sub- time series) of observed *in- situ* soil moisture data, HSM, Noah and Mosaic dataset using db3 wavelet upto 9 dyadic levels.

A3. Trend and monthly error estimation for the Hybrid soil moisture (HSM)

Soil moisture (SM) follows a seasonal trend and the errors in estimation of the monthly SM varies from month to month depending on the part of the year. We use a bootstrap based approach to obtain approximate quartiles of the percentage absolute error in estimating SM for respective months. This approach is explained through a schematic presented in Figure. A0-3.

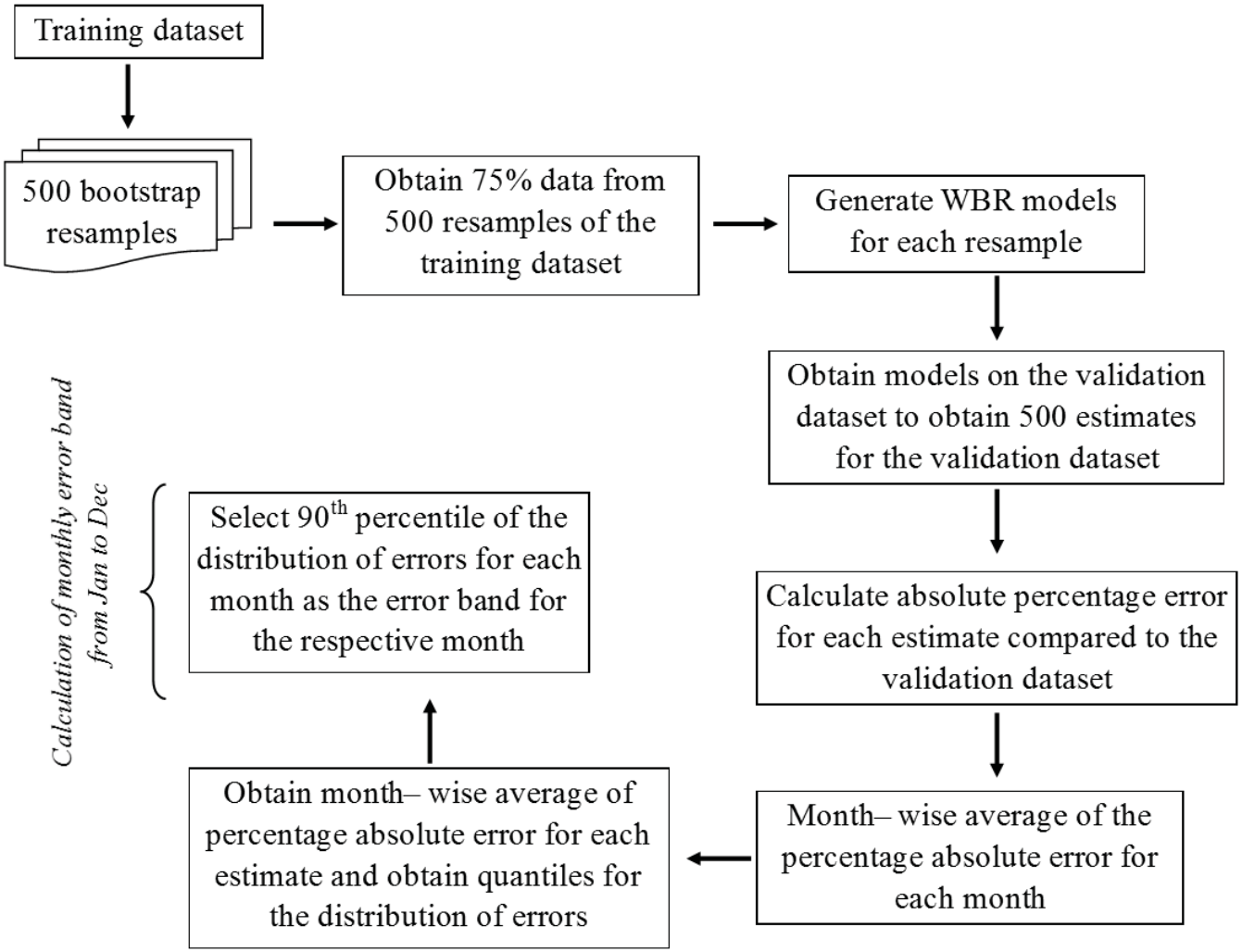

Figure. A0-3: Schematic for obtaining monthly error percentiles for the estimated Hybrid Soil Moisture using a bootstrap resampling approach

Figure. A0-4 provides box plots for the estimated percentage absolute error from Jan to Dec for each layer along with the variation in the values of the HSM for each month as obtained from the validation dataset. It is interesting to note that the estimated error band follows the same trend as that of SM. While the values of SM fall down during summers, so does the per cent absolute error in estimating the SM. While the values for SM are highest during the winter months, the percent absolute error as well increases in magnitude. The values for 10^{th}, 50^{th} and 90^{th} percentiles for the per cent absolute error for the three soil layers are provided in Table A0-1. The value of the absolute error percentage at 90^{th} percentile is chosen to be the error band for the respective month of each layer. Figure. A0-5 provides line plots of observed v/s estimated SM for validation and total dataset with month-wise error bands.

Table A0-1: Month-wise values for the 10th, 50th and 90th percentile of absolute error (%) in estimation of the Hybrid Soil Moisture for the three soil layers. The monthly 90^{th} percentile provides the error band in the estimation of the Hybrid Soil Moisture for the respective month.

	Percentile value of monthly absolute error (%) for HSM estimations								
	Layer 1			***Layer 2***			***Layer 3***		
	10^{th}	90^{th}	50^{th}	10^{th}	90^{th}	50^{th}	10^{th}	90^{th}	50^{th}
Jan	23.5	21.5	22.5	24.2	21.8	23.0	26.6	23.6	25.0
Feb	24.0	21.8	22.9	25.4	22.8	24.1	28.0	24.9	26.4
Mar	22.3	20.6	21.4	25.5	23.4	24.4	28.4	25.8	27.1
Apr	20.3	18.7	19.5	23.9	21.9	22.9	28.4	26.0	27.2
May	18.4	16.6	17.5	21.6	19.5	20.6	26.0	23.4	24.7
June	18.1	16.3	17.2	21.4	19.4	20.4	25.6	23.0	24.2
July	17.5	15.7	16.6	20.5	18.4	19.4	25.1	22.4	23.6
Aug	16.8	14.8	15.8	19.7	17.5	18.5	23.8	20.9	22.2
Sep	17.4	15.4	16.4	20.2	17.8	19.0	23.3	20.4	21.7
Oct	17.4	15.5	16.4	20.2	17.8	19.0	23.6	20.7	22.0
Nov	18.8	16.9	17.9	20.7	18.3	19.5	23.7	20.8	22.2
Dec	21.2	19.2	20.2	22.6	20.2	21.4	25.3	22.4	23.7

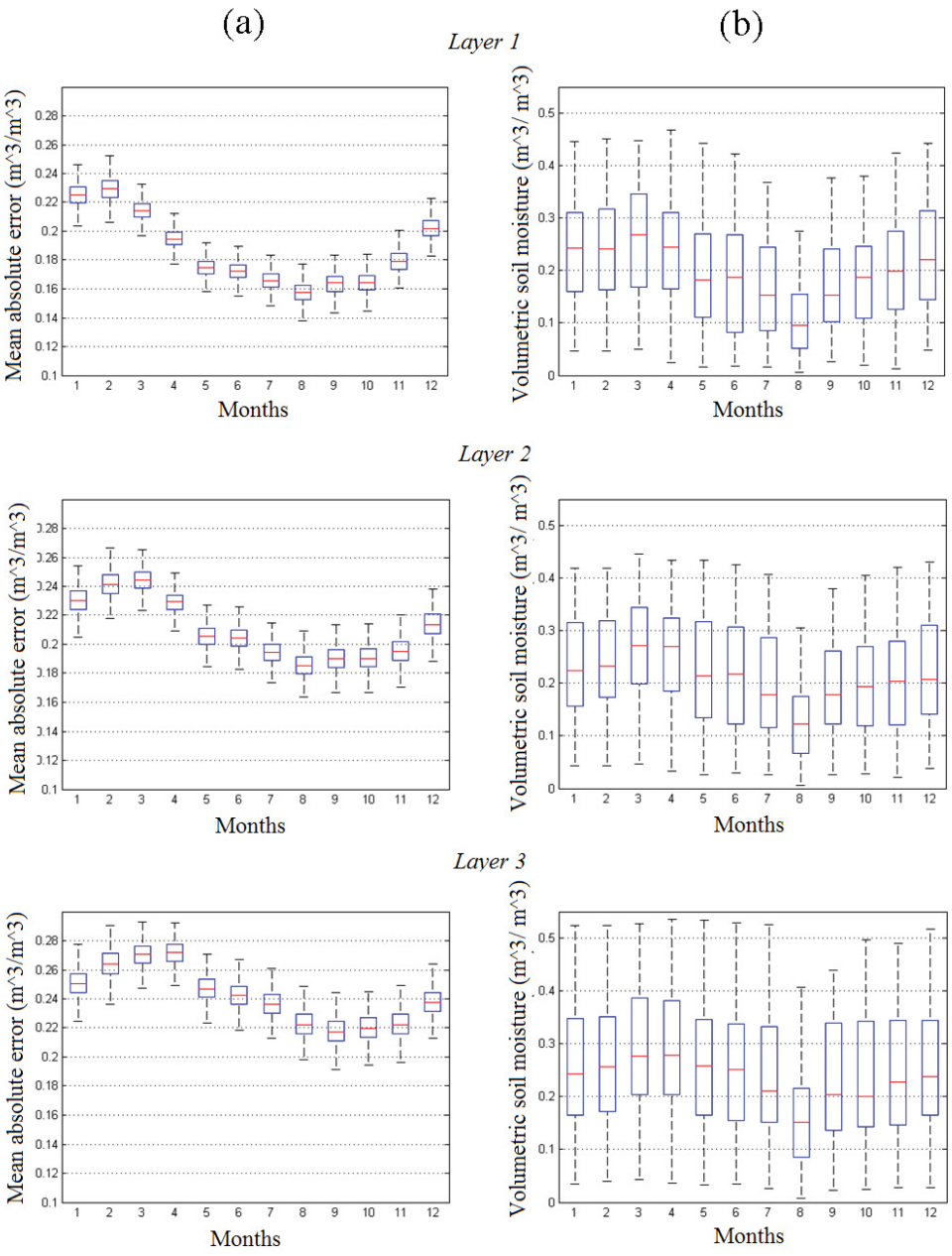

Figure. A0-4: Box plots for (a) Mean Absolute error (%) in estimation of the validation dataset using WBR models from the resampled training dataset. The absolute error (in percent) in estimating the validation dataset using the WBR models on the resampled dataset is averaged month- wise thus giving 500 values for each month corresponding to each resample. (b) Monthly *in- situ* soil moisture across control stations

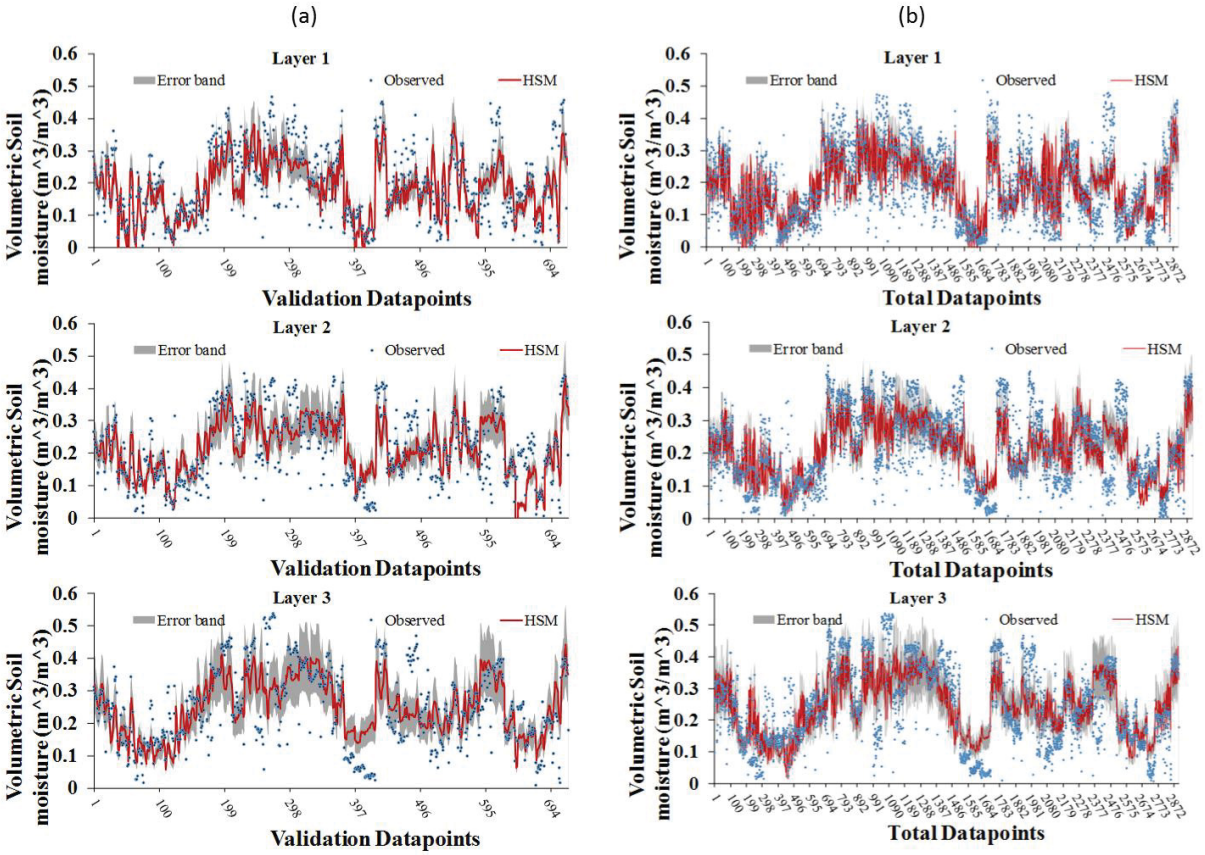

Figure. A0-5: Line plots of *in- situ* soil moisture v/s HSM for all three layers with month-wise error band for (a) Validation and (b) Total dataset

Further, a model implementation scheme is employed where the models are developed for all but one station are implemented on the remaining station ("*skip one take rest* ") and the performance of the model is evaluated in order to demonstrate the ability of the models to perform for all geographies with a reasonable accuracy. The process is repeated till all control stations are covered. The values of correlation between the observed SM data and HSM as obtained by the above-mentioned approach for each station is obtained and is shown spatially in Figure. A0-6. To assess the variability in the correlation value between the observed SM and HSM as obtained from the reliability scheme in this section, the correlation values obtained for each layer across all stations are plotted in a boxplot as shown in Figure. A0-7. The mean of correlation values of HSM with

observed SM for all control stations is found to be closer to 0.75 for layer 1 and 0.6 for both layers 2 and 3. There are a few exceptions where the models aren't able to provide HSM with high correlation with observed SM, but number of such occurrences is very small. This indicates that the models can be relied upon for further analysis.

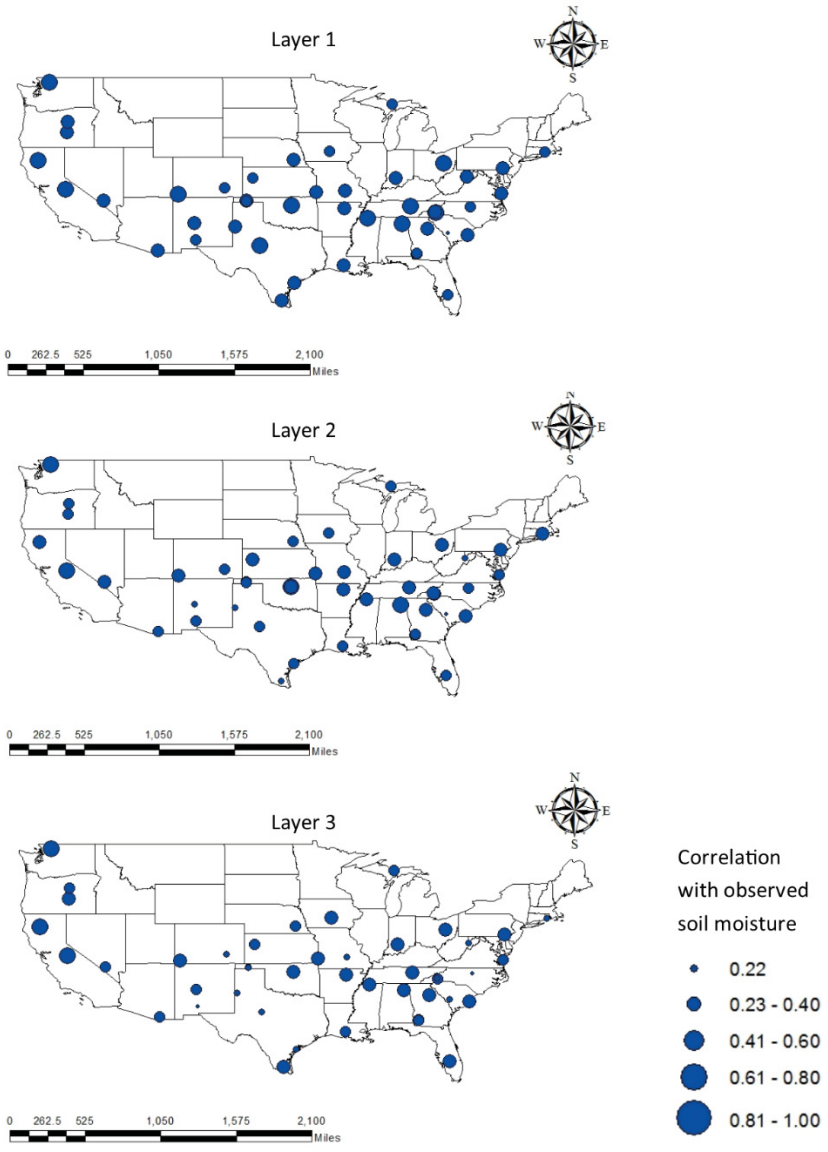

Figure. A0-6: Correlation values between *in- situ* soil moisture and the Hybrid Soil Moisture obtained by the reliability scheme for each station

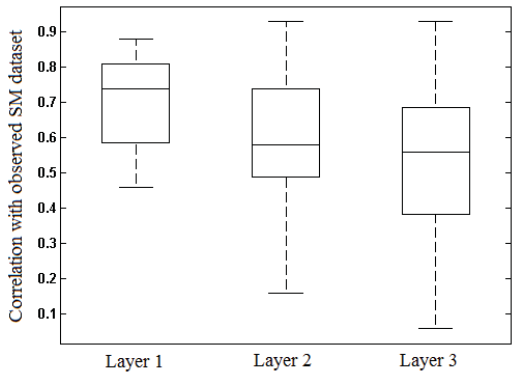

Figure. A0-7: Correlation values between the Hybrid Soil Moisture and *in- situ* soil moisture from the control stations as obtained after the "*skip one take rest*" implementation scheme

It can be observed from Figure. A0-6 and Figure. A0-7 the generalized modeling approach adopted in this study is reasonably accurate for most of the regions and hence can be used for further analysis with reasonable confidence. The error in estimation in soil moisture increases from Layer 1 to Layer 3 (Figure. A0-5). Hence the overall correlation of the HSM with observed dataset is low for the deeper layers compared to the top layer. This is because the correlation of simulated SM from both Noah and Mosaic with the *in- situ* SM decreases with increasing depth of the soil layer from the surface thus providing lesser information for the model to emulate in the estimation of the *in- situ* SM.

A4. Climatology (average annual precipitation, Maximum and minimum annual temperatures) of 50 watersheds based on 1979- 2013 data

Basin	Watershed	PREC (mm)	Tmin (°C)	Tmax (°C)
0301	30101	96.4	-14.0	37.9
	30102	100.2	-12.2	38.7
	30103	108.0	-10.4	38.1
0302	30201	113.1	-10.0	38.7
	30202	120.3	-9.3	38.3
0303	30301	111.4	-10.0	38.9
	30302	121.5	-9.6	39.6
	30303	131.5	-8.5	39.4
0304	30401	105.7	-10.9	38.7
	30402	122.1	-8.3	39.4
	30403	119.8	-7.9	40.1
0305	30501	109.0	-11.0	38.2
	30502	121.8	-6.0	40.1
	30503	108.2	-9.0	39.3
0306	30601	111.6	-8.7	39.2
	30602	116.6	-6.0	40.1
	30603	112.6	-6.8	40.3
	30604	123.9	-5.5	40.0
0307	30701	113.9	-8.1	39.8
	30702	115.8	-7.6	39.7
	30703	121.7	-6.0	40.0
	30704	131.3	-4.7	39.8
0308	30801	150.8	-0.5	37.8
	30802	144.4	-2.3	38.4
0309	30901	159.7	0.6	38.4
	30902	167.8	2.3	36.5

Basin	Watershed	PREC (mm)	Tmin (°C)	Tmax (°C)
0310	31001	153.7	-0.7	39.3
	31002	141.1	0.4	37.1
	31003	144.0	-2.2	38.8
0311	31101	145.3	-4.1	39.5
	31102	132.0	-5.2	39.6
0312	31201	142.1	-7.1	39.0
0313	31301	122.5	-9.1	38.3
	31302	120.5	-7.4	39.5
	31303	130.4	-4.9	39.2
0314	31401	137.8	-4.9	37.8
	31402	132.3	-5.8	40.0
	31403	133.3	-7.1	39.8
0315	31501	121.6	-11.3	37.8
	31502	124.0	-9.6	38.6
	31503	129.0	-7.9	39.9
0316	31601	130.3	-9.7	39.7
	31602	128.9	-10.1	39.1
	31603	135.2	-7.3	40.0
0317	31701	134.6	-7.8	40.4
	31702	134.8	-7.4	40.5
	31703	143.2	-6.0	39.8
0318	31801	135.1	-8.9	39.9
	31802	135.6	-7.7	40.0
	31803	137.4	-6.5	40.2

A5. Flow hydrographs: SWAT simulation vs USGS observed discharge

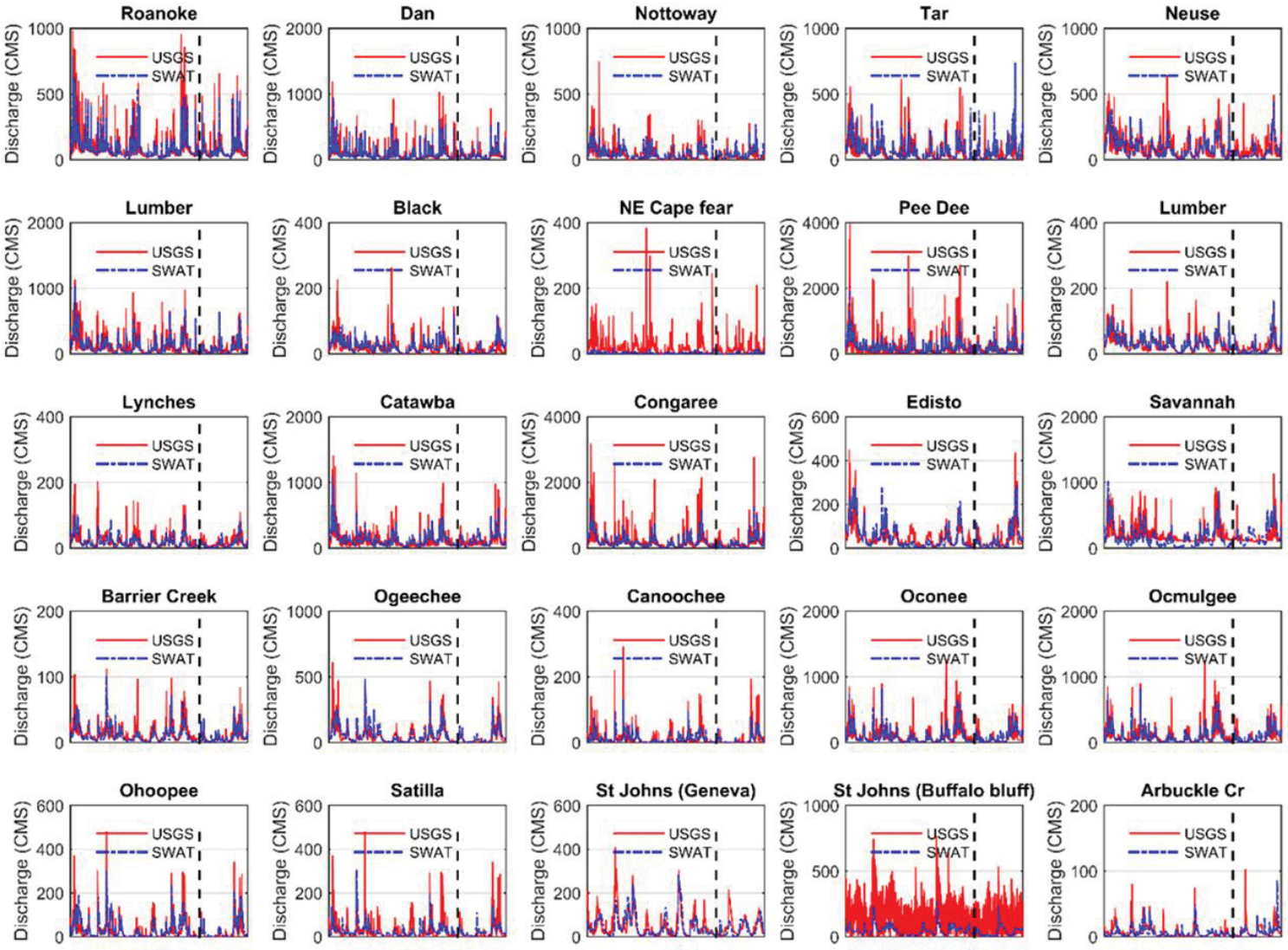

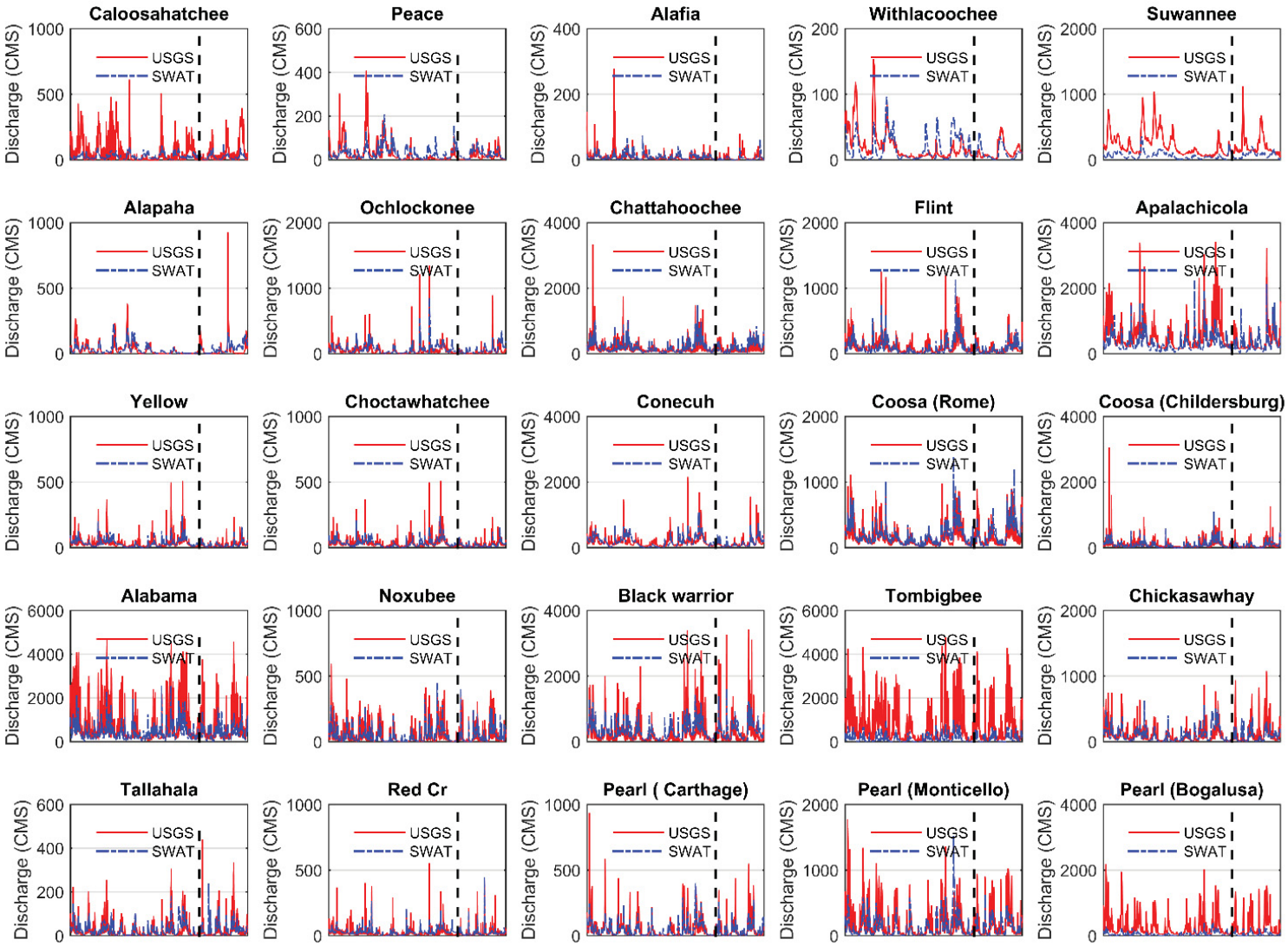
Caloosahatchee
Peace
Alafia
Withlacoochee
Suwannee
Alapaha
Ochlockonee
Chattahoochee
Flint
Apalachicola
Yellow
Choctawhatchee
Conecuh
Coosa (Rome)
Coosa (Childersburg)
Alabama
Noxubee
Black warrior
Tombigbee
Chickasawhay
Tallahala
Red Cr
Pearl (Carthage)
Pearl (Monticello)
Pearl (Bogalusa)
Discharge (CMS)
USGS
SWAT

A6. Performance statistics of SWAT model calibration and validation for 50 watersheds.

				Calibration (2000-2010)					Validation (2011-2013)				
Basin	Lon	Lat	USGS stations	Rsq	NSE	NRMSE	NMAE	WI	Rsq	NSE	NRMSE	NMAE	WI
0301	-78.74	36.92	02066000	0.60	0.59	0.06	0.03	0.52	0.62	0.61	0.07	0.04	0.54
	-79.09	36.64	02075500	0.48	0.43	0.06	0.03	0.45	0.50	0.19	0.07	0.04	0.37
	-77.17	36.77	02047000	0.49	0.49	0.06	0.03	0.46	0.45	-0.11	0.12	0.08	0.10
0302	-77.37	35.62	02084000	0.52	0.51	0.10	0.05	0.56	0.35	-2.05	0.24	0.13	0.11
	-77.30	35.31	02091814	0.59	0.57	0.10	0.06	0.70	0.49	0.36	0.12	0.09	0.57
0303	-78.96	34.44	02134500	0.64	0.64	0.08	0.05	0.65	0.53	0.40	0.10	0.06	0.47
	-78.29	34.76	02106500	0.40	0.40	0.07	0.04	0.45	0.34	-0.30	0.14	0.09	0.18
	-77.83	34.83	02108000	0.37	-0.25	0.09	0.05	0.37	0.34	-0.27	0.11	0.06	0.39
0304	-79.87	34.95	02129000	0.52	0.49	0.05	0.02	0.46	0.49	0.41	0.07	0.04	0.56
	-78.96	34.44	02134500	0.51	0.50	0.09	0.05	0.62	0.65	0.47	0.09	0.07	0.59
	-79.75	34.05	02132000	0.41	0.39	0.09	0.05	0.52	0.51	0.35	0.10	0.08	0.62
0305	-80.88	34.84	02147020	0.56	0.56	0.05	0.03	0.56	0.56	0.51	0.07	0.05	0.48
	-81.05	33.99	02169500	0.51	0.51	0.05	0.03	0.51	0.58	0.54	0.05	0.03	0.59
	-80.39	33.03	02175000	0.68	0.57	0.07	0.05	0.67	0.73	0.70	0.07	0.05	0.68
0306	-81.94	33.37	02197000	0.46	0.26	0.15	0.11	0.57	0.18	-0.41	0.13	0.09	-0.08
	-81.65	32.93	02198000	0.53	0.44	0.08	0.05	0.62	0.73	0.71	0.06	0.04	0.73
	-81.42	32.19	02202500	0.57	0.54	0.08	0.04	0.55	0.81	0.80	0.06	0.03	0.72
	-81.89	32.18	02203000	0.46	0.46	0.05	0.03	0.43	0.64	0.61	0.07	0.03	0.46
0307	-82.89	32.54	02223500	0.59	0.57	0.07	0.04	0.63	0.50	0.45	0.13	0.09	0.40
	-83.46	32.28	02215000	0.59	0.57	0.07	0.04	0.63	0.50	0.45	0.13	0.09	0.40
	-82.18	32.08	02225500	0.54	0.48	0.07	0.04	0.50	0.68	0.64	0.07	0.04	0.52
	-81.87	31.22	02228000	0.27	0.24	0.08	0.05	0.32	0.48	0.46	0.09	0.05	0.28
0308	-81.04	28.71	02234000	0.63	0.62	0.09	0.06	0.68	0.43	0.39	0.14	0.10	0.63
	-81.68	29.60	02244040	0.41	-0.62	0.20	0.16	0.51	0.03	-1.05	0.24	0.19	0.46
0309	-81.30	27.44	02270500	0.41	0.37	0.09	0.05	0.50	0.18	-0.13	0.11	0.06	0.31
	-81.70	26.72	02292900	0.19	0.01	0.14	0.08	0.40	0.29	0.06	0.19	0.10	0.42
0310	-81.88	27.22	02296750	0.33	0.32	0.09	0.05	0.26	0.48	0.00	0.19	0.14	0.12
	-82.21	27.87	02301500	0.18	0.15	0.04	0.02	0.23	0.16	-0.24	0.12	0.06	0.38
	-82.35	28.99	02313000	0.27	0.19	0.15	0.10	0.42	0.45	0.37	0.18	0.12	0.58
0311	-82.94	29.59	02323500	0.29	-0.58	0.20	0.14	0.49	0.05	-0.68	0.17	0.12	0.43
	-83.03	30.70	02317500	0.44	0.43	0.05	0.02	0.31	0.31	0.30	0.06	0.03	0.09
0312	-84.67	30.18	02330150	0.42	0.37	0.06	0.03	0.30	0.22	-0.12	0.08	0.04	-0.02
0313	-84.90	33.48	02338000	0.56	0.54	0.04	0.02	0.52	0.40	-0.55	0.20	0.14	0.10
	-84.02	31.73	02350512	0.51	0.46	0.08	0.05	0.57	0.53	0.51	0.10	0.07	0.57
	-85.03	30.43	02358700	0.39	0.17	0.13	0.08	0.54	0.38	0.30	0.09	0.06	0.45
0314	-86.92	30.57	02369600	0.43	0.43	0.06	0.03	0.45	0.35	0.31	0.09	0.05	0.44
	-85.90	30.45	02366500	0.43	0.43	0.06	0.03	0.45	0.35	0.31	0.09	0.05	0.44
	-87.06	31.07	02374250	0.39	0.34	0.07	0.05	0.45	0.47	0.47	0.08	0.04	0.46
0315	-85.26	34.20	02397000	0.67	0.65	0.08	0.05	0.64	0.61	0.51	0.13	0.10	0.54
	-86.36	33.29	02407000	0.41	0.39	0.03	0.01	0.47	0.39	0.38	0.06	0.03	0.44
	-87.55	31.62	02428400	0.48	0.22	0.16	0.10	0.52	0.33	0.19	0.15	0.10	0.50
0316	-88.30	32.92	02448500	0.57	0.56	0.08	0.04	0.53	0.51	0.50	0.13	0.07	0.40
	-87.84	32.78	02466030	0.54	0.53	0.07	0.04	0.45	0.50	0.47	0.09	0.06	0.30
	-88.13	31.76	02469761	0.52	-0.28	0.21	0.13	0.49	0.38	-0.30	0.23	0.15	0.48
0317	-88.55	31.15	02478500	0.45	0.43	0.11	0.07	0.50	0.29	0.25	0.14	0.07	0.40
	-89.11	31.33	02474500	0.45	0.42	0.08	0.05	0.35	0.28	0.27	0.09	0.05	0.25
	-88.78	30.74	02479300	0.38	0.37	0.05	0.03	0.16	0.61	0.61	0.06	0.03	0.35
0318	-89.53	32.71	02482550	0.54	0.53	0.05	0.03	0.54	0.56	0.55	0.09	0.05	0.56
	-90.09	31.55	02488500	0.37	0.32	0.11	0.06	0.51	0.59	0.46	0.18	0.11	0.56
	-89.82	30.79	02489500	0.42	-0.19	0.17	0.10	0.46	0.67	-0.18	0.27	0.16	0.48

A7. Watershed-wise water balance plots from simulated hydrologic variables using calibrated SWAT model implementation for a period of January 1982- through December 2013.

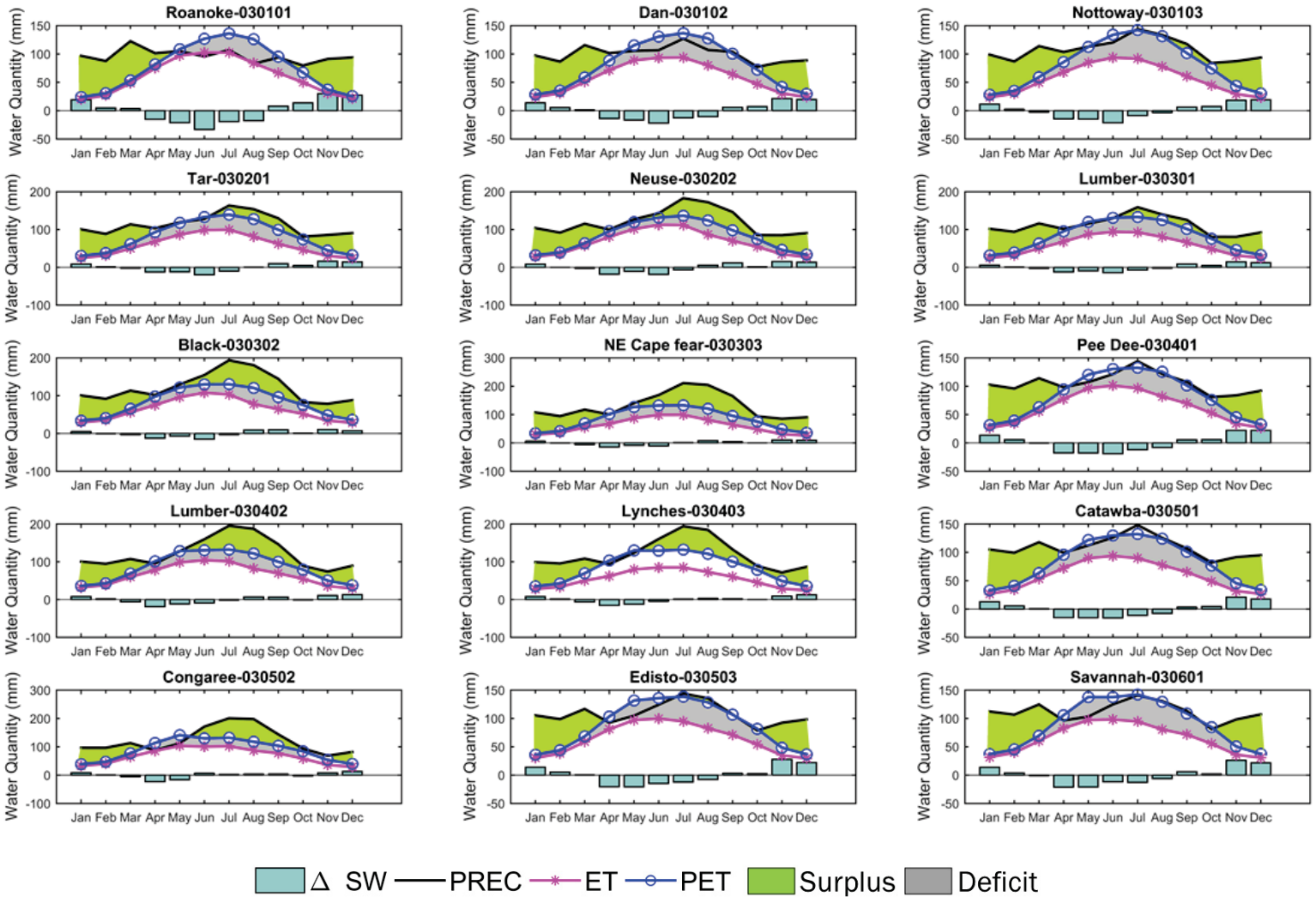

(Contd..) Watershed-wise water balance plots from simulated hydrologic variables using calibrated SWAT model implementation for a period of January 1982- through December 2013.

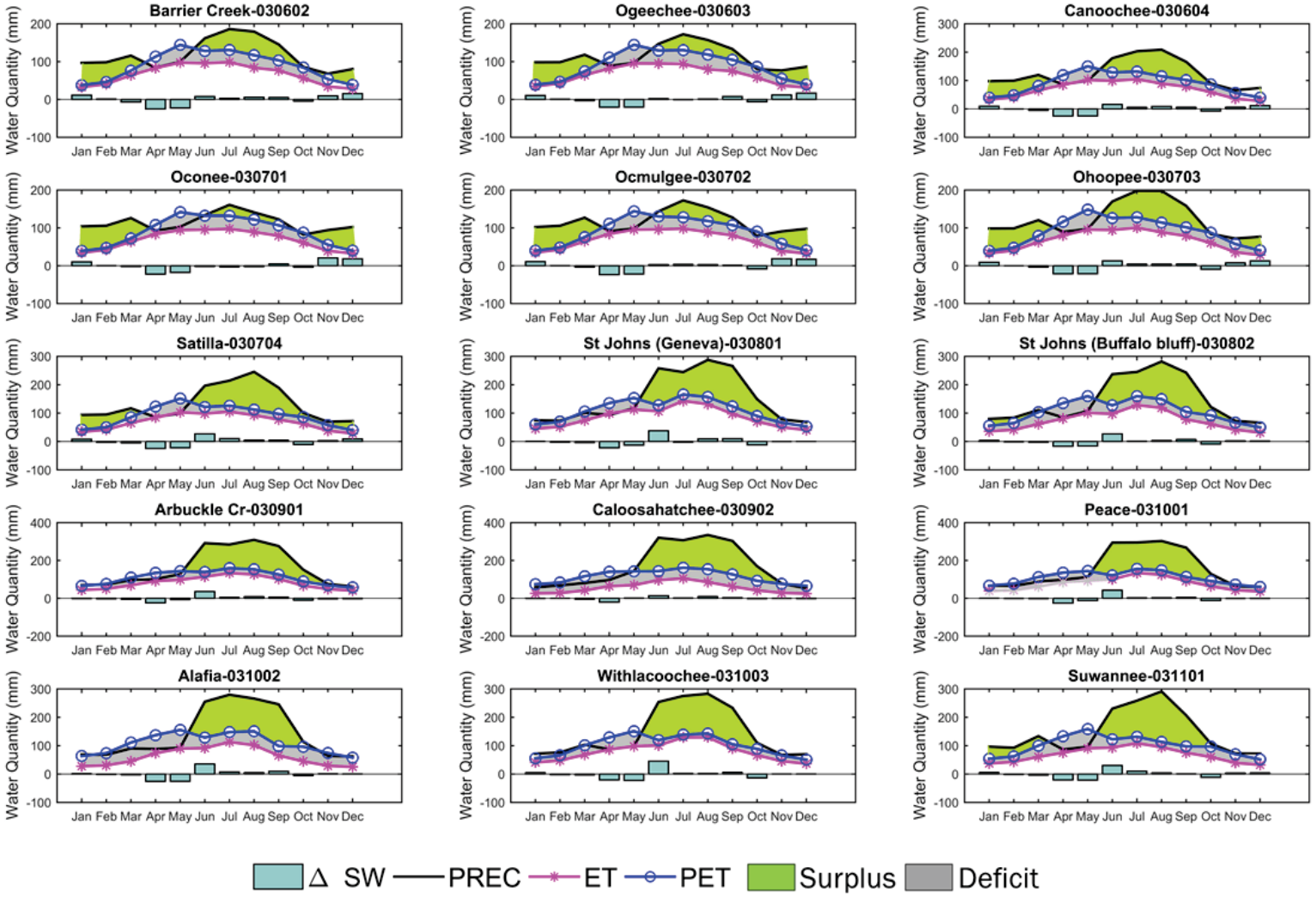

(Contd..) Watershed-wise water balance plots from simulated hydrologic variables using calibrated SWAT model implementation for a period of January 1982- through December 2013.

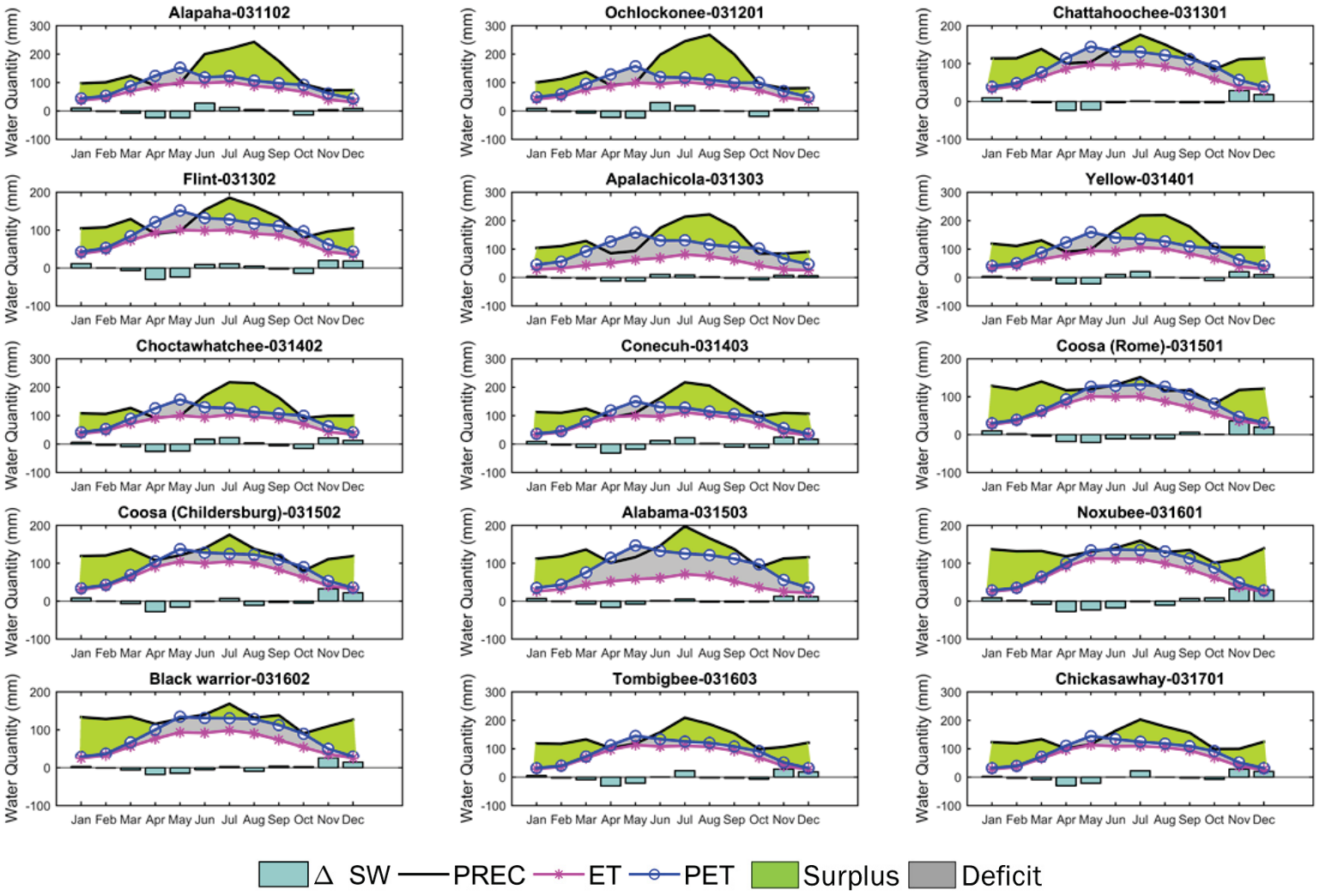

(Contd..) Watershed-wise water balance plots from simulated hydrologic variables using calibrated SWAT model implementation for a period of January 1982- through December 2013.

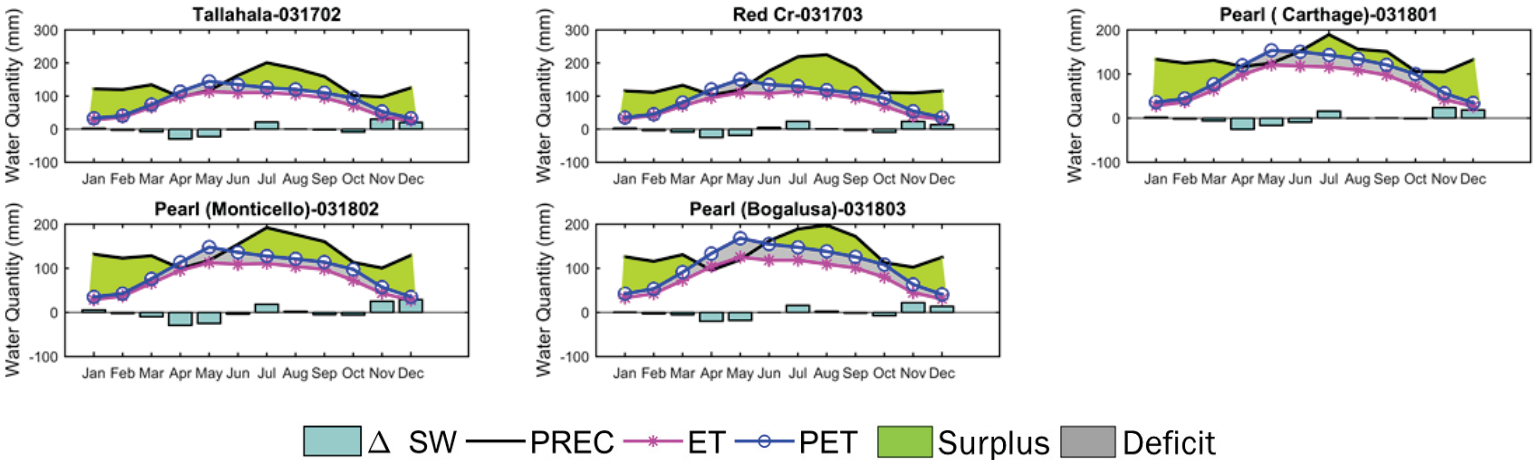

A8. Watershed-wise time series of the forecasted hydrologic variables (precipitation, actual evapotranspiration, potential evapotranspiration and soil moisture simulated using SWAT- CFSv2 hybrid models.

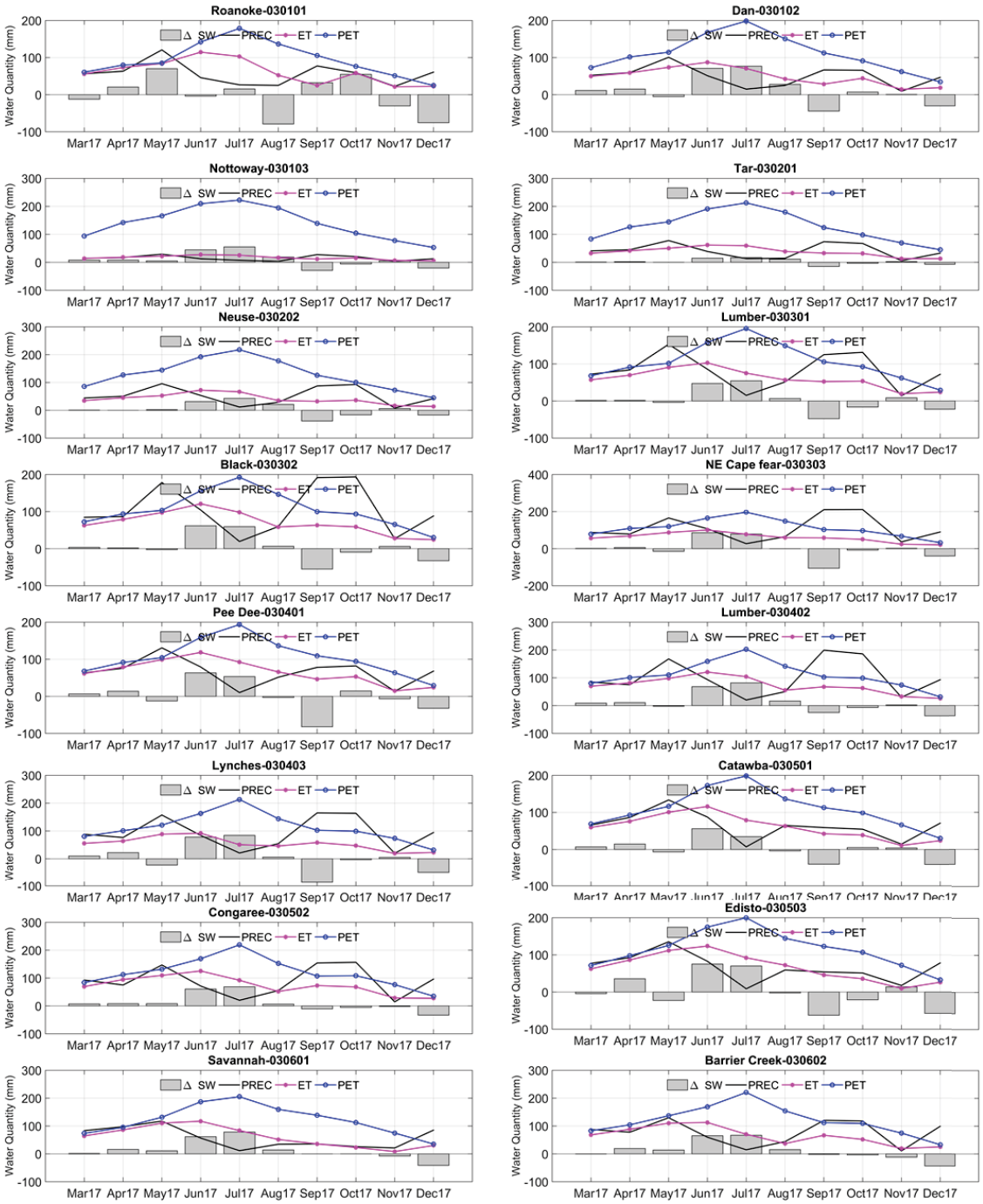

(Contd..) Watershed-wise time series of the forecasted hydrologic variables (precipitation, actual evapotranspiration, potential evapotranspiration and soil moisture simulated using SWAT- CFSv2 hybrid models.

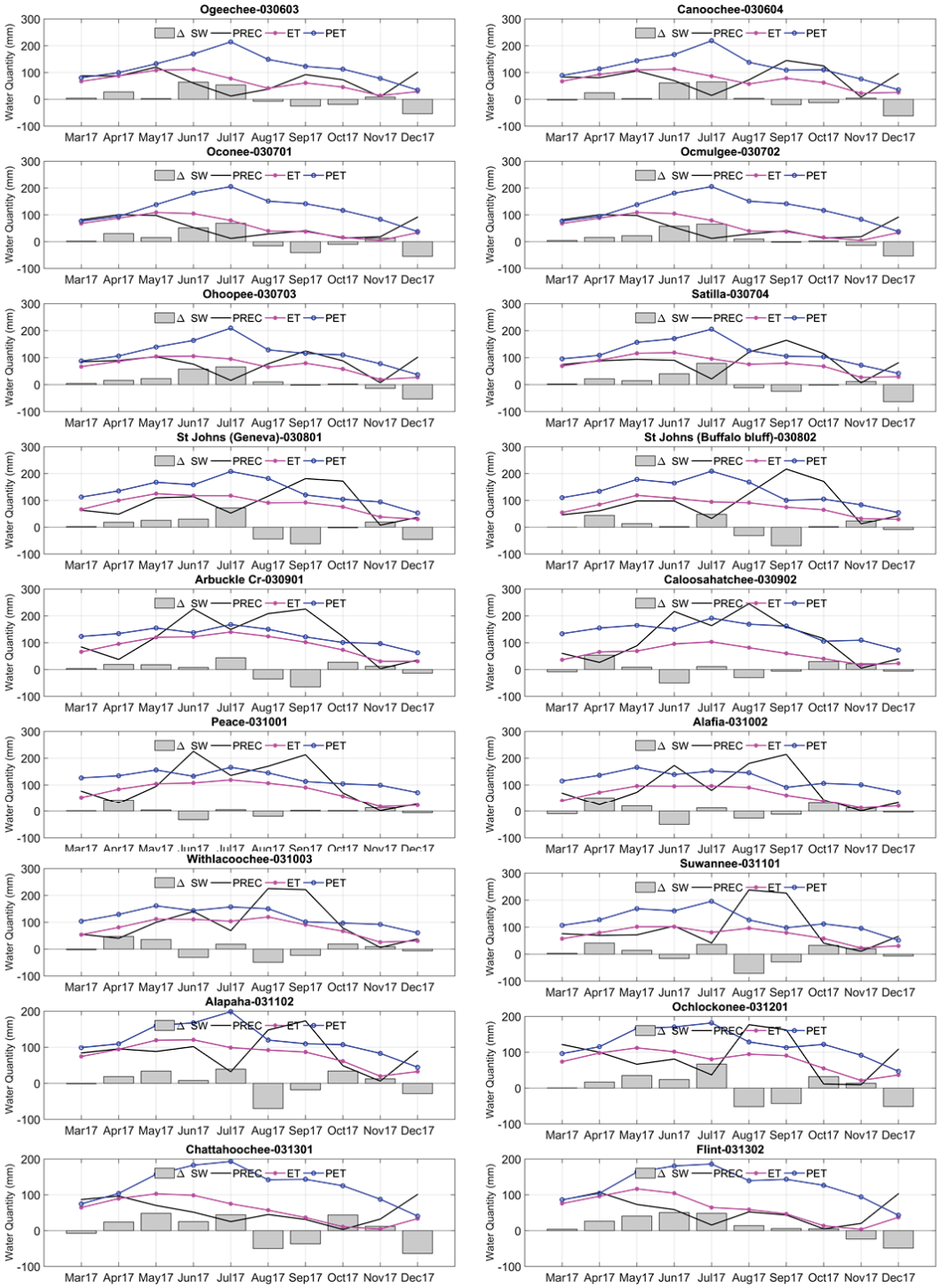

(Contd..) Watershed-wise time series of the forecasted hydrologic variables (precipitation, actual evapotranspiration, potential evapotranspiration and soil moisture simulated using SWAT- CFSv2 hybrid models.

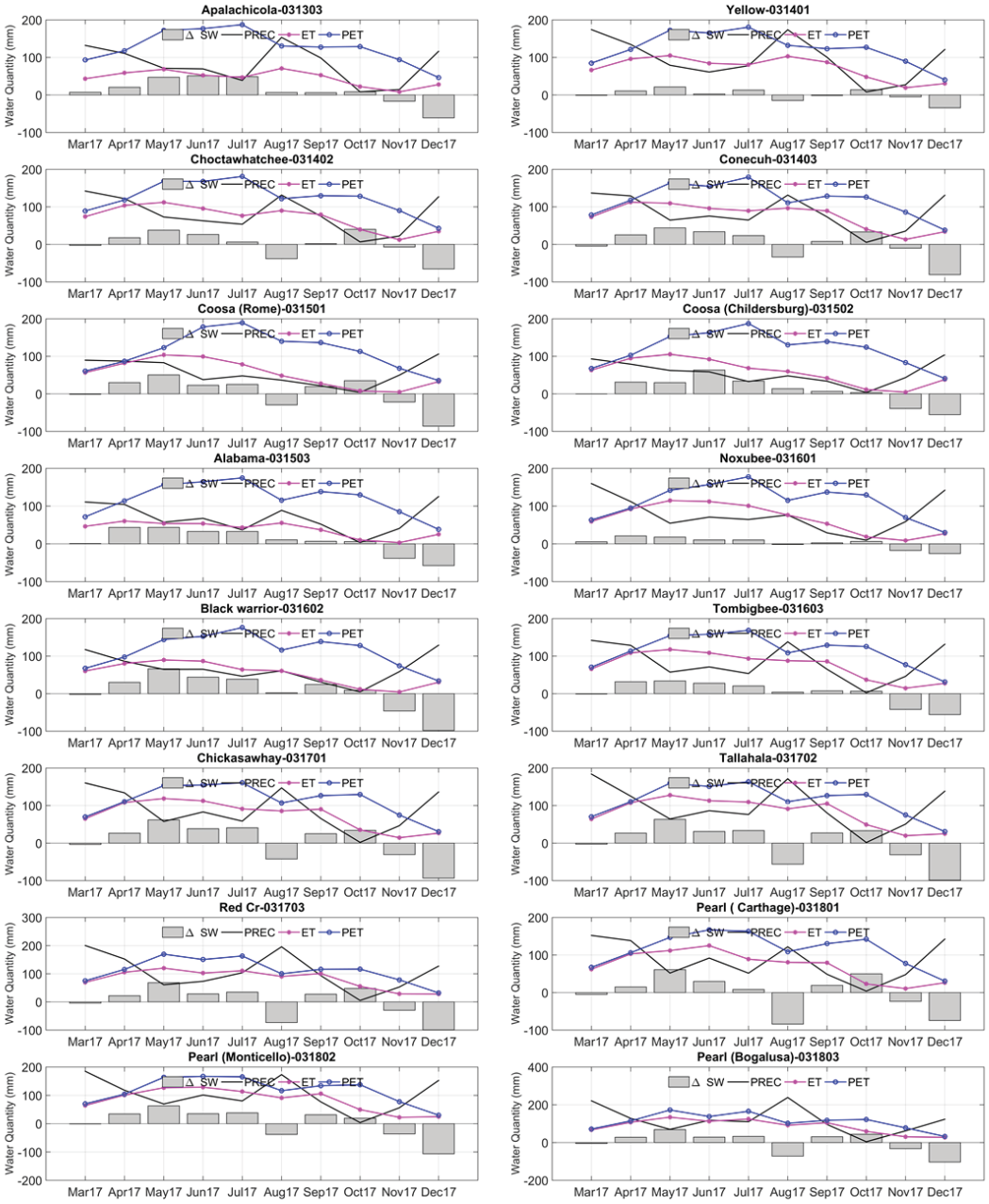

A9. List of hydroclimatological indices for used in the preliminary analysis

The variables which showed high correlation with hydrologic variables for across all watersheds are selected for further evaluation using HydroFit tool provided by HydroMetriks, LLC.

Index Name	**Index Abbreviation**
SOI	Southern Oscillation Index
ONI	Oceanic Niño Index
N12	Niño 1+2 Region
N3	Niño 3 Region
N34	Niño 3.4 Region
N4	Niño 4 Region
EPI	ENSO Precipitation Index
TNI	Trans-Niño Index
MEI	Multivariate ENSO Index
NAO	North Atlantic Oscillation
TNA	Tropical Northern Atlantic Index
TSA	Tropical Southern Atlantic Index
NTA	North Tropical Atlantic Index
AMO	Atlantic Multidecadal Oscillation
AMM	Atlantic Meridional Mode
CAR	Caribbean SST Index
PDO	Pacific Decadal Oscillation
NOI	Northern Oscillation Index
NP	North Pacific pattern
EPNP	East Pacific/North Pacific pattern
WP	Western Pacific pattern
PNA	Pacific/North American pattern
AO	Arctic Oscillation
AAO	Antarctic Oscillation
EAWR	Eastern Asia/Western Russia Index
WHWP	Western Hemisphere Warm Pool
QBO	Quasi-Biennial Oscillation
CIP	Central Indian Precipitation
SF	Solar Flux
MJO9	Madden-Julian Oscillation @ 20E
MJO10	Madden-Julian Oscillation @ 70E
MJO1	Madden-Julian Oscillation @ 80E
MJO2	Madden-Julian Oscillation @ 100E
MJO3	Madden-Julian Oscillation @ 120E

A10. Correlation of hydroclimatological indices with drought indices and hydrologic variables

	SW									
	MEI	Nino 1+2	Nina 4	Nina 3.4	PDO	BEST	ONI	TNI	WHWP	TSA
30101	0.37	0.27	0.22	0.29	0.41	0.36	0.36	-0.12	-0.15	-0.13
30102	0.39	0.21	0.23	0.28	0.45	0.38	0.36	-0.11	-0.17	-0.12
30103	0.31	0.31	0.12	0.24	0.43	0.31	0.30	-0.07	-0.27	-0.08
30201	0.31	0.19	0.15	0.20	0.39	0.31	0.31	-0.07	-0.23	-0.09
30202	0.30	0.21	0.11	0.16	0.39	0.29	0.29	-0.01	-0.21	-0.07
30301	0.32	0.09	0.17	0.18	0.35	0.31	0.31	-0.02	-0.16	-0.10
30302	0.30	0.07	0.13	0.13	0.35	0.28	0.27	0.01	-0.10	-0.04
30303	0.36	0.03	0.23	0.22	0.38	0.34	0.33	-0.06	-0.07	-0.11
30401	0.38	0.19	0.21	0.26	0.40	0.38	0.37	-0.09	-0.20	-0.17
30402	0.40	0.09	0.23	0.24	0.44	0.38	0.38	-0.07	-0.12	-0.10
30403	0.48	0.07	0.34	0.35	0.46	0.46	0.45	-0.12	-0.09	-0.14
30501	0.41	0.17	0.24	0.28	0.44	0.40	0.39	-0.10	-0.21	-0.20
30502	0.39	0.07	0.27	0.25	0.39	0.40	0.40	-0.10	-0.09	-0.10
30503	0.43	0.20	0.27	0.30	0.41	0.43	0.43	-0.12	-0.17	-0.19
30601	0.39	0.18	0.24	0.27	0.37	0.39	0.41	-0.07	-0.14	-0.17
30602	0.43	0.10	0.31	0.30	0.43	0.44	0.45	-0.14	-0.09	-0.12
30603	0.39	0.10	0.26	0.24	0.39	0.41	0.41	-0.09	-0.09	-0.11
30604	0.41	0.06	0.33	0.28	0.39	0.43	0.44	-0.16	-0.03	-0.10
30701	0.37	0.11	0.26	0.25	0.36	0.38	0.40	-0.09	-0.06	-0.12
30702	0.37	0.01	0.30	0.25	0.34	0.38	0.40	-0.10	0.01	-0.12
30703	0.39	0.06	0.31	0.26	0.38	0.41	0.42	-0.14	-0.03	-0.10
30704	0.39	-0.02	0.37	0.27	0.36	0.42	0.42	-0.20	0.03	-0.14
30801	0.34	-0.14	0.36	0.21	0.30	0.39	0.36	-0.25	0.01	-0.15
30802	0.34	-0.12	0.34	0.21	0.31	0.37	0.35	-0.22	0.02	-0.13
30901	0.36	-0.07	0.32	0.24	0.36	0.40	0.37	-0.19	-0.04	-0.16
30902	0.34	-0.06	0.27	0.23	0.33	0.36	0.32	-0.14	-0.07	-0.14
31001	0.35	-0.07	0.31	0.22	0.38	0.39	0.36	-0.20	-0.04	-0.13
31002	0.37	-0.06	0.33	0.21	0.36	0.40	0.39	-0.24	-0.02	-0.13
31003	0.34	-0.11	0.34	0.21	0.33	0.38	0.37	-0.23	0.02	-0.10
31101	0.39	-0.04	0.37	0.29	0.40	0.41	0.41	-0.20	0.04	-0.11
31102	0.39	0.02	0.37	0.29	0.37	0.42	0.44	-0.20	0.03	-0.13
31201	0.35	-0.05	0.35	0.28	0.27	0.37	0.39	-0.14	0.12	-0.11
31301	0.32	0.14	0.20	0.22	0.34	0.33	0.34	-0.05	-0.01	-0.10
31302	0.35	0.09	0.25	0.24	0.36	0.36	0.38	-0.07	0.02	-0.06
31303	0.45	0.01	0.38	0.36	0.34	0.45	0.46	-0.13	0.09	-0.15
31401	0.30	-0.01	0.24	0.20	0.26	0.33	0.32	-0.06	0.04	-0.15
31402	0.31	0.00	0.25	0.22	0.30	0.34	0.34	-0.08	0.05	-0.11
31403	0.29	0.03	0.23	0.20	0.28	0.34	0.33	-0.08	-0.03	-0.15
31501	0.36	0.15	0.22	0.27	0.33	0.37	0.37	-0.05	-0.14	-0.21
31502	0.27	0.09	0.14	0.17	0.29	0.29	0.28	0.03	-0.09	-0.14
31503	0.36	0.03	0.26	0.26	0.34	0.38	0.36	-0.04	0.00	-0.18
31601	0.35	0.16	0.18	0.20	0.34	0.36	0.35	0.00	-0.13	-0.19
31602	0.29	0.09	0.14	0.17	0.29	0.30	0.29	0.03	-0.13	-0.18
31603	0.23	0.03	0.14	0.11	0.22	0.26	0.25	0.00	-0.04	-0.16
31701	0.22	0.01	0.13	0.10	0.24	0.25	0.22	-0.01	-0.04	-0.17
31702	0.21	0.02	0.14	0.09	0.23	0.25	0.23	-0.06	-0.05	-0.18
31703	0.21	-0.06	0.20	0.13	0.19	0.27	0.24	-0.09	0.02	-0.17
31801	0.29	0.18	0.12	0.14	0.31	0.29	0.31	0.02	-0.11	-0.16
31802	0.24	0.10	0.12	0.12	0.26	0.27	0.27	-0.02	-0.13	-0.18
31803	0.17	0.11	0.10	0.08	0.21	0.22	0.21	-0.08	-0.08	-0.18

	PCP									
	MEI	Nino 1+2	Nina 4	Nina 3.4	PDO	BEST	ONI	TNI	WHWP	TSA
30101	0.20	0.06	0.15	0.18	0.23	0.20	0.21	-0.07	-0.05	-0.11
30102	0.18	0.06	0.12	0.15	0.22	0.18	0.18	-0.04	-0.09	-0.10
30103	0.15	0.10	0.07	0.13	0.21	0.15	0.15	-0.02	-0.11	-0.06
30201	0.15	0.07	0.08	0.14	0.19	0.16	0.15	-0.02	-0.10	-0.06
30202	0.18	0.08	0.11	0.17	0.19	0.18	0.18	-0.02	-0.08	-0.05
30301	0.21	0.07	0.12	0.17	0.22	0.21	0.20	-0.01	-0.07	-0.08
30302	0.21	0.07	0.13	0.20	0.20	0.21	0.20	-0.02	-0.05	-0.05
30303	0.21	0.05	0.15	0.20	0.16	0.21	0.21	-0.04	-0.03	-0.05
30401	0.23	0.07	0.16	0.20	0.21	0.24	0.23	-0.05	-0.09	-0.13
30402	0.25	0.06	0.18	0.24	0.21	0.26	0.26	-0.04	-0.05	-0.08
30403	0.29	0.07	0.21	0.26	0.22	0.29	0.30	-0.05	-0.04	-0.10
30501	0.24	0.08	0.18	0.21	0.21	0.26	0.25	-0.06	-0.09	-0.15
30502	0.26	0.04	0.21	0.25	0.20	0.27	0.29	-0.09	-0.06	-0.11
30503	0.24	0.08	0.19	0.22	0.19	0.25	0.26	-0.06	-0.08	-0.14
30601	0.20	0.06	0.16	0.18	0.17	0.21	0.22	-0.05	-0.08	-0.13
30602	0.24	0.02	0.21	0.23	0.18	0.25	0.27	-0.09	-0.04	-0.09
30603	0.23	0.02	0.21	0.22	0.18	0.25	0.27	-0.07	-0.03	-0.08
30604	0.26	0.01	0.24	0.24	0.20	0.27	0.29	-0.10	-0.03	-0.07
30701	0.21	0.02	0.21	0.21	0.15	0.23	0.25	-0.08	0.01	-0.07
30702	0.23	0.02	0.22	0.22	0.16	0.25	0.26	-0.09	0.04	-0.06
30703	0.26	0.02	0.23	0.24	0.20	0.27	0.29	-0.08	-0.01	-0.08
30704	0.30	0.02	0.27	0.26	0.26	0.32	0.32	-0.10	-0.01	-0.08
30801	0.25	0.01	0.24	0.23	0.24	0.28	0.24	-0.09	-0.10	-0.11
30802	0.28	0.00	0.24	0.23	0.26	0.29	0.26	-0.07	-0.05	-0.09
30901	0.24	0.00	0.22	0.21	0.25	0.26	0.23	-0.10	-0.11	-0.09
30902	0.25	0.01	0.19	0.23	0.26	0.26	0.24	-0.06	-0.10	-0.08
31001	0.24	-0.02	0.23	0.21	0.25	0.27	0.24	-0.11	-0.06	-0.09
31002	0.26	-0.03	0.25	0.23	0.25	0.28	0.25	-0.08	-0.01	-0.09
31003	0.26	-0.01	0.23	0.22	0.27	0.28	0.24	-0.06	-0.04	-0.09
31101	0.28	0.01	0.24	0.22	0.27	0.30	0.28	-0.07	-0.01	-0.09
31102	0.29	0.02	0.26	0.25	0.25	0.32	0.31	-0.09	0.00	-0.08
31201	0.24	-0.01	0.22	0.21	0.19	0.27	0.26	-0.06	0.02	-0.06
31301	0.18	0.02	0.17	0.16	0.14	0.21	0.21	-0.06	0.03	-0.08
31302	0.22	0.02	0.22	0.22	0.16	0.26	0.26	-0.09	0.06	-0.04
31303	0.23	0.02	0.20	0.22	0.16	0.26	0.27	-0.05	0.03	-0.05
31401	0.21	0.03	0.18	0.20	0.14	0.25	0.24	-0.04	0.04	-0.07
31402	0.20	0.01	0.18	0.19	0.16	0.23	0.23	-0.05	0.04	-0.04
31403	0.20	0.01	0.18	0.17	0.17	0.25	0.23	-0.07	0.02	-0.09
31501	0.14	0.02	0.12	0.12	0.11	0.17	0.15	-0.05	-0.06	-0.19
31502	0.17	0.03	0.15	0.15	0.13	0.19	0.19	-0.02	-0.03	-0.13
31503	0.18	0.02	0.16	0.15	0.13	0.22	0.21	-0.03	-0.01	-0.14
31601	0.17	0.04	0.10	0.10	0.14	0.17	0.16	0.02	-0.05	-0.19
31602	0.15	0.05	0.08	0.10	0.13	0.17	0.14	0.04	-0.07	-0.18
31603	0.20	0.03	0.17	0.16	0.13	0.23	0.20	-0.01	0.03	-0.15
31701	0.19	0.02	0.16	0.15	0.13	0.21	0.19	-0.02	0.03	-0.15
31702	0.20	0.04	0.17	0.17	0.13	0.22	0.20	-0.03	0.03	-0.13
31703	0.20	0.02	0.20	0.20	0.11	0.24	0.22	-0.05	0.06	-0.12
31801	0.18	0.04	0.11	0.12	0.16	0.18	0.18	0.03	-0.02	-0.14
31802	0.19	0.05	0.14	0.16	0.14	0.21	0.20	-0.02	-0.02	-0.12
31803	0.19	0.05	0.18	0.18	0.11	0.23	0.21	-0.05	0.03	-0.12

Figure. A0-8: Correlation of monthly SW (left) and Precipitation (right) percentiles with 10 hydroclimatic indices

	SURQ									
	MEI	Nino 1+2	Nina 4	Nina 3.4	PDO	BEST	ONI	TNI	WHWP	TSA
30101	0.16	0.19	0.08	0.15	0.24	0.18	0.17	-0.08	-0.13	-0.07
30102	0.17	0.17	0.08	0.14	0.26	0.19	0.17	-0.06	-0.16	-0.08
30103	0.18	0.18	0.08	0.17	0.27	0.19	0.17	-0.04	-0.16	-0.05
30201	0.17	0.16	0.08	0.18	0.24	0.19	0.17	-0.03	-0.17	-0.05
30202	0.27	0.14	0.14	0.22	0.29	0.27	0.24	-0.04	-0.17	-0.07
30301	0.21	0.17	0.08	0.18	0.25	0.21	0.20	0.01	-0.12	-0.07
30302	0.23	0.14	0.11	0.20	0.23	0.20	0.21	0.00	-0.09	0.01
30303	0.28	0.07	0.19	0.24	0.22	0.26	0.26	-0.04	-0.05	-0.03
30401	0.25	0.20	0.13	0.21	0.25	0.26	0.24	-0.06	-0.16	-0.13
30402	0.33	0.11	0.20	0.27	0.29	0.31	0.32	-0.04	-0.11	-0.08
30403	0.37	0.11	0.25	0.32	0.29	0.35	0.37	-0.07	-0.09	-0.11
30501	0.25	0.16	0.16	0.22	0.24	0.26	0.25	-0.08	-0.12	-0.12
30502	0.32	0.09	0.24	0.28	0.23	0.33	0.36	-0.11	-0.08	-0.09
30503	0.30	0.20	0.19	0.25	0.24	0.30	0.30	-0.09	-0.11	-0.12
30601	0.19	0.14	0.14	0.18	0.18	0.21	0.22	-0.06	-0.09	-0.01
30602	0.29	0.08	0.23	0.27	0.23	0.30	0.33	-0.10	-0.06	-0.07
30603	0.29	0.08	0.23	0.26	0.22	0.29	0.32	-0.07	-0.01	-0.03
30604	0.32	0.05	0.26	0.27	0.24	0.31	0.34	-0.10	-0.01	-0.05
30701	0.25	0.10	0.22	0.24	0.18	0.25	0.28	-0.08	0.03	0.02
30702	0.26	0.12	0.21	0.25	0.20	0.27	0.30	-0.07	0.04	0.02
30703	0.32	0.08	0.24	0.27	0.24	0.31	0.34	-0.08	0.01	-0.05
30704	0.34	0.11	0.24	0.26	0.21	0.34	0.35	-0.07	0.03	-0.05
30801	0.23	0.09	0.09	0.12	0.21	0.22	0.15	0.11	0.02	-0.02
30802	0.25	0.12	0.10	0.17	0.21	0.25	0.22	0.11	0.08	0.02
30901	0.32	0.01	0.20	0.21	0.35	0.31	0.27	-0.02	-0.08	-0.11
30902	0.37	0.00	0.22	0.25	0.37	0.35	0.32	0.00	-0.11	-0.13
31001	0.28	-0.03	0.24	0.22	0.28	0.29	0.26	-0.09	0.02	-0.11
31002	0.31	-0.03	0.23	0.21	0.31	0.30	0.26	-0.03	0.06	-0.08
31003	0.22	0.03	0.07	0.14	0.21	0.17	0.16	0.22	0.15	0.02
31101	0.29	0.07	0.19	0.21	0.26	0.30	0.28	-0.02	0.02	-0.06
31102	0.34	0.08	0.25	0.27	0.26	0.36	0.36	-0.08	0.03	-0.06
31201	0.23	0.02	0.14	0.15	0.12	0.24	0.25	-0.02	0.03	-0.01
31301	0.16	0.15	0.11	0.15	0.16	0.20	0.19	-0.06	0.00	0.02
31302	0.25	0.11	0.21	0.23	0.20	0.28	0.29	-0.08	0.09	0.02
31303	0.24	0.02	0.17	0.19	0.15	0.26	0.28	-0.03	0.05	-0.04
31401	0.23	0.07	0.14	0.18	0.13	0.25	0.27	0.00	0.10	-0.04
31402	0.15	0.06	0.10	0.13	0.11	0.17	0.20	-0.03	0.07	0.02
31403	0.20	0.07	0.15	0.17	0.16	0.24	0.25	-0.05	0.06	-0.03
31501	0.09	0.14	0.04	0.08	0.11	0.12	0.12	-0.05	-0.08	-0.09
31502	0.16	0.14	0.13	0.18	0.14	0.19	0.21	-0.03	-0.08	-0.08
31503	0.22	0.06	0.18	0.18	0.17	0.26	0.26	-0.02	-0.01	-0.14
31601	0.20	0.20	0.07	0.12	0.22	0.21	0.19	0.04	-0.11	-0.19
31602	0.17	0.18	0.07	0.11	0.19	0.19	0.18	0.05	-0.12	-0.17
31603	0.27	0.18	0.14	0.19	0.18	0.28	0.27	0.05	0.02	-0.18
31701	0.21	0.13	0.11	0.13	0.16	0.23	0.21	0.02	0.01	-0.17
31702	0.21	0.14	0.13	0.15	0.12	0.23	0.22	0.00	0.03	-0.16
31703	0.18	0.03	0.17	0.15	0.02	0.22	0.21	-0.05	0.12	-0.12
31801	0.21	0.16	0.07	0.11	0.24	0.19	0.20	0.06	-0.12	-0.14
31802	0.23	0.16	0.13	0.17	0.21	0.25	0.25	-0.01	-0.10	-0.12
31803	0.21	0.11	0.17	0.16	0.08	0.23	0.24	-0.02	0.06	-0.10

	PET									
	MEI	Nino 1+2	Nina 4	Nina 3.4	PDO	BEST	ONI	TNI	WHWP	TSA
30101	-0.22	-0.02	-0.13	-0.17	-0.29	-0.21	-0.20	0.05	0.09	0.16
30102	-0.24	-0.03	-0.15	-0.18	-0.30	-0.23	-0.21	0.06	0.10	0.15
30103	-0.22	-0.07	-0.13	-0.18	-0.33	-0.22	-0.21	0.08	0.13	0.10
30201	-0.22	-0.04	-0.14	-0.17	-0.30	-0.21	-0.20	0.06	0.10	0.10
30202	-0.24	-0.05	-0.16	-0.20	-0.29	-0.23	-0.23	0.07	0.10	0.11
30301	-0.26	-0.03	-0.17	-0.21	-0.30	-0.25	-0.24	0.05	0.10	0.14
30302	-0.24	-0.04	-0.15	-0.19	-0.29	-0.23	-0.22	0.05	0.09	0.10
30303	-0.22	-0.03	-0.15	-0.17	-0.23	-0.21	-0.21	0.06	0.07	0.10
30401	-0.26	-0.03	-0.15	-0.20	-0.29	-0.25	-0.23	0.03	0.12	0.18
30402	-0.26	-0.04	-0.17	-0.20	-0.30	-0.25	-0.24	0.05	0.09	0.11
30403	-0.29	-0.04	-0.19	-0.22	-0.29	-0.28	-0.27	0.05	0.09	0.12
30501	-0.26	-0.02	-0.15	-0.19	-0.29	-0.24	-0.23	0.03	0.14	0.19
30502	-0.29	-0.04	-0.21	-0.23	-0.27	-0.29	-0.28	0.08	0.07	0.14
30503	-0.26	-0.02	-0.16	-0.19	-0.26	-0.25	-0.24	0.03	0.13	0.20
30601	-0.24	-0.03	-0.14	-0.17	-0.26	-0.23	-0.23	0.03	0.13	0.19
30602	-0.29	-0.03	-0.21	-0.22	-0.25	-0.29	-0.29	0.09	0.07	0.16
30603	-0.29	-0.02	-0.22	-0.22	-0.26	-0.29	-0.29	0.08	0.08	0.17
30604	-0.32	-0.01	-0.26	-0.25	-0.26	-0.33	-0.32	0.12	0.05	0.17
30701	-0.26	-0.02	-0.19	-0.20	-0.26	-0.25	-0.26	0.08	0.09	0.14
30702	-0.28	-0.02	-0.23	-0.23	-0.25	-0.29	-0.29	0.10	0.04	0.14
30703	-0.32	-0.02	-0.26	-0.25	-0.27	-0.33	-0.33	0.12	0.06	0.18
30704	-0.31	-0.02	-0.28	-0.25	-0.27	-0.33	-0.33	0.15	0.06	0.18
30801	-0.30	0.01	-0.29	-0.25	-0.26	-0.33	-0.29	0.19	0.07	0.14
30802	-0.29	0.00	-0.27	-0.24	-0.24	-0.32	-0.29	0.19	0.08	0.13
30901	-0.28	0.03	-0.28	-0.23	-0.24	-0.31	-0.28	0.19	0.08	0.14
30902	-0.23	0.06	-0.24	-0.21	-0.21	-0.26	-0.24	0.15	0.06	0.12
31001	-0.28	0.03	-0.25	-0.21	-0.28	-0.31	-0.28	0.16	0.10	0.11
31002	-0.32	-0.01	-0.28	-0.25	-0.30	-0.34	-0.31	0.16	0.08	0.10
31003	-0.30	0.00	-0.26	-0.24	-0.27	-0.33	-0.30	0.17	0.08	0.11
31101	-0.30	-0.02	-0.27	-0.25	-0.27	-0.32	-0.32	0.16	0.06	0.14
31102	-0.32	-0.02	-0.29	-0.26	-0.29	-0.34	-0.34	0.15	0.05	0.16
31201	-0.27	0.01	-0.26	-0.25	-0.21	-0.29	-0.30	0.12	0.01	0.17
31301	-0.23	-0.03	-0.16	-0.18	-0.23	-0.24	-0.24	0.05	0.05	0.12
31302	-0.27	-0.02	-0.22	-0.21	-0.24	-0.28	-0.28	0.09	0.02	0.13
31303	-0.28	0.00	-0.25	-0.23	-0.24	-0.31	-0.30	0.12	0.02	0.15
31401	-0.26	-0.03	-0.19	-0.21	-0.22	-0.28	-0.26	0.06	0.03	0.16
31402	-0.27	-0.01	-0.22	-0.22	-0.24	-0.29	-0.28	0.10	0.04	0.15
31403	-0.24	-0.03	-0.18	-0.20	-0.23	-0.27	-0.25	0.07	0.06	0.14
31501	-0.24	-0.05	-0.11	-0.16	-0.25	-0.23	-0.22	-0.02	0.11	0.16
31502	-0.23	-0.04	-0.13	-0.16	-0.23	-0.22	-0.21	0.01	0.05	0.13
31503	-0.23	-0.03	-0.15	-0.17	-0.23	-0.24	-0.22	0.04	0.06	0.13
31601	-0.24	-0.05	-0.11	-0.14	-0.25	-0.23	-0.21	-0.03	0.05	0.16
31602	-0.23	-0.05	-0.10	-0.14	-0.24	-0.22	-0.20	-0.03	0.07	0.14
31603	-0.23	-0.04	-0.13	-0.16	-0.23	-0.24	-0.22	0.01	0.07	0.14
31701	-0.23	-0.03	-0.13	-0.16	-0.23	-0.24	-0.22	0.01	0.08	0.13
31702	-0.24	-0.02	-0.15	-0.17	-0.22	-0.25	-0.23	0.04	0.08	0.14
31703	-0.25	-0.02	-0.18	-0.19	-0.21	-0.28	-0.25	0.07	0.06	0.15
31801	-0.23	-0.01	-0.13	-0.13	-0.23	-0.23	-0.20	0.00	0.05	0.14
31802	-0.21	0.00	-0.13	-0.16	-0.17	-0.22	-0.20	0.01	0.04	0.14
31803	-0.22	-0.01	-0.18	-0.18	-0.19	-0.26	-0.23	0.09	0.09	0.15

Figure. A0-9: Correlation of monthly SURQ (left) and PET (right) percentiles with 10 hydroclimatic indices

SM- DJF										
	MEI	Nino 1+2	Nina 4	Nina 3.4	PDO	BEST	ONI	TNI	WHWP	TSA
30101	0.48	0.32	0.49	0.43	0.47	0.55	0.45	-0.37	-0.17	-0.05
30102	0.47	0.31	0.42	0.38	0.45	0.53	0.41	-0.30	-0.23	-0.05
30103	0.41	0.27	0.34	0.32	0.40	0.48	0.34	-0.24	-0.28	-0.11
30201	0.38	0.25	0.33	0.30	0.39	0.46	0.32	-0.25	-0.28	-0.04
30202	0.39	0.28	0.31	0.30	0.41	0.47	0.32	-0.20	-0.30	-0.01
30301	0.40	0.29	0.32	0.32	0.39	0.47	0.34	-0.19	-0.25	-0.04
30302	0.38	0.25	0.32	0.29	0.44	0.47	0.31	-0.22	-0.28	0.04
30303	0.41	0.28	0.31	0.33	0.36	0.47	0.34	-0.17	-0.29	-0.12
30401	0.48	0.33	0.42	0.40	0.42	0.54	0.42	-0.28	-0.25	-0.08
30402	0.46	0.33	0.36	0.38	0.45	0.52	0.40	-0.21	-0.28	-0.05
30403	0.53	0.38	0.42	0.45	0.40	0.58	0.47	-0.24	-0.23	-0.15
30501	0.47	0.31	0.41	0.39	0.41	0.53	0.41	-0.29	-0.28	-0.14
30502	0.46	0.32	0.41	0.39	0.43	0.54	0.41	-0.28	-0.28	-0.08
30503	0.52	0.34	0.49	0.45	0.40	0.57	0.47	-0.35	-0.20	-0.14
30601	0.48	0.31	0.47	0.43	0.37	0.54	0.45	-0.33	-0.19	-0.17
30602	0.49	0.33	0.46	0.44	0.43	0.56	0.46	-0.32	-0.26	-0.11
30603	0.51	0.34	0.47	0.45	0.44	0.57	0.47	-0.32	-0.23	-0.13
30604	0.50	0.35	0.48	0.45	0.46	0.56	0.46	-0.33	-0.20	-0.04
30701	0.52	0.34	0.51	0.49	0.37	0.56	0.49	-0.33	-0.13	-0.18
30702	0.54	0.38	0.51	0.51	0.40	0.59	0.51	-0.31	-0.14	-0.13
30703	0.52	0.38	0.49	0.47	0.46	0.58	0.48	-0.32	-0.17	-0.03
30704	0.54	0.39	0.51	0.48	0.54	0.58	0.50	-0.32	-0.11	-0.04
30801	0.58	0.43	0.49	0.50	0.46	0.59	0.52	-0.27	-0.09	-0.02
30802	0.58	0.46	0.47	0.50	0.53	0.58	0.52	-0.23	-0.06	-0.01
30901	0.53	0.40	0.43	0.44	0.39	0.54	0.47	-0.21	-0.17	-0.09
30902	0.46	0.35	0.30	0.36	0.30	0.46	0.38	-0.09	-0.22	-0.14
31001	0.57	0.46	0.45	0.48	0.43	0.57	0.50	-0.21	-0.12	-0.02
31002	0.53	0.39	0.46	0.46	0.39	0.55	0.47	-0.27	-0.13	-0.04
31003	0.52	0.42	0.44	0.46	0.46	0.52	0.47	-0.20	-0.01	0.03
31101	0.59	0.49	0.52	0.54	0.54	0.62	0.55	-0.27	-0.08	0.04
31102	0.54	0.41	0.53	0.50	0.51	0.59	0.51	-0.34	-0.10	-0.02
31201	0.58	0.49	0.52	0.55	0.41	0.59	0.55	-0.24	0.02	0.01
31301	0.49	0.39	0.45	0.46	0.43	0.53	0.46	-0.24	-0.02	0.01
31302	0.57	0.45	0.51	0.53	0.46	0.61	0.53	-0.24	-0.07	-0.03
31303	0.63	0.49	0.54	0.61	0.37	0.66	0.62	-0.24	-0.08	-0.11
31401	0.60	0.46	0.58	0.60	0.41	0.65	0.60	-0.30	0.04	0.06
31402	0.59	0.46	0.55	0.58	0.41	0.64	0.58	-0.25	-0.01	0.00
31403	0.53	0.36	0.54	0.53	0.46	0.59	0.53	-0.35	-0.06	-0.01
31501	0.36	0.25	0.34	0.33	0.29	0.42	0.34	-0.23	-0.16	-0.12
31502	0.40	0.31	0.33	0.36	0.40	0.44	0.37	-0.17	-0.09	-0.07
31503	0.43	0.36	0.28	0.37	0.49	0.48	0.40	-0.08	-0.11	-0.10
31601	0.42	0.31	0.35	0.35	0.38	0.48	0.37	-0.22	-0.11	-0.11
31602	0.32	0.26	0.21	0.26	0.34	0.37	0.28	-0.10	-0.19	-0.10
31603	0.44	0.31	0.41	0.42	0.42	0.49	0.42	-0.24	-0.04	-0.06
31701	0.37	0.26	0.31	0.33	0.34	0.41	0.33	-0.15	-0.06	-0.15
31702	0.36	0.25	0.33	0.34	0.37	0.39	0.34	-0.20	-0.06	-0.09
31703	0.46	0.26	0.45	0.44	0.40	0.51	0.44	-0.30	-0.07	-0.04
31801	0.35	0.26	0.27	0.31	0.33	0.37	0.32	-0.13	-0.02	-0.15
31802	0.42	0.35	0.32	0.38	0.37	0.43	0.39	-0.11	0.02	-0.05
31803	0.33	0.16	0.37	0.34	0.21	0.37	0.34	-0.29	-0.06	-0.14

SM- MAM										
	MEI	Nino 1+2	Nina 4	Nina 3.4	PDO	BEST	ONI	TNI	WHWP	TSA
30101	0.47	0.25	0.34	0.42	0.30	0.45	0.43	-0.12	0.32	-0.17
30102	0.53	0.27	0.37	0.46	0.43	0.54	0.47	-0.15	0.38	-0.05
30103	0.46	0.26	0.24	0.36	0.35	0.44	0.37	-0.03	0.34	-0.01
30201	0.42	0.26	0.20	0.33	0.28	0.41	0.34	0.00	0.32	-0.05
30202	0.43	0.32	0.16	0.35	0.29	0.43	0.35	0.07	0.36	-0.06
30301	0.37	0.35	0.09	0.29	0.13	0.34	0.29	0.17	0.35	-0.11
30302	0.34	0.32	-0.01	0.23	0.11	0.31	0.24	0.21	0.33	-0.03
30303	0.49	0.36	0.21	0.41	0.31	0.48	0.42	0.07	0.42	-0.03
30401	0.48	0.33	0.24	0.41	0.23	0.47	0.41	0.00	0.37	-0.19
30402	0.51	0.32	0.22	0.42	0.38	0.51	0.43	0.00	0.40	-0.02
30403	0.61	0.42	0.34	0.53	0.41	0.59	0.54	-0.03	0.48	-0.06
30501	0.51	0.35	0.29	0.45	0.32	0.52	0.45	-0.04	0.37	-0.22
30502	0.38	0.31	0.14	0.32	0.19	0.37	0.32	0.07	0.34	-0.08
30503	0.50	0.37	0.30	0.45	0.24	0.50	0.45	-0.02	0.39	-0.19
30601	0.36	0.33	0.15	0.31	0.14	0.34	0.32	0.09	0.35	-0.09
30602	0.53	0.34	0.34	0.49	0.35	0.52	0.50	-0.08	0.44	-0.04
30603	0.38	0.30	0.18	0.34	0.19	0.37	0.34	0.04	0.36	0.01
30604	0.48	0.30	0.36	0.47	0.29	0.48	0.47	-0.12	0.41	-0.02
30701	0.35	0.25	0.22	0.31	0.15	0.34	0.31	-0.01	0.33	0.09
30702	0.40	0.26	0.30	0.37	0.19	0.40	0.38	-0.08	0.36	0.06
30703	0.45	0.29	0.36	0.44	0.24	0.45	0.45	-0.11	0.39	-0.01
30704	0.47	0.24	0.43	0.47	0.30	0.50	0.48	-0.23	0.36	-0.06
30801	0.46	0.10	0.53	0.48	0.41	0.54	0.49	-0.42	0.23	-0.10
30802	0.51	0.13	0.52	0.52	0.39	0.57	0.52	-0.39	0.28	-0.10
30901	0.47	0.13	0.48	0.46	0.42	0.54	0.47	-0.34	0.24	-0.10
30902	0.46	0.16	0.40	0.43	0.43	0.52	0.43	-0.26	0.23	-0.12
31001	0.49	0.11	0.50	0.48	0.45	0.56	0.49	-0.39	0.24	-0.10
31002	0.56	0.18	0.58	0.56	0.49	0.61	0.57	-0.43	0.32	-0.05
31003	0.52	0.16	0.59	0.56	0.48	0.58	0.57	-0.44	0.32	0.01
31101	0.51	0.19	0.49	0.52	0.45	0.54	0.52	-0.31	0.35	0.01
31102	0.45	0.22	0.46	0.47	0.30	0.48	0.47	-0.26	0.34	-0.06
31201	0.37	0.19	0.40	0.40	0.20	0.41	0.41	-0.21	0.27	-0.16
31301	0.42	0.24	0.30	0.38	0.25	0.41	0.38	-0.09	0.32	0.00
31302	0.44	0.28	0.36	0.42	0.27	0.44	0.42	-0.12	0.36	0.06
31303	0.63	0.37	0.53	0.63	0.43	0.64	0.63	-0.23	0.48	-0.05
31401	0.41	0.24	0.38	0.42	0.20	0.45	0.42	-0.16	0.29	-0.13
31402	0.42	0.20	0.39	0.42	0.24	0.46	0.42	-0.21	0.27	-0.07
31403	0.31	0.21	0.28	0.31	0.12	0.36	0.32	-0.10	0.21	-0.15
31501	0.37	0.28	0.20	0.34	0.10	0.35	0.34	0.01	0.34	-0.11
31502	0.24	0.25	0.06	0.21	0.00	0.22	0.21	0.13	0.28	-0.01
31503	0.45	0.36	0.30	0.43	0.29	0.47	0.44	-0.04	0.40	-0.17
31601	0.36	0.32	0.15	0.32	0.01	0.35	0.32	0.09	0.34	-0.14
31602	0.31	0.28	0.08	0.27	0.04	0.29	0.27	0.12	0.32	-0.06
31603	0.25	0.22	0.16	0.23	-0.01	0.27	0.23	0.02	0.21	-0.12
31701	0.34	0.27	0.20	0.30	0.01	0.36	0.30	0.01	0.29	-0.13
31702	0.40	0.31	0.29	0.38	0.03	0.43	0.38	-0.05	0.32	-0.18
31703	0.29	0.20	0.30	0.31	0.02	0.35	0.30	-0.11	0.20	-0.21
31801	0.33	0.27	0.15	0.29	-0.01	0.33	0.29	0.05	0.28	-0.14
31802	0.34	0.29	0.24	0.35	-0.06	0.38	0.35	-0.02	0.25	-0.35
31803	0.36	0.27	0.37	0.39	-0.03	0.41	0.38	-0.14	0.27	-0.27

Figure. A0-10: Correlation of monthly DJF(left) and MAM (right) percentiles with of SW with 10 hydroclimatic indices

	SM- JJA									
	MEI	Nino 1+2	Nina 4	Nina 3.4	PDO	BEST	ONI	TNI	WHWP	TSA
30101	0.33	0.07	0.22	0.34	0.46	0.27	0.41	-0.08	-0.08	-0.37
30102	0.31	0.03	0.22	0.31	0.54	0.27	0.39	-0.11	-0.11	-0.34
30103	0.24	-0.05	0.15	0.21	0.52	0.19	0.31	-0.15	-0.18	-0.29
30201	0.26	-0.03	0.18	0.23	0.51	0.21	0.33	-0.15	-0.15	-0.28
30202	0.30	0.01	0.19	0.25	0.51	0.22	0.34	-0.11	-0.09	-0.25
30301	0.31	0.02	0.21	0.28	0.53	0.27	0.37	-0.12	-0.11	-0.30
30302	0.32	0.04	0.18	0.26	0.56	0.25	0.34	-0.09	-0.06	-0.30
30303	0.32	0.05	0.20	0.27	0.54	0.23	0.36	-0.09	-0.03	-0.26
30401	0.33	0.03	0.23	0.31	0.51	0.28	0.40	-0.12	-0.11	-0.34
30402	0.32	0.03	0.20	0.27	0.57	0.26	0.36	-0.11	-0.08	-0.30
30403	0.33	0.00	0.26	0.31	0.56	0.30	0.41	-0.17	-0.11	-0.33
30501	0.35	0.03	0.24	0.33	0.55	0.30	0.42	-0.13	-0.11	-0.37
30502	0.33	-0.01	0.31	0.35	0.54	0.34	0.42	-0.22	-0.03	-0.36
30503	0.35	0.03	0.28	0.36	0.51	0.33	0.44	-0.15	-0.07	-0.39
30601	0.35	0.04	0.28	0.37	0.48	0.34	0.44	-0.14	-0.04	-0.39
30602	0.35	0.01	0.33	0.39	0.50	0.37	0.45	-0.22	-0.02	-0.36
30603	0.35	0.03	0.32	0.39	0.52	0.37	0.45	-0.19	-0.02	-0.37
30604	0.35	0.02	0.36	0.40	0.49	0.39	0.47	-0.23	-0.02	-0.36
30701	0.35	0.05	0.31	0.38	0.47	0.35	0.44	-0.15	0.03	-0.37
30702	0.31	0.04	0.31	0.37	0.41	0.32	0.41	-0.16	0.08	-0.33
30703	0.35	0.03	0.34	0.39	0.51	0.37	0.46	-0.20	0.01	-0.37
30704	0.35	0.03	0.42	0.42	0.46	0.38	0.49	-0.26	0.04	-0.38
30801	0.23	-0.04	0.30	0.28	0.38	0.33	0.35	-0.26	-0.13	-0.30
30802	0.26	-0.03	0.40	0.35	0.38	0.35	0.43	-0.32	-0.04	-0.32
30901	0.25	-0.01	0.27	0.28	0.44	0.30	0.37	-0.19	-0.11	-0.31
30902	0.14	-0.06	0.22	0.20	0.36	0.24	0.28	-0.21	-0.15	-0.17
31001	0.23	-0.02	0.30	0.29	0.48	0.32	0.38	-0.23	-0.09	-0.27
31002	0.27	-0.01	0.39	0.36	0.49	0.41	0.44	-0.29	-0.08	-0.25
31003	0.25	-0.03	0.40	0.34	0.44	0.38	0.43	-0.33	-0.06	-0.29
31101	0.28	0.01	0.36	0.36	0.41	0.33	0.43	-0.25	0.03	-0.31
31102	0.31	0.03	0.37	0.39	0.43	0.35	0.45	-0.23	0.04	-0.35
31201	0.27	0.06	0.29	0.33	0.29	0.28	0.38	-0.14	0.08	-0.27
31301	0.28	0.05	0.26	0.34	0.35	0.28	0.37	-0.11	0.11	-0.27
31302	0.26	0.03	0.29	0.33	0.37	0.28	0.37	-0.16	0.13	-0.25
31303	0.23	0.02	0.24	0.29	0.29	0.29	0.34	-0.14	0.02	-0.31
31401	0.19	0.08	0.11	0.18	0.22	0.21	0.24	-0.02	0.05	-0.31
31402	0.20	0.05	0.14	0.22	0.30	0.23	0.27	-0.06	0.04	-0.28
31403	0.23	0.06	0.15	0.25	0.30	0.27	0.30	-0.06	0.00	-0.34
31501	0.34	0.08	0.24	0.37	0.42	0.34	0.43	-0.08	-0.06	-0.41
31502	0.30	0.12	0.18	0.31	0.38	0.27	0.37	-0.01	0.06	-0.32
31503	0.31	0.11	0.22	0.34	0.39	0.31	0.39	-0.04	0.04	-0.38
31601	0.49	0.23	0.31	0.45	0.58	0.38	0.52	0.02	0.07	-0.44
31602	0.39	0.18	0.18	0.35	0.50	0.31	0.43	0.05	0.00	-0.43
31603	0.36	0.17	0.20	0.33	0.40	0.30	0.38	0.03	0.12	-0.39
31701	0.37	0.15	0.26	0.36	0.51	0.30	0.41	-0.03	0.15	-0.38
31702	0.35	0.11	0.31	0.39	0.47	0.33	0.43	-0.10	0.13	-0.39
31703	0.27	0.09	0.29	0.33	0.26	0.33	0.35	-0.12	0.14	-0.34
31801	0.47	0.20	0.31	0.44	0.59	0.36	0.51	0.00	0.07	-0.39
31802	0.44	0.18	0.34	0.46	0.51	0.39	0.52	-0.05	0.02	-0.37
31803	0.34	0.11	0.37	0.42	0.36	0.37	0.45	-0.15	0.13	-0.36

	SM- SON									
	MEI	Nino 1+2	Nina 4	Nina 3.4	PDO	BEST	ONI	TNI	WHWP	TSA
30101	0.28	0.06	0.27	0.28	0.53	0.34	0.33	-0.21	-0.33	-0.19
30102	0.29	0.11	0.21	0.24	0.55	0.33	0.30	-0.11	-0.45	-0.21
30103	0.26	0.08	0.19	0.22	0.50	0.30	0.28	-0.13	-0.48	-0.20
30201	0.26	0.09	0.17	0.20	0.50	0.28	0.27	-0.09	-0.49	-0.19
30202	0.25	0.10	0.14	0.17	0.51	0.26	0.23	-0.05	-0.48	-0.16
30301	0.25	0.12	0.16	0.21	0.53	0.28	0.27	-0.06	-0.49	-0.13
30302	0.30	0.20	0.19	0.23	0.52	0.30	0.27	0.00	-0.37	-0.11
30303	0.26	0.10	0.19	0.19	0.47	0.29	0.24	-0.10	-0.46	-0.18
30401	0.31	0.11	0.22	0.23	0.59	0.34	0.30	-0.13	-0.54	-0.29
30402	0.38	0.20	0.26	0.30	0.61	0.38	0.36	-0.08	-0.49	-0.20
30403	0.42	0.22	0.31	0.36	0.64	0.44	0.42	-0.11	-0.50	-0.27
30501	0.35	0.13	0.26	0.26	0.62	0.37	0.33	-0.13	-0.53	-0.32
30502	0.49	0.30	0.37	0.42	0.68	0.50	0.47	-0.07	-0.44	-0.23
30503	0.40	0.16	0.31	0.32	0.61	0.41	0.39	-0.14	-0.50	-0.35
30601	0.44	0.22	0.35	0.37	0.61	0.44	0.43	-0.10	-0.44	-0.38
30602	0.45	0.24	0.35	0.39	0.67	0.46	0.44	-0.11	-0.46	-0.26
30603	0.48	0.30	0.36	0.39	0.68	0.47	0.45	-0.05	-0.40	-0.24
30604	0.45	0.26	0.39	0.41	0.62	0.47	0.46	-0.13	-0.39	-0.23
30701	0.46	0.29	0.38	0.39	0.62	0.44	0.45	-0.07	-0.31	-0.32
30702	0.42	0.28	0.35	0.37	0.59	0.40	0.42	-0.04	-0.29	-0.28
30703	0.44	0.27	0.36	0.38	0.60	0.44	0.43	-0.09	-0.37	-0.21
30704	0.44	0.23	0.42	0.40	0.59	0.48	0.45	-0.18	-0.37	-0.26
30801	0.33	0.08	0.28	0.25	0.50	0.38	0.30	-0.19	-0.42	-0.33
30802	0.30	0.09	0.23	0.20	0.52	0.34	0.25	-0.14	-0.45	-0.28
30901	0.32	0.11	0.24	0.24	0.53	0.35	0.30	-0.13	-0.48	-0.38
30902	0.27	0.11	0.15	0.16	0.51	0.28	0.24	-0.05	-0.53	-0.40
31001	0.31	0.09	0.23	0.21	0.55	0.35	0.28	-0.13	-0.51	-0.32
31002	0.32	0.09	0.29	0.25	0.53	0.37	0.30	-0.18	-0.43	-0.30
31003	0.32	0.09	0.31	0.26	0.51	0.38	0.31	-0.21	-0.37	-0.33
31101	0.39	0.16	0.35	0.32	0.58	0.41	0.37	-0.17	-0.37	-0.33
31102	0.44	0.22	0.42	0.40	0.55	0.47	0.45	-0.18	-0.33	-0.30
31201	0.40	0.27	0.37	0.35	0.45	0.41	0.38	-0.08	-0.16	-0.29
31301	0.32	0.23	0.27	0.28	0.49	0.30	0.32	0.00	-0.25	-0.28
31302	0.36	0.27	0.28	0.31	0.56	0.33	0.35	0.01	-0.26	-0.21
31303	0.39	0.21	0.35	0.34	0.52	0.42	0.38	-0.15	-0.33	-0.32
31401	0.30	0.19	0.25	0.25	0.46	0.32	0.29	-0.07	-0.32	-0.24
31402	0.32	0.21	0.26	0.27	0.46	0.33	0.31	-0.04	-0.29	-0.18
31403	0.33	0.17	0.30	0.27	0.49	0.35	0.31	-0.11	-0.40	-0.25
31501	0.37	0.20	0.30	0.31	0.48	0.39	0.35	-0.07	-0.42	-0.42
31502	0.32	0.22	0.22	0.24	0.52	0.31	0.28	0.02	-0.45	-0.25
31503	0.32	0.17	0.25	0.24	0.52	0.33	0.29	-0.07	-0.48	-0.24
31601	0.37	0.21	0.28	0.28	0.53	0.37	0.32	-0.05	-0.50	-0.25
31602	0.29	0.14	0.20	0.21	0.48	0.30	0.26	-0.05	-0.56	-0.26
31603	0.18	0.09	0.15	0.13	0.34	0.20	0.16	-0.05	-0.42	-0.15
31701	0.08	-0.02	0.11	0.04	0.26	0.13	0.06	-0.13	-0.46	-0.09
31702	0.05	-0.08	0.12	0.03	0.23	0.11	0.05	-0.20	-0.45	-0.09
31703	0.08	-0.02	0.15	0.09	0.26	0.15	0.10	-0.19	-0.38	-0.13
31801	0.35	0.22	0.30	0.28	0.47	0.37	0.32	-0.07	-0.45	-0.17
31802	0.12	0.01	0.13	0.08	0.34	0.16	0.11	-0.13	-0.50	-0.09
31803	-0.02	-0.14	0.09	-0.01	0.21	0.04	0.00	-0.24	-0.41	-0.08

Figure. A0-11: Correlation of monthly JJA (left) and SON (right) percentiles with of SW with 10 hydroclimatic indices

	PCP- DJF									
	MEI	Nino 1+2	Nina 4	Nina 3.4	PDO	BEST	ONI	TNI	WHWP	TSA
30101	0.42	0.39	0.29	0.37	0.27	0.46	0.37	-0.06	0.07	-0.15
30102	0.48	0.48	0.32	0.43	0.19	0.51	0.42	0.00	0.14	-0.09
30103	0.51	0.56	0.36	0.47	0.16	0.52	0.45	0.03	0.26	0.05
30201	0.54	0.58	0.35	0.48	0.12	0.56	0.47	0.05	0.19	-0.01
30202	0.60	0.63	0.39	0.54	0.11	0.61	0.54	0.03	0.17	-0.04
30301	0.61	0.61	0.41	0.54	0.22	0.64	0.54	0.01	0.14	0.03
30302	0.65	0.68	0.40	0.58	0.13	0.64	0.60	0.07	0.17	0.00
30303	0.67	0.70	0.45	0.64	0.06	0.65	0.65	0.03	0.23	0.05
30401	0.53	0.51	0.37	0.48	0.20	0.57	0.48	-0.03	0.11	-0.03
30402	0.72	0.77	0.46	0.66	0.20	0.69	0.67	0.07	0.26	0.06
30403	0.65	0.73	0.45	0.64	0.11	0.64	0.64	0.07	0.34	0.05
30501	0.45	0.43	0.33	0.42	0.19	0.49	0.41	-0.04	0.10	-0.02
30502	0.52	0.56	0.42	0.54	0.05	0.50	0.53	-0.03	0.30	-0.05
30503	0.43	0.45	0.31	0.42	0.11	0.45	0.41	0.02	0.21	-0.03
30601	0.34	0.36	0.27	0.36	-0.03	0.34	0.35	0.02	0.25	-0.10
30602	0.39	0.40	0.36	0.42	0.08	0.37	0.41	-0.10	0.26	-0.06
30603	0.34	0.37	0.31	0.38	0.02	0.34	0.37	-0.05	0.23	-0.08
30604	0.42	0.38	0.43	0.45	0.12	0.40	0.44	-0.19	0.27	0.01
30701	0.43	0.45	0.37	0.47	-0.06	0.45	0.45	-0.03	0.26	-0.13
30702	0.47	0.48	0.40	0.49	-0.05	0.49	0.48	-0.04	0.24	-0.18
30703	0.40	0.38	0.41	0.43	0.09	0.39	0.43	-0.15	0.26	-0.01
30704	0.53	0.49	0.52	0.55	0.22	0.53	0.54	-0.21	0.35	0.11
30801	0.44	0.43	0.32	0.40	0.17	0.41	0.41	-0.04	0.06	-0.04
30802	0.45	0.48	0.33	0.43	0.23	0.40	0.43	0.00	0.21	0.08
30901	0.47	0.46	0.31	0.41	0.15	0.44	0.42	0.00	0.00	-0.10
30902	0.58	0.54	0.36	0.50	0.19	0.55	0.51	0.02	-0.01	-0.07
31001	0.43	0.43	0.29	0.37	0.15	0.40	0.38	-0.01	0.06	-0.05
31002	0.47	0.47	0.33	0.41	0.15	0.43	0.42	-0.01	0.16	0.02
31003	0.50	0.56	0.35	0.46	0.21	0.45	0.46	0.06	0.26	0.11
31101	0.42	0.36	0.44	0.42	0.19	0.46	0.42	-0.23	0.21	0.00
31102	0.48	0.42	0.49	0.49	0.17	0.51	0.49	-0.22	0.26	0.04
31201	0.39	0.29	0.44	0.40	0.14	0.42	0.39	-0.24	0.13	-0.03
31301	0.36	0.35	0.31	0.40	-0.09	0.39	0.38	-0.05	0.21	-0.24
31302	0.49	0.50	0.42	0.52	-0.05	0.52	0.51	-0.05	0.24	-0.23
31303	0.46	0.44	0.43	0.49	0.04	0.47	0.48	-0.10	0.22	-0.07
31401	0.53	0.50	0.52	0.59	0.03	0.54	0.57	-0.15	0.39	0.04
31402	0.48	0.47	0.46	0.54	-0.01	0.51	0.53	-0.11	0.31	0.00
31403	0.40	0.40	0.40	0.48	-0.09	0.44	0.46	-0.11	0.31	-0.10
31501	0.24	0.24	0.15	0.25	-0.04	0.25	0.25	0.03	0.18	-0.20
31502	0.18	0.13	0.13	0.21	-0.11	0.21	0.20	-0.03	0.07	-0.36
31503	0.11	0.07	0.11	0.17	-0.16	0.18	0.16	-0.06	0.04	-0.39
31601	0.06	0.10	-0.02	0.08	-0.09	0.07	0.08	0.09	0.09	-0.28
31602	0.13	0.17	0.00	0.14	-0.03	0.13	0.14	0.12	0.06	-0.32
31603	0.18	0.18	0.14	0.24	-0.06	0.21	0.23	-0.01	0.18	-0.26
31701	0.12	0.13	0.11	0.20	-0.08	0.15	0.19	-0.03	0.16	-0.29
31702	0.13	0.12	0.16	0.21	-0.08	0.15	0.20	-0.09	0.16	-0.33
31703	0.35	0.32	0.36	0.43	-0.04	0.36	0.42	-0.14	0.28	-0.10
31801	0.02	0.03	-0.02	0.06	-0.09	0.02	0.05	0.05	0.11	-0.27
31802	0.00	0.00	0.04	0.08	-0.07	0.00	0.07	-0.03	0.17	-0.32
31803	0.21	0.19	0.24	0.30	-0.06	0.24	0.29	-0.13	0.19	-0.27

	PCP- MAM									
	MEI	Nino 1+2	Nina 4	Nina 3.4	PDO	BEST	ONI	TNI	WHWP	TSA
30101	0.41	0.52	0.17	0.35	0.17	0.36	0.34	0.22	0.42	-0.12
30102	0.37	0.44	0.12	0.29	0.16	0.32	0.29	0.21	0.39	-0.02
30103	0.26	0.26	0.04	0.17	0.11	0.23	0.17	0.14	0.26	0.06
30201	0.27	0.30	0.04	0.18	0.08	0.24	0.18	0.17	0.28	0.02
30202	0.30	0.34	0.02	0.20	0.06	0.27	0.20	0.20	0.34	0.00
30301	0.38	0.47	0.05	0.29	0.11	0.33	0.28	0.28	0.44	-0.06
30302	0.28	0.28	0.02	0.18	0.02	0.26	0.19	0.14	0.29	-0.08
30303	0.28	0.22	0.07	0.20	0.06	0.27	0.21	0.07	0.25	-0.05
30401	0.42	0.50	0.15	0.37	0.11	0.37	0.36	0.22	0.45	-0.13
30402	0.28	0.30	0.03	0.20	0.03	0.25	0.21	0.16	0.30	-0.12
30403	0.33	0.33	0.11	0.28	0.05	0.30	0.28	0.12	0.34	-0.11
30501	0.43	0.49	0.23	0.40	0.06	0.40	0.40	0.13	0.44	-0.17
30502	0.22	0.13	0.17	0.22	-0.09	0.23	0.22	-0.09	0.22	-0.12
30503	0.38	0.42	0.21	0.36	0.02	0.34	0.35	0.11	0.39	-0.10
30601	0.22	0.24	0.10	0.19	-0.03	0.19	0.19	0.07	0.27	0.08
30602	0.25	0.19	0.24	0.28	-0.08	0.26	0.27	-0.10	0.29	-0.02
30603	0.23	0.18	0.22	0.25	-0.05	0.22	0.25	-0.07	0.29	0.15
30604	0.31	0.21	0.34	0.36	-0.01	0.34	0.36	-0.16	0.32	-0.08
30701	0.18	0.12	0.18	0.18	-0.04	0.17	0.17	-0.08	0.22	0.22
30702	0.21	0.14	0.25	0.23	-0.02	0.22	0.23	-0.12	0.25	0.15
30703	0.28	0.18	0.31	0.32	-0.01	0.29	0.32	-0.15	0.30	0.00
30704	0.30	0.13	0.38	0.36	0.07	0.35	0.36	-0.26	0.25	-0.14
30801	0.23	-0.07	0.37	0.30	0.17	0.32	0.29	-0.38	0.08	-0.15
30802	0.33	0.11	0.42	0.38	0.17	0.40	0.38	-0.28	0.24	-0.21
30901	0.23	-0.11	0.35	0.27	0.22	0.33	0.27	-0.40	0.06	-0.07
30902	0.25	-0.08	0.33	0.24	0.26	0.35	0.24	-0.38	0.04	-0.15
31001	0.33	-0.02	0.40	0.35	0.26	0.42	0.35	-0.40	0.16	-0.09
31002	0.41	0.13	0.45	0.43	0.31	0.47	0.44	-0.31	0.29	-0.09
31003	0.32	0.08	0.43	0.38	0.26	0.39	0.39	-0.31	0.22	-0.12
31101	0.27	0.13	0.32	0.31	0.14	0.32	0.32	-0.18	0.24	-0.11
31102	0.27	0.14	0.36	0.33	0.09	0.32	0.33	-0.21	0.26	-0.10
31201	0.26	0.17	0.32	0.31	0.01	0.30	0.31	-0.14	0.25	-0.10
31301	0.22	0.18	0.20	0.20	0.01	0.22	0.20	-0.06	0.21	0.08
31302	0.22	0.15	0.28	0.25	0.02	0.25	0.24	-0.14	0.21	0.09
31303	0.20	0.12	0.26	0.24	-0.03	0.23	0.24	-0.12	0.18	0.00
31401	0.30	0.26	0.29	0.34	-0.03	0.35	0.33	-0.04	0.25	-0.09
31402	0.22	0.18	0.24	0.25	0.03	0.26	0.25	-0.07	0.18	0.03
31403	0.26	0.18	0.29	0.28	0.02	0.31	0.28	-0.11	0.19	-0.03
31501	0.17	0.18	0.11	0.16	-0.17	0.14	0.16	0.03	0.22	-0.06
31502	0.11	0.14	0.11	0.12	-0.13	0.10	0.11	0.01	0.17	0.07
31503	0.11	0.16	0.13	0.12	-0.11	0.14	0.12	0.01	0.12	-0.02
31601	0.11	0.14	0.07	0.11	-0.18	0.11	0.10	0.07	0.10	-0.07
31602	0.00	0.13	-0.02	0.00	-0.22	-0.02	-0.01	0.15	0.06	0.04
31603	0.21	0.25	0.19	0.22	-0.15	0.24	0.21	0.03	0.17	-0.16
31701	0.24	0.23	0.22	0.26	-0.14	0.27	0.23	-0.01	0.19	-0.16
31702	0.25	0.23	0.30	0.29	-0.17	0.28	0.27	-0.08	0.23	-0.16
31703	0.25	0.20	0.35	0.31	-0.15	0.31	0.28	-0.15	0.18	-0.21
31801	0.16	0.10	0.13	0.16	-0.12	0.16	0.15	-0.01	0.09	-0.06
31802	0.23	0.18	0.32	0.29	-0.16	0.28	0.28	-0.15	0.15	-0.25
31803	0.26	0.28	0.40	0.34	-0.15	0.31	0.32	-0.13	0.26	-0.17

Figure. A0-12: Correlation of monthly DJF (left) and MAM (right) percentiles with of PCP with 10 hydroclimatic indices

	PCP- JJA									
	MEI	Nino 1+2	Nina 4	Nina 3.4	PDO	BEST	ONI	TNI	WHWP	TSA
30101	0.09	-0.19	0.10	0.15	0.33	0.16	0.23	-0.26	-0.38	-0.29
30102	0.13	-0.19	0.14	0.19	0.36	0.21	0.28	-0.28	-0.38	-0.30
30103	0.15	-0.17	0.16	0.20	0.39	0.22	0.30	-0.26	-0.41	-0.30
30201	0.14	-0.17	0.15	0.19	0.36	0.19	0.29	-0.26	-0.38	-0.25
30202	0.16	-0.15	0.17	0.21	0.38	0.20	0.31	-0.25	-0.34	-0.22
30301	0.18	-0.12	0.17	0.22	0.41	0.25	0.32	-0.23	-0.32	-0.25
30302	0.22	-0.08	0.18	0.24	0.43	0.22	0.34	-0.19	-0.26	-0.25
30303	0.18	-0.12	0.16	0.22	0.38	0.18	0.31	-0.21	-0.26	-0.19
30401	0.15	-0.17	0.14	0.18	0.38	0.21	0.27	-0.25	-0.33	-0.26
30402	0.22	-0.11	0.19	0.24	0.44	0.26	0.34	-0.23	-0.28	-0.26
30403	0.22	-0.14	0.24	0.27	0.44	0.29	0.36	-0.28	-0.28	-0.27
30501	0.17	-0.15	0.15	0.20	0.38	0.22	0.29	-0.23	-0.30	-0.27
30502	0.20	-0.18	0.26	0.28	0.42	0.29	0.36	-0.33	-0.24	-0.26
30503	0.14	-0.18	0.16	0.20	0.35	0.22	0.28	-0.27	-0.29	-0.28
30601	0.15	-0.17	0.18	0.22	0.33	0.22	0.29	-0.27	-0.24	-0.29
30602	0.18	-0.17	0.25	0.26	0.37	0.28	0.34	-0.31	-0.22	-0.26
30603	0.19	-0.15	0.23	0.26	0.39	0.27	0.33	-0.28	-0.20	-0.28
30604	0.21	-0.14	0.27	0.29	0.35	0.31	0.36	-0.30	-0.19	-0.28
30701	0.15	-0.16	0.19	0.22	0.32	0.20	0.28	-0.26	-0.13	-0.24
30702	0.13	-0.16	0.20	0.22	0.29	0.19	0.26	-0.26	-0.07	-0.20
30703	0.23	-0.10	0.26	0.29	0.37	0.31	0.37	-0.26	-0.15	-0.31
30704	0.28	-0.04	0.27	0.32	0.41	0.32	0.40	-0.20	-0.12	-0.32
30801	0.21	-0.01	0.11	0.17	0.42	0.24	0.27	-0.09	-0.31	-0.33
30802	0.28	0.03	0.19	0.26	0.40	0.30	0.35	-0.10	-0.20	-0.31
30901	0.12	-0.10	0.09	0.10	0.36	0.16	0.21	-0.15	-0.32	-0.27
30902	0.17	-0.03	0.09	0.14	0.42	0.21	0.25	-0.09	-0.28	-0.26
31001	0.15	-0.09	0.16	0.15	0.39	0.23	0.26	-0.18	-0.28	-0.25
31002	0.20	-0.08	0.22	0.20	0.45	0.30	0.30	-0.23	-0.26	-0.22
31003	0.21	-0.04	0.19	0.20	0.42	0.27	0.30	-0.18	-0.24	-0.26
31101	0.29	0.01	0.23	0.30	0.40	0.34	0.39	-0.16	-0.10	-0.36
31102	0.25	-0.06	0.25	0.30	0.38	0.31	0.38	-0.22	-0.12	-0.32
31201	0.20	-0.05	0.20	0.24	0.32	0.28	0.32	-0.17	-0.07	-0.29
31301	0.13	-0.11	0.17	0.22	0.22	0.16	0.25	-0.19	-0.01	-0.18
31302	0.09	-0.16	0.19	0.19	0.26	0.15	0.23	-0.25	-0.01	-0.13
31303	0.12	-0.08	0.13	0.18	0.25	0.18	0.24	-0.15	-0.05	-0.23
31401	0.13	-0.02	0.07	0.14	0.21	0.16	0.19	-0.07	-0.03	-0.26
31402	0.12	-0.06	0.09	0.16	0.24	0.17	0.21	-0.11	-0.05	-0.21
31403	0.18	-0.02	0.13	0.21	0.30	0.22	0.27	-0.11	-0.05	-0.28
31501	0.18	-0.08	0.11	0.23	0.31	0.21	0.28	-0.14	-0.20	-0.33
31502	0.21	0.04	0.09	0.22	0.31	0.17	0.28	-0.01	-0.06	-0.27
31503	0.23	0.06	0.10	0.23	0.31	0.22	0.29	-0.01	-0.04	-0.30
31601	0.44	0.25	0.22	0.38	0.51	0.31	0.43	0.11	0.05	-0.45
31602	0.38	0.22	0.13	0.33	0.42	0.27	0.39	0.12	-0.02	-0.45
31603	0.36	0.19	0.19	0.32	0.43	0.29	0.37	0.05	0.10	-0.39
31701	0.39	0.22	0.21	0.34	0.49	0.31	0.38	0.06	0.13	-0.39
31702	0.38	0.20	0.22	0.34	0.46	0.33	0.39	0.02	0.10	-0.40
31703	0.32	0.16	0.26	0.32	0.30	0.34	0.35	-0.04	0.16	-0.37
31801	0.49	0.32	0.21	0.40	0.54	0.34	0.46	0.17	0.07	-0.39
31802	0.40	0.24	0.16	0.33	0.46	0.32	0.39	0.11	-0.01	-0.32
31803	0.36	0.19	0.23	0.34	0.35	0.35	0.39	0.02	0.07	-0.33

	PCP- SON									
	MEI	Nino 1+2	Nina 4	Nina 3.4	PDO	BEST	ONI	TNI	WHWP	TSA
30101	0.15	0.07	0.17	0.17	0.41	0.17	0.18	-0.11	0.00	-0.06
30102	0.08	0.07	0.07	0.08	0.33	0.10	0.10	0.00	-0.06	-0.14
30103	0.05	0.10	0.01	0.06	0.24	0.08	0.06	0.06	-0.06	-0.11
30201	0.03	0.06	-0.01	0.03	0.25	0.06	0.03	0.05	-0.09	-0.13
30202	0.07	0.05	0.02	0.05	0.29	0.10	0.05	0.00	-0.11	-0.07
30301	0.10	0.09	0.05	0.08	0.37	0.12	0.11	0.02	-0.10	-0.11
30302	0.12	0.05	0.09	0.10	0.30	0.15	0.09	-0.08	-0.10	-0.03
30303	0.13	0.03	0.12	0.12	0.23	0.17	0.11	-0.11	-0.05	-0.07
30401	0.14	0.07	0.14	0.13	0.36	0.19	0.16	-0.06	-0.15	-0.20
30402	0.24	0.09	0.24	0.25	0.33	0.30	0.26	-0.17	-0.14	-0.13
30403	0.37	0.26	0.29	0.35	0.44	0.39	0.37	-0.07	-0.14	-0.17
30501	0.24	0.12	0.24	0.21	0.44	0.28	0.25	-0.09	-0.17	-0.25
30502	0.36	0.25	0.21	0.28	0.51	0.34	0.31	0.01	-0.24	-0.22
30503	0.33	0.22	0.29	0.28	0.43	0.34	0.31	-0.05	-0.14	-0.29
30601	0.35	0.27	0.27	0.28	0.43	0.32	0.31	0.03	-0.16	-0.28
30602	0.33	0.24	0.18	0.22	0.55	0.30	0.26	0.04	-0.26	-0.17
30603	0.36	0.31	0.22	0.26	0.49	0.33	0.30	0.09	-0.20	-0.16
30604	0.29	0.18	0.14	0.17	0.59	0.26	0.22	0.01	-0.38	-0.06
30701	0.37	0.30	0.31	0.30	0.39	0.35	0.32	0.02	-0.07	-0.22
30702	0.34	0.28	0.27	0.27	0.42	0.33	0.30	0.02	-0.12	-0.15
30703	0.34	0.24	0.18	0.22	0.57	0.31	0.27	0.03	-0.35	-0.06
30704	0.38	0.25	0.19	0.24	0.65	0.34	0.29	0.04	-0.40	-0.13
30801	0.29	0.13	0.12	0.09	0.48	0.28	0.14	0.00	-0.39	-0.35
30802	0.26	0.11	0.10	0.08	0.52	0.23	0.13	0.00	-0.44	-0.28
30901	0.38	0.24	0.16	0.19	0.57	0.34	0.25	0.08	-0.37	-0.36
30902	0.36	0.30	0.10	0.19	0.54	0.32	0.26	0.18	-0.43	-0.28
31001	0.36	0.24	0.16	0.17	0.56	0.33	0.23	0.09	-0.36	-0.34
31002	0.30	0.21	0.13	0.11	0.46	0.27	0.15	0.12	-0.25	-0.32
31003	0.36	0.25	0.17	0.17	0.57	0.30	0.22	0.10	-0.31	-0.36
31101	0.34	0.23	0.16	0.16	0.63	0.27	0.21	0.06	-0.32	-0.17
31102	0.37	0.26	0.18	0.21	0.61	0.31	0.26	0.06	-0.32	-0.11
31201	0.26	0.23	0.09	0.12	0.47	0.19	0.16	0.10	-0.22	0.00
31301	0.24	0.22	0.21	0.20	0.34	0.22	0.22	0.05	-0.08	-0.16
31302	0.29	0.23	0.23	0.23	0.38	0.28	0.25	0.01	-0.12	-0.14
31303	0.27	0.18	0.14	0.20	0.45	0.25	0.23	-0.01	-0.26	-0.08
31401	0.13	0.06	0.10	0.12	0.33	0.15	0.14	-0.06	-0.23	-0.17
31402	0.15	0.08	0.11	0.14	0.34	0.16	0.15	-0.05	-0.22	-0.12
31403	0.21	0.11	0.23	0.20	0.37	0.24	0.22	-0.11	-0.25	-0.22
31501	0.22	0.13	0.29	0.23	0.22	0.24	0.23	-0.10	-0.03	-0.24
31502	0.31	0.26	0.31	0.28	0.34	0.32	0.30	-0.01	-0.12	-0.13
31503	0.28	0.22	0.27	0.24	0.36	0.28	0.26	-0.03	-0.20	-0.15
31601	0.22	0.00	0.28	0.18	0.35	0.26	0.21	-0.27	-0.39	-0.07
31602	0.21	0.02	0.27	0.18	0.38	0.26	0.21	-0.23	-0.37	-0.04
31603	0.15	0.08	0.20	0.13	0.24	0.19	0.14	-0.12	-0.19	-0.06
31701	0.08	0.03	0.13	0.04	0.16	0.12	0.05	-0.11	-0.24	-0.01
31702	0.06	0.03	0.11	0.02	0.16	0.09	0.03	-0.09	-0.22	-0.02
31703	0.08	0.06	0.10	0.06	0.20	0.11	0.07	-0.07	-0.21	-0.13
31801	0.21	0.10	0.20	0.17	0.30	0.22	0.19	-0.11	-0.32	-0.05
31802	0.12	0.02	0.15	0.12	0.24	0.15	0.14	-0.15	-0.23	0.06
31803	0.03	-0.02	0.11	0.00	0.16	0.08	0.01	-0.13	-0.19	-0.10

Figure. A0-13: Correlation of monthly JJA (left) and SON (right) percentiles with of PCP with 10 hydroclimatic indices

SURQ- DJF										
	MEI	Nino 1+2	Nina 4	Nina 3.4	PDO	BEST	ONI	TNI	WHWP	TSA
30101	0.43	0.37	0.31	0.34	0.42	0.48	0.35	-0.12	-0.07	-0.01
30102	0.45	0.41	0.30	0.37	0.30	0.51	0.37	-0.05	-0.07	-0.02
30103	0.52	0.53	0.37	0.46	0.24	0.56	0.45	-0.01	0.16	0.09
30201	0.56	0.59	0.35	0.48	0.19	0.59	0.48	0.06	0.09	0.05
30202	0.64	0.61	0.45	0.55	0.34	0.69	0.55	-0.05	0.02	-0.01
30301	0.58	0.56	0.37	0.49	0.33	0.62	0.50	0.00	0.00	0.14
30302	0.65	0.69	0.39	0.55	0.33	0.65	0.57	0.09	0.06	0.16
30303	0.64	0.63	0.44	0.60	0.23	0.64	0.60	-0.01	0.05	0.04
30401	0.54	0.46	0.38	0.46	0.30	0.60	0.46	-0.10	-0.09	0.02
30402	0.69	0.67	0.48	0.62	0.31	0.71	0.64	-0.04	0.00	0.05
30403	0.62	0.58	0.48	0.60	0.16	0.66	0.60	-0.09	0.09	0.02
30501	0.48	0.40	0.34	0.40	0.30	0.53	0.41	-0.08	-0.09	0.04
30502	0.56	0.47	0.50	0.57	0.18	0.61	0.58	-0.22	0.05	-0.01
30503	0.57	0.48	0.46	0.53	0.32	0.62	0.53	-0.14	0.08	0.08
30601	0.50	0.48	0.39	0.50	0.17	0.54	0.49	-0.03	0.25	0.15
30602	0.48	0.41	0.43	0.48	0.21	0.51	0.49	-0.18	0.11	-0.02
30603	0.51	0.46	0.40	0.51	0.16	0.56	0.52	-0.08	0.11	-0.04
30604	0.51	0.41	0.46	0.50	0.28	0.52	0.51	-0.22	0.07	-0.03
30701	0.46	0.45	0.36	0.47	0.06	0.51	0.47	0.00	0.22	0.04
30702	0.48	0.48	0.36	0.49	0.04	0.53	0.49	0.01	0.20	-0.04
30703	0.52	0.47	0.42	0.51	0.23	0.54	0.52	-0.10	0.11	-0.02
30704	0.58	0.50	0.46	0.50	0.41	0.57	0.52	-0.13	0.06	0.01
30801	0.39	0.46	0.24	0.29	0.14	0.38	0.29	0.09	0.13	0.04
30802	0.46	0.61	0.19	0.38	0.40	0.39	0.39	0.27	0.20	0.27
30901	0.52	0.55	0.33	0.42	0.26	0.50	0.43	0.03	0.02	-0.09
30902	0.55	0.56	0.30	0.44	0.27	0.52	0.46	0.10	-0.07	0.02
31001	0.44	0.54	0.29	0.38	0.26	0.42	0.38	0.06	0.21	-0.02
31002	0.49	0.55	0.32	0.42	0.31	0.46	0.43	0.04	0.23	0.05
31003	0.36	0.53	0.16	0.32	0.24	0.30	0.33	0.30	0.33	0.22
31101	0.42	0.36	0.37	0.35	0.22	0.44	0.36	-0.14	0.09	0.08
31102	0.57	0.48	0.48	0.52	0.28	0.59	0.53	-0.16	0.08	0.00
31201	0.47	0.35	0.44	0.42	0.15	0.50	0.42	-0.17	0.10	0.00
31301	0.39	0.36	0.33	0.40	0.11	0.46	0.39	-0.07	0.19	0.03
31302	0.53	0.51	0.43	0.54	0.13	0.60	0.53	-0.05	0.20	0.00
31303	0.47	0.42	0.43	0.49	0.07	0.50	0.49	-0.12	0.15	-0.03
31401	0.58	0.55	0.55	0.65	0.01	0.59	0.64	-0.15	0.36	0.17
31402	0.43	0.43	0.40	0.50	-0.06	0.45	0.49	-0.08	0.35	0.15
31403	0.47	0.45	0.44	0.55	-0.05	0.49	0.54	-0.12	0.29	0.05
31501	0.26	0.24	0.21	0.26	0.17	0.33	0.26	-0.03	0.24	0.04
31502	0.19	0.10	0.19	0.21	0.07	0.26	0.20	-0.13	0.08	-0.20
31503	0.22	0.13	0.23	0.29	0.04	0.30	0.28	-0.15	0.06	-0.23
31601	0.17	0.14	0.10	0.17	0.10	0.19	0.17	-0.03	0.06	-0.19
31602	0.22	0.20	0.12	0.21	0.19	0.24	0.21	0.00	0.09	-0.16
31603	0.39	0.39	0.30	0.43	0.21	0.42	0.42	-0.03	0.21	-0.02
31701	0.26	0.23	0.26	0.33	0.13	0.28	0.31	-0.11	0.21	-0.06
31702	0.24	0.23	0.26	0.32	0.06	0.26	0.30	-0.11	0.24	-0.11
31703	0.45	0.45	0.46	0.54	0.01	0.45	0.53	-0.17	0.32	0.11
31801	0.10	0.03	0.07	0.11	0.08	0.12	0.09	-0.05	0.11	-0.20
31802	0.22	0.19	0.19	0.25	0.14	0.22	0.23	-0.05	0.25	-0.23
31803	0.35	0.36	0.33	0.43	-0.02	0.36	0.42	-0.10	0.26	-0.01

SURQ- MAM										
	MEI	Nino 1+2	Nina 4	Nina 3.4	PDO	BEST	ONI	TNI	WHWP	TSA
30101	0.43	0.43	0.25	0.38	0.31	0.42	0.37	0.05	0.37	-0.25
30102	0.45	0.44	0.23	0.37	0.32	0.44	0.36	0.09	0.41	-0.11
30103	0.29	0.26	0.14	0.21	0.18	0.29	0.21	0.05	0.24	-0.03
30201	0.29	0.31	0.15	0.22	0.15	0.30	0.22	0.08	0.27	-0.05
30202	0.47	0.52	0.15	0.37	0.31	0.46	0.36	0.21	0.49	-0.05
30301	0.43	0.57	0.07	0.32	0.22	0.39	0.31	0.33	0.48	-0.18
30302	0.40	0.45	0.11	0.30	0.16	0.39	0.30	0.17	0.38	-0.09
30303	0.47	0.42	0.19	0.39	0.27	0.46	0.39	0.10	0.43	-0.04
30401	0.50	0.54	0.19	0.43	0.28	0.46	0.42	0.20	0.50	-0.15
30402	0.50	0.49	0.13	0.40	0.28	0.45	0.40	0.19	0.47	-0.08
30403	0.46	0.44	0.15	0.41	0.18	0.42	0.40	0.15	0.45	-0.09
30501	0.52	0.51	0.27	0.47	0.23	0.49	0.46	0.10	0.48	-0.14
30502	0.25	0.12	0.19	0.26	-0.04	0.26	0.26	-0.12	0.24	-0.07
30503	0.50	0.46	0.26	0.45	0.21	0.45	0.44	0.08	0.47	-0.05
30601	0.25	0.23	0.12	0.21	0.10	0.21	0.21	0.03	0.31	0.20
30602	0.29	0.18	0.28	0.32	-0.05	0.29	0.31	-0.15	0.32	0.01
30603	0.28	0.20	0.21	0.29	-0.03	0.25	0.28	-0.05	0.36	0.21
30604	0.42	0.30	0.35	0.44	0.05	0.41	0.43	-0.11	0.48	0.07
30701	0.24	0.15	0.16	0.23	0.03	0.20	0.22	-0.05	0.30	0.34
30702	0.26	0.18	0.22	0.26	0.01	0.24	0.25	-0.08	0.30	0.22
30703	0.38	0.25	0.33	0.39	0.04	0.35	0.39	-0.13	0.43	0.14
30704	0.49	0.30	0.41	0.50	0.17	0.49	0.51	-0.17	0.51	0.04
30801	0.35	0.23	0.25	0.34	0.36	0.33	0.34	-0.01	0.39	0.31
30802	0.49	0.46	0.39	0.51	0.45	0.48	0.51	0.01	0.56	0.01
30901	0.44	0.11	0.37	0.43	0.47	0.47	0.43	-0.25	0.30	0.14
30902	0.58	0.29	0.44	0.55	0.55	0.63	0.54	-0.20	0.37	-0.13
31001	0.39	0.04	0.41	0.39	0.35	0.45	0.40	-0.38	0.22	-0.02
31002	0.45	0.23	0.39	0.45	0.48	0.46	0.46	-0.18	0.41	0.13
31003	0.28	0.39	0.09	0.26	0.37	0.18	0.26	0.31	0.46	0.36
31101	0.36	0.31	0.29	0.37	0.30	0.38	0.39	-0.03	0.41	-0.02
31102	0.42	0.28	0.38	0.44	0.18	0.43	0.44	-0.14	0.46	0.00
31201	0.32	0.29	0.22	0.33	0.06	0.32	0.34	0.03	0.37	0.01
31301	0.24	0.21	0.12	0.21	0.10	0.21	0.21	0.03	0.27	0.20
31302	0.30	0.25	0.25	0.30	0.08	0.29	0.29	-0.04	0.32	0.16
31303	0.33	0.25	0.29	0.34	0.04	0.33	0.34	-0.07	0.34	0.12
31401	0.44	0.41	0.32	0.44	-0.02	0.42	0.44	0.04	0.44	0.08
31402	0.16	0.13	0.15	0.16	-0.01	0.13	0.16	-0.01	0.17	0.35
31403	0.29	0.20	0.29	0.30	-0.01	0.29	0.30	-0.08	0.27	0.20
31501	0.16	0.17	-0.01	0.11	-0.12	0.11	0.12	0.11	0.20	-0.06
31502	0.05	0.08	0.03	0.05	-0.17	0.02	0.05	0.03	0.13	0.16
31503	0.14	0.19	0.11	0.14	-0.09	0.14	0.14	0.05	0.15	0.01
31601	0.15	0.22	0.07	0.14	-0.16	0.13	0.13	0.12	0.14	-0.12
31602	0.04	0.22	-0.06	0.04	-0.16	0.00	0.03	0.24	0.10	0.04
31603	0.40	0.48	0.25	0.40	-0.10	0.38	0.40	0.13	0.39	-0.26
31701	0.35	0.43	0.17	0.35	-0.10	0.33	0.33	0.17	0.33	-0.25
31702	0.27	0.39	0.17	0.28	-0.14	0.24	0.26	0.15	0.31	-0.18
31703	0.38	0.38	0.32	0.39	-0.17	0.39	0.38	0.03	0.33	-0.23
31801	0.22	0.22	0.10	0.21	0.02	0.18	0.21	0.08	0.19	0.02
31802	0.24	0.27	0.23	0.29	-0.07	0.25	0.28	-0.02	0.23	-0.13
31803	0.26	0.41	0.27	0.29	-0.13	0.22	0.28	0.10	0.35	0.01

Figure. A0-14: Correlation of monthly DJF (left) and MAM (right) percentiles with of SURQ with 10 hydroclimatic indices

	SURQ- JJA									
	MEI	Nino 1+2	Nina 4	Nina 3.4	PDO	BEST	ONI	TNI	WHWP	TSA
30101	0.00	-0.18	0.02	0.09	0.18	0.09	0.14	-0.19	-0.35	-0.30
30102	0.07	-0.19	0.11	0.16	0.26	0.17	0.23	-0.24	-0.35	-0.28
30103	0.14	-0.15	0.13	0.20	0.35	0.20	0.29	-0.23	-0.37	-0.30
30201	0.12	-0.17	0.13	0.18	0.32	0.18	0.28	-0.24	-0.37	-0.25
30202	0.14	-0.13	0.14	0.19	0.32	0.15	0.27	-0.21	-0.29	-0.21
30301	0.16	-0.11	0.15	0.21	0.33	0.23	0.29	-0.20	-0.30	-0.28
30302	0.17	-0.07	0.12	0.20	0.33	0.15	0.28	-0.15	-0.27	-0.26
30303	0.16	-0.12	0.14	0.20	0.33	0.15	0.28	-0.19	-0.26	-0.20
30401	0.12	-0.14	0.14	0.20	0.24	0.18	0.26	-0.22	-0.28	-0.28
30402	0.19	-0.09	0.16	0.22	0.38	0.22	0.31	-0.18	-0.25	-0.29
30403	0.25	-0.10	0.24	0.29	0.40	0.29	0.37	-0.24	-0.20	-0.32
30501	0.17	-0.13	0.18	0.25	0.25	0.26	0.31	-0.23	-0.25	-0.26
30502	0.24	-0.12	0.31	0.33	0.35	0.33	0.37	-0.29	-0.16	-0.30
30503	0.17	-0.13	0.23	0.27	0.20	0.26	0.32	-0.25	-0.20	-0.25
30601	0.12	-0.19	0.25	0.24	0.22	0.23	0.27	-0.30	-0.18	-0.20
30602	0.22	-0.13	0.30	0.32	0.34	0.32	0.37	-0.29	-0.15	-0.31
30603	0.26	-0.08	0.35	0.36	0.35	0.36	0.40	-0.27	-0.07	-0.32
30604	0.27	-0.07	0.38	0.38	0.32	0.40	0.42	-0.30	-0.06	-0.33
30701	0.15	-0.14	0.25	0.26	0.28	0.25	0.28	-0.26	-0.07	-0.21
30702	0.13	-0.15	0.24	0.24	0.29	0.24	0.26	-0.27	-0.05	-0.20
30703	0.29	-0.03	0.38	0.39	0.34	0.41	0.42	-0.25	-0.01	-0.36
30704	0.28	0.01	0.30	0.35	0.24	0.36	0.37	-0.16	0.00	-0.28
30801	0.38	0.20	0.21	0.30	0.32	0.34	0.35	0.04	0.01	-0.37
30802	0.24	0.12	0.11	0.17	0.15	0.25	0.21	0.03	-0.04	-0.15
30901	0.27	0.00	0.19	0.22	0.42	0.26	0.32	-0.12	-0.19	-0.33
30902	0.25	-0.01	0.20	0.22	0.43	0.28	0.33	-0.13	-0.25	-0.29
31001	0.28	-0.01	0.27	0.27	0.38	0.32	0.35	-0.18	-0.16	-0.34
31002	0.36	0.09	0.35	0.34	0.47	0.42	0.42	-0.14	-0.08	-0.33
31003	0.26	0.19	0.09	0.15	0.20	0.24	0.19	0.12	0.04	-0.19
31101	0.32	0.06	0.24	0.32	0.31	0.38	0.38	-0.11	-0.02	-0.35
31102	0.32	0.02	0.32	0.39	0.36	0.42	0.44	-0.18	0.00	-0.31
31201	0.19	-0.04	0.20	0.26	0.25	0.32	0.31	-0.16	-0.04	-0.28
31301	0.07	-0.18	0.19	0.20	0.17	0.20	0.21	-0.25	-0.06	-0.15
31302	0.08	-0.17	0.22	0.20	0.26	0.20	0.22	-0.27	0.00	-0.11
31303	0.20	0.01	0.17	0.25	0.26	0.25	0.30	-0.09	0.00	-0.28
31401	0.18	0.01	0.14	0.19	0.26	0.24	0.24	-0.06	0.05	-0.26
31402	0.20	-0.01	0.17	0.25	0.28	0.26	0.29	-0.10	0.03	-0.22
31403	0.19	-0.03	0.16	0.23	0.30	0.28	0.29	-0.12	0.00	-0.26
31501	-0.04	-0.27	0.03	0.08	0.26	0.05	0.10	-0.26	-0.24	-0.21
31502	0.16	-0.02	0.11	0.21	0.25	0.20	0.25	-0.07	-0.11	-0.27
31503	0.30	0.13	0.16	0.30	0.34	0.31	0.35	0.02	0.01	-0.33
31601	0.52	0.30	0.35	0.51	0.53	0.43	0.53	0.08	0.14	-0.58
31602	0.48	0.30	0.24	0.44	0.47	0.40	0.49	0.14	0.05	-0.55
31603	0.47	0.26	0.33	0.46	0.44	0.45	0.49	0.05	0.19	-0.46
31701	0.51	0.29	0.34	0.49	0.55	0.47	0.51	0.05	0.20	-0.52
31702	0.52	0.29	0.34	0.50	0.50	0.48	0.51	0.04	0.18	-0.54
31703	0.29	0.09	0.30	0.30	0.29	0.36	0.30	-0.13	0.26	-0.40
31801	0.61	0.43	0.31	0.54	0.60	0.47	0.59	0.22	0.07	-0.50
31802	0.53	0.31	0.29	0.51	0.50	0.49	0.56	0.11	-0.01	-0.43
31803	0.49	0.26	0.35	0.48	0.36	0.49	0.51	0.01	0.16	-0.42

	SURQ- SON									
	MEI	Nino 1+2	Nina 4	Nina 3.4	PDO	BEST	ONI	TNI	WHWP	TSA
30101	-0.02	-0.09	0.07	0.03	0.24	0.07	0.06	-0.18	-0.15	-0.10
30102	-0.07	-0.11	-0.04	-0.06	0.26	-0.01	-0.03	-0.09	-0.21	-0.15
30103	-0.07	-0.05	-0.06	-0.04	0.15	-0.01	-0.03	-0.04	-0.17	-0.10
30201	-0.14	-0.14	-0.15	-0.14	0.16	-0.08	-0.12	-0.03	-0.25	-0.12
30202	-0.03	-0.14	-0.05	-0.07	0.25	0.03	-0.03	-0.12	-0.38	-0.17
30301	-0.08	-0.12	-0.05	-0.07	0.24	-0.02	-0.04	-0.07	-0.14	-0.06
30302	0.02	-0.03	-0.02	-0.03	0.26	0.03	-0.03	-0.05	-0.06	0.12
30303	0.08	-0.02	0.07	0.05	0.23	0.12	0.05	-0.11	-0.08	-0.06
30401	0.02	-0.12	0.07	0.01	0.34	0.11	0.06	-0.18	-0.33	-0.31
30402	0.17	-0.01	0.15	0.15	0.41	0.24	0.18	-0.18	-0.34	-0.19
30403	0.34	0.16	0.29	0.32	0.52	0.39	0.36	-0.16	-0.30	-0.29
30501	0.07	-0.06	0.11	0.04	0.40	0.14	0.09	-0.15	-0.24	-0.30
30502	0.32	0.17	0.20	0.26	0.60	0.34	0.30	-0.03	-0.32	-0.27
30503	0.17	0.03	0.17	0.10	0.43	0.21	0.15	-0.11	-0.28	-0.46
30601	0.11	0.08	0.05	0.03	0.44	0.11	0.07	0.06	-0.19	-0.29
30602	0.32	0.20	0.19	0.21	0.66	0.28	0.26	0.02	-0.27	-0.15
30603	0.35	0.25	0.24	0.24	0.63	0.32	0.28	0.04	-0.20	-0.14
30604	0.21	0.08	0.13	0.15	0.55	0.22	0.19	-0.05	-0.37	-0.01
30701	0.39	0.32	0.36	0.32	0.47	0.36	0.34	0.04	0.06	-0.20
30702	0.33	0.27	0.31	0.27	0.45	0.32	0.28	0.02	0.02	-0.14
30703	0.23	0.12	0.16	0.16	0.49	0.24	0.19	-0.03	-0.32	-0.04
30704	0.17	0.09	0.13	0.15	0.37	0.19	0.18	-0.03	-0.28	-0.10
30801	0.10	0.13	-0.01	0.00	0.27	0.09	0.01	0.15	-0.15	-0.20
30802	0.12	0.04	0.09	0.08	0.28	0.15	0.08	-0.03	-0.16	-0.09
30901	0.29	0.23	0.09	0.14	0.48	0.26	0.19	0.13	-0.38	-0.40
30902	0.31	0.28	0.07	0.16	0.49	0.27	0.23	0.19	-0.47	-0.33
31001	0.33	0.22	0.17	0.18	0.44	0.32	0.22	0.07	-0.23	-0.27
31002	0.18	0.11	0.07	0.04	0.31	0.18	0.06	0.09	-0.20	-0.25
31003	0.20	0.19	0.12	0.16	0.31	0.19	0.16	0.12	-0.05	-0.19
31101	0.25	0.14	0.14	0.14	0.49	0.21	0.17	0.01	-0.25	-0.10
31102	0.21	0.10	0.16	0.15	0.44	0.21	0.18	-0.05	-0.28	-0.13
31201	0.04	0.06	-0.03	-0.04	0.20	0.01	-0.02	0.09	-0.15	0.04
31301	0.06	0.07	0.15	0.06	0.26	0.09	0.07	0.00	0.05	-0.14
31302	0.22	0.18	0.24	0.18	0.33	0.22	0.18	-0.01	0.07	-0.17
31303	0.08	0.04	0.01	0.02	0.29	0.07	0.04	-0.01	-0.22	-0.12
31401	-0.08	-0.06	-0.05	-0.07	0.19	-0.06	-0.08	-0.02	-0.06	-0.14
31402	-0.07	-0.02	-0.03	-0.04	0.11	-0.03	-0.05	-0.01	-0.01	-0.06
31403	0.02	0.01	0.12	0.04	0.23	0.05	0.04	-0.08	-0.06	-0.15
31501	0.10	0.04	0.23	0.11	0.13	0.17	0.11	-0.10	0.06	-0.14
31502	0.24	0.20	0.29	0.24	0.30	0.28	0.25	-0.03	-0.06	-0.11
31503	0.19	0.16	0.22	0.15	0.32	0.21	0.18	-0.03	-0.22	-0.19
31601	0.17	-0.04	0.21	0.11	0.34	0.22	0.14	-0.23	-0.49	-0.08
31602	0.07	-0.11	0.18	0.04	0.33	0.16	0.07	-0.24	-0.41	-0.09
31603	-0.04	-0.04	0.01	-0.11	0.19	-0.02	-0.08	0.00	-0.29	-0.15
31701	-0.05	-0.08	0.03	-0.11	0.14	-0.02	-0.10	-0.09	-0.25	0.04
31702	-0.03	-0.05	0.11	-0.05	0.07	0.02	-0.05	-0.12	-0.10	0.02
31703	-0.08	-0.04	0.03	-0.06	-0.02	-0.03	-0.06	-0.07	0.00	-0.04
31801	0.11	0.00	0.14	0.07	0.27	0.14	0.10	-0.11	-0.42	-0.01
31802	0.02	-0.12	0.13	0.05	0.18	0.09	0.05	-0.22	-0.31	0.05
31803	-0.10	-0.13	0.07	-0.08	0.03	-0.04	-0.09	-0.16	0.00	-0.07

Figure. A0-15: Correlation of monthly JJA (left) and SON (right) percentiles with of SURQ with 10 hydroclimatic indices

	PET- DJF									
	MEI	Nino 1+2	Nina 4	Nina 3.4	PDO	BEST	ONI	TNI	WHWP	TSA
30101	-0.23	-0.17	-0.13	-0.16	-0.32	-0.27	-0.18	0.05	0.24	0.17
30102	-0.23	-0.16	-0.13	-0.15	-0.31	-0.30	-0.17	0.07	0.27	0.16
30103	-0.29	-0.18	-0.19	-0.21	-0.34	-0.36	-0.23	0.11	0.30	0.19
30201	-0.25	-0.14	-0.18	-0.18	-0.21	-0.32	-0.20	0.13	0.30	0.24
30202	-0.28	-0.18	-0.19	-0.21	-0.17	-0.34	-0.23	0.13	0.31	0.25
30301	-0.23	-0.15	-0.12	-0.15	-0.23	-0.30	-0.17	0.07	0.33	0.24
30302	-0.21	-0.13	-0.11	-0.14	-0.13	-0.28	-0.16	0.07	0.36	0.29
30303	-0.24	-0.15	-0.15	-0.19	-0.11	-0.28	-0.20	0.08	0.33	0.31
30401	-0.19	-0.15	-0.05	-0.11	-0.19	-0.25	-0.13	-0.02	0.29	0.21
30402	-0.27	-0.19	-0.13	-0.20	-0.16	-0.32	-0.22	0.04	0.34	0.31
30403	-0.26	-0.17	-0.12	-0.18	-0.17	-0.31	-0.21	0.05	0.38	0.32
30501	-0.16	-0.11	-0.04	-0.09	-0.18	-0.22	-0.11	0.00	0.31	0.21
30502	-0.31	-0.17	-0.19	-0.25	-0.20	-0.36	-0.28	0.15	0.41	0.40
30503	-0.12	-0.06	0.00	-0.06	-0.11	-0.18	-0.08	0.01	0.36	0.31
30601	-0.07	-0.03	0.04	-0.02	-0.07	-0.13	-0.05	-0.03	0.33	0.34
30602	-0.31	-0.18	-0.17	-0.24	-0.21	-0.35	-0.27	0.12	0.41	0.40
30603	-0.27	-0.15	-0.14	-0.20	-0.19	-0.32	-0.23	0.11	0.41	0.40
30604	-0.44	-0.26	-0.34	-0.39	-0.28	-0.48	-0.42	0.24	0.33	0.36
30701	-0.15	-0.06	-0.06	-0.10	-0.10	-0.22	-0.12	0.08	0.37	0.34
30702	-0.24	-0.14	-0.14	-0.18	-0.18	-0.30	-0.21	0.12	0.34	0.33
30703	-0.45	-0.27	-0.34	-0.39	-0.28	-0.49	-0.41	0.24	0.30	0.34
30704	-0.50	-0.31	-0.42	-0.46	-0.32	-0.53	-0.49	0.29	0.25	0.28
30801	-0.48	-0.27	-0.40	-0.40	-0.37	-0.49	-0.43	0.28	0.25	0.09
30802	-0.50	-0.27	-0.47	-0.47	-0.29	-0.54	-0.50	0.35	0.25	0.17
30901	-0.51	-0.32	-0.39	-0.42	-0.37	-0.53	-0.44	0.21	0.18	0.12
30902	-0.46	-0.32	-0.32	-0.37	-0.28	-0.48	-0.39	0.13	0.14	0.12
31001	-0.54	-0.37	-0.41	-0.46	-0.39	-0.56	-0.49	0.20	0.17	0.12
31002	-0.57	-0.37	-0.49	-0.51	-0.35	-0.59	-0.54	0.29	0.13	0.08
31003	-0.53	-0.30	-0.47	-0.48	-0.34	-0.56	-0.50	0.34	0.23	0.09
31101	-0.40	-0.25	-0.38	-0.38	-0.17	-0.44	-0.40	0.26	0.26	0.17
31102	-0.48	-0.32	-0.42	-0.45	-0.23	-0.52	-0.47	0.27	0.22	0.23
31201	-0.41	-0.33	-0.29	-0.38	-0.17	-0.41	-0.40	0.11	0.19	0.38
31301	-0.23	-0.15	-0.09	-0.17	-0.21	-0.30	-0.19	0.04	0.31	0.26
31302	-0.28	-0.19	-0.17	-0.22	-0.24	-0.35	-0.25	0.11	0.32	0.24
31303	-0.40	-0.25	-0.32	-0.36	-0.23	-0.48	-0.39	0.22	0.29	0.22
31401	-0.36	-0.21	-0.29	-0.33	-0.25	-0.42	-0.36	0.21	0.22	0.13
31402	-0.37	-0.18	-0.29	-0.32	-0.26	-0.45	-0.35	0.24	0.34	0.28
31403	-0.36	-0.18	-0.27	-0.30	-0.28	-0.43	-0.33	0.22	0.27	0.20
31501	-0.13	-0.14	0.04	-0.07	-0.19	-0.19	-0.09	-0.11	0.26	0.21
31502	-0.20	-0.18	-0.02	-0.12	-0.23	-0.25	-0.14	-0.07	0.24	0.18
31503	-0.29	-0.20	-0.15	-0.22	-0.25	-0.35	-0.25	0.07	0.25	0.24
31601	-0.14	-0.19	0.06	-0.06	-0.24	-0.20	-0.09	-0.15	0.22	0.15
31602	-0.16	-0.22	0.04	-0.08	-0.25	-0.21	-0.11	-0.16	0.18	0.10
31603	-0.31	-0.26	-0.16	-0.26	-0.23	-0.36	-0.28	0.02	0.15	0.16
31701	-0.29	-0.27	-0.13	-0.24	-0.20	-0.34	-0.27	-0.03	0.12	0.13
31702	-0.25	-0.17	-0.14	-0.20	-0.12	-0.31	-0.23	0.06	0.20	0.21
31703	-0.34	-0.19	-0.28	-0.30	-0.21	-0.40	-0.33	0.22	0.25	0.17
31801	-0.20	-0.18	-0.03	-0.12	-0.25	-0.26	-0.15	-0.06	0.17	0.15
31802	-0.38	-0.41	-0.18	-0.33	-0.11	-0.39	-0.35	-0.08	0.04	0.32
31803	-0.22	-0.10	-0.17	-0.20	-0.05	-0.27	-0.22	0.15	0.26	0.27

	PET- MAM									
	MEI	Nino 1+2	Nina 4	Nina 3.4	PDO	BEST	ONI	TNI	WHWP	TSA
30101	-0.41	-0.32	-0.18	-0.35	-0.25	-0.38	-0.37	-0.04	-0.29	0.15
30102	-0.43	-0.33	-0.17	-0.36	-0.27	-0.41	-0.38	-0.07	-0.33	0.12
30103	-0.47	-0.29	-0.22	-0.40	-0.34	-0.45	-0.41	0.01	-0.35	0.02
30201	-0.40	-0.30	-0.12	-0.33	-0.27	-0.38	-0.34	-0.11	-0.33	0.00
30202	-0.40	-0.33	-0.12	-0.32	-0.21	-0.39	-0.34	-0.13	-0.35	0.07
30301	-0.42	-0.37	-0.13	-0.34	-0.21	-0.41	-0.36	-0.14	-0.36	0.12
30302	-0.42	-0.40	-0.08	-0.33	-0.18	-0.38	-0.34	-0.20	-0.41	0.05
30303	-0.37	-0.38	-0.04	-0.29	-0.11	-0.31	-0.29	-0.23	-0.40	0.05
30401	-0.43	-0.39	-0.13	-0.35	-0.23	-0.40	-0.37	-0.14	-0.35	0.15
30402	-0.46	-0.40	-0.14	-0.37	-0.21	-0.42	-0.38	-0.16	-0.43	0.01
30403	-0.46	-0.40	-0.16	-0.38	-0.24	-0.42	-0.39	-0.13	-0.41	0.04
30501	-0.44	-0.40	-0.12	-0.36	-0.23	-0.40	-0.37	-0.15	-0.37	0.16
30502	-0.43	-0.41	-0.19	-0.36	-0.16	-0.41	-0.37	-0.10	-0.40	0.06
30503	-0.43	-0.42	-0.14	-0.35	-0.20	-0.39	-0.36	-0.15	-0.38	0.15
30601	-0.39	-0.36	-0.15	-0.33	-0.17	-0.37	-0.34	-0.10	-0.34	0.14
30602	-0.43	-0.39	-0.24	-0.38	-0.14	-0.42	-0.39	-0.04	-0.40	0.10
30603	-0.46	-0.39	-0.30	-0.44	-0.19	-0.47	-0.44	0.01	-0.42	0.07
30604	-0.45	-0.35	-0.30	-0.41	-0.20	-0.46	-0.42	0.03	-0.41	0.09
30701	-0.42	-0.33	-0.24	-0.37	-0.19	-0.41	-0.38	-0.01	-0.38	-0.02
30702	-0.48	-0.36	-0.30	-0.43	-0.20	-0.48	-0.44	0.04	-0.44	0.00
30703	-0.45	-0.34	-0.34	-0.43	-0.19	-0.47	-0.43	0.08	-0.41	0.08
30704	-0.44	-0.27	-0.36	-0.42	-0.25	-0.49	-0.43	0.14	-0.35	0.11
30801	-0.39	-0.03	-0.46	-0.41	-0.30	-0.49	-0.41	0.40	-0.17	0.07
30802	-0.42	-0.10	-0.42	-0.43	-0.29	-0.50	-0.43	0.32	-0.22	0.07
30901	-0.33	0.02	-0.44	-0.34	-0.25	-0.43	-0.34	0.41	-0.08	0.15
30902	-0.23	0.01	-0.32	-0.23	-0.17	-0.30	-0.23	0.29	-0.03	0.17
31001	-0.39	-0.09	-0.42	-0.38	-0.31	-0.48	-0.38	0.31	-0.16	0.16
31002	-0.46	-0.18	-0.47	-0.46	-0.34	-0.53	-0.46	0.30	-0.26	0.09
31003	-0.50	-0.19	-0.46	-0.49	-0.34	-0.56	-0.49	0.29	-0.31	0.03
31101	-0.46	-0.20	-0.39	-0.45	-0.36	-0.51	-0.45	0.23	-0.32	0.08
31102	-0.46	-0.26	-0.36	-0.43	-0.30	-0.50	-0.44	0.15	-0.35	0.08
31201	-0.31	-0.15	-0.31	-0.33	-0.17	-0.37	-0.33	0.16	-0.22	0.23
31301	-0.42	-0.30	-0.22	-0.37	-0.18	-0.41	-0.38	0.01	-0.37	0.06
31302	-0.50	-0.37	-0.34	-0.47	-0.21	-0.50	-0.47	0.06	-0.46	0.05
31303	-0.45	-0.22	-0.38	-0.44	-0.24	-0.49	-0.45	0.20	-0.35	0.10
31401	-0.44	-0.24	-0.36	-0.45	-0.17	-0.48	-0.45	0.16	-0.34	0.22
31402	-0.43	-0.20	-0.36	-0.43	-0.20	-0.47	-0.43	0.19	-0.31	0.16
31403	-0.38	-0.21	-0.27	-0.38	-0.11	-0.42	-0.38	0.12	-0.30	0.14
31501	-0.39	-0.33	-0.13	-0.34	-0.14	-0.39	-0.34	-0.08	-0.34	0.16
31502	-0.40	-0.30	-0.20	-0.38	-0.13	-0.40	-0.37	-0.01	-0.35	0.12
31503	-0.39	-0.23	-0.23	-0.36	-0.13	-0.41	-0.36	0.07	-0.31	0.07
31601	-0.51	-0.40	-0.26	-0.47	-0.10	-0.52	-0.47	-0.02	-0.45	0.19
31602	-0.47	-0.36	-0.22	-0.43	-0.12	-0.47	-0.43	-0.04	-0.41	0.17
31603	-0.42	-0.25	-0.24	-0.39	-0.13	-0.44	-0.38	0.06	-0.33	0.11
31701	-0.42	-0.27	-0.23	-0.38	-0.10	-0.44	-0.38	0.04	-0.32	0.16
31702	-0.46	-0.33	-0.30	-0.43	-0.06	-0.50	-0.43	0.07	-0.37	0.23
31703	-0.48	-0.31	-0.38	-0.47	-0.11	-0.51	-0.47	0.12	-0.35	0.21
31801	-0.45	-0.33	-0.24	-0.40	-0.04	-0.46	-0.40	0.01	-0.38	0.18
31802	-0.28	-0.19	-0.17	-0.28	0.11	-0.32	-0.28	0.03	-0.18	0.35
31803	-0.44	-0.31	-0.38	-0.44	-0.01	-0.50	-0.43	0.16	-0.32	0.31

Figure. A0-16: Correlation of monthly DJF (left) and MAM (right) percentiles with of PET with 10 hydroclimatic indices

	PET- JJA									
	MEI	Nino 1+2	Nina 4	Nina 3.4	PDO	BEST	ONI	TNI	WHWP	TSA
30101	-0.15	0.13	-0.10	-0.23	-0.28	-0.21	-0.28	0.20	0.32	0.43
30102	-0.16	0.14	-0.11	-0.22	-0.33	-0.21	-0.29	0.22	0.34	0.38
30103	-0.15	0.18	-0.09	-0.19	-0.39	-0.17	-0.27	0.24	0.34	0.30
30201	-0.13	0.18	-0.08	-0.16	-0.34	-0.14	-0.24	0.23	0.32	0.23
30202	-0.15	0.19	-0.12	-0.18	-0.34	-0.16	-0.26	0.26	0.29	0.23
30301	-0.21	0.11	-0.11	-0.21	-0.40	-0.21	-0.30	0.19	0.29	0.29
30302	-0.19	0.14	-0.13	-0.20	-0.43	-0.18	-0.29	0.23	0.25	0.26
30303	-0.12	0.21	-0.11	-0.16	-0.32	-0.13	-0.24	0.28	0.26	0.22
30401	-0.22	0.10	-0.11	-0.21	-0.39	-0.22	-0.30	0.18	0.31	0.36
30402	-0.23	0.12	-0.15	-0.22	-0.45	-0.21	-0.31	0.22	0.25	0.31
30403	-0.21	0.15	-0.16	-0.21	-0.43	-0.23	-0.30	0.25	0.28	0.32
30501	-0.21	0.13	-0.12	-0.20	-0.42	-0.23	-0.29	0.21	0.33	0.37
30502	-0.19	0.18	-0.21	-0.24	-0.41	-0.26	-0.31	0.33	0.24	0.35
30503	-0.21	0.12	-0.14	-0.22	-0.42	-0.23	-0.31	0.21	0.30	0.38
30601	-0.22	0.11	-0.15	-0.22	-0.45	-0.21	-0.31	0.20	0.25	0.36
30602	-0.20	0.16	-0.22	-0.26	-0.38	-0.26	-0.33	0.30	0.22	0.36
30603	-0.24	0.12	-0.24	-0.30	-0.43	-0.28	-0.37	0.28	0.21	0.37
30604	-0.20	0.17	-0.28	-0.31	-0.37	-0.30	-0.37	0.34	0.18	0.39
30701	-0.23	0.11	-0.23	-0.28	-0.44	-0.25	-0.35	0.25	0.22	0.34
30702	-0.21	0.12	-0.27	-0.31	-0.38	-0.25	-0.36	0.27	0.15	0.36
30703	-0.23	0.14	-0.28	-0.32	-0.40	-0.30	-0.38	0.31	0.18	0.41
30704	-0.19	0.16	-0.29	-0.32	-0.30	-0.30	-0.37	0.35	0.18	0.43
30801	-0.16	0.13	-0.34	-0.30	-0.18	-0.38	-0.36	0.36	0.31	0.37
30802	-0.12	0.21	-0.31	-0.28	-0.13	-0.33	-0.33	0.42	0.28	0.36
30901	-0.06	0.17	-0.21	-0.17	-0.13	-0.22	-0.23	0.30	0.33	0.29
30902	0.05	0.24	-0.13	-0.07	-0.18	-0.11	-0.13	0.31	0.27	0.13
31001	0.06	0.23	-0.04	-0.02	-0.19	-0.08	-0.10	0.26	0.40	0.13
31002	-0.05	0.18	-0.18	-0.14	-0.22	-0.23	-0.23	0.31	0.33	0.16
31003	-0.05	0.25	-0.27	-0.20	-0.13	-0.28	-0.28	0.45	0.39	0.25
31101	-0.14	0.18	-0.28	-0.27	-0.25	-0.29	-0.34	0.36	0.21	0.34
31102	-0.22	0.14	-0.31	-0.34	-0.34	-0.32	-0.39	0.34	0.15	0.40
31201	-0.13	0.16	-0.22	-0.24	-0.28	-0.22	-0.30	0.28	0.11	0.30
31301	-0.12	0.15	-0.17	-0.20	-0.32	-0.17	-0.25	0.24	0.15	0.29
31302	-0.14	0.17	-0.25	-0.26	-0.32	-0.20	-0.30	0.30	0.11	0.32
31303	-0.12	0.15	-0.20	-0.22	-0.27	-0.23	-0.27	0.26	0.14	0.35
31401	-0.15	0.01	-0.10	-0.16	-0.23	-0.23	-0.22	0.09	0.10	0.38
31402	-0.11	0.11	-0.12	-0.16	-0.28	-0.20	-0.22	0.18	0.14	0.33
31403	-0.14	0.08	-0.12	-0.17	-0.30	-0.21	-0.23	0.16	0.18	0.38
31501	-0.22	0.05	-0.11	-0.22	-0.37	-0.20	-0.29	0.10	0.23	0.36
31502	-0.15	0.09	-0.18	-0.22	-0.33	-0.19	-0.26	0.18	0.14	0.34
31503	-0.14	0.10	-0.16	-0.19	-0.34	-0.19	-0.24	0.19	0.15	0.36
31601	-0.32	-0.13	-0.18	-0.31	-0.46	-0.23	-0.37	-0.01	0.05	0.41
31602	-0.23	-0.03	-0.15	-0.24	-0.40	-0.19	-0.29	0.06	0.11	0.38
31603	-0.20	0.00	-0.13	-0.21	-0.37	-0.22	-0.26	0.08	0.17	0.40
31701	-0.24	-0.03	-0.16	-0.25	-0.42	-0.25	-0.31	0.08	0.18	0.38
31702	-0.27	-0.05	-0.20	-0.29	-0.43	-0.30	-0.36	0.10	0.16	0.36
31703	-0.25	-0.02	-0.23	-0.28	-0.37	-0.35	-0.34	0.15	0.13	0.38
31801	-0.27	-0.07	-0.20	-0.29	-0.53	-0.22	-0.35	0.07	0.04	0.38
31802	-0.22	-0.03	-0.14	-0.22	-0.42	-0.21	-0.30	0.08	0.12	0.19
31803	-0.28	-0.02	-0.27	-0.34	-0.40	-0.38	-0.40	0.18	0.17	0.35

	PET- SON									
	MEI	Nino 1+2	Nina 4	Nina 3.4	PDO	BEST	ONI	TNI	WHWP	TSA
30101	-0.37	-0.24	-0.28	-0.35	-0.51	-0.38	-0.37	0.06	0.30	0.13
30102	-0.36	-0.23	-0.28	-0.34	-0.48	-0.38	-0.37	0.07	0.35	0.18
30103	-0.30	-0.19	-0.24	-0.29	-0.41	-0.32	-0.32	0.08	0.30	0.14
30201	-0.34	-0.23	-0.25	-0.31	-0.43	-0.36	-0.34	0.04	0.31	0.14
30202	-0.34	-0.19	-0.27	-0.32	-0.45	-0.38	-0.35	0.10	0.36	0.15
30301	-0.38	-0.22	-0.27	-0.34	-0.51	-0.40	-0.38	0.09	0.43	0.17
30302	-0.32	-0.15	-0.28	-0.31	-0.44	-0.37	-0.34	0.16	0.37	0.15
30303	-0.32	-0.12	-0.31	-0.31	-0.39	-0.37	-0.33	0.21	0.35	0.18
30401	-0.38	-0.22	-0.28	-0.33	-0.50	-0.40	-0.38	0.08	0.46	0.25
30402	-0.34	-0.15	-0.28	-0.31	-0.48	-0.38	-0.35	0.16	0.42	0.23
30403	-0.36	-0.18	-0.28	-0.32	-0.50	-0.39	-0.37	0.12	0.44	0.24
30501	-0.37	-0.21	-0.26	-0.31	-0.46	-0.39	-0.36	0.08	0.50	0.29
30502	-0.38	-0.17	-0.32	-0.33	-0.51	-0.42	-0.37	0.16	0.44	0.34
30503	-0.35	-0.17	-0.26	-0.29	-0.47	-0.38	-0.35	0.10	0.52	0.31
30601	-0.34	-0.16	-0.25	-0.28	-0.48	-0.36	-0.33	0.11	0.51	0.32
30602	-0.36	-0.15	-0.31	-0.31	-0.49	-0.40	-0.36	0.17	0.47	0.36
30603	-0.36	-0.17	-0.28	-0.29	-0.51	-0.39	-0.34	0.13	0.49	0.32
30604	-0.38	-0.14	-0.33	-0.33	-0.51	-0.43	-0.38	0.20	0.47	0.37
30701	-0.35	-0.16	-0.30	-0.29	-0.48	-0.39	-0.34	0.15	0.47	0.30
30702	-0.35	-0.15	-0.31	-0.30	-0.46	-0.39	-0.34	0.17	0.45	0.30
30703	-0.39	-0.15	-0.34	-0.34	-0.51	-0.43	-0.39	0.20	0.47	0.37
30704	-0.36	-0.11	-0.34	-0.31	-0.50	-0.41	-0.36	0.24	0.48	0.39
30801	-0.30	-0.09	-0.22	-0.20	-0.46	-0.33	-0.26	0.16	0.45	0.47
30802	-0.24	-0.05	-0.17	-0.14	-0.47	-0.28	-0.20	0.14	0.48	0.42
30901	-0.35	-0.14	-0.29	-0.26	-0.53	-0.37	-0.33	0.15	0.42	0.47
30902	-0.31	-0.13	-0.25	-0.25	-0.48	-0.33	-0.30	0.13	0.39	0.43
31001	-0.34	-0.12	-0.26	-0.23	-0.53	-0.36	-0.30	0.14	0.48	0.46
31002	-0.37	-0.16	-0.28	-0.26	-0.54	-0.39	-0.32	0.13	0.48	0.50
31003	-0.30	-0.11	-0.22	-0.19	-0.47	-0.32	-0.26	0.13	0.47	0.48
31101	-0.35	-0.12	-0.29	-0.27	-0.51	-0.39	-0.33	0.18	0.47	0.45
31102	-0.38	-0.13	-0.33	-0.31	-0.50	-0.42	-0.36	0.20	0.50	0.37
31201	-0.38	-0.12	-0.34	-0.32	-0.44	-0.42	-0.37	0.21	0.45	0.33
31301	-0.35	-0.18	-0.28	-0.29	-0.47	-0.37	-0.33	0.11	0.43	0.27
31302	-0.34	-0.16	-0.29	-0.29	-0.45	-0.38	-0.33	0.14	0.44	0.28
31303	-0.34	-0.17	-0.26	-0.28	-0.46	-0.37	-0.33	0.11	0.45	0.33
31401	-0.30	-0.16	-0.18	-0.23	-0.46	-0.31	-0.27	0.04	0.45	0.28
31402	-0.34	-0.20	-0.24	-0.27	-0.48	-0.36	-0.32	0.05	0.44	0.29
31403	-0.31	-0.16	-0.22	-0.24	-0.47	-0.33	-0.29	0.06	0.45	0.29
31501	-0.37	-0.17	-0.28	-0.30	-0.51	-0.38	-0.35	0.11	0.48	0.28
31502	-0.31	-0.14	-0.25	-0.26	-0.49	-0.33	-0.30	0.11	0.45	0.25
31503	-0.29	-0.14	-0.23	-0.23	-0.45	-0.32	-0.28	0.09	0.45	0.28
31601	-0.28	-0.13	-0.21	-0.22	-0.42	-0.29	-0.26	0.09	0.52	0.23
31602	-0.28	-0.11	-0.20	-0.21	-0.43	-0.29	-0.25	0.09	0.51	0.29
31603	-0.28	-0.14	-0.21	-0.23	-0.44	-0.30	-0.27	0.08	0.48	0.24
31701	-0.27	-0.13	-0.19	-0.22	-0.44	-0.29	-0.26	0.08	0.53	0.18
31702	-0.25	-0.11	-0.19	-0.21	-0.40	-0.27	-0.25	0.10	0.55	0.15
31703	-0.26	-0.12	-0.20	-0.23	-0.44	-0.29	-0.27	0.11	0.52	0.17
31801	-0.30	-0.18	-0.23	-0.25	-0.46	-0.32	-0.29	0.07	0.52	0.18
31802	-0.27	-0.11	-0.24	-0.24	-0.39	-0.29	-0.28	0.15	0.53	0.12
31803	-0.22	-0.04	-0.22	-0.21	-0.37	-0.26	-0.25	0.20	0.53	0.15

Figure. A0-17: Correlation of monthly JJA (left) and SON (right) percentiles with of PET with 10 hydroclimatic indices

References

[1] Abatzoglou, J.T., Barbero, R., Wolf, J.W., Holden, Z.A., 2014. Tracking interannual streamflow variability with drought indices in the US pacific northwest. Journal of Hydrometeorology, 15(5): 1900-1912.

[2] Abbaspour, K., Genuchten, M.v., Schulin, R., Schläppi, E., 1997. A sequential uncertainty domain inverse procedure for estimating subsurface flow and transport parameters. Water Resources Research, 33(8): 1879-1892.

[3] Abbaspour, K., Johnson, C., Van Genuchten, M.T., 2004. Estimating uncertain flow and transport parameters using a sequential uncertainty fitting procedure. Vadose Zone Journal, 3(4): 1340-1352.

[4] Abbaspour, K. et al., 2015. A continental-scale hydrology and water quality model for Europe: Calibration and uncertainty of a high-resolution large-scale SWAT model. Journal of Hydrology, 524: 733-752.

[5] Abbaspour, K.C., 2011. SWAT-CUP4: SWAT calibration and uncertainty programs–a user manual. Swiss Federal Institute of Aquatic Science and Technology, Eawag.

[6] Adamowski, J.F., 2008. River flow forecasting using wavelet and cross-wavelet transform models. Hydrological processes, 22(25): 4877-4891.

[7] Agarwal, A., Maheswaran, R., Kurths, J., Khosa, R., 2016a. Wavelet Spectrum and Self-Organizing Maps-Based Approach for Hydrologic Regionalization-a Case Study in the Western United States. Water Resources Management: 1-15.

[8] Agarwal, A. et al., 2016b. Hydrologic regionalization using wavelet-based multiscale entropy method. Journal of Hydrology, 538: 22-32.

[9] Agarwal, A., Marwan, N., Rathinasamy, M., Merz, B., Kurths, J., Multi-scale event synchronization analysis for unravelling climate processes: A wavelet-based approach.

[10] AghaKouchak, A., 2014. A baseline probabilistic drought forecasting framework using standardized soil moisture index: application to the 2012 United States drought. Hydrology and Earth System Sciences, 18(7): 2485-2492.

[11] AghaKouchak, A., 2015. A multivariate approach for persistence-based drought prediction: Application to the 2010–2011 East Africa drought. Journal of Hydrology, 526: 127-135.

[12] AghaKouchak, A., Hao, Z., Nakhjiri, N., 2014. Drought Monitoring and Prediction Tools. Google Patents.

[13] Ajami, N.K., Duan, Q., Sorooshian, S., 2007. An integrated hydrologic Bayesian multimodel combination framework: Confronting input, parameter, and model structural uncertainty in hydrologic prediction. Water Resources Research, 43(1).

[14] Alapaty, K., Raman, S., Niyogi, D.S., 1997. Uncertainty in the specification of surface characteristics: A study of prediction errors in the boundary layer. Boundary-Layer Meteorology, 82(3): 475-502.

[15] Alvarez-Garreton, C. et al., 2015. Improving operational flood ensemble prediction by the assimilation of satellite soil moisture: comparison between lumped and semi-distributed schemes. Hydrology and Earth System Sciences, 19(4): 1659-1676.

[16] Anderson, M.C. et al., 2013. An intercomparison of drought indicators based on thermal remote sensing and NLDAS-2 simulations with US Drought Monitor classifications. Journal of Hydrometeorology, 14(4): 1035-1056.

[17] Anderson, M.C., Norman, J.M., Mecikalski, J.R., Otkin, J.A., Kustas, W.P., 2007. A climatological study of evapotranspiration and moisture stress across the continental United States based on thermal remote sensing: 1. Model formulation. Journal of Geophysical Research: Atmospheres, 112(D10).

[18] Arnold, J.G. et al., 2012. SWAT: Model use, calibration, and validation. Transactions of the ASABE, 55(4): 1491-1508.

[19] Arnold, J.G., Srinivasan, R., Muttiah, R.S., Williams, J.R., 1998. Large area hydrologic modeling and assessment part I: Model development1. Wiley Online Library.

[20] Bangira, T., Maathuis, B.H., Dube, T., Gara, T.W., 2015. Investigating flash floods potential areas using ASCAT and TRMM satellites in the Western Cape Province, South Africa. Geocarto International, 30(7): 737-754.

[21] Barnett, T.P. et al., 1999. Origins of the midlatitude Pacific decadal variability. Geophysical Research Letters, 26(10): 1453-1456.

[22] Beebee, R.A., Manga, M., 2004. Variation in the relationship between snowmelt runoff and ENSO and PDO. Wiley Online Library.

[23] Bell, J.E. et al., 2013. US Climate Reference Network soil moisture and temperature observations. Journal of Hydrometeorology, 14(3): 977-988.

[24] Best, M.J. et al., 2015. The plumbing of land surface models: benchmarking model performance. Journal of Hydrometeorology, 16(3): 1425-1442.

[25] Betts, A.K., Chen, F., Mitchell, K.E., Janjic, Z.I., 1997. Assessment of the land surface and boundary layer models in two operational versions of the NCEP Eta model using FIFE data. Monthly Weather Review, 125(11): 2896-2916.

[26] Beven, K., Freer, J., 2001. Equifinality, data assimilation, and uncertainty estimation in mechanistic modelling of complex environmental systems using the GLUE methodology. Journal of hydrology, 249(1): 11-29.

[27] Bouchet, R., 1963. Evapotranspiration réelle et potentielle, signification climatique. IAHS Publ, 62: 134-142.

[28] Box, G.E., Jenkins, G.M., 1976. Time series analysis: forecasting and control, revised ed. Holden-Day.

[29] Brabson, B., Lister, D., Jones, P., Palutikof, J., 2005. Soil moisture and predicted spells of extreme temperatures in Britain. Journal of Geophysical Research: Atmospheres, 110(D5).

[30] Brocca, L. et al., 2010. Improving runoff prediction through the assimilation of the ASCAT soil moisture product. Hydrology and Earth System Sciences, 14(10): 1881.

[31] Brown, M.E. et al., 2013. NASA's soil moisture active passive (SMAP) mission and opportunities for applications users. Bulletin of the American Meteorological Society, 94(8): 1125-1128.

[32] Budyko, M.I., 1971. Climate and life.

[33] Cao, W., Bowden, W.B., Davie, T., Fenemor, A., 2006. Multi-variable and multi-site calibration and validation of SWAT in a large mountainous catchment with high spatial variability. Hydrological Processes, 20(5): 1057-1073.

[34] Chen, F., 2007. The Noah land surface model in WRF: a short tutorial, NCAR, LSM Group Meeting, Apr.

[35] Chen, F., Janjić, Z., Mitchell, K., 1997. Impact of atmospheric surface-layer parameterizations in the new land-surface scheme of the NCEP mesoscale Eta model. Boundary-Layer Meteorology, 85(3): 391-421.

[36] Chen, M., Zhuang, Q., He, Y., 2014. An efficient method of estimating downward solar radiation based on the MODIS observations for the use of land surface modeling. Remote Sensing, 6(8): 7136-7157.

[37] Chou, C.-M., Wang, R.-Y., 2002. On-line estimation of unit hydrographs using the wavelet-based LMS algorithm. Hydrological sciences journal, 47(5): 721-738.

[38] Ciabatta, L. et al., 2016. Rainfall-runoff modelling by using SM2RAIN-derived and state-of-the-art satellite rainfall products over Italy. International Journal of Applied Earth Observation and Geoinformation, 48: 163-173.

[39] Coulibaly, P., Burn, D.H., 2004. Wavelet analysis of variability in annual Canadian streamflows. Water Resources Research, 40(3).

[40] Crow, W.T., Wood, E.F., 2002. The value of coarse-scale soil moisture observations for regional surface energy balance modeling. Journal of Hydrometeorology, 3(4): 467-482.

[41] D'Odorico, P., Ridolfi, L., Porporato, A., Rodriguez-Iturbe, I., 2000. Preferential states of seasonal soil moisture: The impact of climate fluctuations. Water Resources Research, 36(8): 2209-2219.

[42] Dai, A., 2011. Drought under global warming: a review. Wiley Interdisciplinary Reviews: Climate Change, 2(1): 45-65.

[43] Dai, X., Wang, P., Chou, J., 2003. Multiscale characteristics of the rainy season rainfall and interdecadal decaying of summer monsoon in North China. Chinese Science Bulletin, 48(24): 2730-2734.

[44] Daubechies, I., 1990. The wavelet transform, time-frequency localization and signal analysis. IEEE transactions on information theory, 36(5): 961-1005.

[45] Delworth, T.L., Manabe, S., 1988. The influence of potential evaporation on the variabilities of simulated soil wetness and climate. Journal of Climate, 1(5): 523-547.

[46] Dile, Y.T., Srinivasan, R., 2014. Evaluation of CFSR climate data for hydrologic prediction in data-scarce watersheds: an application in the Blue Nile River Basin. JAWRA Journal of the American Water Resources Association, 50(5): 1226-1241.

[47] Dirmeyer, P.A., 2013. Characteristics of the water cycle and land–atmosphere interactions from a comprehensive reforecast and reanalysis data set: CFSv2. Climate Dynamics, 41(3-4): 1083-1097.

[48] Dorigo, W. et al., 2013. Global automated quality control of in situ soil moisture data from the International Soil Moisture Network. Vadose Zone Journal, 12(3).

[49] Dracup, J.A., Kahya, E., 1994. The relationships between US streamflow and La Niña events. Water Resources Research, 30(7): 2133-2141.

[50] Duan, Q., Ajami, N.K., Gao, X., Sorooshian, S., 2007. Multi-model ensemble hydrologic prediction using Bayesian model averaging. Advances in Water Resources, 30(5): 1371-1386.

[51] Dutra, E. et al., 2013. The 2010–2011 drought in the Horn of Africa in ECMWF reanalysis and seasonal forecast products. International Journal of Climatology, 33(7): 1720-1729.

[52] Ek, M. et al., 2003. Implementation of Noah land surface model advances in the National Centers for Environmental Prediction operational mesoscale Eta model. Journal of Geophysical Research: Atmospheres, 108(D22).

[53] Enfield, D.B., Mestas-Nuñez, A.M., Mayer, D.A., Cid-Serrano, L., 1999. How ubiquitous is the dipole relationship in tropical Atlantic sea surface temperatures? Journal of Geophysical Research: Oceans, 104(C4): 7841-7848.

[54] Engström, J., Waylen, P., 2017a. The changing hydroclimatology of Southeastern US. Journal of Hydrology, 548: 16-23.

[55] Engström, J., Waylen, P., 2017b. Drivers of long-term precipitation and runoff variability in the southeastern USA. Theoretical and Applied Climatology: 1-14.

[56] Entekhabi, D., Eagleson, P.S., 1989. Land surface hydrology parameterization for atmospheric general circulation models including subgrid scale spatial variability. Journal of climate, 2(8): 816-831.

[57] Famiglietti, J., Wood, E., 1994. Multiscale modeling of spatially variable water and energy balance processes. Water Resources Research, 30(11): 3061-3078.

[58] Famiglietti, J., Wood, E.F., 1995. Effects of spatial variability and scale on areally averaged evapotranspiration. Water Resources Research, 31(3): 699-712.

[59] Famiglietti, J.S., Ryu, D., Berg, A.A., Rodell, M., Jackson, T.J., 2008. Field observations of soil moisture variability across scales. Water Resources Research, 44(1).

[60] Fernandez, C., Ley, E., Steel, M.F., 2001a. Benchmark priors for Bayesian model averaging. Journal of Econometrics, 100(2): 381-427.

[61] Fernandez, C., Ley, E., Steel, M.F., 2001b. Model uncertainty in cross-country growth regressions. Journal of applied Econometrics, 16(5): 563-576.

[62] Feyereisen, G., Strickland, T., Bosch, D., Sullivan, D., 2007. Evaluation of SWAT manual calibration and input parameter sensitivity in the Little River watershed. Trans. ASABE, 50(3): 843-855.

[63] Ford, T.W., McRoberts, D.B., Quiring, S.M., Hall, R.E., 2015. On the utility of in situ soil moisture observations for flash drought early warning in Oklahoma, USA. Geophysical Research Letters, 42(22): 9790-9798.

[64] Fragoso, T.M., Neto, F.L., 2015. Bayesian model averaging: A systematic review and conceptual classification. arXiv preprint arXiv:1509.08864.

[65] Fredj, E., Roarty, H., Kohut, J., Smith, M., Glenn, S., 2016. Gap Filling of the Coastal Ocean Surface Currents from HFR Data: Application to the Mid-Atlantic Bight HFR Network. Journal of Atmospheric and Oceanic Technology, 33(6): 1097-1111.

[66] Fu, C., James, A.L., Yao, H., 2015. Investigations of uncertainty in SWAT hydrologic simulations: a case study of a Canadian Shield catchment. Hydrological Processes, 29(18): 4000-4017.

[67] Fuka, D. et al., 2013. Using the Climate Forecast System Reanalysis dataset to improve weather input data for watershed models. Hydrol. Proc. DOI, 10.

[68] Garcia, D., 2010. Robust smoothing of gridded data in one and higher dimensions with missing values. Computational statistics & data analysis, 54(4): 1167-1178.

[69] Garnaud, C., Bélair, S., Carrera, M.L., McNairn, H., Pacheco, A., 2017. Field-Scale Spatial Variability of Soil Moisture and L-Band Brightness Temperature from Land Surface Modeling. Journal of Hydrometeorology, 18(3): 573-589.

[70] Garner, G., Van Loon, A.F., Prudhomme, C., Hannah, D.M., 2015. Hydroclimatology of extreme river flows. Freshwater Biology, 60(12): 2461-2476.

[71] Gassman, P., Reyes, M., Green, C., Arnold, J., 2007. THE SOIL AND WATER ASSESSMENT TOOL: HISTORICAL DEVELOPMENT, APPLICATIONS, AND FUTURE RESEARCH DIRECTIONS Invited Review Series. Transactions of the American Society of Agricultural and Biological Engineers, 50(4): 1211-1250.

[72] Griensven, A.v., Maharjan, S., Alemayehu, T., 2014. Improved simulation of evapotranspiration for land use and climate change impact analysis at catchment scale.

[73] Gringorten, I.I., 1963. A plotting rule for extreme probability paper. Journal of Geophysical Research, 68(3): 813-814.

[74] Guetter, A.K., Georgakakos, K.P., 1996. Are the El Niño and La Niña predictors of the Iowa River seasonal flow? Journal of Applied Meteorology, 35(5): 690-705.

[75] Hain, C.R., Crow, W.T., Mecikalski, J.R., Anderson, M.C., Holmes, T., 2011. An intercomparison of available soil moisture estimates from thermal infrared and passive microwave remote sensing and land surface modeling. Journal of Geophysical Research: Atmospheres, 116(D15).

[76] Hansen, J.W., 2005. Integrating seasonal climate prediction and agricultural models for insights into agricultural practice. Philosophical Transactions of the Royal Society of London B: Biological Sciences, 360(1463): 2037-2047.

[77] Hao, Z., AghaKouchak, A., 2014. A nonparametric multivariate multi-index drought monitoring framework. Journal of Hydrometeorology, 15(1): 89-101.

[78] Hayes, M., Svoboda, M., Wall, N., Widhalm, M., 2011. The Lincoln declaration on drought indices: universal meteorological drought index recommended. Bulletin of the American Meteorological Society, 92(4): 485-488.

[79] Hobbins, M.T. et al., 2016. The evaporative demand drought index. Part I: Linking drought evolution to variations in evaporative demand. Journal of Hydrometeorology, 17(6): 1745-1761.

[80] Hoeting, J.A., Madigan, D., Raftery, A.E., Volinsky, C.T., 1999. Bayesian model averaging: a tutorial. Statistical science: 382-401.

[81] Homer, C.G. et al., 2015. Completion of the 2011 National Land Cover Database for the conterminous United States-Representing a decade of land cover change information. Photogrammetric Engineering and Remote Sensing, 81(5): 345-354.

[82] Huang, B. et al., 2015. Extended reconstructed sea surface temperature version 4 (ERSST. v4). Part I: Upgrades and intercomparisons. Journal of climate, 28(3): 911-930.

[83] Hunt, E.D., Hubbard, K.G., Wilhite, D.A., Arkebauer, T.J., Dutcher, A.L., 2009. The development and evaluation of a soil moisture index. International Journal of Climatology, 29(5): 747.

[84] Huntington, J., Szilagyi, J., Tyler, S., Pohll, G., 2011. Evaluating the complementary relationship for estimating evapotranspiration from arid shrublands. Water Resources Research, 47(5).

[85] Iglesias, A., Garrote, L., Cancelliere, A., Cubillo, F., Wilhite, D.A., 2009. Coping with drought risk in agriculture and water supply systems: Drought management and policy development in the Mediterranean, 26. Springer Science & Business Media.

[86] Jaksa, W.T., Sridhar, V., Huntington, J.L., Khanal, M., 2013. Evaluation of the complementary relationship using Noah Land Surface Model and North American Regional Reanalysis (NARR) data to estimate evapotranspiration in semiarid ecosystems. Journal of Hydrometeorology, 14(1): 345-359.

[87] Jimenez, C., Prigent, C., Aires, F., 2009. Toward an estimation of global land surface heat fluxes from multisatellite observations. Journal of Geophysical Research: Atmospheres, 114(D6).

[88] Jin, X., Sridhar, V., 2012. Impacts of Climate Change on Hydrology and Water Resources in the Boise and Spokane River Basins1. Wiley Online Library.

[89] Jung, M., Reichstein, M., Bondeau, A., 2009. Towards global empirical upscaling of FLUXNET eddy covariance observations: validation of a model tree ensemble approach using a biosphere model. Biogeosciences, 6(10): 2001-2013.

[90] Kahya, E., Dracup, J.A., 1993. US streamflow patterns in relation to the El Niño/Southern Oscillation. Water Resources Research, 29(8): 2491-2503.

[91] Kang, H. et al., 2016. Modification of SWAT auto-calibration for accurate flow estimation at all flow regimes. Paddy and Water Environment, 14(4): 499-508.

[92] Kang, H., Sridhar, V., 2017. Combined statistical and spatially distributed hydrological model for evaluating future drought indices in Virginia. Journal of Hydrology Regional Studies (In Press).

[93] Karl, T., Koss, W.J., 1984. Regional and national monthly, seasonal, and annual temperature weighted by area, 1895-1983. National Climatic Data Center.

[94] Karl, T.R., 1983. Some spatial characteristics of drought duration in the United States. Journal of Climate and Applied Meteorology, 22(8): 1356-1366.

[95] Katz, R.W., Parlange, M.B., Tebaldi, C., 2003. Stochastic modeling of the effects of large-scale circulation on daily weather in the southeastern US, Issues in the Impacts of Climate Variability and Change on Agriculture. Springer, pp. 189-216.

[96] Keshavarz, M.R., Vazifedoust, M., Alizadeh, A., 2014. Drought monitoring using a Soil Wetness Deficit Index (SWDI) derived from MODIS satellite data. Agricultural Water Management, 132: 37-45.

[97] Khong, A., Wang, J.K., Quiring, S.M., Ford, T.W., 2015. Soil moisture variability in Iowa. International Journal of Climatology, 35(10): 2837-2848.

[98] Kim, G., Barros, A.P., 2002. Space–time characterization of soil moisture from passive microwave remotely sensed imagery and ancillary data. Remote sensing of environment, 81(2): 393-403.

[99] Kim, J., Mohanty, B.P., Shin, Y., 2015. Effective soil moisture estimate and its uncertainty using multimodel simulation based on Bayesian Model Averaging. Journal of Geophysical Research: Atmospheres, 120(16): 8023-8042.

[100] Kim, S., 2004. Wavelet analysis of precipitation variability in northern California, USA. KSCE Journal of Civil Engineering, 8(4): 471-477.

[101] Kim, T.-W., Valdés, J.B., 2003. Nonlinear model for drought forecasting based on a conjunction of wavelet transforms and neural networks. Journal of Hydrologic Engineering, 8(6): 319-328.

[102] Koren, V. et al., 1999. A parameterization of snowpack and frozen ground intended for NCEP weather and climate models. Journal of Geophysical Research: Atmospheres, 104(D16): 19569-19585.

[103] Koster, R.D. et al., 2004. Regions of strong coupling between soil moisture and precipitation. Science, 305(5687): 1138-1140.

[104] Koster, R.D., Suarez, M.J., 1994. The components of a 'SVAT'scheme and their effects on a GCM's hydrological cycle. Advances in Water Resources, 17(1-2): 61-78.

[105] Koster, R.D., Suarez, M.J., 1996. Energy and water balance calculations in the Mosaic LSM.

[106] Kundzewicz, Z.W., Hirabayashi, Y., Kanae, S., 2010. River floods in the changing climate—observations and projections. Water Resources Management, 24(11): 2633-2646.

[107] Labosier, C.F., Quiring, S.M., 2013. Hydroclimatology of the Southeastern USA. Climate Research, 57(2): 157-171.

[108] Laiolo, P. et al., 2016. Impact of different satellite soil moisture products on the predictions of a continuous distributed hydrological model. International Journal of Applied Earth Observation and Geoinformation, 48: 131-145.

[109] Lakshmi, V., Piechota, T., Narayan, U., Tang, C., 2004. Soil moisture as an indicator of weather extremes. Geophysical research letters, 31(11).

[110] Leamer, E.E., 1978. Specification searches: Ad hoc inference with nonexperimental data, 53. John Wiley & Sons Incorporated.

[111] Li, B., Avissar, R., 1994. The impact of spatial variability of land-surface characteristics on land-surface heat fluxes. Journal of Climate, 7(4): 527-537.

[112] Limaye, A.S., Boyington, T.M., Cruise, J.F., Bulusu, A., Brown, E., 2001. MACROSCALE HYDROLOGIC MODELING FOR REGIONAL CLIMATE ASSESSMENT STUDIES IN THE SOUTHEASTERN UMTED STATES. JAWRA Journal of the American Water Resources Association, 37(3): 709-722.

[113] Liu, W. et al., 2010. Actual evapotranspiration estimation for different land use and land cover in urban regions using Landsat 5 data. Journal of Applied Remote Sensing, 4(1): 041873.

[114] Liu, Y., Yang, W., Wang, X., 2008. Development of a SWAT extension module to simulate riparian wetland hydrologic processes at a watershed scale. Hydrological Processes, 22(16): 2901-2915.

[115] Liu, Y. et al., 2015. Evapotranspiration in Northern Eurasia: Impact of forcing uncertainties on terrestrial ecosystem model estimates. Journal of Geophysical Research: Atmospheres, 120(7): 2647-2660.

[116] Livezey, R.E., Smith, T.M., 1999. Covariability of aspects of North American climate with global sea surface temperatures on interannual to interdecadal timescales. Journal of Climate, 12(1): 289-302.

[117] Lu, J., Sun, G., McNulty, S.G., Amatya, D.M., 2003. Modeling actual evapotranspiration from forested watersheds across the Southeastern United States. JAWRA Journal of the American Water Resources Association, 39(4): 886-896.

[118] Lu, R., 2002. Decomposition of interdecadal and interannual components for North China rainfall in rainy season. Chinese Journal of Atmosphere (in Chinese), 26: 611-624.

[119] Luo, L., Wood, E.F., 2007. Monitoring and predicting the 2007 US drought. Geophysical Research Letters, 34(22).

[120] Ma, F., Yuan, X., Ye, A., 2015. Seasonal drought predictability and forecast skill over China. Journal of Geophysical Research: Atmospheres, 120(16): 8264-8275.

[121] Mace, R.E., Yang, B., Pu, B., 2015. Early warning of summer drought over Texas and the south central United States: spring conditions as a harbinger of summer drought.

[122] Madadgar, S., Moradkhani, H., 2013. A Bayesian framework for probabilistic seasonal drought forecasting. Journal of Hydrometeorology, 14(6): 1685-1705.

[123] Madadgar, S., Moradkhani, H., 2014. Spatio-temporal drought forecasting within Bayesian networks. Journal of Hydrology, 512: 134-146.

[124] Maheswaran, R., Khosa, R., 2012a. Comparative study of different wavelets for hydrologic forecasting. Computers & Geosciences, 46: 284-295.

[125] Maheswaran, R., Khosa, R., 2012b. Wavelet–Volterra coupled model for monthly stream flow forecasting. Journal of Hydrology, 450: 320-335.

[126] Makkonen, L., 2006. Plotting positions in extreme value analysis. Journal of Applied Meteorology and Climatology, 45(2): 334-340.

[127] Mallat, S., 1999. A Wavelet Tour of Signal Processing, (Wavelet Analysis & Its Applications).

[128] Mantua, N.J., Hare, S.R., Zhang, Y., Wallace, J.M., Francis, R.C., 1997. A Pacific interdecadal climate oscillation with impacts on salmon production. Bulletin of the american Meteorological Society, 78(6): 1069-1079.

[129] Manuel, J., 2008. Drought in the Southeast: Lessons for Water Management. Environmental Health Perspectives, 116(4): 168-171.

[130] Mao, J. et al., 2015. Disentangling climatic and anthropogenic controls on global terrestrial evapotranspiration trends. Environmental Research Letters, 10(9): 094008.

[131] Marek, G.W. et al., 2016. Estimating evapotranspiration for dryland cropping systems in the semiarid Texas High Plains using SWAT. JAWRA Journal of the American Water Resources Association.

[132] Martinez-Martinez, E., Nejadhashemi, A.P., Woznicki, S.A., Love, B.J., 2014. Modeling the hydrological significance of wetland restoration scenarios. Journal of environmental management, 133: 121-134.

[133] McEvoy, D.J., 2015. Physically based evaporative demand as a drought metric: Historical analysis and seasonal prediction, Citeseer.

[134] McEvoy, D.J. et al., 2016a. The Evaporative Demand Drought Index. Part II: CONUS-wide assessment against common drought indicators. Journal of Hydrometeorology, 17(6): 1763-1779.

[135] McEvoy, D.J., Huntington, J.L., Mejia, J.F., Hobbins, M.T., 2016b. Improved seasonal drought forecasts using reference evapotranspiration anomalies. Geophysical Research Letters, 43(1): 377-385.

[136] McKee, T.B., Doesken, N.J., Kleist, J., 1993. The relationship of drought frequency and duration to time scales, Proceedings of the 8th Conference on Applied Climatology. American Meteorological Society Boston, MA, pp. 179-183.

[137] Mishra, A., VP, S., VR, D., 2009. Drought characterization: a probabilistic approach. Stochastic Environmental Research and Risk Assessment, 23(1): 41-55.

[138] Mishra, A.K., Singh, V.P., 2010. A review of drought concepts. Journal of Hydrology, 391(1): 202-216.

[139] Mitchell, K.E. et al., 2004a. The multi-institution North American Land Data Assimilation System (NLDAS): Utilizing multiple GCIP products and partners in a continental distributed hydrological modeling system. Journal of Geophysical Research: Atmospheres, 109(D7).

[140] Mitchell, K.E. et al., 2004b. The multi-institution North American Land Data Assimilation System (NLDAS): Utilizing multiple GCIP products and partners in a continental distributed hydrological modeling system. Journal of Geophysical Research: Atmospheres (1984–2012), 109(D7).

[141] Mitra, S., 2014. Anthropogenic and Climate Impacts on Groundwater Resources in the Lower Apalachicola-Chattahoochee-Flint River Basin, Auburn University.

[142] Mo, K.C., 2008. Model-based drought indices over the United States. Journal of Hydrometeorology, 9(6): 1212-1230.

[143] Mo, K.C., Chen, L.-C., Shukla, S., Bohn, T.J., Lettenmaier, D.P., 2012a. Uncertainties in North American land data assimilation systems over the contiguous United States. Journal of Hydrometeorology, 13(3): 996-1009.

[144] Mo, K.C. et al., 2011. Drought indices based on the Climate Forecast System Reanalysis and ensemble NLDAS. Journal of Hydrometeorology, 12(2): 181-205.

[145] Mo, K.C., Shukla, S., Lettenmaier, D.P., Chen, L.C., 2012b. Do Climate Forecast System (CFSv2) forecasts improve seasonal soil moisture prediction? Geophysical Research Letters, 39(23).

[146] Moreda, F., Koren, V., Zhang, Z., Reed, S., Smith, M., 2006. Parameterization of distributed hydrological models: learning from the experiences of lumped modeling. Journal of Hydrology, 320(1): 218-237.

[147] Mozny, M. et al., 2012. Use of a soil moisture network for drought monitoring in the Czech Republic. Theoretical and Applied Climatology, 107(1-2): 99-111.

[148] Mu, Q., Zhao, M., Kimball, J.S., McDowell, N.G., Running, S.W., 2013. A remotely sensed global terrestrial drought severity index. Bulletin of the American Meteorological Society, 94(1): 83-98.

[149] Mueller, B. et al., 2013. Benchmark products for land evapotranspiration: LandFlux-EVAL multi-data set synthesis. Hydrology and Earth System Sciences.

[150] Mueller, B. et al., 2011. Evaluation of global observations-based evapotranspiration datasets and IPCC AR4 simulations. Geophysical Research Letters, 38(6).

[151] Muttiah, R.S., Wurbs, R.A., 2002. Scale-dependent soil and climate variability effects on watershed water balance of the SWAT model. Journal of Hydrology, 256(3): 264-285.

[152] Nag, B., Misra, V., Bastola, S., 2014. Validating ENSO teleconnections on Southeastern US winter hydrology. Earth Interactions, 18(15): 1-23.

[153] Nanda, T., Sahoo, B., Beria, H., Chatterjee, C., 2016. A wavelet-based non-linear autoregressive with exogenous inputs (WNARX) dynamic neural network model for real-time flood forecasting using satellite-based rainfall products. Journal of Hydrology, 539: 57-73.

[154] Narayan, U., Lakshmi, V., 2008. Characterizing subpixel variability of low resolution radiometer derived soil moisture using high resolution radar data. Water resources research, 44(6).

[155] Neitsch, S.L., Arnold, J.G., Kiniry, J.R., Williams, J.R., 2011. Soil and water assessment tool theoretical documentation version 2009, Texas Water Resources Institute.

[156] Oglesby, R.J., Marshall, S., Erickson, D.J., Roads, J.O., Robertson, F.R., 2002. Thresholds in atmosphere–soil moisture interactions: Results from climate model studies. Journal of Geophysical Research: Atmospheres, 107(D14).

[157] Oldak, A., Jackson, T.J., Pachepsky, Y., 2002. Using GIS in passive microwave soil moisture mapping and geostatistical analysis. International Journal of Geographical Information Science, 16(7): 681-698.

[158] Otkin, J.A. et al., 2016. Assessing the evolution of soil moisture and vegetation conditions during the 2012 United States flash drought. Agricultural and Forest Meteorology, 218: 230-242.

[159] Palmer, W.C., 1965. Meteorological drought, 30. US Department of Commerce, Weather Bureau Washington, DC.

[160] Parrish, M.A., Moradkhani, H., DeChant, C.M., 2012. Toward reduction of model uncertainty: Integration of Bayesian model averaging and data assimilation. Water Resources Research, 48(3).

[161] Partal, T., Kişi, Ö., 2007. Wavelet and neuro-fuzzy conjunction model for precipitation forecasting. Journal of Hydrology, 342(1): 199-212.

[162] Pederson, N. et al., 2012. A long-term perspective on a modern drought in the American Southeast. Environmental Research Letters, 7(1): 014034.

[163] Peters-Lidard, C., Pan, F., 2002. Re-thinking the contradictions of soil moisture spatial variability, AGU Fall Meeting Abstracts, pp. 1042.

[164] Peterson, T.C., Stott, P.A., Herring, S., 2012. Explaining extreme events of 2011 from a climate perspective. Bulletin of the American Meteorological Society, 93(7): 1041-1067.

[165] Polhamus, A., Fisher, J.B., Tu, K.P., 2013. What controls the error structure in evapotranspiration models? Agricultural and forest meteorology, 169: 12-24.

[166] Pulwarty, R.S., Sivakumar, M.V., 2014. Information systems in a changing climate: Early warnings and drought risk management. Weather and Climate Extremes, 3: 14-21.

[167] Quiring, S.M. et al., 2015. The North American soil moisture database: development and applications. Bulletin of the American Meteorological Society(2015).

[168] Raftery, A.E., Gneiting, T., Balabdaoui, F., Polakowski, M., 2005. Using Bayesian model averaging to calibrate forecast ensembles. Monthly Weather Review, 133(5): 1155-1174.

[169] Rathinasamy, M., Adamowski, J., Khosa, R., 2013. Multiscale streamflow forecasting using a new Bayesian Model Average based ensemble multi-wavelet Volterra nonlinear method. Journal of Hydrology, 507: 186-200.

[170] Rathinasamy, M., Agarwal, A., Parmar, V., Khosa, R., Bairwa, A., 2017. Partial wavelet coherence analysis for understanding the standalone relationship between Indian Precipitation and Teleconnection patterns. arXiv preprint arXiv:1702.06568.

[171] Robinson, J., Hubbard, K., 1990. Soil water assessment model for several crops in the High Plains. Agronomy Journal, 82(6): 1141-1148.

[172] Rojas, R., Feyen, L., Dassargues, A., 2008. Conceptual model uncertainty in groundwater modeling: Combining generalized likelihood uncertainty estimation and Bayesian model averaging. Water Resources Research, 44(12).

[173] Ropelewski, C.F., Halpert, M.S., 1986. North American precipitation and temperature patterns associated with the El Niño/Southern Oscillation (ENSO). Monthly Weather Review, 114(12): 2352-2362.

[174] Rouholahnejad, E. et al., 2012. A parallelization framework for calibration of hydrological models. Environmental Modelling & Software, 31: 28-36.

[175] Roundy, J.K., Ferguson, C.R., Wood, E.F., 2014. Impact of land-atmospheric coupling in CFSv2 on drought prediction. Climate dynamics, 43(1-2): 421-434.

[176] Saha, S. et al., 2010. The NCEP climate forecast system reanalysis. Bulletin of the American Meteorological Society, 91(8): 1015.

[177] Sahay, R.R., Sehgal, V., 2014. Wavelet-ANFIS models for forecasting monsoon flows: Case study for the Gandak River (India). Water Resources, 41(5): 574-582.

[178] Schmidt, N., Lipp, E., Rose, J., Luther, M., 2001. ENSO influences on seasonal rainfall and river discharge in Florida. Journal of Climate, 14(4): 615-628.

[179] Seager, R., Tzanova, A., Nakamura, J., 2009. Drought in the southeastern United States: causes, variability over the last millennium, and the potential for future hydroclimate change. Journal of Climate, 22(19): 5021-5045.

[180] Sehgal, Tiwari, M.K., Chandranath, C., 2014a. Wavelet bootstrap multiple linear regression based hybrid modeling for daily river discharge forecasting. Water resources management, 28(10): 2793-2811.

[181] Sehgal, V., Lakhanpal, A., Maheswaran, R., Khosa, R., Sridhar, V., 2016. Application of multi scale wavelet entropy and multi-resolution Volterra models for climatic downscaling: a case study of Krishna basin, India. Journal of Hydrology, Under Review.

[182] Sehgal, V., Sahay, R.R., Chatterjee, C., 2014b. Effect of utilization of discrete wavelet components on flood forecasting performance of wavelet based ANFIS models. Water resources management, 28(6): 1733-1749.

[183] Sehgal, V., Sridhar, V., 2017. Retrospective drought analysis using SWAT-simulated hydrologic variables and implementation of SWAT-CFSv2 coupled models for near-real time seasonal drought forecasting. Under review.

[184] Sehgal, V., Sridhar, V., Tyagi, A., 2017. Stratified drought analysis using a stochastic ensemble of simulated and in-situ soil moisture observations. Journal of Hydrology, 545: 226-250.

[185] Sehgal, V., Tiwari, M.K., Chatterjee, C., 2014c. Wavelet bootstrap multiple linear regression based hybrid modeling for daily river discharge forecasting. Water resources management, 28(10): 2793-2811.

[186] Sen, A., 2012. Streamflow variability in the Southern Appalachians and atmospheric teleconnections. River research and applications, 28(5): 630-636.

[187] Seneviratne, S.I., Lüthi, D., Litschi, M., Schär, C., 2006. Land–atmosphere coupling and climate change in Europe. Nature, 443(7108): 205-209.

[188] Seong, C., Sridhar, V., 2017. Hydroclimatic variability and change in the Chesapeake Bay Watershed. Journal of Water and Climate Change, 8(2): 254-273.

[189] Shafiee-Jood, M., Cai, X., Chen, L., Liang, X.Z., Kumar, P., 2014. Assessing the value of seasonal climate forecast information through an end-to-end forecasting framework: Application to US 2012 drought in central Illinois. Water Resources Research, 50(8): 6592-6609.

[190] Shah, R.D., Mishra, V., 2016. Utility of Global Ensemble Forecast System (GEFS) Reforecast for Medium-Range Drought Prediction in India. Journal of Hydrometeorology, 17(6): 1781-1800.

[191] Sheffield, J., Goteti, G., Wen, F., Wood, E.F., 2004a. A simulated soil moisture based drought analysis for the United States. Journal of Geophysical Research: Atmospheres (1984–2012), 109(D24).

[192] Sheffield, J., Goteti, G., Wen, F., Wood, E.F., 2004b. A simulated soil moisture based drought analysis for the United States. Journal of Geophysical Research: Atmospheres, 109(D24).

[193] Sheffield, J., Wood, E.F., 2012. Drought: past problems and future scenarios. Routledge.

[194] Sheffield, J. et al., 2014. A drought monitoring and forecasting system for sub-Sahara African water resources and food security. Bulletin of the American Meteorological Society, 95(6): 861-882.

[195] Shiklomanov, I.A., 1998. World water resources: a new appraisal and assessment for the 21st century: a summary of the monograph World water resources. Unesco.

[196] Sims, A.P., Raman, S., 2002. Adopting drought indices for estimating soil moisture: A North Carolina case study. Geophysical Research Letters, 29(8).

[197] Singh, R., Prasad, V.H., Bhatt, C., 2004. Remote sensing and GIS approach for assessment of the water balance of a watershed/evaluation par télédétection et SIG du bilan hydrologique d'un bassin versant. Hydrological sciences journal, 49(1): 131-141.

[198] Sittel, M.C., 1994. Marginal probabilities of the extremes of ENSO events for temperature and precipitation in the southeastern United States. Center for Ocean-Atmosphere Prediction Studies. Florida State University.

[199] Sivapalan, M., Wood, E., 1986. Spatial heterogeneity and scale in the infiltration response of catchments, Scale problems in hydrology. Springer, pp. 81-106.

[200] Smith, C.A., Sardeshmukh, P.D., 2000. The effect of ENSO on the intraseasonal variance of surface temperatures in winter. International Journal of Climatology, 20(13): 1543-1557.

[201] Smith, L.C., Turcotte, D.L., Isacks, B.L., 1998. Stream flow characterization and feature detection using a discrete wavelet transform. Hydrological processes, 12(2): 233-249.

[202] Sohrabi, M.M., Ryu, J.H., Abatzoglou, J., Tracy, J., 2015. Development of soil moisture drought index to characterize droughts. Journal of Hydrologic Engineering, 20(11): 04015025.

[203] Sommerlot, A.R., Wagena, M.B., Fuka, D.R., Easton, Z.M., 2016. Coupling the short-term global forecast system weather data with a variable source area hydrologic model. Environmental Modelling & Software, 86: 68-80.

[204] Sridhar, V., Anderson, K.A., 2017. Human-induced modifications to land surface fluxes and their implications on water management under past and future climate change conditions. Agricultural and Forest Meteorology, 234: 66-79.

[205] Sridhar, V., Hubbard, K., 2009. Estimation of the water balance using observed soil water in the Nebraska sandhills. Journal of Hydrologic Engineering, 15(1): 70-78.

[206] Sridhar, V., Hubbard, K.G., You, J., Hunt, E.D., 2008. Development of the soil moisture index to quantify agricultural drought and its "user friendliness" in severity-area-duration assessment. Journal of Hydrometeorology, 9(4): 660-676.

[207] Sridhar, V. et al., 2013. Evaluating bias-corrected AMSR-E soil moisture using in situ observations and model estimates. Vadose Zone Journal, 12(3).

[208] Sridhar, V., Wedin, D.A., 2009. Hydrological behaviour of grasslands of the Sandhills of Nebraska: water and energy-balance assessment from measurements, treatments, and modelling. Ecohydrology, 2(2): 195-212.

[209] Su, B., Wang, A., Wang, G., Wang, Y., Jiang, T., 2016. Spatiotemporal variations of soil moisture in the Tarim River basin, China. International Journal of Applied Earth Observation and Geoinformation, 48: 122-130.

[210] Sun, S. et al., 2017. Modeling Evapotranspiration over China's Landmass from 1979 to 2012 Using Multiple Land Surface Models: Evaluations and Analyses. Journal of Hydrometeorology, 18(4): 1185-1203.

[211] Svoboda, M., LeComte, D., Hayes, M., Heim, R., 2002. The drought monitor. Bulletin of the American Meteorological Society, 83(8): 1181.

[212] SWAT, 2017. SWAT literature database for peer- reviewed journal articles.

[213] Tallaksen, L.M., Van Lanen, H.A., 2004. Hydrological drought: processes and estimation methods for streamflow and groundwater, 48. Elsevier.

[214] Tang, C., Piechota, T.C., 2009. Spatial and temporal soil moisture and drought variability in the Upper Colorado River Basin. Journal of Hydrology, 379(1): 122-135.

[215] Teuling, A.J., Troch, P.A., 2005. Improved understanding of soil moisture variability dynamics. Geophysical Research Letters, 32(5).

[216] Tootle, G.A. et al., 2009. The 2009-2010 El Nino: Hydrologic relief to US regions. EOS Transactions, 90(50): 481.

[217] Torrence, C., Webster, P.J., 1998. The annual cycle of persistence in the El Nño/Southern Oscillation. Quarterly Journal of the Royal Meteorological Society, 124(550): 1985-2004.

[218] Torrence, C., Webster, P.J., 1999. Interdecadal changes in the ENSO-monsoon system. Journal of Climate, 12(8): 2679-2690.

[219] Trenberth, K., Overpeck, J., Solomon, S., 2004. Exploring drought and its implications for the future. Eos, Transactions American Geophysical Union, 85(3): 27-27.

[220] Trenberth, K.E., 1984. Some effects of finite sample size and persistence on meteorological statistics. Part I: Autocorrelations. Monthly Weather Review, 112(12): 2359-2368.

[221] Trenberth, K.E., Fasullo, J.T., 2012. Climate extremes and climate change: The Russian heat wave and other climate extremes of 2010. Journal of Geophysical Research: Atmospheres, 117(D17).

[222] Trenberth, K.E., Fasullo, J.T., Kiehl, J., 2009. Earth's global energy budget. Bulletin of the American Meteorological Society, 90(3): 311-323.

[223] Trenberth, K.E., Stepaniak, D.P., 2001. Indices of El Niño evolution. Journal of Climate, 14(8): 1697-1701.

[224] Twine, T.E., Kucharik, C.J., Foley, J.A., 2005. Effects of El Niño–Southern Oscillation on the climate, water balance, and streamflow of the Mississippi River basin. Journal of Climate, 18(22): 4840-4861.

[225] Uniyal, B., Jha, M.K., Verma, A.K., 2015. Parameter identification and uncertainty analysis for simulating streamflow in a river basin of Eastern India. Hydrological Processes, 29(17): 3744-3766.

[226] USGS, 2017. Boundary Descriptions and Names of Regions, Subregions, Accounting Units and Cataloging Units.

[227] Van Liew, M.W., Arnold, J., Bosch, D., 2005. Problems and potential of autocalibrating a hydrologic model. Transactions of the ASAE, 48(3): 1025-1040.

[228] Van Loon, A., Van Lanen, H., 2012. A process-based typology of hydrological drought. Hydrology and Earth System Sciences, 16(7): 1915.

[229] Vinukollu, R.K., Wood, E.F., Ferguson, C.R., Fisher, J.B., 2011. Global estimates of evapotranspiration for climate studies using multi-sensor remote sensing data: Evaluation of three process-based approaches. Remote Sensing of Environment, 115(3): 801-823.

[230] Vrugt, J.A., Robinson, B.A., 2007. Treatment of uncertainty using ensemble methods: Comparison of sequential data assimilation and Bayesian model averaging. Water Resources Research, 43(1).

[231] Walter, I.A. et al., 2000. ASCE's standardized reference evapotranspiration equation, Watershed management and operations management 2000, pp. 1-11.

[232] Wang, A., Bohn, T.J., Mahanama, S.P., Koster, R.D., Lettenmaier, D.P., 2009. Multimodel ensemble reconstruction of drought over the continental United States. Journal of Climate, 22(10): 2694-2712.

[233] Wang, A., Lettenmaier, D.P., Sheffield, J., 2011. Soil moisture drought in China, 1950-2006. Journal of Climate, 24(13): 3257-3271.

[234] Wang, A., Zeng, X., Shen, S.S., Zeng, Q.-C., Dickinson, R.E., 2006. Time scales of land surface hydrology. Journal of Hydrometeorology, 7(5): 868-879.

[235] Wang, C., Enfield, D.B., 2001. The tropical Western Hemisphere warm pool. Geophysical Research Letters, 28(8): 1635-1638.

[236] Wang, G., Garcia, D., Liu, Y., De Jeu, R., Dolman, A.J., 2012. A three-dimensional gap filling method for large geophysical datasets: Application to global satellite soil moisture observations. Environmental Modelling & Software, 30: 139-142.

[237] Wang, H., Kumar, A., 2015. Assessing the impact of ENSO on drought in the US Southwest with NCEP climate model simulations. Journal of Hydrology, 526: 30-41.

[238] Wang, H., Ting, M., 2000. Covariabilities of winter US precipitation and Pacific sea surface temperatures. Journal of Climate, 13(20): 3711-3719.

[239] Wang, W., Ding, J., 2003. Wavelet network model and its application to the prediction of hydrology. Nature and Science, 1(1): 67-71.

[240] Wang, X., Yang, W., Melesse, A.M., 2008. Using hydrologic equivalent wetland concept within SWAT to estimate streamflow in watersheds with numerous wetlands. Transactions of the ASAE (American Society of Agricultural Engineers), 51(1): 55.

[241] Wetterhall, F., Winsemius, H., Dutra, E., Werner, M., Pappenberger, E., 2015. Seasonal predictions of agro-meteorological drought indicators for the Limpopo basin. Hydrology and Earth System Sciences, 19(6): 2577-2586.

[242] Wilhite, D.A., Glantz, M.H., 1985. Understanding: the drought phenomenon: the role of definitions. Water international, 10(3): 111-120.

[243] Wilhite, D.A., Wood, D., Meyer, S., 1987. Climate-related impacts in the United States during the 1982-83 El Nino.

[244] Wilks, D., 2011. Empirical distributions and exploratory data analysis. Statistical Methods in the Atmospheric Sciences: 41-44.

[245] Williams, J., Jones, C., Dyke, P., 1984. A modeling approach to determining the relationship between erosion and soil productivity. Trans. Asae, 27(1): 129-144.

[246] Willmott, C.J., Robeson, S.M., Matsuura, K., 2012. A refined index of model performance. International Journal of Climatology, 32(13): 2088-2094.

[247] Willmott, C.J., Robeson, S.M., Matsuura, K., Ficklin, D.L., 2015. Assessment of three dimensionless measures of model performance. Environmental Modelling & Software, 73: 167-174.

[248] Wolter, K., Timlin, M.S., 1998. Measuring the strength of ENSO events: how does 1997/98 rank? Weather, 53(9): 315-324.

[249] Wolter, K., Timlin, M.S., 2011. El Niño/Southern Oscillation behaviour since 1871 as diagnosed in an extended multivariate ENSO index (MEI. ext). International Journal of Climatology, 31(7): 1074-1087.

[250] Wood, A.W., 2008. The University of Washington Surface Water Monitor: An experimental platform for national hydrologic assessment and prediction, American Meteorology Society annual meeting, 22nd conference on hydrology, New Orleans. p.

[251] Wood, A.W., Maurer, E.P., Kumar, A., Lettenmaier, D.P., 2002. Long-range experimental hydrologic forecasting for the eastern United States. Journal of Geophysical Research: Atmospheres, 107(D20).

[252] Wu, H., 2016. Integrated sensitivity analysis, calibration, and uncertainty propagation analysis approaches for supporting hydrological modeling, Memorial University of Newfoundland.

[253] Xia, Y. et al., 2014a. Uncertainties, correlations, and optimal blends of drought indices from the NLDAS multiple land surface model ensemble. Journal of Hydrometeorology, 15(4): 1636-1650.

[254] Xia, Y. et al., 2014b. Application of USDM statistics in NLDAS-2: Optimal blended NLDAS drought index over the continental United States. Journal of Geophysical Research: Atmospheres, 119(6): 2947-2965.

[255] Xia, Y. et al., 2012. Continental-scale water and energy flux analysis and validation for the North American Land Data Assimilation System project phase 2 (NLDAS-2): 1. Intercomparison and application of model products. Journal of Geophysical Research: Atmospheres, 117(D3).

[256] Xu, Z., Pang, J., Liu, C., Li, J., 2009. Assessment of runoff and sediment yield in the Miyun Reservoir catchment by using SWAT model. Hydrological Processes, 23(25): 3619-3630.

[257] Yan, D. et al., 2013. Modified Palmer drought severity index based on distributed hydrological simulation. Mathematical Problems in Engineering, 2013.

[258] Yang, J., Reichert, P., Abbaspour, K., Xia, J., Yang, H., 2008. Comparing uncertainty analysis techniques for a SWAT application to the Chaohe Basin in China. Journal of Hydrology, 358(1): 1-23.

[259] Yuan, X., Wood, E.F., 2013. Multimodel seasonal forecasting of global drought onset. Geophysical Research Letters, 40(18): 4900-4905.

[260] Yuan, X. et al., 2013. Probabilistic seasonal forecasting of African drought by dynamical models. Journal of Hydrometeorology, 14(6): 1706-1720.

[261] Zang, Y., Wallace, J., Battisti, D., 1997. ENSO-like interdecadal variability: 1900–1993. Journal of Climate, 10: 1004-1020.

[262] Zhang, L., Dawes, W., Walker, G., 2001. Response of mean annual evapotranspiration to vegetation changes at catchment scale. Water resources research, 37(3): 701-708.

[263] Zhang, L., Zhang, H., Zhang, Q., Li, Y., Zhao, J., 2016a. On the potential application of land surface models for drought monitoring in China. Theoretical and Applied Climatology: 1-17. DOI:10.1007/s00704-016-1730-0

[264] Zhang, X., Tang, Q., Liu, X., Leng, G., Li, Z., 2017. Soil Moisture Drought Monitoring and Forecasting Using Satellite and Climate Model Data over Southwestern China. Journal of Hydrometeorology, 18(1): 5-23.

[265] Zhang, Y. et al., 2010. Using long-term water balances to parameterize surface conductances and calculate evaporation at 0.05 spatial resolution. Water Resources Research, 46(5).

[266] Zhang, Y. et al., 2016b. Multi-decadal trends in global terrestrial evapotranspiration and its components. Scientific reports, 6.

[267] Zhu, J., Ju, W., Ren, Y., 2010. Effects of land cover types and forest age on evapotranspiration detected by remote sensing in Xiamen City, China, Geoinformatics, 2010 18th International Conference on. IEEE, pp. 1-5.

[268] Zou, L., Xia, J., She, D., 2017. Drought Characteristic Analysis Based on an Improved PDSI in the Wei River Basin of China. Water, 9(3): 178.